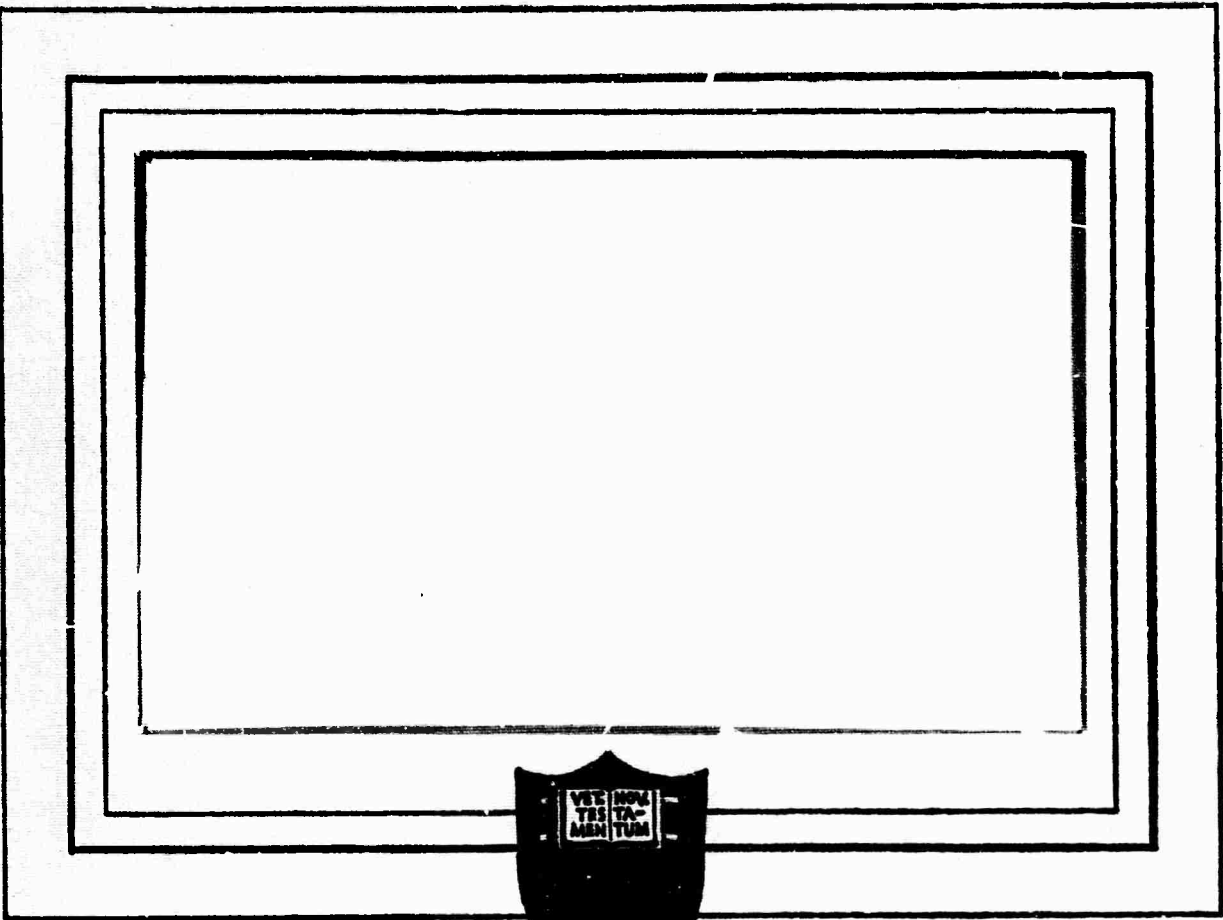


AD634278



CLEARINGHOUSE FOR FEDERAL SCIENTIFIC AND TECHNICAL INFORMATION			
Hardcopy	Microfiche		
\$ 7.00	\$ 1.50	310 PP	72
ARCHIVE COPY			

DDC
JUN 27 1966

1. Distribution of this document is unlimited.

PRINCETON UNIVERSITY
DEPARTMENT OF
AEROSPACE AND MECHANICAL SCIENCES

DISCLAIMER NOTICE

THIS DOCUMENT IS THE BEST
QUALITY AVAILABLE.

COPY FURNISHED CONTAINED
A SIGNIFICANT NUMBER OF
PAGES WHICH DO NOT
REPRODUCE LEGIBLY.

DEPARTMENT OF THE AIR FORCE
AIR FORCE OFFICE OF SCIENTIFIC RESEARCH
PROPULSION RESEARCH DIVISION

AFOSR Grant - 448-63
Project Task No. 920F-3814

Sponsored by:

Advanced Research Projects Agency
ARPA Order No. 317-62, Am. No. 9

SOLID PROPELLANT COMBUSTION INSTABILITY:
STATIONARY BURNING OF SOLID ROCKET PROPELLANTS (U)

Aerospace and Mechanical Sciences Report No. 751

Scientific Report
1 June 1963 - 30 September 1964


by

R. H. Woodward Waesche - Assistant-in-Research

and

Martin Summerfield - Professor of Aerospace Propulsion

Transmitted by:


for Martin Summerfield
Principal Investigator

Reproduction, translation, publication, use and disposal in whole or in part by or for the United States Government is permitted.

August 1965

Guggenheim Laboratories for the Aerospace Propulsion Sciences
Department of Aerospace and Mechanical Sciences
PRINCETON UNIVERSITY
Princeton, New Jersey

BLANK PAGE

ABSTRACT

One of the major unsolved problems in the field of solid propellant rockets is the phenomenon of combustion instability, which is characterized by the amplification of a small pressure disturbance (a part of the spectrum of noise connected with any system involving combustion and flow) to high levels of intensity. The high intensity disturbances can be periodic in nature, with frequencies characteristic of one or more of the acoustic modes of the motor cavity, and this type of instability is the main subject of interest.

Since many factors influenced the severity and type of a particular case of combustion instability, an attempt has been made, based on the morphological method introduced by Zwicky, to separate and analyze the different components of a particular instability. It has been found that a particular case can be described by four elements: (1) the physical coupling that drives the oscillation, (2) the damping mechanism that limits the amplitude, (3) the degree of linearity, and (4) the oscillation mode or modes.

One result of a literature review is to show that the most often encountered source of the self-amplification of a disturbance is the dynamic coupling of the oscillatory pressure field and the combustion zone near the surface. From a consideration of flame zone structure, it is possible to predict the ranges of steady-state pressure and oscillation frequency over which different processes are affected by the oscillating field. Extensive theoretical studies of this coupling have been carried out in an attempt to understand the mechanism of the self-amplification, and the ranges of applicability are discussed.

A number of experiments carried out at other laboratories to determine the acoustic admittance characterizing the interaction between the combustion zone and varying pressure are reviewed and discussed. A knowledge of the admittance is important, since it is then possible to indicate whether the propellant in question will generate instability in a full-scale rocket motor.

The acoustic admittance is composed of two parts - a dynamic burning rate function and a dynamic flame temperature function. This thesis is focussed on the determination of the dynamic flame temperature function, partly because it is an aspect of the measurement of acoustic admittance, but mainly because it provides a means of diagnosing the character of the burning rate - pressure interaction.

Five different experiments have been analyzed here for the measurement of acoustic admittance of a burning solid propellant, including a "detuning" test, shock wave reflection, thickness measurement, particle track techniques, and composition or temperature wave studies. Detailed consideration shows that, while most are unsuitable, the most promising is the temperature wave measurement.

Since the gas temperature is meaningful only when observed in coordination with pressure, the combined effect should be reported as the entropy of the gas, so that a measurement of the entropy variation of the gas emerging from the flame zone of a solid propellant burning under varying

pressure should lead to a determination of the interaction behavior.

At the lowest frequencies, ("zero-frequency" regime), two simple cases are thought to exist for the entropy variation: (1) the emergent gas is characterized by constant entropy during an oscillation, like a sound wave reflection; (2) the flame temperature is constant, leading to entropy waves carried (i.e., convected) with the burnt gases. These convection waves would be seen as a time-and space-varying temperature field above the burning surface with wavelengths of the order of a few centimeters and efflux velocities of the order of a few hundreds of centimeters per second. Waves appearing to have some of the expected properties have been observed photographically by W. A. Wood of the Rohm & Haas Company. Entropy variations more complex than these simple cases should occur at higher frequencies. The predicted behavior of the entropy variation is related to the model chosen for the flame zone, and it is shown that there should exist different regions of interaction, depending on the combustion pressure and the frequency of the pressure disturbances.

An experimental study of the entropy behavior has been made, using a 2-inch diameter T-tube combustor as the source of oscillating pressure for a wide range of frequencies, amplitudes, and pressures. The acoustic interaction was studied with high-speed cinematography, a streak camera, and spectral radiometry with sodium doping. No entropy variation from an end burning grain was found over the pressures (250-1150 psi) and frequencies (75-1600 cps) used for the different compositions tested, which included pure ammonium perchlorate composite propellants and plastisol nitrocellulose-types. It has also been found that the waves observed by Wood are not one-dimensional entropy waves and that these waves are obtainable, for some obscure reason, only by using an uninhibited side-burning test specimen. A mechanism for these waves is postulated.

Absence of the predicted entropy waves leads to the belief that the flame zone model used as a basis for anticipating such waves is apparently in error. Possible errors in the model are discussed, together with some experiments aimed at the magnitude of the errors.

The conclusion to be drawn from this research on the unsteady combustion of solid propellants is that further knowledge of steady-state combustion mechanisms is required. The dynamic coupling involved can be explained only when a firmer understanding of these mechanisms is obtained.

ACKNOWLEDGEMENTS

This research was supported by the Air Force Office of Scientific Research and its financial sponsorship is greatly appreciated.

Doctor Joseph Wenograd was responsible for the administrative details of the project. In addition, he provided valuable suggestions as well as friendship. Many stimulating discussions were held with Professor Reuel Shinnar, under whose direction the theoretical work in Chapter X was performed.

Mr. Lubomyr Kurylko provided invaluable aid in propellant processing and formulations, as well as assisting in the final phases of assembling this report. The majority of the propellant processing was carried out under the direction of Mr. Chris Felsheim, who also contributed many helpful suggestions to the assembly of the experimental apparatus.

Special thanks are due to the two laboratory technicians on this project, Mr. Roy Crosby and Mr. Samuel Morris. Mr. Crosby was a great help in the photographic aspects of the work, and Mr. Morris was responsible for the instrumentation required. Both provided numerous helpful suggestions in addition to their indispensable work in carrying out the research. Above all, both provided good humor and friendship which are deeply appreciated.

Numerous of the other personnel at the Guggenheim Laboratories provided assistance. The Drafting Room, under Mr. Tony Poli, provided graphs and figures, principally by Mrs. Ann Jansak and Mrs. Kathryn Walter. Mr. Donald Neiler provided the excellent photographs for this report. Typing of the draft was carried out skillfully by Miss Yolanda Pastor. The report in its final form was typed by Miss Claire Hartmann and Miss Susan Blomer.

TABLE OF CONTENTS

		<u>PAGE</u>
TITLE PAGE		i
ABSTRACT		ii
ACKNOWLEDGEMENTS		iv
TABLE OF CONTENTS		v
LIST OF TABLES		viii
LIST OF FIGURES		i
CHAPTER	I	THE OCCURRENCE OF COMBUSTION INSTABILITY IN SOLID PROPELLANT ROCKET MOTORS
		1
	A.	Introduction and Definitions
		1
	B.	An Account of the Observed Instabilities and Practical Fixes
		1
	C.	Characteristic Effects of Combustion Instability
		3
CHAPTER	II	THE MORPHOLOGY OF COMBUSTION OSCILLATIONS
		7
	A.	The Principles of Morphology
		7
	B.	The Philosophy of Morphology
		7
	C.	Organization of a System and Notation
		7
	D.	Detailed Description of Elements with Diagram
		8
	E.	Energy Sources
		8
	F.	Physical Coupling Mechanisms
		9
	G.	Damping Mechanisms
		10
	H.	Degree of Linearity
		12
	I.	Gasdynamic Behavior
		13
CHAPTER	III	THEORIES OF ELEMENTAL PROCESSES IN COMBUSTION INSTABILITY - A LITERATURE SURVEY
		15
	A.	Background - "Singing Flames"
		15
	B.	Argument for Pressure Coupling
		16
	C.	Theories on the Coupling of Pressure with a Surface Flame
		16
	D.	The Coupling of Velocity with a Surface Flame
		19
	E.	The Coupling of Pressure with a Distributed Flame Zone
		24
	F.	Damping Effects
		26
	H.	Nonlinear Effects
		34
	I.	A Perspective View
		35
CHAPTER	IV	A DETAILED DISCUSSION OF PRESSURE COUPLING WITH THE SURFACE FLAME ZONE
		36
	A.	Introduction
		36
	B.	Pressure-Frequency Regimes
		36
	C.	Theories of Pressure Coupling
		39

CHAPTER	V	EXPERIMENTAL STUDIES ON THE NATURE OF THE PRESSURE - SURFACE FLAME COUPLING	51
		A. Introduction	51
		B. Self-Excited Pressure Oscillations	52
		C. Combustors with External Sound Source	59
		D. Combustors with External Single-Pulse Wave	61
CHAPTER	VI	CONSIDERATION OF POSSIBLE EXPERIMENTS TO MEASURE ACOUSTIC ADMITTANCE	64
		A. Introduction	64
		B. Acoustic Methods	64
		C. Shock-Wave Reflection	70
		D. Instantaneous Thickness Measurement	75
		E. Particle-Track Method	79
		F. Composition-Wave Observation	83
CHAPTER	VII	ACOUSTIC ADMITTANCE AND ENTROPY WAVES	84
		A. The Acoustic Admittance Equation	84
		B. Importance of	84
		C. Characteristics of the Zero-Frequency Regime	85
		D. Entropy Variation and Admittance	91
CHAPTER	VIII	EXPERIMENTAL APPARATUS	93
		A. Oscillator Selection	93
		B. T-Burner Design	93
		C. Ignition and Controls	94
		D. Instrumentation	95
		E. Photographic Equipment	96
		F. T-Motor Performance Parameters	96
		G. Window Design	100
		H. Temperature Measurements	103
		I. Photomultiplier Design and Calibration	108
CHAPTER	IX	EXPERIMENTAL RESULTS	111
CHAPTER	X	DAMPING MECHANISM STUDIES	119
CHAPTER	XI	CONCLUSIONS AND FUTURE EXPERIMENTS	132
APPENDICES			
		A. Acoustic Admittance	
		B. Cavity Acoustics	
		C. Thickness Measurement with X-Rays and Photo- multiplier	
		D. Flame Temperature Calculations	
		E. Polyurethane Processing and Motor Casting Procedure	
		F. "D" Line Contour Calculations	

- G. Plastisol Processing Procedure
- H. dp/dt Experiment
- I. List of Equipment
- J. List of Chemicals

REFERENCES

FIGURES

LIST OF TABLES

I	Pressure behind reflected shock	VI-75
II	Time and distance to reach 95% of gas velocity	VI-81
III	Particle in oscillating gas flow	VI-81
IV	Persistence of Entropy Wave	VII-90
V	Effect of Heat Loss	VIII-99
VI	Measured Spectral Line Widths for LP-3 Strands	VIII-106
VII	Measured Spectral line Widths for Plastisol Specimens	VIII-107
VIII	Photomultiplier Calibration	VIII-109
IX	Photomultiplier Calibration	VIII-109
X	Photomultiplier Calibration	VIII-110
XI	Observation of Luminosity Waves (AUP85T)	IX-112
XII	Observation of Luminosity Waves (AUP80)	IX-112
XIII	Observation of Luminosity Waves (AUP + Na)	IX-113
XIV	Testing Standoff Effect	IX-114
XV	Test Conditions for Plastisol Samples	IX-115
XVI	Test Conditions for Inhibited and Uninhibited Samples	IX-117
XVII	Parameters Used in Calculations	X-126

<u>Fig. No.</u>	<u>Title</u>	<u>Page</u>
1	Oscillatory vs. unstable burning	I-1
2	Pressure-time curves for tubular JPN ballistic grain	I-2
3	Pressure change due to oscillatory burning	I-4
4	Apparatus used by Price to obtain the effect of oscillatory burning on propellant burning rate	I-4
5	Change in burning rate as a function of acoustic environment for combustion oscillations at 4200 cps for double-base propellants	I-5
6	Change in burning rate as a function of acoustic environment for combustion oscillations at 4200 cps AP-PBAA composite propellant	I-5
7	Ratio of burning rate under oscillatory conditions to the steady-state burning rate as a function of frequency	I-5
8	Apparatus used by Watermeier to determine effect of oscillations on burning rate	I-5
9	Star grain geometry with rotating tangential mode	I-6
10	Acoustic sources and sinks in a solid propellant rocket motor	II-8
11	History of pressure pulse for conditions of amplification	II-9
12	Morphological lattice space of combustion oscillations	II-10
13	Model used by Green	III-20
14	Results of Green theory for resonance and near-resonance conditions	III-20
15	Dependence of severity of irregular burning on pressure	III-22
16	Demonstration on non-linear instability	III-23
17	Non-linear instability tests in stable and unstable regimes	III-23
18	Non-acoustic instability (note frequency dependence on pressure)	III-24
19	Chuffing	III-24
20	Effect of propellant compressibility on response function	III-29
21	Pressure-frequency regimes of acoustic interaction with combustion zone	IV-37
22	Response functions obtained by Hart-McClure and by Cheng with fixed and variable time lag	IV-42
23	Combustion zone model used by Hart and McClure	IV-42
24	A typical response vs frequency curve calculated by Hart and McClure (amplification in shaded area)	IV-44
25	Effect of temperature sensitivity on response function	IV-44
26	Domains of stability and instability	IV-50
27	T-burner used by Price	V-52
28	T-burner for oscillatory burning experiments	V-52
29	Response functions for two propellants as measured by different laboratories	V-57
30	Four-nozzle resonant chamber used by Watermeier	V-57
31	The effect of binder composition upon the response function of a propellant	V-57
32	The effect of burning rate modifiers upon the response function	V-57

<u>Fig. No.</u>	<u>Title</u>	<u>Page</u>
33	Propellant response function plotted against frequency and against frequency divided by the square of the burning rate	V-57
34	Comparison of admittance data for three methods	V-59
35	Technique used to increase the propellant burning surface	V-59
36	Oscillator used by Foner for measuring solid propellant response	V-59
37	Modified Mawardi impedance measurement	V-60
38	Solid-Propellant acoustic oscillator with transparent (quartz) combustion chamber used by Nachbar	V-61
39	Wave splitter apparatus used by Lawhead	V-62
40	Pressure along a tube	VI-66
41	Variation of microphone pressure with frequency	VI-67
42	Shock reflection from rigid end wall with outgassing	VI-72
43	Expected result - particle track method	VI-80
44	Experiment to observe particle track in product gas stream	VI-80
45	Size selection criterion for relative amplitude 90%	VI-82
46	Entropy wave properties in an acoustic field	VI-83
47	Pressure and temperature as a function of time for gas packets emitted from the flame	VII-87
48	Cross-section of T-burner	VIII-93
49	Experimental arrangement for observation of temperature waves under oscillating pressure in T-burner	VIII-94
50	T-burner test section	VIII-94
51	Sample holder with specimen mounted	VIII-94
52	Solid propellant test cell	VIII-94
53	Assembled igniter	VIII-94
54	Igniter components prior to assembly	VIII-94
55	Basic firing circuit for oscillator driver	VIII-94
56	Control panel	VIII-95
57	Dynisco pressure transducer	VIII-95
58	Instrumentation Panel	VIII-95
59	Burning rate of candidate driverpropellants	VIII-97
60	Operating characteristics of t-motor at 430 cps with driver containing 80% B.M. AP, 20% PBAA, 2% copper chromite	VIII-98
61	Operating characteristics of t-motor at 270 cps with driver containing 80% B.M. AP, 20% PBAA, 2% copper chromite	VIII-98
62	LP-3 burning rate	VIII-98
63	Operating characteristics of t-motor at 430 cps with driver containing 80% B.M. AP, 20% LP-3	VIII-98
64	Burning rate vs pressure for propellant containing 85% trimodal AP, 15% Polyurethane	VIII-98
65	Operating characteristics of t-motor with driver containing 85% trimodal AP, 15% Polyurethane	VIII-98
66	Effect of mean pressure and frequency on pressure wave form in t-burner	VIII-99

<u>Fig. No.</u>	<u>Title</u>	<u>Page</u>
67	Effect of spacer length on oscillation amplitude	VIII-99
68	Effect of driver grain length on oscillation amplitude	VIII-99
69	Original test section	VIII-100
70	Comparison of new and old windows (new on left)	VIII-102
71	Optical system for obtaining sodium line width of burning solid propellant	VIII-105
72	Experimental Apparatus for obtaining spectrum of propellant burning in test section	VIII-106
73	Spectrum of Propellant Combustion Gases with Filtered Radiation from Tungsten Lamp Superimposed	VIII-107
74	Photometric temperature measuring apparatus	VIII-108
75	Photomultiplier circuit	VIII-108
76	Brightness temperature vs current for 18A/T10/2P6V Bulb	VIII-108
77	Brightness temperature vs current for 18A/T10/2P-6V Bulb	VIII-108
78	Photomultiplier output vs brightness temperature	VIII-108
79	Photomultiplier output vs brightness temperature	VIII-108
80	Photomultiplier output vs brightness temperature	VIII-108
81	Streak photograph for uninhibited test specimen	IX-115
82	Burning rate vs pressure for plastisol propellant P-5	IX-115
83	Streak photograph for inhibited test specimen	IX-117
84	Streak photograph for uninhibited test specimen	IX-117
85	Computed variation of $Re(\tilde{\theta}_f \bar{P}/\bar{T}_f \tilde{\phi})$ with frequency for different values of heat of surface reaction (H) (m = 1)	X-125
86	Computed variation of $Re(y)$ with frequency for different values of heat of surface reaction (H) (m = 1)	X-125
87	Computed variation of phase angle δ with frequency for different values of heat of surface reaction (H) (m = 1)	X-125
88	Computed variation of $\tilde{\theta}_f \bar{P}/\bar{T}_f \tilde{\phi}$ with frequency for different values of heat of surface reaction (H) (m = 1)	X-125
89	Computed variation of $Re(\tilde{\theta}_f \bar{P}/\bar{T}_f \tilde{\phi})$ with frequency for different values of burning rate (H = - 200)	X-125
90	Computed variation of $Re(\tilde{\theta}_f \bar{P}/\bar{T}_f \tilde{\phi})$ with frequency for different values of burning rate (H = - 100)	X-125
91	Computed variation of $Re(\tilde{\theta}_f \bar{P}/\bar{T}_f \tilde{\phi})$ with frequency for two values of E, the activation energy of surface reaction (H = - 200)	X-125
92	Computed variation of $Re(\tilde{\theta}_f \bar{P}/\bar{T}_f \tilde{\phi})$ with frequency for different values of surface temperature (H = - 100)	X-125
93	Effect of heat transfer parameter α on $Re(\tilde{\theta}_f \bar{P}/\bar{T}_f \tilde{\phi})$ (H = - 200)	X-129
94	Effect of heat transfer parameter α on $Re(\tilde{\theta}_f \bar{P}/\bar{T}_f \tilde{\phi})$ (H = - 100)	X-129
95	Portion of the Oscillograph Record of Radiometer and Pressure Output	IX-113
B-1	Standing and spinning forms of the first tangential mode	B-2

<u>Fig. No.</u>	<u>Title</u>	<u>Page</u>
B-2	Oscillation pattern for transverse modes	B-2
C-1	X-ray thickness measurement	C-7
F-1	Emissivity of combustion gases vs wave length	F-4
F-2	Emissivity of combustion gases vs wave length	F-4
F-3	Emissivity of combustion gases vs wave length	F-4
F-4	Emissivity of combustion gases vs wave length	F-4
H-1	Pressure vs time in (dp/dt) experiment	H-1
H-2	Pressure vs luminosity in (dp/dt) experiment	H-1
H-3	Pressure vs temperature in (dp/dt) experiment	H-1

CHAPTER I

THE OCCURRENCE OF COMBUSTION INSTABILITY IN SOLID PROPELLANT ROCKET MOTORS

Introduction and Definitions

When a ballistician is presented with a specified thrust-time curve for a solid propellant rocket, he is usually able to meet these specifications through a selection from the wide variety of binders available and a judicious balancing of burning rate modifiers and grain configuration. He can get some indication as to his success by small-scale tests of the design. However, one big question can usually not be answered before the full-scale motor is tested. This question concerns the possibility of occurrence of combustion instability.

Combustion instability takes two basic forms - oscillatory burning and unstable burning, shown in Figure 1. Oscillatory burning is characterized by pressure oscillations around the steady-state pressure, with frequencies which usually correspond to one or more of the Rayleigh modes of the grain configuration cavity. Unstable burning is characterized by variations (often large-scale) of the pressure from the design value which cannot be blamed on a grain irregularity, nozzle difficulty, etc. It has been found that unstable burning has associated with it, and is preceded by, the pressure oscillations characteristic of oscillatory burning.

Although oscillatory and unstable burning in solid propellant rockets have been reported since 1941, it is only recently that investigations of this phenomenon have been of other than a short-term, quick-fix character. Various engineering remedies for suppression of combustion instability have been used since the problem was first encountered. A number of these remedies will be discussed later. Unfortunately, a more fundamental understanding of the combustion instability of a solid propellant is needed since the large motors in use today and being designed for tomorrow are far too expensive, with too much lead time, to use the engineering methods which sufficed in the past.

An Account of the Observed Instabilities and Practical Fixes

The first known encounters with combustion instability occurred in Great Britain early in World War II. Boys and Schofield found (1) that unexplainable motor case ruptures were occurring in test firings of a small aircraft rocket using a simple tubular grain burning internally and externally. When they used heavier motor cases, it was found that the pressure was, at times, jumping to new steady-state values which were sometimes nearly twice the design pressure. These increases were accompanied by severe localized increases in burning rate, with the propellant surface showing signs of rippling or pitting. They found that putting a

rod or flat "tongue" along the axis of the grain perforation cured the difficulty. In addition, it was found that drilling radial hole opening to the inner cavity brought about stability (2).

Similar results are reported by Wimpress (3), who summarizes the work performed at the California Institute of Technology during World War II. Based on geometric considerations, a simple circular tube was used as the propellant grain design, since it would give an almost neutral pressure-time curve without the need of inhibition. However, it was found that JPN ballistite tubular grains burned with severe secondary peaks (Figure 2). When the outer surface was inhibited, allowing burning to take place only in the perforation, even more severe peaks occurred. Partially burned grains showed the inner surfaces to be pitted and rippled, while the outer surfaces were smooth. In addition, the grain would sometimes split longitudinally. Wimpress reports that the most common stabilization procedure was the drilling of radial holes through the grain. A number of considerations in the number and size of the holes is presented. In addition, non-burning axial rods were placed in the center of the perforation to cure stability. It was also found that non-circular axial perforations were more stable.

The original experiments reported above were made with recording instruments and pressure gauges with frequency responses of less than 100 cps. Investigators at the Naval Ordnance Test Station later found evidence of high-frequency pressure oscillations in rocket motors when tests were performed with higher response instrumentation (4). In a continuation of this work, Swanson (5) found that the secondary peaks recorded by low-response equipment were present only when accompanied by high-frequency pressure oscillations.

Smith and Sprenger (6) conducted the first systematic experimental study using high-frequency instrumentation into combustion instability. They found that secondary peaks were associated with transverse modes in the circular and annular cavities used - longitudinal modes were found with one grain design, but led only to moderate, prolonged pressure increases. The transverse modes found were the tangential ones, and the use of two pickups 90° apart disclosed the fact that the spinning mode was present. It was also found that the shape of the seal at the nozzle end of the grain influenced the type and severity of the oscillations, undoubtedly through the effect on the gas flow and boundary conditions at the end of the grain.

Green performed a number of interesting experiments on different phenomena involved in combustion instability. They were designed to test the effects of two classes of variables - the grain configuration and the propellant's oxidizer concentration and particle size. The first sets of experiments, on charge configuration, were designed to test the predictions of two theories (to be discussed later) as to the acoustic modes to be expected and as to the effect of configuration on stability (7). A ranking of stability, based on low-frequency response records follows: An external burning rod was most stable, followed in order of decreasing

stability by tubular grains, annular charges, and grains with star-shaped cavities. The latter three were all internal-burning grains. (The author performed a similar series of tests at the Rohm & Haas Company with a different propellant system and found similar results (8)). The resulting traces and high-frequency instrumentation data are given in a separate report (9).

The second set of experiments performed by Green was designed to test the belief that instability was more likely in propellants with highest energy content (10). Using seven propellant formulations with different oxidizer particle size and concentration and with burning rate modifiers, he found that the rate of energy release (product of burning rate, propellant density, and heat of explosion), gave a better indication of relative stability than did energy content or burning rate alone. The highest energy propellant was fairly stable, which was attributed to the fact that the burning rate was low, probably because of the coarse oxidizer used.

Summaries of the experimental evidence gathered in the 1950's have been given by Geckler (11) (12), Green (2) (7), Price (13), Wall (14), and Osborn (15). Among the results given in these summaries are the different techniques which were used to cure or alleviate combustion instability. The earliest ones, mentioned previously, were the use of non-burning axial rods and the drilling of radial holes. In addition, the addition of a fore-end free volume, use of baffles, and smoothing the nozzle end of the grain were sometimes found effective. The shapes and sizes of the rods and baffles used seemed like Daliesque, nightmarish creations, with little science to their design. These techniques appeared to work because they would either disrupt any ordered acoustic motion or dampen the acoustic energy in the flow field. It was also noticed that the proximity of a cold metal wall, as in the external burning grains, seemed to promote stability, probably by degrading performance and damping temperature oscillations.

In addition to these purely mechanical means, it was also found that the propellant composition could be adjusted to cure instability. Shuey found (16) that the addition of powdered aluminum could suppress instability. Other metals and additives have been used (17). It is hypothesized that these work either by decoupling the propellant response from the gas pressure oscillations or by attenuating the sound field in the gas phase (18) (19). Experiments on this will be discussed later.

Characteristic Effects of Combustion Instability

As a continuation of the historical review, it is fitting to include a listing of some of the phenomena observed as a result of combustion instability. These observations will serve as a background for the experimental and theoretical work to be discussed in later sections.

As noted originally, combustion instability is noted by either unstable burning or oscillatory burning. It can be marked by sharp

secondary peaks, possible causes of which will be discussed later. The pressure-level can also reach a new value, which can be higher or lower than the value before the onset of oscillations (20) (Figure 3). The pressure increases may come either through burning rate increases or through decreases in mass flow rate through the nozzle (21). Burning rate increases can come about through "erosive burning," by a mechanism to be described shortly. The effective nozzle throat area can be decreased by the centrifugal action caused by the vortex flow associated with the spinning tangential mode mentioned earlier and described in Appendix B. (Evidence of this vortex flow will be given in this section.)

The pressure decreases can result either through burning rate drops which have been reported for some mesa propellants (propellants whose burning rate drops with pressure increase over some range), or through a decrease in combustion efficiency caused by the oscillations.

When only oscillatory burning is present, the characteristic oscillations can cause vibrations in the whole motor system. It is known that vibrations are transmitted into and through the propellant (21) (22) (23) (24) so it is not surprising that the structural system is affected. The vibrations can, of course, cause damage to sensitive guidance systems or fatigue to motor parts. The physical integrity of the grain can be destroyed, leading to severe pressure increases due to extra exposed burning surface. In addition, the initially sinusoidal waves can steepen in many cases to a wave shape not unlike a shock front (25) (26) (27) (28) (14) which can cause even more serious effects.

Large increases in heat transfer to the cavity boundaries are noted during combustion instability, much as in liquid propellant rockets. Different mechanisms may be invoked to explain these increases. It is known, for instance, that standing vortices can exist in laminar channel flow in a resonant acoustic field (29). In addition, Moore and Maslen have shown that the first tangential mode is the one most likely to be amplified by an internal-burning cylindrical grain (30), as was also found in the theories of Grad and Cheng. Since the maximum pressure and velocity changes occur at the wall for this mode, it is not surprising that the presence of the tangential mode can cause large increases in heat transfer. The heat transfer increases probably explain the presence of grooves in the propellant grain noted by Wimpess and by Boys and Schofield.

Vandenkerkchove (31) relates the peaks of unstable burning to large increases in burning rate. These increases result from the increased transport, through turbulence, of hot gas products into (for double-base propellants) the fizz zone.

One of the most controversial effects of combustion instability has been the change which occurs in mean and local regression rate of the propellant. Price has performed a series of experiments of increasing sophistication (20) (32) (33) to correlate the change in burning rate with the local acoustic environment along a grain (Figure 4). For double-

base propellant systems, it was found that the burning rate was increased at velocity antinodes (pressure nodes) and decreased at velocity nodes (pressure antinodes) (Figure 5). One significant result was that the burning rate and pressure showed violent increases when the tangential mode frequency was an integral multiple of the frequency of an unstable axial mode (Figure 6).

Eisel (35) found, using a one-dimensional design with propellant only at the pressure antinode, that the burning rates of both composite and double-base propellant were reduced for burning under oscillating pressure. The reduction was greater at higher frequencies for both classes of propellant, but the effect of steady-state pressure was different for the two types (Figure 6). The effect of oscillating pressure was greater at increased steady-state pressure for the composite propellants, but less for the double-base propellants, probably as a result of the different effect of pressure on the combustion-zone structure for the two classes.

Nadaud studied the effect of a sound field on burning rate, using an 80 watt speaker into a tube containing burning propellant (36). For non-metallized propellant, it was found that, at certain frequencies, the burning rate increased markedly at the velocity antinodes, but not at pressure antinodes. The increase was a function of the power delivered to the loud-speaker. For metallized propellants, however, very little burning rate increase was obtained (Figure 7).

Watermeier (37) used a siren to generate an oscillatory pressure in a strand burner containing a burning strand of a plateau-type double-base propellant. It was found that the burning rate increased when the siren frequency was close to a resonant frequency of the burner chamber.

Yamazaki et al. (38) employed a tweeter, covering the frequency range from 1.5 to 13 kilocycles, with a constant wattage input to give an oscillating pressure field for propellants burning at pressures from 1 to 70 atmospheres in a modified strand burner. For a polysulfide propellant containing 70% ammonium perchlorate, the burning rate at a given pressure increased 10-20% at a definite frequency, and this frequency decreased with increasing pressure. At the lower pressures, the frequency for maximum regression rate was relatively constant (close to the cavity natural frequency), and no increase in rate was observed at the highest pressure (1000 psi). For different propellants and catalysts, the frequency at which the regression rate became a maximum moved to higher frequency as the rate increased. From matching pressure with the frequency for maximum rate increase, they calculate that the thickness of the flame zone mixed by the sound waves extended from a few hundred to a few thousand microns above the surface.

Watermeier later attempted to obtain the effect of acoustic erosivity (39) using an adaptation of the resonant tube used by others for acoustic admittance measurements, which will be described later. The experiment is shown schematically in Figure 8. The test samples

are at a velocity antinode, and the burning rate is determined by a Fairchild movie camera. Oscillations of 160 psi amplitude were attained at a mean pressure of 300 psi, giving a particle velocity (using acoustic theory) of 800 ft/sec. No burning rate increase was obtained.

An intriguing effect of combustion instability is, in many cases, to cause a violent roll torque on the whole motor assembly (24) (40). This can be traced back to the presence of rotational flow in the cavity, set up by the sound field (41). Photographs through the head-end of chambers had disclosed swirling motion in the gas (42) (43) (Figure 9) which, in one case, "scrubbed" the viewing window clean of reaction products. Green also reported that cruciform grains were observed to rotate inside motor chambers during firing (44). A recent experimental program has led to the photographing of a large number of vortices of different classes, depending on the acoustic mode present (45) (46) (47). Sotter has shown, following Mager (48), that the rapidly spinning gases can cause a drop in gas velocity when they pass through the nozzle, thus decreasing the mass flow rate by as much as 40%.

Some general observations as to the occurrence of combustion instability can also be made. Oscillations from as low as 6 cycles per second to 55,000 cycles per second have been recorded (49). Instability is more severe when the initial propellant temperature is some value not near the middle of its conditioning range (50). It is usually found that increasing the chamber pressure leads to a relative stability increase, at least as measured by relative pressure amplitudes (51) (52) (53). In fact, some investigators have found that there is an upper pressure limit above which instability does not occur (53) (24). Another observation is the fact that certain modes of oscillation appear and disappear through a single firing, giving rise to oscillations of varying amplitude (52), because of the geometrical changes in the cavity resulting from propellant consumption.

CHAPTER II

THE MORPHOLOGY OF COMBUSTION OSCILLATIONS

The Principles of Morphology

The preceding summary of a few of the phenomena connected with combustion oscillations gives some indication of the complexity of the problem. It is easily seen that there are many factors determining the occurrence, type, and severity of oscillations for a given motor design. In order to obtain an understanding of the problem or, indeed, to attempt to use the results of one theory or experiment and to apply them to another set of conditions, these factors must be sorted out and classified, so that their interplay can be studied in a more orderly manner. Once the factors are classified, the various ways in which they can combine must be examined. An analogous problem is the one faced by the grammarian in his study of word formation, and the scientist can profit from the grammarian's study of morphology to probe the makeup of possible words, using parallel techniques to investigate possible combinations of factors which could lead to different resultant phenomena (54).

As used in this particular context, the principle of morphology is based on separating the various distinctive components of the problem to be studied and analyzing the various combinations which can result from choices of the components. In this way, the characteristic roles of the different components in determining the attributes of the resultants can be distinguished. Moreover, it then becomes possible to make an intelligent prediction of the effects a change in one of the components will have on a combination whose characteristics were well known before the component was altered.

The Philosophy of Morphology

The organization of such a morphological system, then, is a key part of the morphology, and great care must be taken in defining the characteristics of the different components. The mere act of definition, however, helps a great deal in the treatment of the problem, for the researcher, in so doing, is forced to look into the basic aspects of the problem, usually gaining fresh insight as a result.

Organization of a System and Notation

One way in which a many-component system can be represented is through the notation of a vector space on which lattice points are entered. The different axes of the system, known as the base vectors, represent the different determining variables of the problem. The number of variables, n , determines the dimension of the lattice space. Along each base vector (axis) are ranged the different types of behavior for a given variable. The choice for a particular variable defines one coordinate of the resultant vector, which is completely specified, for an n -dimensional system,

by the choice of n coordinates. The n -tuple of coordinates gives a point in the n -dimensional lattice space. In this treatment of combustion instability, the number n has been chosen to be four. It would be possible to define other axes, but the choice $n = 4$ permits a sufficient degree of specification to give a good indication of the character of a given point in the 4-dimensional lattice space. It must be emphasized that, once again, the technique of analogy is being invoked, since the vector space is being used only as a convenient means of representation of the many combinations. For instance, there is not continuous variation along the axes, and the rules of vector algebra have no bearing here. However, discrete coordinates do not exist, as there is a great amount of overlapping, especially on some axes.

Detailed Description of Elements with Diagram

In choosing the axes for a morphology of combustion oscillations, we must consider the various components of a particular oscillation. In observing an oscillation, we measure two things - the frequency of oscillation and the amplitude. The frequency can be related, as will be seen shortly, to the mode of oscillation. The initial amplitude or growth of the oscillation define the degree of linearity of the particular problem. The amplitude is, in turn, determined by two factors - the driving force of the oscillation and the damping mechanism which limits the magnitude of the oscillation. As a result, the four axes representing a particular case of combustion oscillation are defined as follows:

- (1) The physical coupling that drives the oscillation
- (2) The damping mechanism that limits the amplitude
- (3) The degree of linearity of the theory of experiment in question
- (4) The particular oscillation mode treated in the theory or encountered in the experiment.

The components of these four axes will now be discussed in detail.

Energy Sources

To help in visualizing the problem, Figure 10 shows some of the sources of gains and losses for a solid propellant motor (55). Others can be listed, and will be mentioned in the detailed description of the four axes. It will be noticed that the burning zone has been indicated as a source or sink, depending on the particular nature of the problem. One way to specify this behavior of the burning zone (and of the other components of the acoustic field) is through the concept of acoustic admittance, which was first used for solid propellants by Hart and McClure (56). As shown in Appendix A, the sign of the real part of the acoustic admittance is the important quantity in determining whether a wave incident on a surface will be reflected with increased or decreased amplitude.

In any case, it appears, both from theoretical and experimental viewpoints, that the major energy source for the acoustic system resides in the combustion zone at the propellant surface. For ordinary propellants,

pressures, and frequencies, this zone is thin enough, compared to acoustic wavelengths, to enable the propellant to be considered as a surface defining the boundary conditions for most acoustical considerations (the boundary condition will, of course, have to involve the behavior of the burning zone as well as the cold propellant behavior). Cases may arise, which will be discussed later, where the concept of a surface boundary condition no longer holds. The boundary condition is significant, since the major gain of the acoustic system results from the coupling of some cavity fluctuation to an energy source at the surface. It has been estimated that as much as 10 percent of the combustion energy can go into gas oscillations (13). Smith and Sprenger found (6) that acoustical energy was fed by about 5% of the combustion energy from the rate of amplitude increase. This rate of increase corresponded to an energy feed which was more than 20 times the rate of conversion of combustion energy into kinetic energy of gas flow.

Physical Coupling Mechanisms

A wide variety of coupling mechanisms can be envisioned between the propellant combustion and the cavity. As will be discussed later, the dominant coupling is likely to occur between the surface flame zone and fluctuations in pressure (or some gasdynamic property directly related to pressure). This coupling, by which the propellant amplifies a small perturbation, is related to the physicochemical structure of the combustion zone (57). It can be assumed (58) that: (a) a pressure fluctuation will change the gaseous rate and the gas temperature gradient adjacent to the solid surface; (b) the changed gradient means a modified flux level and consequently a change in surface temperature and distribution of temperature in the solid; (c) this brings about a new linear pyrolysis rate at the surface; and (d) the cycle is completed when the ensuing change in gas evolution rate modifies the structure of the gaseous zone. The overall effect is that the pressure fluctuation has induced a burning rate fluctuation with a certain magnitude and having a certain phase with relation to the pressure fluctuation. This effect can be seen diagrammatically in Figure 11 (13).

Another type of coupling is based on the action of changes in the flow field. This coupling, which can be regarded as velocity-surface flame coupling, depends on the changes in convection resulting from the oscillating gas velocity parallel to the surface. In liquid propellant motors, this can be an important factor, and can be thought of in terms of a shear and gas displacement interacting with a spray of liquid droplets, leading to changes in atomization, mixing, and effective mixture ratio. In the case of solid propellants, a slightly different situation arises, owing to the sensitivity of many propellants to erosive burning. This sensitivity is caused by the varying effects of convective heat transfer as part of the energy balance in the combustion zone. In the case of many solid propellants, the role of convection is a large one, and small changes in the gas velocity parallel to the surface bring about large changes in propellant regression rate. When the velocity is oscil-

lating, it is possible to have situations arise where the regression rate fluctuations can couple to the velocity fluctuations, bringing about amplification.

It should be remarked, at this point, that both of these couplings are sensitive to the frequency at which the gasdynamic property fluctuates. Depending on the frequency, the fluctuation can couple to any number of combustion processes. If the fluctuation has a period which is long compared to a particular step in the combustion process, then the behavior of the step can be considered quasi-steady for the fluctuation frequency in question. This point will be referred to later, but should be kept in mind. In the case of the morphology, this frequency sensitivity may be regarded as defining a subspace in the four-dimensional vector field.

Other couplings between the cavity and the propellant combustion are also possible. For instance, variations in the thermal radiation from the cavity to the propellant could disturb the energy balance, leading to variations in the regression rate. Another possibility is that the fluctuations in the chamber pressure could cause stress coupling, especially for brittle propellants, where the incident pressure wave could interact with the surface structure of the burning propellant, causing microscopic (or macroscopic) cracking or "crazing". This surface failure would bring about an increase in the burning area, and would be most serious at low propellant temperature or high oscillation frequencies (high loading rates), where the viscoelastic polymer is most likely to show "glassy" behavior (59).

Thus far, in discussing couplings, it has been assumed that the combustion zone is a thin one, and may be considered as a surface in defining boundary conditions, as mentioned earlier. In many cases, however, combustion reactions occur over an extended zone. This is particularly true for highly metallized propellants at low or intermediate pressures (< 25 atmospheres) or for many propellants at low pressures (< 10 atmospheres). As a result, the chamber is filled with a mixture of partially reacted gases. When a rise in instantaneous pressure occurs, either as a result of combustion "noise" or from some other source, the resulting compression and temperature increase may bring about something like a thermal explosion in the gas phase, giving a further pressure increase and completing the combustion reaction. When the pressure drops again, a partially reacted mixture builds up once more, and the process can be repeated. In this case, we can say that the pressure has coupled with a distributed flame zone to drive combustion oscillations.

These five couplings are shown on axis I of the vector field (Figure 12). Other coupling mechanisms can be mentioned but these five will suffice in showing how the field is built up.

Damping Mechanisms

In discussing the damping mechanisms which can offset the driving forces listed above, it is helpful to return to Figure 10 in

order to observe the various means by which acoustic energy can be dissipated. Here are seen four separate components which can absorb this energy: the nozzle, the propellant, the walls, and the gas itself.

The nozzle is the primary acoustic sink for many rocket motors, especially for inviscid flow. Not only is energy transported through the nozzle by the propellant combustion gases, but, in addition, for many axial modes of oscillation, the greatest pressure fluctuation occurs at the nozzle plane. The inertia of the gas in the convergent section causes a phase difference between the velocity and pressure oscillations of the gas entering the nozzle, allowing work to be done by the acoustic field. Moreover, for a long entrance section, there will be dispersion of the reflected waves, decreasing the chance of a resonant situation occurring. All these will lead to varying amounts of reflection and transmission of acoustic energy in the nozzle. As a result, the nozzle will be given as the first damping mechanism in the morphological diagram.

Another boundary of the rocket cavity is the solid propellant itself. The propellant, being a non-rigid material, can deform under compression, absorbing energy in the process. As a result, part of the energy in an incident pressure wave will be taken up by the propellant and, aside from the effect on the burning zone, the reflected wave would have a smaller amplitude. In addition, the response of the solid to the pressure wave might take a finite time, giving rise to possible interference through an improper phase between the reflected wave and a subsequent incident wave.

The inert boundaries of the cavity are also possible absorbers of acoustic energy. The primary loss would be caused by the viscous dissipation resulting from friction between the inert parts and the gas particles moving in the gasdynamic disturbance. In addition, non-reactive boundaries, being (typically) colder than the combustion gases, could receive energy from the gases, both by radiative and by convective heat transfer. Both of these mechanisms help to explain the role of "resonance rods", which can act both by absorbing mechanical and thermal energy from the acoustic field and by breaking up the flow patterns of the field, although the latter mechanism is probably more important. As a result, the two damping mechanisms from the inert parts are viscous dissipation and heat losses.

The combustion gases themselves also can absorb acoustic energy. The primary mechanism is the absorption of energy, through relaxation processes, to the internal energy of the gaseous molecules. (Chemical reaction relaxations could also enter, but their role is less clear.) Additional energy can be lost to the gases if there are any condensed particles present in the gas. This energy transfer occurs as a result of viscous dissipation, and can be a major acoustic sink for a propellant which has a large amount of combustion products in the condensed phase.

The six acoustic energy sinks mentioned above are listed on the "damping mechanism" axis of Figure 12. In summary, they are: nozzle losses (acoustic and flow), viscoelastic losses in the propellant, viscous dissipation by inert components, heat losses to inert components, relaxation losses to the gases, and viscous dissipation by condensed particles in the gas. These energy sinks may prevent instability from occurring, even when the burning solid propellant is amplifying small disturbances.

Degree of Linearity

The interplay of the coupling mechanisms and the damping mechanisms directly affects the next axis of the vector field, which is the degree of linearity of the theory or experiment. If the driving force is only slightly greater than the sum of the damping terms, the rate of growth of the amplitude of the oscillation will probably be small. In this case, linearized perturbation theory can be used, where "linearized" implies that all deviations from the mean values are so small that only first-order terms need be taken into account. These theories, where only linear processes are considered, can be referred to as acoustic theories. It should be remarked that this type of theory will only predict whether an infinitesimal disturbance will be attenuated or magnified, and does not deal with the maximum amplitude to which a disturbance will grow.

For large disturbances, terms of higher order than the first need to be considered. These are the concern of non-linear theories, which deal with the large amplitude oscillations not treated by acoustic theory. Care must be taken in the consideration of finite amplitudes, since often a "linear" theory will hold to large amplitudes, but many cases are known where a motor is stable to small perturbations but unstable for large perturbations (27).

Frequently, the pressure variation of a large amplitude disturbance is so great that the disturbance loses its sinusoidal appearance and steepens into a shock wave, although mean flow effects will also bring about the wave form change. The treatment of this type of disturbance may be quite different from that for sinusoidal disturbances, since the rates of pressure change can be much higher, and the velocity of propagation will vary with the strength of the shock more than is the case for an ordinary acoustic disturbance, but the same linearity distinction may still be made.

The linearity axis, then, contains two points: linear disturbances with small amplitude waves and non-linear disturbances with large amplitude waves. The points on this axis of the vector space are not discrete, in contrast to those on the other three, and a great deal of confusion can arise from the different properties of overlapping points. Moreover, the accuracy of the results of a theoretical treatment will depend on the degree of linearity assumed.

Gasdynamic Behavior

The fourth axis to be considered is linked with the gasdynamic behavior of the disturbance in the cavity. A knowledge of the acoustics of a cylindrical cavity is required for an understanding of the flow patterns involved in the oscillations, and a discussion of the Rayleigh modes for a cylindrical cavity closed at both ends with rigid walls is given in Appendix B.

It should be remarked parenthetically at the outset that the term "reverberant" is used for the Rayleigh modes of a cavity rather than "acoustic" because the term "acoustic" is most often used in the sense mentioned under the discussion of linearity, i.e., to refer to small amplitude disturbances where linear theories and processes are sufficient to describe the wave behavior.

The particular reverberant mode which is likely to occur is a function of the motor geometry. Transverse modes are favored over axial modes in general, owing to the large acoustic losses which exist at the nozzle end for an axial mode. Counterbalancing this are at least two factors. These are the effect of wave length and wave velocity on the aerodynamic sound produced by the subsonic flow at the nozzle end of the grain (44, 60) and viscous attenuation acting on the high-frequency transverse modes. It is found that, as a result, the small, short rockets of the 1950's characteristically oscillated in transverse modes while the larger rockets of today, often with higher loading density, oscillate in axial modes (61). The tangential modes are usually the only transverse modes which are definitely encountered.

The effect of the reverberant mode is related to the pressure-velocity distribution characteristic of the mode. As a result, the reverberant modes can be broken into three general classes: axial modes, standing transverse modes, and spinning tangential modes. As mentioned earlier, the damping effect of the nozzle is greatest for the axial modes. In addition, the greatest changes in pressure and velocity occur near the surface for transverse modes, so that velocity and heat transfer effects are greatest for transverse modes. These effects are intensified for the case in which the nodal and antinodal points of the mode rotate in the cavity, as occurs for the spinning tangential mode. This effect has already been mentioned in the work of Smith and Sprenger (62). As a result of these considerations, it can be seen that the effect of the reverberant mode on the burning is greatest for the spinning tangential mode and least for the axial mode.

The spatial distribution of the disturbances is different for another type of oscillation mode, whose occurrence depends on the relation between combustion process times and the characteristic gasdynamic times for the rocket chamber. If some process time is comparable to the oscillatory period for a natural frequency of the cavity, then a resonant system is possible and one of the reverberant modes

mentioned above can be amplified. If, however, the process time is long compared to any oscillatory period for the chamber, no reverberant wave motion can couple itself to the combustion process so as to be reinforced.

For cases involving long combustion process times, the chamber as a whole might oscillate as a capacitive system, with a characteristic gasdynamic reaction time depending on the volume and the throat area, as opposed to the wave-type motion of reverberant modes. In this case, the term "non-acoustic instability" is often used, since the overall pressure variations have frequencies (determined by motor residence times = L^*/C^*) which are lower than those of the lowest acoustic mode of the grain cavity, although "capacitive instability" is a more descriptive term. This type instability is analogous to the phenomenon known as "chugging" in liquid propellant rockets (63).

The importance of capacitive instability is that, while the combustion process time involved may be, under certain particular conditions (e.g., low pressure, special composition), long compared to the reverberant oscillation periods for today's motors, the large rockets proposed for the future will have longer periods, so that even these processes can couple to a wave motion, with further disastrous amplification.

In summary, then, the base vector for the four-dimensional space which is concerned with the gasdynamics of the oscillation mode has four points: axial modes, standing transverse modes, spinning tangential modes, and capacitive modes.

This completes the treatment of the lattice space. There are 240 possible points present, which shows how formidable an understanding of instability is. The remarks of McClure (64) on the subject of combustion instability are quite apt:

"This collection of characteristics provides a varied and exotic means for a theorist who would enjoy these delicacies, but to devour this feast at one sitting would almost surely result in a case of extreme indigestion rather than an appreciation of the finer flavors of such a varied fare. As a consequence it seems wise, in fact necessary, to separate the main courses wherever possible, and to attack them one at a time."

A well-defined theory, then, will specify the points of the vector space to which it is applicable. The experimentalist, on the other hand, cannot deal with pure points, but with a mixture. The particular points of the morphology which are applicable should be remembered in both the design of the experiment and the interpretation of the results. The idea of accurate classification is important whenever sets of theories and/or experiments are compared and discussed.

CHAPTER III

THEORIES OF ELEMENTAL PROCESSES IN COMBUSTION INSTABILITY - A LITERATURE SURVEY

I. Background - "Singing Flames"

Combustion instability in solid propellant rockets is only one case of periodic disturbances connected with heat release. The original observation of this connection was the "singing flame", first observed by Higgins (65) in 1777. Since that time, a variety of periodic phenomena have been recorded. These can occur in a solid or a volume of gas, and result from the expansion of a heated body, which does mechanical work in compressing or displacing some other part of the body. Wood reports on a large variety of cases where the proper phase relation occurs, so that periodic vibrations are set up (66). Recent surveys of the field have been made by Putnam and Dennis (67) and by Roginskii (68). Oscillatory combustion has been observed in diffusion flames fed by long pipes (singing flame) (65), in flash tubes (69), in tunnel type burners (refractory tubes) (70), and in turbojets and ramjets (71), as well as in liquid and gaseous rockets (72) (73). There has been a section of a Combustion Symposium dedicated to oscillatory combustion phenomena.

Singing flames are discussed, together with striking photographs, by Gaydon and Wolfhard (74). There are two explanations for singing flames, one by Jones (75), the other by Rayleigh (76). The latter explanation, known as the "Rayleigh Criterion", is generally taken as the physical basis for oscillatory combustion. According to Rayleigh, "If heat be periodically communicated to, and abstracted from, a mass of air vibrating (for example) in a cylinder bounded by a piston, the effect produced will depend upon the phase of the vibration at which the transfer of heat takes place. If heat be given to the air at the moment of greatest condensation, or be taken from it at the moment of greatest rarefaction, the vibration is encouraged. On the other hand, if heat be given at the moment of greatest rarefaction, or abstracted at the moment of greatest condensation, the vibration is discouraged." In the case of the singing flame, the oscillations are coupled between the gas supply tube (inner tube) and the burning zone. Any vibration in the burning zone is transmitted to the supply tube, so that the gas in the supply tube will undergo pressure oscillations in the gas supply. Coupling occurs and the initial oscillation grows if the maxima in the supply fluctuations occur in phase with the pressure maxima in the burning zone, since (assuming no combustion time lag) the combustion of the extra gas will further raise the pressure in the burning zone. As a result, the occurrence or non-occurrence or sustained oscillation depends on the relative lengths of the burner and supply tubes, and on the speed of sound in the fuel gases.

The same type of explanation can be given for "gauze tones" which occur without a flame, but with only cooling off of a wire mesh.

First observed by Rijke (77), the tones are produced by a vertical pipe with wire mesh at the bottom. When the mesh is heated and then allowed to cool, a high intensity tone is emitted by the wire. Rayleigh connects the generation of sound with the varying heat transfer from the mesh to the air (78). As he notes, the influence of ordinary pressure and density variations is unfavorable, since the air receives less heat from the wire when the air temperature is raised by compression. However, the heat transfer is affected by the varying motion of the air superimposed on the mean flow. When the mesh is at the bottom, conditions are right for amplification, since the velocity fluctuations lead the temperature fluctuation by 90° . When the mesh is in the top part of tube, however, fresh air arrives at the moment of greatest rarefaction, which has an unfavorable effect. Experiments have shown that the gauze tones exist only where the mesh is at the bottom, which supports Rayleigh's hypothesis.

Explanations for solid propellant combustion instability are not quite so simple, although Diederichsen has commented (79) on the similarity between oscillations in a gauze burner and in the regions of nodes in a solid propellant rocket motor.

The discussion of the morphology of combustion oscillations (Chapter II) introduced a number of mechanisms for amplifying or attenuating disturbances. These mechanisms will now be studied in greater detail.

II. Argument for Pressure Coupling

The previous section has shown that, in the case of solid propellant combustion, there are a number of physical mechanisms for driving oscillations. However, the existence of a pressure-coupled mechanism as one possible type of coupling is pointed out by Price (49), who performed a series of tests using propellant charges made up partly of dummy propellant and partly of real propellant. The amount and location, relative to the longitudinal acoustic modes, of the "live" propellant were varied in an attempt to find where the propellant was most efficient in driving oscillations. It was found that "combustion near the pressure antinodes supports instability more effectively than combustion elsewhere in the acoustic mode, and the results of the whole study indicate that this is true for a variety of propellants (all propellants tested)."

III. Theories on the Coupling of Pressure with a Surface Flame

The experiment just described is only a part of the mass of persuasive evidence that one of the most common forms of instability is one that is generated by the coupling of the combustion processes at the surface with pressure fluctuations. The majority of theoretical treatments of combustion oscillations have been focused on this class of physical coupling, and have used linear perturbation theory to predict whether a small pressure disturbance will increase with time or will be damped out by the losses in the acoustic field. Details of these theories will be given in a later chapter, but, as part of the description of the elemental processes in combustion instability, some salient points of the treatments

will be listed, together with some predictions of the individual theories.

The first theoretical treatment of solid propellant combustion instability was advanced by Grad (80), who based the amplification of an incident pressure disturbance on the reaction of the burning rate to the pressure change, with unstable frequency regions being predicted by a fixed time lag, which represented the time required by the reactions at the burning surface to reach equilibrium. His theory found that the most unstable mode was a spiral one, which, some consideration shows, is a spinning tangential mode moving downstream with the main gas flow. The secondary peaks of unstable burning were assumed to be caused by the reaction of the burning rate to this spiral mode, and his theory indicated that the most unstable propellants were those with a large value of "n" in the Vieille's equation for steady-state burning rate, $r = c_1^n$ (62).

The concept of a time lag was also used by Cheng (81), but an extra degree of sophistication was injected by the assumption that the time lag was a function of pressure. Cheng's theoretical treatment, like Grad's, predicted that the fundamental spiral mode would be most unstable, but the frequency-dependent time lag treatment led to the prediction that a large value of n would give a more stable propellant. In addition, Cheng's theory dealt specifically with tendencies toward instability. For instance, it was predicted that increasing the effective length of the nozzle would improve stability, a internal-burning grain was the most unstable, and that the grain became more unstable during the run as the effective L/D of the motor cavity decreased. It was found that the pressure-sensitive time lag had to lie in certain ranges for the tendency toward instability to occur, a prediction criticized by Price (82), who pointed out that instability has been observed over a broad frequency spectrum.

Misunderstanding of the details of Cheng's theory led to some controversy in the published literature. Green (42) (44) (83) commented that it was unnecessary to have a pressure-dependent burning rate for instability. In addition, he disagreed with Cheng's ranking of the stability of grain geometry and of the L/D effect, and felt that viscous effects should have been taken into account, especially at the end of the grain. Cheng (84) replied that it was only necessary that the vapor phase reactions vary with pressure for instability to occur. Moreover, he stated that, since his theory was intended only to predict tendencies toward instability, severity of instability could not be predicted, and that viscous effects could be neglected, since they were only important at large amplitudes. Equally important, in Cheng's mind, was the idea that, in the experimental investigation of trends, only one factor should be varied at a time. (The very occurrence of such a controversy, largely based on misunderstanding, points up the significance of consideration of a morphology.)

A more refined treatment of pressure-surface flame coupling was given by Hart and McClure (85). Instead of assuming some type of a priori time lag, their model allowed the reaction to give a phase lag which, if it were of the right order of magnitude, would lead to amplification of a pressure disturbance. Like Cheng's, their original theory dealt with the tendency

toward instability, but, unlike Cheng, they found that the unstable region of frequency covered a broad band, rather than being sharply peaked. (Cheng showed that a modified time-lag model could give the same result, as will be described when these theories are discussed in greater detail in the following chapter). The later work of Hart and McClure extended the linear perturbation theory to finite amplitude disturbances, and also considered the participation of the propellant as a viscoelastic medium in the oscillations. Perhaps the most important contribution of Hart and McClure was, however, the representation, in terms of a response function, of the propellant's tendency to amplify or attenuate a disturbance. This concept more clearly brought in the idea of gains and losses of acoustic energy, and gave an idea of a means of estimating the contribution of some part of the rocket motor to the acoustic field.

An extension of the Hart-McClure theory was advanced by Williams (86), who took into account the effect of a distributed gaseous reaction zone, rather than the collapsed zone previously assumed. As a result, the diffusion of reactants, neglected by Hart and McClure, was taken into account. However, this extra step introduced great complexity to the problem, so that only very special cases were tractable.

A group of theories is based on the response of the solid phase to a pressure perturbation. (The applicable frequency range will be discussed in Chapter IV). The physical processes involved, based on thermal flame theory and an Arrhenius type pyrolysis law, are as follows. When the pressure increases, the combustion zone moves nearer the surface quickly, then moves slowly as the surface temperature responds to the new pressure. However, the initial mass flux from the surface does not correspond to that for the new pressure because the surface temperature has not yet reached the corresponding value. As the combustion zone-surface relation is relatively fixed, the mass balance must be maintained through the zone, so that the gas temperature drops until the surface temperature reaches the new steady-state value corresponding to the new pressure. To accomplish the temperature drop, heat is transferred from the gas to the solid, leading to a revision of the heat balance in the solid phase. Unstable burning could then occur if the solid phase temperature distribution does not match the heat transfer and surface temperature conditions.

The first formulation of this method of attack on the theory of the coupling of pressure with the surface flame zone was by Akiba and Tanno (87), who dealt with the equilibration of the thermal profile in the solid phase as a means of amplification. Using the non-steady heat conduction equation in the solid, together with quasi-steady state arguments for burning rate, they found that, for $L^* \left(= \frac{\text{chamber volume}}{\text{throat area}} \right)$ less than some value varying with pressure to the (-2 n) power, instability would occur.

The same model was used by Sehgal and Strand (88), who introduced more variables and a greater degree of mathematical sophistication to the treatment of the problem. As a result, they were able to predict stability regions for individual propellants. The same pressure versus L^* relation

was found as in the Akiba-Tanno model.

Price (89) also considered the role of the solid state in amplifying a pressure perturbation. His theory considered the balance between the thermal gradient for steady-state conditions and for perturbed conditions, and found that, for a rate of pressure change greater than some critical amount, the propellant would, in turn, gasify at a higher rate, giving amplification.

Another theory dealing with heat conduction in the solid phase was advanced by Smith (90), who assumed a burning rate oscillation and solved the conduction equation in the solid to find what heat transfer would cause the assumed oscillation. The results of the solution are that while, at low frequencies, the burning rate is in phase with pressure, at high frequencies (the exact magnitude depending on propellant parameters), the burning rate could lead the oscillations in pressure by as much as $\pi/4$. The lead effect was assumed to come from the fact that the burning rate would overshoot in response to a step function in pressure because, for a short time, the propellant initial temperature is higher at some fixed point near the surface. At high frequencies, this overshoot could lead to a magnification of burning rate fluctuations, so that amplification was more likely to occur at the higher frequencies.

Dennison and Baum (91) dealt with the solid-phase response as well, but their analysis was far more comprehensive. They perturb laminar flame conditions for the steady state and use transient heat conduction in the solid to study the effect of frequency. They assume a Lewis Number of 1, a single-step combustion reaction, no solid-phase reaction, an Arrhenius law decomposition, no erosive burning, and a homogeneous propellant. No assumption is made as to the pressure dependence of burning rate. It was found that, for a wide range of conditions, the surface mass-flux perturbation could attain a large amplitude, increasing either monotonically or sinusoidally.

IV. The Coupling of Velocity with a Surface Flame

The second element of the morphology to be discussed concerns the driving of oscillations by the coupling of the surface flame to fluctuations in flow velocity parallel to the surface. Cheng (81) stated that velocity effects were unimportant at small amplitudes, so neglected them in his treatment, which only predicts tendencies. He did, however, emphasize that, for large amplitudes, the velocity mechanism was important in supplying the necessary driving energy (92). Smith and Sprenger (93) felt that the travelling tangential mode was important in generating peaks, because of the substantial increase in the rate of heat transfer resulting from the velocity change near the surface.

The first extensive analysis of velocity coupling was made by Green (94), and later modified by Nachbar and Green (95). These treatments are based on the effect of small amplitude oscillations in parallel flow conditions, and treat "resonance" points, where unstable burning will occur,

rather than oscillatory burning. Three parts of the reaction are considered in the model shown in Fig. 13: heat conduction in the solid phase, a phase change governed by a quasi-steady Arrhenius law, and an oscillating convective heat transfer from the hot gases flowing over the propellant surface. The instantaneous burning rate was assumed to depend on surface temperature, which fluctuated owing to the heat transfer oscillations, but with a time lag τ assumed.

This time delay, τ , was the time "required for transition of the propellant matter from an ordered solid state at a temperature ($T - \theta$), where θ is a small temperature difference, through a semi-ordered 'surface' region at mean temperature T to a disordered gaseous state at temperature ($T + \theta$)." This delay is based on the fact that the burning "surface" is actually a zone of finite thickness for many propellants, where it might exist as a liquid containing gas bubbles (96). In addition, τ may include, for composite propellants, the time required for diffusion and mixing of the fuel and oxidizer components.

The model is first solved for steady-state, then the solutions are perturbed to find the response for oscillations in the gas flow. The major aim of the model is the determination of the behavior of the average burning rate as a function of frequency. It was found that, for certain combinations of frequency and time lag, a resonance condition existed where the surface temperature would fluctuate as much as 300 K, leading to a large increase in burning rate (Fig. 14).

The analysis led to the prediction that stability was increased by a minimum time lag, low burning rate sensitivity to changes in pressure and temperature, high surface temperature, and increases in propellant thermal conductivity, density, and heat capacity. The possibility of instability was increased by decreasing E , the activation energy of the surface reaction, by increasing flame temperature, by increasing the heat of phase change ΔH_s , by increasing or decreasing the initial temperature away from ambient, and by increasing the steady-state pressure. It was also predicted that instability was more likely to occur at velocity nodes for oscillating flow or at the stagnation point for steady flow.

Although the Green model was, admittedly, an idealized one based on linear behavior, it has resulted in some controversy. Cheng (97) objects to the notion of inherent instability, pointing out that this notion implies only a weak coupling between combustion and the gas field, which violates the principal manifestation of combustion instability, i.e., severe oscillations in the gas. Price (98) points to the idea of the thermal boundary layer's being so little affected by combustion, in addition to objecting to the representation of the gas phase heat process in terms of a gas-dynamic boundary layer. He also objects to "resonance frequencies," as noted before (82).

Applications of the theory to some instability tests and effects have led to arguments in the literature between Price and Nachbar and Green (99), (100), (101), (11). These were largely concerned with the

tests mentioned earlier on burning rate changes in combustion instability, but a major contention was the lack of evidence for any dramatic change in burning rate with changes in composition or frequency over a wide range. Green and Nachbar attribute this result to the fact that Price's results are in a design where acoustic damping has been markedly reduced from typical motor design. The failure of the theory to explain the burning rate results was blamed on the linearization of the equations and their resulting non-applicability to non-linear situations. However, Nachbar and Green did admit (101) that they had overstepped the limits of their theory in attempting to place the location of the maximum burning rate change with respect to the velocity oscillations in the acoustic wave.

Cheng (97) also objects to the linear nature of the theory from the standpoint that it does not serve to determine stability boundaries, but only to indicate possible instability at "resonance." He further indicates how the formulation of the theory could have been altered to give the amplification for an initial condition, rather than the amplitude of the limiting standing oscillation.

It should be re-emphasized at this point that much of the difficulty in interpretation and usage of the theory was caused by, once again, a failure to visualize the particular lattice point occupied by the Green-Nachbar treatment. Cheng raised a very valid objection when he pointed out that a linear theory had been used to predict non-linear results.

Barrere used an extension of the Green-Nachbar theory, once again assuming that the driving force was the fluctuating heat transfer related to the fluctuating gas velocity (102), but he generalized the theory for different distributions of the time lag. In his treatment, Barrere uses a standoff distance from the surface to the combustion zone ϵ . This oscillates with the behavior

$$\epsilon = \bar{\epsilon} + \Delta \epsilon e^{i\omega t} \quad (1)$$

where ϵ varies in phase with the temperature, not with the burning rate. There is, once again, a time lag which represents the time required to convert the solid into gas. This time lag is different from Green's, however, because, as Barrere notes, the appearance of the surface of composite grains has been shown to be quite jagged (103), (104). As a result, the combustion zones are unequal, so that the time lag can no longer be assumed unique and constant. Barrere's analysis then shows that distributed combustion times increase stability, so that composite propellants are more likely to be stable than homogeneous ones, and composites with broad oxidizer particle cuts should be more stable than composites with unimodal grinds. The effect of aluminum as a stabilizing additive could be explained by the different times required to gasify the propellant matrix and the

aluminum. Barrere continues this idea in a later article (105) where the different zones of combustion found by Bastress (103) are used to explain qualitatively some generalizations of experimental observations. The same argument is used by Vandenkerckhove (106) to explain Landsbaum's results (107), i.e., the relative severity of oscillations increased with pressure to some point, after which a sharp dropoff was noted (Figure 15). This behavior was linked to the appearance of the surface as follows. At low pressures the oxidizer crystals protrude, but as the pressure increases, the surface becomes smoother, allowing more erosive response to gas oscillations. At some point, however, fuel peaks will appear, preventing the velocity oscillations from reaching the oxidizer crystals. The smoothness of double base propellant surfaces and the protrusion of fuel peaks in ammonium nitrate propellants would explain the behavior of these types.

Shinnar and Dishon (108) also studied the effect of velocity fluctuations on the heat transfer and, hence, on the burning rate. One important difference exists between their treatment and the other theories of velocity coupling, namely, the lack of an a priori time lag. Instead, they included an equation for the diffusion of heat through a gas film of thickness δ . The gas temperature was assumed constant on one side of this thermal boundary layer, so that heat transfer depended on the value of δ . Surface decomposition obeyed an Arrhenius law with surface heat of phase change L , and heat transfer in the solid was considered.

The possible existence of unstable conditions was investigated by a stability analysis for small perturbations, so that stability boundaries were obtained in terms of the physical properties of the propellant. No numerical results are shown, but qualitative discussion of the results showed that stability was increased by a highly endothermic phase change and decreased by an exothermic one. The thermal boundary layer thickness had to fall in some range for instability to exist, and the action of turbulators in suppressing instability was ascribed to their diminution of the gas film thickness, thereby improving heat transfer. It was postulated that decreasing δ below some minimum value might lead to complete stability. The effect of δ , in general, seems to be much the same as Green's time lag. They do admit that the validity of drawing conclusions from small perturbations and extending them to large disturbances is questionable, but state that when damping for small perturbations is found, the propellant is "obviously stable." This statement appears to be somewhat in error, as will be discussed shortly.

Hart, McClure, and their co-workers used a different approach to the effect of velocity fluctuations, extending the notion of a response function, originally used for pressure-coupled oscillations only, to the case where flow effects became important. It was found (64) that erosive burning can play a large role in determining stability, and that the type of erosion—steady or acoustic—determines the relative importance of erosive burning. Acoustic erosivity can, in some cases, cause a motor which is stable at low amplitudes to be unstable at moderate amplitudes (109), contrary to the statement of Shinnar and Dishon. Acoustic erosion can also limit the amplitude of oscillation (110), and change the waveform of the

oscillation.

Experiments on the effect of velocity coupling have been based on the production of a finite pressure and flow disturbance by a source external from the motor. Typically, these experiments are made for a motor where the damping terms are ordinarily sufficient to override the driving sources, so that the motor would operate stably. As a result, these experiments deal with non-linear velocity-coupled instability, a point which must be kept in mind when drawing inferences from their results. Once again, the aim of the morphology concept is to prevent such possible misunderstandings.

The pressure disturbance, together with its accompanying flow, was first produced artificially by Dickinson at CARDE (111). A full description of the technique and of the pulsing unit is given in a report by Morris (112). The technique involved the use of four black powder charges at the head end of an internal-burning tubular grain, which were fired sequentially as the pressure rose during the run owing to the grain geometry (Figure 16). The charges produced a compression wave with a pressure ratio, at reflection, of approximately 1.4. If the motor was stable in the operating region to a disturbance of the magnitude chosen, the pressure would return to the steady-state design value. If the motor was operating in an unstable regime, the amplitude of the disturbance would grow to some limiting value (Figure 17).

Extensive studies have been conducted with this technique at CARDE, typically by Brownlee, whose results have been summarized recently in a pair of reports (113), (114). He found that, during unstable operation, pressure, thrust, and burning rate always increased. Instability occurred for a given motor and propellant only above a certain critical pressure, which decreased as the initial grain temperature was lowered. In general, propellants with high burning rates were stable to higher pressure than those with low burning rates. The influence of aluminum corresponded to this burning rate criterion, as that amount and particle size which gave the highest burning rate gave the highest stability to non-linear initiation. Burning rate modifiers also followed the same trend as lithium fluoride, a depressant, increased propellant sensitivity markedly, while copper chromite, an accelerator, increased the stability of the propellant. Finally, it was found that results from scaling were somewhat irregular, so that small motors went unstable for different operating conditions than large motors. In comparing his work with Horton's work with linear, pressure-coupled response functions (115), (116), Brownlee found that his results with lithium fluoride, copper chromite, and aluminum and their stability effects agreed with Horton. However, the effects of aluminum particle size (115) and pressure (117) were different. Brownlee conducted a concurrent program on erosive burning (118) and the results of that program, plus the experience of others, led him to hypothesize that the stability of a propellant to non-linear initiation was inversely proportional to its tendency toward erosive burning, showing the potential importance of velocity coupling.

Brownlee reported that, in some cases, tangential instability

occurred when the axial mode was fully excited (119). At the onset of the tangential mode, the axial mode ceased, and the burning rate increased 50 to 70%, possibly due to the greater velocity effect.

Dickinson continued work with non-linear pulsed initiation at Stanford Research Institute (120). Using a different binder (PBAA as opposed to the polyurethane used by Brownlee), it was found that instability, like erosion, was increased by reducing the burning rate. In fact, it was found that propellants with burning rates above 0.6 inches per second would not go unstable, even at pressures as high as 2500 psi. Among these high burning rate propellants were some with potassium perchlorate as oxidizer. Interesting results were obtained when coarse (600 μ) ammonium perchlorate was added to the oxidizer and when 30 μ aluminum was used, rather than 6 μ (121). In both cases, the pressure level at which instability would begin dropped. This effect was related to the structure of the flame zone and its relative sensitivity to increased mixing or convective heat transfer owing to the passage of the velocity disturbance.

The pulse technique has been used by Sotter (47) to study stability in transverse modes, rather than the axial modes encountered by the above investigators. Tangential nitrogen jets induce a vortex which triggers the travelling tangential mode, and, in many cases, the motor continues to operate unstably after the jet is cut off. This phenomenon is explained by acoustic erosivity effects, since mean flow will not exist in a transverse manner except when excited by a transverse pulse or when vortex flow exists, and this mean flow is necessary for erosion effects.

V. The Coupling of Pressure with a Distributed Flame Zone

The discussion of the morphological element concerning the coupling of variations in pressure with a flame zone distributed through the cavity is a complex one, owing to the large number of variables involved. The fundamental difficulty is that a new dimension has been introduced, since the combustion reactions may not go to completion in the ordinary sense. Two separate experimental phenomena are observed - one where the pressure fluctuates, as in ordinary combustion instability (122), (Fig. 18) the other where intermediate high-pressure combustion of propellant is interrupted by long periods where combustion (if any) takes place at pressures near atmospheric (123) (Fig. 19). The latter phenomenon is known as "chuffing," while the former is often similar to the "chugging" of liquid propellant engines. Whether the two are related is a matter of some contention, but it has been observed that they are often both observed on the same firing (124).

Huffington conducted the first series of motor experiments on chuffing (125), and formulated a thermal explosion theory, based on his earlier experiments with cordite (126), which agreed with estimates based on the Frank-Kamenetzsky theory (127). The theory, which was later expanded by Glennow and Huffington (128), is based on the postulate that burning during these non-steady periods is thermal explosive in nature, governed by a condensed phase exothermic reaction. Huggett (129), on the

other hand, postulated that chuffing in double-base propellant was caused by spontaneous ignition of a combustible gas mixture formed from the exothermic decomposition of layers of propellant in the solid phase. Yount and Angelus (122) mention these two possibilities, but suggest that, in some cases, reactive species are either swept from the motor or at least far enough from the grain surface to cut off the ordinary energy feedback to the solid required for combustion.

The same type of mechanism is invoked by Price (89) to explain instability in cases where incomplete reaction of the propellant can occur. He postulates that the chamber fills with an explosive mixture, which might react by a thermal explosion mechanism, similar to that invoked by Hufington to explain chuffing.

The distributed flame zone is also important in the case of metallized propellants. Angelus has hypothesized that the occurrence of capacitive instability in double-base propellants containing aluminum or magnesium at pressures below 500 psi is related to the burning behavior of the metal in the propellant gas. The metals will have an ignition lag because metal ignition temperatures are higher (130) than experimentally determined surface temperatures (131). In Angelus' later work (52), he extended this belief to the hypothesis that unburned metal collects on the surface and burns during the rising portion of the pressure-time curve, increasing the swing in pressure. Some experimental evidence to support this hypothesis has been given by Shanfield (132).

Some confusion exists concerning the frequency of oscillation in this particular type of instability. Angelus gives data which show frequency increasing with pressure for a number of different metallized propellants (124), but no mention is made of the dependence on L^* . He does, however, state that the frequencies were not comparable to Helmholtz modes, and that one round oscillated at a constant frequency, while burning for 18 seconds at constant steady-state pressure, even though the free volume was changing. Moreover, the Mg/Al ratio changes the frequency significantly. In later ABL work, Yount and Angelus (122) reported the same linear increase of frequency with pressure, and stated that frequency increased with increasing conditioning chamber temperature. However, they also stated that charge size changes did not influence the frequency, and the plotted increase of frequency with pressure is so slight that it might easily be caused by more efficient combustion or higher gas temperature. Eisel (133) extended the original work of Angelus (124) to lower pressure, and found that the frequency of oscillation increased from 6 to 36 cps as the pressure increase from 0 to 80 psig. In this motor, there was no L^* effect, since the pressure rise was controlled only by a bleed.

These data indicate that there may be some cases where the oscillation frequency is of a capacitive nature and is related to the gas-dynamic filling time of the cavity, but that the frequency may be determined by some other mechanism for many cases.

Further light on the subject was shed by Price (134), who reported on tests with a large number of propellants. It was found that the

perchlorate particle size, the aluminum concentration, and the binder could all affect the dependence (if any) of frequency on pressure. It is obvious, then, that several different mechanisms may be operating in the low pressure range, where the flame zone is distributed over an appreciable portion of the chamber volume. A partial explanation for the pressure-independent case may be that the combustion process may tend to oscillate at some characteristic frequency. For instance, Eisel et al. (133) found that the frequency data were correlated well by assuming that combustion produced a pulse with every surface recession of 90μ . Such a characteristic oscillation might become serious if there were a natural cavity mode to which it might couple.

These data indicate that, for some cases, a different type of coupling is probably important. It is, however, difficult to assign these experimental results to a definite lattice point in the morphology, which is often a difficulty when dealing with experimental data.

By far the most elegant theoretical treatment of the interaction of pressure with a distributed flame zone was advanced by Cheng (135), who considered metal-containing propellants which had appreciable metal combustion in the chamber volume. This combustion was represented as generating a large number of distributed heat sources, and the effect of these sources on the sound field was studied. Two separate cases were studied - one where the strength of the heat sources was assumed independent of pressure oscillations, the other where the heat source oscillated, but only one dimension was used. In the case of insensitive heat sources, the effect depended on the distortion of the acoustic wave by the non-uniform temperature field and the resulting change in nozzle damping. It was found that, when the burning surface acted as the external boundary of the chamber volume, the effect was stabilizing.

The effect of the pressure-sensitive heat sources is more complex. For example, the fundamental longitudinal mode (and odd harmonics) would be damped, but the second harmonic (and even harmonics) would be amplified, so that a motor might be driven unstable. Moreover, the heat sources might drive a chugging type of instability, which is an interesting result, since the theory antedated publication of Angelus' original work on instability in metallized propellants burning at low pressure. In summary, the theory predicted that the direct effect of an element of the reactive additive on driving or suppressing instability was simply related to the position where the element burned with respect to the standing acoustic wave in the chamber. The effect was most pronounced for an element burning in the region of the pressure antinode.

VI. Damping Effects

Thus far in the discussion of the elements of the morphology, emphasis has been placed on the axis of the lattice space which is concerned with the mechanisms by which combustion oscillations can be driven. We will now turn our attention to the axis dealing with damping effects, which can either limit the amplitude or, if they outweigh the driving terms, completely

suppress oscillations.

A. Nozzle

Some of the early experimenters noticed that the nozzle configuration could have a large effect on the occurrence and severity of combustion instability. Some specific examples were reported at the Fourth Combustion Symposium. As mentioned earlier, Smith and Sprenger (6) found that, by appropriate choice of end seal, the same motor could be made to burn over a range from smooth, oscillation-free operation to extremely rough operation. Ellis et al. (136), using optical techniques to study instability in a liquid propellant engine, observed that changes in the convergent angle of the nozzle changed the intensity and distribution of a disturbance reflected from the nozzle.

Grad, in his treatment of combustion instability (80), used a simplified model for the nozzle boundary condition. He followed Morse's treatment (137) of a tube with a hole at one end, and arrived at qualitative results only. The justification for this treatment was that the nozzle boundary condition was not thought to be important in determining stability.

The first theoretical study of the nozzle was made by Tsien (138), who calculated the "transfer function," which is the ratio of the fractional increase in mass flow through the nozzle to the fractional increase in pressure, as a function of frequency. The nozzle entrance conditions were assumed isothermal, and a linear velocity distribution in the nozzle was assumed (63), only if there were no velocity oscillations at the entrance, so that the assumption of unity was approached only at very low frequencies. As the frequency increased, the lead component of the transfer function increased, and at high frequency, the mass flow rate fluctuated a good deal more than the pressure.

Crocco (139), (140) extended Tsien's treatment to non-isothermal entrance conditions and replaced the transfer function with the acoustic admittance. Like Tsien, he assumed the nozzle was shaped such that the velocity increased linearly with distance in the subsonic portion, and also treated axial modes only. The results, even at low frequencies, differed significantly from Tsien's. By assuming isentropic entrance conditions, he was able to extend the calculations to cover all frequencies. The following are some of the results: (1) For a given entrance Mach number, the real part of the admittance increases with frequency, while the phase goes from 0 to a large portion of 90° back to 0° . (2) When the length of the subsonic portion is increased, the admittance value effectively shifts to that for a higher frequency. (3) For a given geometry, the stabilizing effect of the nozzle is greater for oscillations of higher frequency. (4) As a result of (2) and (3), for a given entrance Mach number and frequency, the stabilizing effect is greater for a longer subsonic entrance section. Crocco also commented that the use of a "short" nozzle boundary condition, i.e., constant Mach number at the combustion chamber exit, underestimated the damping ability of the nozzle, but was a useful first approximation.

Cheng, in his treatment of solid-propellant instability (81), used the Crocco treatment in determining stability. In later work (141), however, he investigated the effect of the quasi-steady assumption on stability, and found that, at low frequencies, stability was increased by the unsteady flow, owing to the volumetric effect of the nozzle, which effectively increased the capacity of the chamber to store combustion gases. At high frequencies, stability was also increased, but the mechanism was dissipation of the energy of the disturbance by the unsteady flow. The relative effects of changes in Mach number and nozzle length were the same as before.

Crocco later extended the treatment for the axial modes from the linear velocity variation previously assumed to a general velocity variation (142), and found the same trends to hold. The magnitudes of the admittances and the predicted effects of configuration changes were later verified experimentally (143) (144).

The first extension of the treatment of nozzle admittance to a three-dimensional case was reported by Scala (145), who noted that, for transverse modes, the contribution of the nozzle was typically small. The full derivation of the admittance for transverse modes was given later by Crocco (146), once again assuming a nozzle shape which gave a linear velocity profile. The calculations for these modes were presented by Reardon (147) for both the linear velocity profile and the velocity profile which results from a conical nozzle. The results show that, for all but the smallest entrance velocities, the nozzle has a destabilizing effect for transverse modes. Increasing the nozzle entrance velocity by decreasing the contraction ratio further increases the destabilizing effect. For a conical converging nozzle, at low entrance velocities, similar trends are found, but higher magnitudes. As the entrance velocity increases, the values resulting from the two velocity profiles become comparable. The trends from these predictions were verified experimentally using liquid propellant rocket firings (148). A further extension was made later for the case where tangential velocity oscillations existed, as in the swirling modes (149). A further destabilizing influence was found.

Another treatment of the boundary condition of the nozzle was given by Culick (150). His treatment was for the three-dimensional, axisymmetric case, and was based on the use of a non-orthogonal coordinate system defined in such a way that one coordinate surface coincided with the nozzle. Rather than using the velocity fluctuations, as done by Crocco, Culick used the perturbation velocity potential. Culick states (151) that the most important approximations seemed to be the linearity of the velocity gradient and the use of a slender nozzle. He also found that the nozzle had no stabilizing influence for transverse modes, and the effects for axial modes matched those of Crocco, which is significant, since different approaches were used. The mean flow damped oscillations by convection of energy through the nozzle, but a slight destabilizing effect also appeared, since convection causes a part of the pressure fluctuation at the nozzle entrance to be in phase with velocity fluctuation at that plane, allowing net work to be done on the pressure waves in the chamber during each cycle. Culick's calculations had one intriguing result - he found that damping was

inversely proportional to the characteristic chamber length, so that a scaling up of a particular design without a corresponding increase in nozzle length was likely to lead to instability. The decrease in stability resulted from a decrease in the effective nozzle damping at lower frequencies. Culick also shows that the tendency of the fundamental mode to appear before harmonics is related to the frequency sensitivity of the nozzle damping.

Additional work has been carried out on the effect of the nozzle, but for a different location of the nozzle. The treatments mentioned before concerned the case most often encountered in rocket design, i.e., the nozzle is at one end of the motor. For some test firings, however, the motor is side-vented through an orifice, usually mounted in the center of the motor. This configuration, known as a T-motor, is important in the study of combustion instability, and will be discussed in some detail in Chapter V. It is best, therefore, to postpone a full discussion of the effect of the orifice for side-vented burners until that time.

B. Propellant Physicals

In the consideration of most acoustic fields, the usual assumption is that the bounding surfaces are rigid walls, i.e., that an incident pressure pulse is reflected with no change in amplitude and no phase lag. In the case of the acoustic cavity of a solid propellant rocket motor, however, the propellant itself forms the major part of the boundary, and can play a large role in determining the acoustic properties of the motor. Bird, McClure, and Hart (152) have mentioned that the relative effect of the solid viscoelastic properties depends on the relation of the web thickness to the damping length in the solid. For a long damping length (small viscous loss), the effect can be strong at times when the solid participates in the oscillatory motion. For a short length, there will be a large viscous loss, so that the propellant cannot sustain oscillatory motion. Instead, the main factor determining the acoustic loss to the solid will be the degree of impedance mismatch between the solid and gas phases. In the theoretical treatments to follow, the former case is assumed.

In their original treatment of pressure coupling (85), Hart and McClure treated the body of the propellant as if it were rigid. In later work, Bird, Haar, Hart, and McClure (153) studied the effect of treating the propellant as a compressible medium. By taking into account the temperature fluctuations in the solid phase, they corrected the response function for different values of compressibility and thermal expansion. It was found that the effect of solid density fluctuations was always to decrease the real value of the response function, thereby lowering the amplification. This is ascribed to the fact that compressibility causes a temperature fluctuation in the solid induction region opposite in phase to that caused by the pressure oscillation. As a result, there is an in-phase oscillation in the thermal gradient at the surface, causing an in-phase variation in heat loss from the surface reaction layer. The effect of thermal expansion is much less marked. Typical results are shown in Fig. 20 (153).

Another revision of the original model gave an excellent explanation for the phenomenon mentioned earlier of "ringing" (52), i.e., at certain times during a run, modes will appear and disappear, so that the pressure oscillations vary in wave form and amplitude. In this revision (154), the propellant was taken as merely one of the components making up a solid propellant rocket when viewed as an acoustic field. It was found that the way in which the grain was mounted had a large effect on the acoustic modes of the cavity, so large, in fact, that a variation of a few thousandths of an inch in the clearance changed completely the modes which the system would support. By investigating the quasi-solid and quasi-gas modes (the modes for a solid shell with a free interior surface or for a gas field with rigid boundaries) (155) (156), it was found that both the solid and gas field had amplifications (or attenuations) which varied with time, so that certain modes would be alternatively damped and amplified during a firing. These calculations explained the results of Angelus (52) with different geometries and grain mountings quite well.

Both of these theoretical treatments were for the high frequency tangential modes. Deters (157) extended the study of the role of the solid phase to the case of the lower frequency axial modes, and found that the intermittent behavior previously mentioned did not occur for the axial modes. He did, however, find that the outer constraint would still make a difference, specifically, that stability was favored by a flexible case rather than a rigid one. Although the effect of the solid changed little during firing, the trend was for the solid phase to have an increasingly stabilizing effect during a firing.

Ryan (158) reported on the experimental coupling of the oscillations in the gas and solid phases. It was found that, when the frequency of the driving gas-phase oscillation was much greater than the natural frequency of the solid, the solid transmitted the oscillation with some attenuation, while for cases where the two frequencies were comparable, the solid could participate, giving amplitudes in the solid greater than those in the gas. The variation in experimental behavior tends to corroborate the existence of the extreme cases mentioned earlier.

In later work, Ryan, Coates, and Baer used a piston arrangement to feed a propellant sample into a constant-volume burner, and found that the solid could absorb energy from the gas when the frequency was such that it matched the resonant value for the solid. The results of the experiments showed viscoelastic properties and acoustic attenuation values which agreed with those found by Nall (159), who used a long rod of propellant to make the first attenuation measurements for propellant. Both a resonant rod method and pulse techniques were used.

In a further extension of their experimental studies of the solid phase, Ryan and Coates investigated the effect of oscillations on the viscoelastic properties of the propellant sample (160), using the piston arrangement mentioned above, and found that viscoelastic properties changed markedly during firing. It was found that both the elasticity and the viscosity of the solid were decreased, even though the temperature inside the sample

was not raised significantly. Since oscillations of the order of only 50 psi amplitude had brought about this change, it was speculated that, for high-amplitude pressure oscillations, this softening of the propellant might be a step in large-scale combustion irregularities. Ryan and Coates calculated that the solid phase response could go quite negative at certain frequencies, which was related to the fact that they often observed two periods of oscillation separated by an oscillation-free period, during which acoustic energy was being transferred to the solid phase.

The experiments of Ryan and Angelus, and the theoretical treatments of the APL group, indicate that the effect of the solid phase as a boundary of the acoustic field is a complex one. Although compressional effects typically act as a loss mechanism, reinforcement of pressure oscillations can occur from the participation of the solid in the acoustic field, a fact which should be kept in mind when considering this particular element of the damping axis.

C. Damping by Walls and Baffles

The remaining boundaries of the acoustic field of a solid propellant rocket are made up of the exposed metal or plastic parts used to contain the pressure generated by the burning propellant. The effect of the walls on the acoustic behavior of a cavity has been studied by Lambert (161), and the results of his theory were applied by Bird, McClure, and Hart to a rocket motor (151). They found that the thermal and viscous losses to the wall would ordinarily be ignorable, especially for a design where only the head cavity wall was exposed. The Lambert treatment was, however, not adequate for a solid propellant motor, since the presence of a flow boundary layer, a thermal boundary layer, and an acoustic boundary layer has to be taken into account.

The acoustic loss calculation was extended to a rocket motor by Cantrell, McClure, and Hart (162). A variational technique was used to find the difference between the results for ordinary gasdynamics without the acoustic field and the results for a resonant cavity, and it was found that the results were rather insensitive to the approximations used in the treatment. The analysis was made only for the axial modes of a 2-dimensional, multiple-half-wavelength rectangular cavity, but was applicable to other geometries when the boundary layer thickness was much smaller than cavity dimensions. This range of applicability results from the fact that, except for low frequencies, the acoustic boundary layer is at least an order of magnitude thinner than the steady-state boundary layers.

It was found that, for a fixed gas temperature outside the boundary layer, the acoustic loss is less for a cold wall. The decrease in acoustic loss results from the diminished velocity amplitude in the colder acoustic boundary layer and the lower kinematic viscosity at lower temperatures.

The acoustic loss values from the modified treatment were still found to be negligible under ordinary considerations (56). For motor designs where there are large exposed inert wall areas, however, the energy

dissipated can be appreciable, as in the case of a cigarette-burning grain or an external-burning cylindrical configuration. The effect of the variable heat loss was noted in T-motor tests at BRL (163), where it was found that preheating the test chamber improved reproducibility of the results. However, the BRL investigators later reported (164) that no difference in cavity damping was observed between a zirconia-coated and an uncoated chamber. The chamber was only $2\frac{1}{4}$ inches long, however, so that the heat-loss effect would not be expected to be great for a $1\text{-}3/16$ " diameter chamber. For larger exposed areas, the acoustic loss would be significant. One case where the efficacy of the wall damping mechanism has been proven is the known ability of resonance rods to absorb acoustical energy under the proper conditions, although the disruptive effect on an acoustical wave may be equally important.

D. Particulate Damping

We now turn our attention to damping mechanisms which are related to phenomena occurring in the burnt gases of the acoustic cavity. The first one to be considered is that which results from the presence of any condensed-phase reaction products in the combustion gases.

Products in the condensed phase are found not only in metal-containing propellants which give oxides, such as alumina, magnesia, or zirconia, that are in the condensed phase at combustion temperatures, but also in non-metallized reactants. Large amounts of soot are observed in the combustion of hydrocarbons, and soot formation plays an important role in optical studies of burning, as will be mentioned later. A study of soot formation in premixed hydrocarbon-air flames (165) indicates that the rate of formation can vary with pressure to a power as high as the third.

The first theoretical treatment of the attenuation of sound in a two-phase medium was made by Epstein and Carhart (18), who considered the dissipation by a particle which moved an amount small compared to its radius, primarily for a water-air fog. The primary damping mechanism is the lack of velocity equilibrium between the gas and the particle, which gives a viscous dissipation of energy (thermal dissipation appears to be less important in rocket motors). Chow (166) later extended the theory to higher-amplitude motion and to small particles, and found the same relations to hold. The theoretical attenuation varies with acoustic frequency, particle concentration, and particle size, with an optimum particle size being predicted for a given frequency and concentration.

The first experimental verification of the theory was made by Zink and Delsasso (19), using a loudspeaker-microphone technique to measure the attenuation of aluminum particles in air. The range of sizes and frequencies was extended by Dobbins (167), who used an acoustic impedance tube technique with an oleic acid aerosol (168). His results also agreed with the theoretical predictions and, combined with the Zink-Delsasso results, showed the existence of a maximum attenuation for a particle size-frequency combination, as predicted by Epstein and Carhart.

An application of the particulate damping mechanism to rocket motors was made by Bird, McClure, and Hart (152). They found that the experimental results of Brownlee and Marble (53) on pressure-frequency stability regimes could be explained by the damping behavior of $\frac{1}{2}$ micron soot particles, at the 1% level, in the combustion gases, using the Epstein-Carhart theory.

The mechanism of instability suppression by aluminum is not so clear. Altman and Neustein suggested (169) that the aluminum oxide particles produced by the burning aluminum damped oscillations in the gas phase by the viscous attenuation mechanism. Originally, experiments seemed to indicate that the primary site of aluminum activity was in the solid phase (16) (17). Recently, however, Horton has reported (115) that, for some propellants, the response function is unchanged by the presence of aluminum. In addition, the condensed phase products caused an increase in damping which agreed qualitatively with the Epstein-Carhart theory, although the theoretical damping was always greater than that observed. Horton also noted an apparent increase in damping with pressure, although the experimental scatter was rather high. The pressure effect is contrary to the calculated findings of Blair (170), who showed that there was no change in damping over a 28-fold change in pressure. However, Blair had assumed constant particle size, and Horton based his pressure effect on the experiments of Sehgal (171), who found that the average particle size of the product alumina increased with chamber pressure. The latter finding is still, however, the subject of some contention (172).

Investigators at Aero Chem (173) measured the absorption coefficient of the gases liberated by an aluminized propellant, using a variable-length resonance tube (174). Although measurements were made only at atmospheric pressure, the frequency behavior of the absorption agreed well with the Epstein-Carhart theory.

In summary, the effects of particulate damping in the combustion gas are well known. In the case of "sooty" propellants, some correlation with stability boundaries can be established. Although the role of aluminum is open to some contention, the condensed products do give some attenuation in the gas phase by a viscous-damping mechanism. The particle sizes of the condensed phase products must be determined before the importance of particulate damping in the suppressant ability of aluminum can be better ascertained.

E. Gas Phase Relaxation

As mentioned in Chapter II, the combustion gases can absorb acoustic energy through relaxation processes. In fact, the absorption of sound has been used to determine vibrational relaxation times in nitrogen as a function of temperature (175). Since the absorption increases with the temperature to (about) the $1-3/4$ power (176), nitrogen relaxation can become important at high temperatures.

Relaxations in chemical reactions could have similar effects, but

those related to incomplete reactions might conceivably amplify. Relaxations in equilibrium shift should tend to dampen a sound wave (152).

Hart and McClure (56) have commented that relaxation losses could be significant at frequencies such that the relaxation time becomes comparable with the period of oscillation. This condition could arise at low chamber pressure and high gas temperature, since relaxation times vary inversely with pressure. As a result, the effect of relaxation can vary widely, even more so if we consider the effects of impurities on relaxation times.

VII. Nonlinear Effects

The theoretical treatments discussed thus far have only concerned themselves with linear effects, that is, only first-order perturbations have been taken into account. As mentioned in the morphology section, a more complete theory would deal with the reaction of the burning surface to a disturbance of any amplitude. Torda and his associates attempted to develop such a theory, starting from first principles, but were unable to make any headway, even with a high-speed computer (177). Hart and McClure refer (56) to recent work where their original linear theory was extended to include second-order pressure effects, but no results were available.

The greatest success in non-linear treatment of the acoustic field has been attained by Sirignano (178), who studied the effect of the nonlinear terms on nozzle damping. He found that the non-linearity became significant only when the oscillation amplitude approached the mean pressure level.

As mentioned earlier, the pressure waveform is distorted at finite amplitudes because of the erosive effects on burning rate, as well as because of mean flow effects. The acoustic energy is transferred from the fundamental to the harmonics where it can be dissipated at a higher rate than in the fundamental mode. Calculations of limiting amplitudes have been made based on the transfer of energy to the second and third harmonic (179), and comparison with actual T-burner tests shows that the predicted values are low by a factor of one to five times.

Experimentally, non-linearity is important in the previously-mentioned CARDE experiments on velocity-coupled instability (113). Here, the size of the disturbance must be great enough to cause flow reversal and allow velocity-coupling erosive mechanisms to become important. In this case, the erosive response of the propellant is the factor that determines the amplitude at which non-linear effects become important.

In general, the subject of stability for finite amplitudes is not as well understood as the stability for small perturbations. Although there is some theoretical treatment of the erosive response, no definitive experimental tests have been made which isolate the magnitude of non-linear erosive effects. In addition, the loss mechanisms are not well characterized at high amplitudes, and the approximate Bolt Beranek and Newman treatment is the only one for limiting amplitudes, even for the pure pressure-coupled case.

VIII. A Perspective View

This somewhat cursory survey of some of the various elements which comprise the morphology of combustion oscillations reveals more clearly how complex a problem is involved. When the theoretician sets out to attack the problem of oscillatory burning, he is confronted with a large number of points in the vector space. Many of the elements of the morphology are not well understood in their simplest form, and it is hard to obtain an understanding of the whole without a thorough knowledge of the parts. The relative importance of the several possible contributing factors must be known, so that the theoretician can have some idea of a realistic approach to the problem at hand and know what factors can be ignored in the range he wishes to investigate, or even have some idea of what range should be investigated.

The task is no simpler for the experimentalist. There is almost no such thing as a pure experiment. For instance, if amplitudes are large enough to make a phenomenon measurable, non-linear effects may enter. The various damping effects are all present, and the experimenter can only endeavor to minimize all but one or two of which he (hopefully) has a good knowledge.

Once again, it must be emphasized that the theoretician and the experimentalist must both keep the idea of the morphology in mind when discussing results of theory or experiment. Far too often in the past, disputes have arisen because those involved were discussing a theory and an experiment which occupied totally different points in the morphological vector space. Too many elements enter to allow the assumption to be made that results of any two treatments of the combustion instability problem can be compared, other than to compare the results of the different approximations made.

CHAPTER IV

A DETAILED DISCUSSION OF PRESSURE COUPLING WITH THE SURFACE FLAME ZONE

I. Introduction

As mentioned in Chapter III, the dominant driving mechanism for combustion oscillations is the coupling of fluctuations in the cavity gas pressure with the surface flame zone. The different theories to be discussed in this chapter illustrate some of the many different approaches which can be used to analyze the problem. For instance, will the flame be premixed, or will diffusive effects have to be considered? Will the burning-rate dependence on pressure be considered as obeying the steady-state law, or will some other dependence be invoked? One important consideration is the method by which the proper phase relation can be established between pressure fluctuations and burning-rate fluctuations so as to give amplification, according to the Rayleigh criterion in its simplest form. One technique commonly used has been the assumption of an arbitrary time lag. Although the use of such an arbitrary lag has been criticized, Cheng (180) points out that a time lag is a physically-sensible way to approximate, by an almost discontinuous variation, the exponential variations arising from Arrhenius behavior and diffusive processes. Moreover, he states that the use of an over-all time lag, first suggested by von Karman (63), is no more arbitrary than the use of an ignition temperature or a film coefficient. Price has commented (51), however, that time-lag theories are less applicable to solid-propellant systems than to the liquid ones first considered, because of the various steps involved in solid combustion, with the result that discrete time lags are less justified.

II. Pressure-Frequency Regimes

Another means of obtaining the proper phase lag for amplification is through the natural equilibration time of any processes. The consideration of such relaxation times determines the region of pressure and frequency to which the results of a model can be applied, as can be seen by analyzing the burning process for an ammonium perchlorate composite propellant.

The combustion zones of ammonium perchlorate propellants possess certain significant features. First, the flame itself must be of the type which is known as a diffusion flame, since the fuel and oxidizer are unmixed in the propellant itself, at least on the dimensional scale of the flame zone. On the basis of previous theoretical and experimental work at the Guggenheim Laboratories (181), (182), it has been described as a "granular diffusion flame." Unlike conventional nitrocellulose propellants, there is no evidence of an intermediate dark layer in the flame zone, which is significant since

BLANK PAGE

such a layer would imply a step having a process time comparable to the period of oscillation under some conditions. The total thickness of the granular diffusion flame is such that process times are significant only at the higher range of frequencies, although finite thickness effects may account for some results to be discussed later. Experiments with fine thermocouples traversing the flame zone indicate that the solid phase does not undergo appreciable reaction before it gasifies at the surface, and that it is primarily a heat-up layer (131). This differs from the situation that is believed to exist in nitrocellulose propellants. Finally, it is known that ammonium perchlorate is itself a monopropellant and possesses a significant burning rate (183), (184), (185), yet this property has not seemed essential in explaining the steady-state burning rates of ammonium perchlorate propellants; it has seemed sufficient to take into account only the overall exothermicity of ammonium perchlorate decomposition and not its monopropellant behavior.

It must be recognized that, abundant as the evidence is for this model description, it is still indirect evidence and the theory might well be in error. Accordingly, the theory should not be taken as the final word in describing the mechanism of ammonium perchlorate propellant combustion.

However, the granular diffusion flame model leads one to expect four distinct regimes of acoustic interaction in a pressure-frequency map (Figure 21). These regimes are based on the various steps of the flame process and the degree to which they will be affected by pressure oscillations. If the period of oscillation is long compared to the time involved in the step, the particular part of the process might not be affected by the pressure variation. A dimensionless time might be defined by:

$$\tau = \frac{\text{process time}}{\text{period of oscillation}} \quad (2)$$

For values of τ less than 1/10, the process will probably be unaffected, as can be seen by considering the waveform of such a small portion of a cycle.

The times involved might be estimated as follows. Assuming a non-reactive composite solid with a one-stage gaseous reaction zone, the gas zone thickness is proportional to $p^{-1/3}$ (181). From continuity, it is found that the characteristic time of the gaseous zone varies as $p^{1/3}$. A typical value at 250 psi, based on a gas efflux velocity of 250 cm/sec and a thickness of 50μ , is 2×10^{-5} seconds. The solid heat-up time varies as $p^{-2/3}$. At 250 psi, the time involved is 6×10^{-3}

seconds, from a thickness of 30μ and a burning rate of 0.5 cm/sec. (The effective depth of a thermal variation will typically be nearly an order of magnitude greater than this, and will increase with propellant diffusivity and decrease with increasing frequency.)

In the area of high pressure and low frequency, the oscillation period is much longer than the overall combustion time of an element of propellant, taken from the moment it first senses the heat of the advancing flame in the solid state to the ultimate completion of reaction in the hot-gas state. In this regime, the "zero-frequency" approximation holds, that is, the flame processes have sufficient time to adjust to any change in an absolute quantity or gradient, so that steady-state conditions can be assumed to prevail at all times. The boundary of the zero-frequency regime is determined by the above-mentioned criterion that the period is ten times the overall combustion time. For shorter oscillation periods (higher frequencies), it is useful to distinguish the two component parts of the combustion time, that is, the solid-phase heat-up time and the (very much) smaller gas-phase diffusion-reaction time. In the "low-frequency" regime, the gas phase can be treated in a quasi-steady fashion, but the solid phase must be treated dynamically. This case will be considered in some detail in a later section. In the "high-frequency" regime, the gas phase would have to be treated dynamically. The boundaries of these regimes are drawn in accord with the pressure and burning-rate effects on the characteristic times mentioned above. The high-frequency regime could be further subdivided if we had an accurate knowledge of the times involved in the various components of the gas-phase combustion reactions. A fourth regime can also be identified, when the pressure is sufficiently high and the flame layer sufficiently thin to make the simple one-dimensional granular diffusion flame model no longer admissible. There is as yet no theoretical description of this regime of combustion, although researchers at Aerojet have correlated burning rates with microscopic physical failures in the solid state (186). In any case, it is reasonable to set the high-pressure region apart as a fourth regime.

Cantrell, Hart, and McClure have recently drawn a similar map (187) to consider the importance of the different flame processes. In their map, the coordinates were burning rate and frequency, but the same general arguments were used. The only differences were that the importance of radiation feedback was considered and that a slightly different criterion was used to draw the boundary of the zone where a lag could exist in the solid heat-up zone.

A similar map for double-base propellants would probably be complex, because of the presence of more zones whose very existence is a strong function of pressure and composition.

III. Theories of Pressure Coupling

A. Grad

The first analysis of combustion instability in solid propellant rocket motors was presented by Grad (80). His treatment was based on the variations in burning rate which resulted from pressure variations. The mechanism was "a small pressure rise near the powder grain leads to a local increase in mass flux, thereby increasing the pressure disturbance; this leads to a further increase in mass flux, etc., and possibly eventually to a cumulative blowup. In other words a resonance effect is expected between oscillation of the gas and the burning rate of the powder."

In his model, Grad assumed the simplest case which could lead to an amplifying phase lag. His excitation mechanism was based on a constant time lag, which represented the time required for the surface to adjust to changes in the gas field.

The mass burning rate, in Grad's model, was assumed to be of the form:

$$\dot{m}(t-\tau) = \dot{m}(t) + \tau \frac{d}{dt} \dot{m}(t), \quad (3)$$

where τ is the time lag.

For a density variation $\rho = \rho_0 + \epsilon e^{iact}$,

$$\text{then} \quad p = p_0 + c^2 \epsilon e^{iact}$$

$$\text{and} \quad T = T_0 + \frac{c^2}{c_p \rho_0} \epsilon e^{iact},$$

where c = sound speed in the gas.

Taking the burning rate as $f(p, T)$, then

$$f(p, t) = f(p_0, T_0) + b c \epsilon e^{iact} \quad (4)$$

The parameter b , which defines the stability of the propellant, was defined by

$$b = \left(\frac{\partial f}{\partial p} + \frac{1}{c_p \rho} \frac{\partial f}{\partial T} \right) c \quad (5)$$

The size of b was important, since instability occurred for $\frac{b}{M} > 1$,

where M was the Mach number of the gas flow at the propellant surface. Grad arrived at this conclusion by defining the parameter $B = b - M$, and using $-B$ as an impedance. For positive values of B , amplification would occur. Although Grad did not state explicitly that b was connected with the steady-state burning properties of the propellant, it is generally assumed that the analysis predicts greatest stability for a propellant whose burning rate is least affected by changes in pressure or conditioning temperature. This fact has been used to criticize the theory (9), since propellants with "plateau" behavior ($n=0$ in the Vieille law (95)) were shown by Smith and Sprenger to burn unstably, Grad's theory also predicted greatest stability for long time constants for the chemical reaction.

In addition, Grad's analysis predicted that a "spiral" mode would be most unstable in the tubular geometry considered. This mode was one which spiralled around the propellant surface, moving downstream and would have explained the appearance of partially-burned grains mentioned earlier. Irregularly shaped perforations were proposed as a means of breaking up this mode, and it was assumed that drilling holes or introducing non-burning axial rods were effective in reducing instability through their interference with this mode.

B. Cheng

Cheng (81) added an extra degree of complexity by the use of a pressure-variable time lag and overall interaction index, much as in the original Crocco-Cheng treatment of liquid combustion instability, which is still the basic theory in that field (188). The time lag τ in Cheng's theory was based on a step in the combustion process, namely, the time between primary decomposition and complete combustion of the intermediate gases. This time lag was assumed to vary with pressure only, expressed as

$$\int_{t-\tau}^t p^m(t') dt' = \text{const.}, \quad (6)$$

where $p(t')$ was taken as the pressure of the burned gas acting on the intermediate gas at time t' , and the constant was taken as the energy that the intermediate product would consume before complete combustion.

The decomposition rate m_b was assumed proportional to p^n , to match the steady-state limit, and was taken independent of flow velocity. As a result, the ratio of the instantaneous rate of burned gas generation and the steady-state burning rate became

$$\frac{m_b(t)}{\bar{m}_b} = \frac{p^m(t)}{p(t-\tau)^{m-n}} \frac{1}{\bar{p}^n(t)} \quad (7)$$

The exponent n was taken as the value in the steady-state law, and was related to solid-phase processes. Concerning the pressure index of interaction of the gaseous phase reaction, Cheng states: "Very little can be said about the value of m except that m should be of the order of unity or smaller than unity, but no much bigger than unity. The value of m of a given propellant will probably depend on the operating chamber pressure and the initial temperature of the solid propellant."

Cheng studied the stability of the steady-state flow for small imposed periodic disturbances. The disturbances were assumed small enough to allow the flow to be considered isentropic, and terms of the order of $(\text{Mach Number})^2$ were ignored. In addition, flow was assumed laminar and axially symmetric. The effect of the nozzle damping was treated in the manner detailed in Chapter III.

In his analysis, Cheng finds that an overall pressure index of interaction S must be greater than a certain minimum value in order to have instability. This index was defined as $S = m - (n/2)$. It should be noted that, as a result, a high value of n would promote stability, contrary to the prediction of Grad. The more important parameter was the value of m , which represented the sensitivity of the rate of the vapor-phase reaction to the chamber oscillations. The many rate-affecting factors, including pressure and temperature of the surrounding gas, determine the magnitude of m . The significance of m can be seen more clearly for the case $n=0$, where the energy to drive amplification is drawn from the accumulated intermediate gaseous products of primary decomposition.

An extensive analysis for different geometries was then made by Cheng, who arrived at the following conclusions. Instability occurred when S_{\min} was exceeded and γ was in a given range for a particular mode.

S_{\min} depended on the mode, the geometry and the burning rate, while the unstable ranges of γ depended on geometry and the propellant S . For tubular grains, the frequency of the spiral mode agreed with acoustical theory, but the axial component differed from the organpipe frequency. The spiral mode (combining transverse and axial motion) was also shown to be most unstable, in agreement with Grad. Stabilization was shown to improve with increases in the effective length of the nozzle. As far as geometrical effects are concerned, Cheng stated that an internal burning grain was most unstable, and that the grain became more unstable through the run. A nonburning rod was predicted to have a stabilizing effect, as was a non-erosible end seal. An external-burning rod was most stable, while a rod in-tube grain (annular burning cavity) was intermediate in stability.

A comparison of the Grad and Cheng models was later made by Cheng (180). He first noted that the Cheng theory was based on a two-parameter scheme - the interaction index and the mean time lag - while the Grad theory only has one parameter - the time lag. The Grad theory

could be made a two-parameter one if the pressure exponent n were allowed to vary from the steady-state value, but the response function would still be different since the Grad theory predicts a fall-off from a value of b for increasing frequency, and the Cheng theory predicts an admittance which increases from an initial value of n to a value of S for $\omega\tau = \pi$, and then oscillates. To give a broad-band amplification, such as results from the Hart-McClure treatment (85), Cheng found that it was necessary to assume that the time lag decreased with frequency (189). Such an assumption is not implausible, since the "steeper" gradients at high frequencies could modify the gas-phase reactions which determine γ . Such a modification could give an answer to Price's criticism (82) that instability has been observed over a broad frequency spectrum, which is contrary to the predictions of the original Cheng treatment, where it was stated that γ had to lie in a certain range for amplification to occur. (Figure 22)

C. Hart and McClure

The first analysis of pressure coupling which did not require the a priori assumption that time lag was made by Hart and McClure (85). They considered that the proper phase would arise from time delays in the feedback loops involved in sustaining combustion, and that, "in particular, if successive perturbations were to occur in the heat release in the reaction region, the resulting increments in mass flow may conceivably arrive in the reaction zone at such a time as to reinforce rather than inhibit the initial perturbation." From a consideration of characteristic times in the combustion process, they decided that chemical reaction times were small compared with the times associated with heat and mass flow in the reaction zone, so that only transfer processes needed to be treated as being time-dependent.

The burning model for the analysis is shown in Figure 23, and has three general steps; nongaseous propellant which vaporizes through an endothermic solid-phase reaction to give intermediate gas products, an induction region where the vapor is heated, and a "flame front" characterized by a flame temperature T_F and a "flame speed" V_F . It was assumed

that the propellant was homogeneous, and that no turbulent gas flow existed. The induction zone was assumed to be small compared to the wavelength of sound, with constant pressure across the zone, which was defined by heat and mass transfer equations. These equations were

$$\frac{\partial}{\partial x} \left[k \left(\frac{\partial T}{\partial x} \right) - m c_p T \right] = \frac{\partial}{\partial t} [c_v \rho T] \quad (8)$$

$$\text{and} \quad \frac{\partial m}{\partial x} = -\frac{\partial \rho}{\partial t} \quad (9)$$

The propellant gas was perfect with constant molecular weight M and had a flow velocity small compared with the speed of sound. The vaporization rate of the solid was an Arrhenius function of the temperature in a thin

surface-reaction zone and a function of the thickness of that zone. Any chemical reactions occurred only in two thin zones, one in the gas phase at a given ignition temperature, one at the solid surface. These zones are collapsed to bounding surfaces, across which mass flux is continuous, but not heat transfer and temperature. This collapse is allowed because of the calculated thickness of such zones (of the order of 10^{-6} centimeters). It was assumed that a quasi-steady dependence of mass flux existed at the surface, namely

$$\frac{dm}{\bar{m}} = \frac{E_s}{RT_s} \left(\frac{dT_s}{T_s} \right) - \left(\frac{dG_s}{\bar{G}_s} \right) \quad (10)$$

where E_s = activation energy of surface reaction

T_s = surface temperature

$G_s = \left(\frac{dT}{dx} \right)$ evaluated at the gas boundary of the solid reaction zone.

At the edge of the hot zone, it was assumed that

$$\frac{\delta m_b}{\bar{m}_b} = n \left(\frac{\delta p}{\bar{p}} \right) + j \left(\frac{\delta T_o}{T_o} \right) \quad (11)$$

where n and j are given by steady-state experiments, and are represented by

$$n = \left[\left(\frac{\bar{p}}{\bar{m}_b} \right) \left(\frac{\partial \bar{m}_b}{\partial \bar{p}} \right) \right]_{T_o} \quad (12a)$$

$$\text{and } j = \left[\left(\frac{T_o}{\bar{m}_b} \right) \left(\frac{\partial \bar{m}_b}{\partial T_o} \right) \right]_p \quad (12b)$$

where T_o = initial propellant temperature

\bar{m}_b = mass burning rate.

The problem is then solved by taking a first order perturbation, using a pressure disturbance as the forcing function, i.e.,

$$p = \bar{p} [1 + \epsilon(t)] \quad (13)$$

and investigating mass flow response

$$m = \bar{m} [1 + \mu(t)] \quad (14)$$

where μ and ϵ are complex quantities having real and imaginary parts.

The values of $\tilde{\mu}$ (complex fractional increment of mass flow) were then solved for. (An expanded discussion of the procedure has been made by Trubridge (190).) In order to connect the sound field with the induction zone, the assumption was made that, since the burning zone thickness was negligible with that of the induction zone, the pressure and mass flow at the boundary between burning-zone and product-gas regions could be approximated by their values at the induction zone boundary. Then, using the definition of the acoustic admittance, Y_p , Hart and McClure stated

$$Y_p = \frac{-V_{pg}}{p} \left[\left(\frac{\tilde{\mu}_1}{\tilde{\epsilon}} \right) - \frac{1}{\gamma} \right] \quad (15)$$

where V_{pg} = mean velocity of gaseous combustion products

p = mean pressure in induction zone

$$\frac{\tilde{\mu}_1}{\tilde{\epsilon}} = \left[\frac{(m_1 - \bar{m})/\bar{m}}{(\tilde{p} - \bar{p})/\bar{p}} \right] = \text{the response function.}$$

As mentioned previously, amplification occurs when the real part of the admittance is negative, so that the criterion for instability was

given by $\text{Re} \frac{\tilde{\mu}_1}{\tilde{\epsilon}} > \frac{1}{\gamma}$. (Comments on this criterion and on the form of Equation

(15) will be made later.) Hart and McClure used this criterion to investigate the effect of different propellant parameters on combustion instability boundaries. Some typical results are shown in Figures 24, 25 (85). It should be noted that amplification occurs over a broad band of frequencies, with no sharp peaks, in contrast to the predictions of the Green and original Cheng models.

The effect of some of the parameters on instability regions was given by Hart and McClure (85). It was found that lowering T_0 generally decreased instability. Increases in stability were found for lower n and j as might have been expected, but cases of amplification were found even for $n=0$. The effect of an increase in the depth of the solid phase reaction zone was to increase instability at high frequencies, which could be attained by increasing T_0/T_s or by decreasing β . The effect of changing the burning rate was largely to change the frequency scale.

The effect of the term \bar{V}_{pg}/p is an interesting one (50). If operation is taking place in a broad amplification region, then the amplification per unit surface is essentially proportional to \bar{V}/p . It may be

rewritten

$$\frac{\bar{V}}{p} = \frac{\bar{m}}{\rho p} = \frac{\bar{m}}{p^2} \frac{RT_s}{M} \quad (16)$$

In this form, the effect of heat release rate $\frac{\bar{m}RT_s}{M}$ is seen clearly, i.e., a high heat-release rate increases the magnitude of Y , hence, the severity of instability. In addition, since burning rate increases less than proportional to pressure, then instability will be more severe at low pressure. Since burning rate is increased by an increase in the initial conditioning temperature, it is seen that instability will be more severe at high temperature. Since, as mentioned above, a lower conditioning temperature has a destabilizing effect on the response function, the combination of the two factors leads to severity at either temperature extreme.

The first revision of the Hart and McClure theory concerns the form of the admittance function as related to the response function. The admittance may be derived as follows:

$$m = \rho v \quad (17)$$

$$\frac{dm}{dp} = \rho \frac{dv}{dp} + v \frac{d\rho}{dp} \quad (18)$$

Since $Y = -\frac{dv}{dp}$, from equation (18) we obtain:

$$Y = \frac{-1}{\rho} \frac{dm}{dp} + \frac{v}{\rho} \frac{d\rho}{dp} \quad (19)$$

which may be rewritten

$$Y = \frac{-v}{p} \left(\frac{p}{\rho v} \frac{dm}{dp} - \frac{p}{\rho} \frac{d\rho}{dp} \right) \quad (20)$$

Then using

$$\tilde{\mu} = \frac{dm}{m}$$

$$\tilde{\epsilon} = \frac{dp}{p}$$

$$\tilde{c} = \frac{d\rho}{\rho}$$

equation (20) becomes

$$Y = \frac{-v}{p} \left(\frac{\tilde{\mu}_1}{\tilde{\epsilon}} - \frac{\tilde{\sigma}_1}{\tilde{\epsilon}} \right) \quad (21)$$

In their original formulation, Hart and McClure evaluated the response function μ/ϵ , and made the simplifying assumption that, since isentropic conditions exist in a sound wave, so that a particle of gas undergoes isentropic compression,

$$\frac{dp}{d\rho} = \frac{\gamma p}{\rho} \quad (22)$$

so

$$\frac{\tilde{\sigma}_1}{\tilde{\epsilon}} = \frac{1}{\gamma} \quad (23)$$

However, as has been pointed out by Summerfield (191), there is a conceptual error in the derivation. The derivative $dp/d\rho$ is to be calculated in the Eulerian sense - at a fixed station in the gas field - since the mass flow equation (17) is defined in Eulerian terms. Therefore, the temperature at the edge of the flame zone must be considered in defining the derivative. One special case, for instance, would be where the temperature is constant.

For a constant temperature,

$$\frac{dp}{d\rho} = RT = \frac{p}{\rho} \quad (24)$$

so

$$\frac{\tilde{\sigma}_1}{\tilde{\epsilon}} = 1 \quad (25)$$

Results of this special case will be discussed later. The McClure derivation would, of course, be true always if the derivative were calculated in the Lagrangian sense, i.e., following the gas particle.

Following this criticism, Hart and McClure reformulated (56) the admittance expression to read

$$Y = \frac{-\bar{v}_1}{p} \left[\frac{\tilde{\mu}_1}{\tilde{\epsilon}} - \frac{1}{\gamma} \left(1 + \frac{\tilde{\zeta}}{\tilde{\epsilon}_1} \right) \right] \quad (26)$$

where

$$\tilde{\zeta} = \left(\frac{\gamma-1}{\gamma} \right) \frac{p_1}{p} - \frac{(T - \bar{T})}{\bar{T}}$$

The term $\tilde{\zeta}/\tilde{\epsilon}$, expresses the degree to which processes at $x = x_1$ are non-isentropic.

In order to evaluate ζ , a knowledge of the temperature response function is required. Calculations to obtain this function have been published (192) by Hart and Cantrell. Similar calculations have been made here, and will be described later.

Another correction to the admittance function has been made by Wood (193), who dealt with the fact that the Hart and McClure analysis was for a homogeneous propellant, rather than for a heterogeneous one, such as a composite propellant would be. In his analysis, Wood treated the oxidizer and binder as having different pressure sensitivities, and found these sensitivities and their relative magnitude to have more importance than the overall pressure exponent for the propellant.

A recent modification to the treatment of pressure coupling has been made by Hart and McClure (187), in which the effect of time-dependent radiative transfer was considered. It was found that, at low frequencies and low burning rates, radiative transfer is the most important dependent mechanism in determining the magnitude of the pressure response function. The influence of time-dependent radiation is less at higher frequencies or for propellants with higher burning rates. In the low-frequency regime, however, radiation can cause a large increase in the response function, which could be an important consideration in explaining some anomalous experimental results to be mentioned in the next chapter.

D. Williams

One of the assumptions made by Hart and McClure in their model was that the gas-phase combustion occurred in a thin zone, so that diffusion of reactants did not have to be considered. An attempt to extend their treatment to include diffusive effects was made by Williams (86). His burning model consisted of a non-reacting solid, surface gasification through an irreversible pyrolysis process, and a distributed gas-phase reaction zone with conduction and diffusion. The simplifying assumption was made that the gas was premixed, based on the statement that such a model had met some success in predicting the steady-state deflagration of pure ammonium perchlorate, so that experimental verification could only be obtained with a pure perchlorate sample. It was further assumed that reaction rates were so slow that no composition change would occur through a sound wave, so species concentrations were frozen and the product gases were isentropic. Pressure perturbations are imposed on the Nachbar-Johnson perchlorate model (194), with only first-order terms being taken into account. A fifth-order, linear, inhomogeneous system of differential equations results, which might be solvable by numerical means. Williams treats only the case of low frequency and large activation energy for the gaseous reactions, and finds that amplification will occur only when the frequency of oscillation approaches the reciprocal of a characteristic gaseous reaction time. He finds the surprising result that gas-phase kinetics affect the response only through the burning rate, which affects only the frequency range. In addition, the model predicts that pure ammonium perchlorate always attenuates sound waves, at least over the frequency range of validity, and that the distributed reaction zone gives more stability. However, the case treated seems over-

simplified, and Hart and McClure (55) refer to it as "a totally unrealistic and misleading over-approximation."

E. Solid Phase Theories

As mentioned in Section II of this Chapter, we can divide the gamut of conditions under which combustion oscillations occur into regimes of pressure and frequency, based on a consideration of the various characteristic times of the several steps in solid propellant combustion. There exists a region, the "low-frequency region", where the gas-phase processes may be regarded as quasi-steady, and where only heat-conduction effects in the solid phase need to be considered as time-dependent.

The first theoretical treatment of this region was advanced by Akiba and Tanno (87). They solved the time-dependent conduction equation for a non-reacting solid, assuming no lag at the surface. The pressure, temperature, burning rate, and thermal gradient were all assumed to vary sinusoidally with time from their steady-state values, with the burning rate also being an Arrhenius function of the surface temperature, the combination of the two giving an eigenvalue for the problem. A transfer function for the burning rate was then derived from a consideration of the energy balance at the surface, which included a heat of phase change. The transfer function for the chamber was defined, which depended on the characteristic chamber exhaust time. From a consideration of the Nyquist criterion, they derived a proportionality relation for the stability boundary, i.e., L^* proportional to (pressure)⁻²ⁿ, and found that, for L^* less than this stability line, amplification would occur.

The same model was used by Sehgal and Strand (88), who developed a more elegant treatment, but arrived at identical transfer functions for the burning rate, the chamber, and the closed-loop feedback between the two. They were able to develop a numerical program for conditional stability, so that specific propellants could be discussed. The same qualitative behavior resulted as from the Akiba-Tanno model.

The following equation resulted from the Sehgal analysis:

$$L^* = \frac{C_D R T_f \tau_{cr} \bar{r}^2 \bar{p}_c^{-2n}}{Ma_g^2} \quad (27)$$

where C_D = discharge coefficient

τ_{cr} = critical chamber time constant

a = constant in Vieille burning-rate law

\bar{p}_c = critical chamber pressure for conditional stability.

It was found that the critical time constant was a strong function of surface temperature, increasing with higher values. Experimentally, it was found that, for aluminized propellants, the L^* -pressure slope was steeper than predicted, although the predicted behavior correlated well with non-metallized propellant.

Admittance calculations have been made here based on the same model, and will be presented in Chapter X of this report.

Price (89) uses a similar concept to consider the role of the solid state in amplification, but arrives at a slightly different solution to a regime of instability. His development is based on the idea that, for steady-state conditions, more heat is stored in the propellant at low pressure than at high pressure (due to the Gentler thermal gradient), so that when a rapid pressure rise occurs, the propellant burns more rapidly as a result of the excess energy content. Price derives the following relation between heat content, heat flux, and rate of pressure change:

$$\left(\frac{dq_s/dp}{dq_r/dt} \right) = - \frac{n L (T_s - T_o)}{\rho a^2 (L + c_p [T_s - T_o]) p^{2n+1}} \quad (28)$$

where dq_s = difference in heat content for steady-state burning at p and at $p + dp$

dq_r = heat transferred to the propellant in time dt for steady-state burning conditions

L = heat of phase change at the surface.

For a typical propellant and a pressure of 100 psi, equation (28) gives a value of 4.5×10^{-5} sec/psi. Assuming that a burning rate increase will occur for $dq_s/dq_r > 0.1$, for the case chosen a rate of pressure rise of the

order of 2 psi per millisecond leads to amplification. The same result would occur for a pressure drop of this order of magnitude.

Price's theory gives the same behavior as the earlier theories for the case where dp/dt is determined by chamber exhaust characteristics, since all three deal with the relation between the characteristic time for the chamber,

$$\tau_{\text{chamber}} = \frac{g V_c M}{C_D A_t R T_f} \quad (29)$$

and a characteristic time for the solid, with the heat of phase change taken into account,

$$\tau_{\text{solid}} = \frac{(T_s - T_o)}{r^2 (L + c_p [T_s - T_o])} \quad (30)$$

The Price solution does, however, allow for a more general case of a pressure disturbance, and gives a clearer picture of the way in which the lag in the solid phase can give amplification.

Dennison and Baum (91) also treated the frequency regime where gas-phase characteristic times were short compared to the oscillation period but solid-phase characteristic times were still an important fraction of the period, but succeeded in including the effects of reactant diffusion as well as those of heat conduction. The gas-phase processes were, however, assumed quasi-steady. The solution was obtained by a combination of perturbing a laminar flame and considering transient heat conduction in the solid. As mentioned in Chapter III, the assumptions included homogeneous propellant, a non-reacting solid, Arrhenius-law decomposition at the surface, a Lewis Number of one, and a single-step combustion reaction of any order. It was further assumed that the molecular weight and thermal conductivity of the gas were constant, and that no back reactions were involved. In order to integrate the gas-phase equations, the change in heat content is neglected in the energy balance with respect to the heat transferred by conduction and the heat produced by chemical reactions. This approximation, made by von Karman (195), is based on the fact that an eigenvalue for the laminar flame speed is primarily dependent on the mass flow ratio of the products near the end of the combustion zone.

After using these approximations to obtain a burning rate, Dennison and Baum then perturb the pressure by a small disturbance, causing small perturbations in the mass flow rate and the temperature, which are determined by considering only first-order terms in the perturbed quantities. The lag in the solid phase gives rise to lags in flame temperature and mass flux. For a step function in pressure, the burning rate can either runaway, oscillate sinusoidally with increasing amplitude, or return to the steady-state value, as shown in Figure 26. The effect of the frequency on the amplitude of the response is shown in Figure 26. However, since the theory is for small perturbations only, the results shown in Figure 26 should only be taken as indicating trends. Moreover, the theory does not give information on the feedback process by which the burning rate change amplifies the original pressure perturbation, but does indicate that large changes in mass flux can result from solid-phase lags, even when diffusive effects are taken into account.

In concluding this discussion of the treatments of pressure coupling with a surface flame zone, it should be noted that every theory considered has used rather restrictive assumptions which limit the range of validity, although the effects of many of the parameters can (hopefully) be predicted. Since there exists no single comprehensive theory for steady-state burning, it is not surprising that the unsteady case has not, as yet, been solved for all regimes. However, it has been found that different models may be applicable to different pressure regimes for steady-state burning, so that treatments of combustion instability may be forced to treat individually the different pressure-frequency regimes detailed at the beginning of this Chapter.

CHAPTER V

EXPERIMENTAL STUDIES ON THE NATURE OF THE PRESSURE- SURFACE FLAME COUPLING

I. Introduction

A survey of the literature on experiments in combustion instability, especially a perusal of two summaries by Price (61) (51) in 1960 and 1964, shows that the experimentalist has grown with the theorist. At first, experiments in the field were primarily phenomenological (6). Next, some variables were deliberately added to the composition and/or configuration, and their effects studied (2) (10). Workers at JPL added some degree of quality control to motor firings and drew still further conclusions as a result (53) (24). For the most part, though, experiments were performed in rocket motors requiring at least ten pounds of propellant per firing, and much of the results were shrouded by a confusing mask of security classification. The successful development of a laboratory burner by Price (99) marked the beginning of the end of the motor-firing era, and experiments have now taken on a much higher degree of sophistication than ten years ago or even six or seven.

The experimentalist has two basic directions to follow. First, he can study those effects which determine stability, but with the increased sophistication obtained from the mistakes of past workers. One particular example is the study of non-linear instability and the ranking of stability through the ability of a system to attenuate a disturbance of a given size. Second, he can attempt to study the gains and losses of individual components of the rocket.

One outstanding example of the second approach, and the subject of this chapter, is the determination of the response function of a burning solid propellant, which represents the degree of acoustic interaction between the pressure and the surface flame. It has been estimated (56) (85) that the specific acoustic admittance of the burning surface will typically be of the order of 10^{-5} - 10^{-6} rayls, so that the amplitude gain on reflection will be of the order of 1% (for an admittance of 1 rayl, a sound pressure of 1 dyne/cm² will produce a linear velocity of 1 cm/sec).

The experimentalist must then ask himself the following questions before deciding on a given experiment: (1) What are the possible physical methods for measuring the acoustic admittance of a propellant flame? (2) Do actual solid propellants, particularly those that exhibit acoustic instability, possess flame structures with a negative real part of the acoustic admittance? (3) Can such measurements of acoustic admittance, by one means or another, be employed to test the efficacy of various instability-suppressing propellant additives? (4) What aspects of the structure of the flame determine the character of the admittance?

BLANK PAGE

Two general experimental directions have been opened up for examination of the nature of the acoustic interaction between pressure and the surface flame. In one case, measurements are made of the oscillatory characteristics of a chamber containing a test propellant. In the other case, direct observation of the propellant or its flame are made while the propellant is burning under a changing pressure. This pressure change can be a single rise (e.g., a shock) or fall (e.g., an expansion) or can be part of a large number of sinusoidal pressure oscillations, either self-excited or externally excited.

II. Self-Excited Pressure Oscillations

Much of the experimental work being carried out today makes use of some modification of Price's T-burner (99), shown in Fig. 27. This was the first successful small-scale laboratory burner, and was used by Price to gain a large amount of information on the effects of combustion instability, as for instance the burning-rate studies mentioned earlier (33) or various side effects (196). In the original design, however, the oscillations were still velocity-coupled, i.e., oscillations in the flow field parallel to the burning surface were present. This fact made the T-motor, in its original form, unsuitable for determination of pressure-surface-flame coupling.

A simple modification of Price's original design was made by Horton (197), who made the T-burner one-dimensional by replacing the cylindrical propellant samples with end-burning samples, as shown in Fig. 28. In this way, the only coupling between the combustion gas and the propellant is pressure coupling, as desired. Horton overcame Price's original difficulty (198) with this configuration by minimizing chamber damping, probably wall and nozzle losses.

The first acoustic-admittance measurements using the one-dimensional T-burner were made by Horton at Utah (199) and continued at NOTS (22), following the suggestions of Price. Since that time, a large body of experimental results has been obtained with the technique.

A. Theory of the Experiment

The theory for the determination of acoustic admittance with the T-burner was developed by Watermeier (163). It may be summarized as follows. The damped wave equation for particle displacement is

$$\frac{\partial^2 \xi}{\partial t^2} + 2k \frac{\partial \xi}{\partial t} - c^2 \frac{\partial^2 \xi}{\partial x^2} = 0 \quad (31)$$

This differs from equation (A-5) in the inclusion of the damping term $2k(\partial \xi / \partial t)$ where $k = R/2 \rho$. R is a damping coefficient which represents the bulk gas damping resulting from all damping mechanisms. For the configuration shown in Fig. 28, all boundaries are rigid, except at $x = l$, where the burning propellant sample is located.

The admittance at $x = \ell$ is given by

$$\eta = \left. \frac{\rho c u}{p} \right|_{x=\ell} = - \left. \frac{(\partial \xi / \partial t)}{c (\partial \xi / \partial x)} \right|_{x=\ell} \quad (32)$$

since $p = -\rho c^2 \frac{\partial \xi}{\partial x}$, as shown in equation (A-7).

By assuming that the pressure oscillations are of the form

$$A f(x) e^{ibt} \quad (33)$$

making algebraic manipulation, and solving equation (31) it is found that

$$\eta = \left(1 + \frac{ik}{b} \right)^{-1} \tanh \frac{i\ell}{c} (b + ik) \quad (34)$$

The real and imaginary parts of b can be obtained from the pressure-time history. From equation (33), it can be seen that

$$\text{Re}(b) = 2 \pi \gamma$$

$$\text{Im}(b) = \frac{\partial}{\partial t} (\ln P) \quad (35)$$

where P is the exponential envelope of the pressure while the propellant is burning.

When the propellant sample burns out, there is a steel plate at $x = \ell$, so that the gas damping determines the exponential decay, which is given by

$$\text{Im}(b) = \frac{\partial}{\partial t} (\ln P_a) = -k \quad (36)$$

where P_a is the exponential envelope of the pressure after burnout.

Evaluation of η from equation (34) is simplified by the fact that the damping and boundary condition has little effect on the undamped,

rigid-end frequency of the cavity. In addition, k/b was found to be small, so that

$$\eta = -\tanh \left\{ \frac{l [\text{Im}(b) + k]}{c} \right\} + \frac{i \tan \left[\frac{l \text{Re}(b)/c}{\cosh^2 \left\{ \frac{l [\text{Im}(b) + k]}{c} \right\}} \right]}{\cosh^2 \left\{ \frac{l [\text{Im}(b) + k]}{c} \right\}} \quad (37)$$

From equations (35) and (36), then, the real part of the admittance ratio becomes

$$\eta = -\tanh \left\{ \frac{l}{c} \left[\frac{\partial}{\partial t} (\ln P) - \frac{\partial}{\partial t} (\ln P_a) \right] \right\}, \quad (38)$$

so that the admittance can be obtained by measuring the growth and decay curves of the pressure amplitude. It is found that the argument of the hyperbolic tangent in equation (38) is small, so that $\tanh x \approx x$. The specific acoustic admittance Y then becomes

$$Y = - \frac{l}{\rho c^2} \left[\frac{\partial}{\partial t} (\ln P) - \frac{\partial}{\partial t} (\ln P_a) \right]. \quad (39)$$

There is, however, one serious error in the derivation of equation (39), and a great deal of controversy has arisen over this point. The original formulation neglected the effect that the mean flow would have on the gains and losses, since the energy present in the flow field can be converted into the acoustic field. McClure, Hart, and Cantrell (200) found that, in the case of the T-burner, the stability criterion could be altered from

$$\text{Re } Y > 0$$

to

$$\text{Re } Y > \frac{\bar{v}}{\gamma \bar{p}}$$

where \bar{v} is the mean flow velocity of the gases leaving the burning zone. As a result, the system could be unstable even for a stable propellant. In other words, the flow field has become a "virtual amplifier." A great deal of discussion as to the modification to be made to the admittance function has taken place.

In their original work, the criterion for amplification of a

disturbance was expressed by McClure and Hart as

$$\operatorname{Re} \left(\frac{\hat{\mu}}{\hat{\epsilon}} \right) > \frac{1}{\gamma}$$

By considering momentum and energy transport, the criterion for a T-burner geometry was changed to (201)

$$\operatorname{Re} \left(\frac{\hat{\mu}}{\hat{\epsilon}} \right) > \frac{\bar{v}}{\gamma \bar{p}},$$

although Horton considered \bar{v} small enough that he reported his results on the basis of $\operatorname{Re}(\gamma) > 0$.

Dyer has made calculations (202) which show that the convective term should alter the criterion to

$$\operatorname{Re} \left(\frac{\hat{\mu}}{\hat{\epsilon}} \right) > \frac{1}{2\gamma},$$

and stated that the difference between his result and the modified McClure result must arise from some other part of the acoustical system of the T-burner. Cantrell and Hart (201), however, state that Dyer's calculations were based on incorrect expressions for the energy flux in the acoustic field. Westervelt has investigated the energy balance between sound and flow (203), and found that energy transfer depends on the coupling at the boundaries. In addition, he found that the attenuation coefficient of the cavity should be modified by a factor containing the Mach Number of the flow.

The effect of flow is a considerable one since the real part of the reduced admittance is, typically, of the same order of magnitude as $1/\gamma$. Some work has been performed at Bolt Beranek and Newman to give more information on the problem. In cold-flow tests (204), it was found that the quality factor of a center-vented cavity was considerably reduced with flow. Measurements on nozzle losses (205) indicate that a very complex dependence of loss on flow is found for Mach numbers greater than 0.02. At about $M = 0.02$, the loss becomes negative for a short time, then returns to a positive value which quickly rises to a maximum at about $M = 0.1$, then decays as M^2 . Although the region of negative loss could result from vortex generation at the nozzle-entrance edges, the strong variation in the loss with Mach Number could be quite critical, especially when the burner is vented into a surge tank, and the behavior of the nozzle as an acoustical component would be quite different during the decay portion of a test than

during burning. The vent losses resulting from acoustic radiation were calculated by Hart and Cantrell (206) to be quite small, but can be significant when the vent is not exactly at the nodal plane. In fact, Smith (107) has calculated that, for a 10-inch cavity with a 5/16-inch-diameter vent, a vent displacement of only 0.001 inches with respect to the nodal plane leads to additional losses resulting from motion of the gases in the vent, and that these losses vary as the square of the separation. Since the separation varies during a firing owing to differential heating, thermal expansion, changes in cavity length with burning, etc., the acoustic radiation losses probably vary during a firing.

Other questions have been raised as to the accuracy of admittance values obtained with the T-burner. Most of these questions are concerned with the method of obtaining the damping factor for the cavity, since the assumption is made that the damping present during the growth of the oscillations is the same as that present during their decay. Owing to the different thermal conditions present, this assumption has been questioned often (56) (208) (209) (210), and is the most tenuous one. The effects of the wall on viscous and thermal damping are different, back-flow of cooled gas may occur, and condensed products may be present at the lower temperatures. Horton has found, in fact, that the decay is not strictly exponential in nature (208).

Horton has given some other objections (22). Among these are the fact that the frequency changes during a firing, so any critical effects on damping and response would be important. The presence of overtones in the wave form would modify interpretation of results severely. The use of linear relations has been questioned, but it appears, from experimental observations, that the growth curve is exponential to surprisingly large amplitudes. Ryan (209) has commented that the use of propellant at one end only leads to an unsymmetrical gas column, and that the mean flow field is different during the decay and growth periods. Another source of error is the wide range of pressure oscillations often encountered, which can cause a change in the boundary layer from a laminar one to a turbulent one, giving a large increase in boundary losses during a test (211).

Of course, one overriding difficulty with the T-burner method of determining acoustic admittance is that it requires a propellant which is marginally stable or unstable. The magnitude of the quantities being measured is, for many cases, comparable with the uncertainties present, so that large scatter is sometimes reported in experimental results.

The large wall-area to propellant-surface area ratio increases the system losses, so that the T-burner is more stable than, for instance, the transverse modes of a cylindrical grain. It seems that amplification is greater at pressures which are often below those used in practical motors.

Despite these many possible sources of error, some experimenters (209) (212) have found that, in the frequency range, 1000-10000 cps, the measured response function is relatively insensitive to vent size, burner

temperature, and the use of a single-ended or double-ended burner. Other experimenters (163) (213) have not found such to be the case, and Foner (213) has commented that the large changes he observed in cavity damping would probably not be noticeable in experiments with rather unstable propellants. Obviously, then, the T-burner as an accurate quantitative tool needs improvement. However, the T-burner does allow isolation of the effect of a number of variables on pressure-surface flame coupling, and some of these effects will be mentioned in the following section.

B. Experiments

The initial data reported from T-burner measurements were from tests at BRL (163), NOTS (212), and Utah (214), and comparisons between results for the same propellant are shown in Fig. 29 (215). It can be seen that, although the results are of the same order of magnitude, the quantitative agreement is rather poor.

The comparison in experimental results is necessary because of different techniques involved by different investigators. In the Utah work (214), the propellant is mounted on a hydraulic ram so that the burning cavity can remain constant or vary in a controlled manner. The BRL investigators (163) use a second piece of propellant to give a more uniform temperature field, but do not take readings until this piece burns out. In this way, the stagnant gas pocket at one end of a single-ended burner does not introduce spurious results.

Watermeier reported (216) on an attempt to improve accuracy by removing some of the uncertainty involved in determination of the decay constant. In order to reduce wall losses, a new combustion chamber was fabricated which had four vent holes rather than one, which would lead to uniform venting, with resultant uniform temperature fields, and reduce flow effects in the orifice (Fig. 30). Although initial results were encouraging, in that losses were reduced and admittance data agreed with results from the single-orifice burner, no further work with the four-orifice burner has been reported.

In addition to the tests mentioned earlier on the damping effect of aluminum, Horton used the T-burner to evaluate the effects of several compositional changes in the binder, in the oxidizer particle size, and in burning rate modifiers (116). Three binders were used -- a polybutadiene-acrylic acid copolymer, a polysulfide, and a polyurethane. Very little effect was found, except that the polyurethanes had a slightly lower response function than the other two propellant systems (Fig. 31). Evaluation of burning rate effects was not clear cut, but the propellants divided themselves into two groups -- one containing coarse oxidizer, the other containing fine oxidizer (Fig. 32).

In order to make further comparisons, the effect of the mean burning rate was removed by plotting the results $\bar{\mu} / \bar{c}$ against ν / r^2 , rather than against ν (Fig. 33). Hart and McClure state that (70) "the unperturbed burning rate is the one parameter whose change merely shifts

the frequency scale", and this shift is a square dependence, because the burning rate appears as a square in the characteristic times involved in the theory. As a result, equivalent frequencies are found for equal values of ν/r^2 , rather than for equal ν .

From the resulting plots, Horton found that changing the particle size only changed the burning rate. The effect of two burning-rate modifiers was somewhat confusing, as copper chromite, a burning-rate accelerator, and lithium fluoride, a burning-rate depressant, increased or decreased stability, depending on the test frequency. The alarming result, from the ballistician's standpoint, is that a modifier added at the 1% level could change the response function by a factor of five, so that minor compositional variations made to match a desired burning rate could easily change a stable motor to an unstable one.

Horton also reported on a series of tests where the only variable was the operating pressure (117). Generally speaking, he found that driving was inversely proportional to pressure. The effect of pressure should be tested more closely, since Price has stated (15) that the pressure dependence predicted by McClure is not always supported by experiment, and that for double-base propellants there seems to be no pressure dependence. Since Horton's results on pressure effect were with double-base propellant, the conflict is intriguing.

One general observation can be made about the response functions which resulted at low frequency. In every case, the response function showed a rapid increase below 1000 cycles per second. Horton (116) attributes this behavior to the uncertainty in the damping constant since "the potential error introduced by this uncertainty becomes very significant at low frequencies where the decay constant is equal to or greater than the growth constant." As a result, the utility of the T-burner as a tool for evaluating response functions seems to be limited to frequencies greater than, say, 1000 cycles per second.

The apparent increase in response function at low frequencies seems to be particularly accentuated for propellants with low burning rates. Although part of the increase may be inherent in the experimental technique, Hart and McClure did find (187) that the inclusion of radiation feedback in their theoretical model could lead to large increases in the acoustic admittance in the low frequency-pressure regime. However, the experimental results still have about the frequency dependence predicted by the Cheng fixed time-lag model.

In addition to the work mentioned earlier on physical properties, the investigators at Utah made some geometric changes in the test configuration, both to check earlier results and to increase the usefulness of the T-burner (209). In one case, there is propellant at one end only, rather than at two ends, as usually employed. The growth rate of oscillations is compared for the two cases, and the admittance obtained from

$$\text{Re}(Y) = \frac{l}{\rho c} (a_1 - a_2), \quad (40)$$

where α_2 and α_1 are the measured growth constants for propellant at both ends and one end, respectively. The method gave comparable results to those obtained using the growth-decay method (Fig. 34). However, the growth-only method gave higher results, which may be due to unsymmetrical temperature effects in the single-ended case.

Another technique uses the geometry shown in Fig. 35. Here, also, the growth rate alone is used and variations in the propellant-burning-surface-area provide variations in the growth rate (209). The tubular section is added to increase the ratio of propellant area to end area, and only a short section is used, so that the wave motion will be relatively undistorted. Admittances obtained with this method agree with those obtained from the other two methods.

One side advantage of the use of extra burning surface is that more acoustic energy input is available to overcome losses, so that less unstable propellants can be characterized as contrasted with the simple end-burning configuration. The effect of the area increase has to be studied carefully before this method can be used widely, however. For instance, some velocity coupling can be introduced.

III. Combustors with External Sound Source

A. Cavity Effects

As previously mentioned, the T-burner technique of measuring propellant response functions has the inherent drawback that the propellant must be unstable before the technique can be used. As a result, several investigators have used external sound sources to provide the time-varying pressure and studied the effect of the burning solid propellant on the acoustic field of the combustor.

Foner (213) kept the basic configuration of the single-ended T-burner, but added an external driving source at the other end (Fig. 36). This driver is phase-locked at one of the resonances of the cavity, and a number of different tests are run to study the growth and damping. First of all, the bandwidth of the resonance can be measured, giving a quality factor Q and a damping constant by

$$\alpha = \frac{\pi \nu}{Q} = \pi \Delta \nu \quad (41)$$

In addition the driver may be cut off for a time t_1 , and the amplitude decay measured. If the amplitude drops from P_0 to P_1 , then

$$\alpha = \frac{1}{t_1} \ln \left(\frac{P_0}{P_1} \right) \quad (42)$$

Another indication of Q can be obtained from the amplitude attained for given conditions, since the amplitude is inversely proportional to the decay constant. Normalization is needed, but trends can be checked.

The values of Q obtained in this manner agree quite well. All show the same behavior - there is an irregular, appreciable change during a test run, so that the damping is obviously changing drastically.

One advantage of this system is that stable propellants can be characterized. Unstable ones can also be studied by using the driver with a 180° phase shift imposed on the driver whenever the amplitude reaches a critical value. Some values of admittance should be available shortly.

Another cavity's pressure behavior was used at Thiokol in an attempt to obtain an acoustic admittance (217). The study was based on a method of O. K. Mawardi (218), which is outlined in an appendix of (217). The method uses a small, heavy-walled metal cavity (20 cc), and was originally intended for use with inert sound absorbers (Fig. 37). A great deal of difficulty was encountered when the equipment was used with burning propellant because of the hot gases generated. Combustion "noise" proved to be high enough to damp out meaningful pressure variations. Some data were obtained over part of the frequency range, but no admittance values could be calculated because of the unknown effect of the vent holes used to release the propellant gases.

Investigators at AeroChem attempted to measure the response function of the propellant surface by measuring the effect on an acoustic signal from a speaker when a sample is burning in an anechoic chamber (219). No results were obtained, because the minimum detectable level change corresponded to an admittance of approximately 2.5×10^{-3} rayls (220). An admittance of 10^{-6} rayls would cause a power change which was approximately 4×10^{-4} of the minimum detectable power change.

Converse (221) has also attempted to use the pressure in a cavity to obtain acoustic admittance, but his external excitation source is of a different type than the speakers used by the three investigators just mentioned. In the Converse experiment, a piece of propellant is glued to the face of a reciprocating piston which closes one end of a long pipe. The amplitude and frequency of the piston movement are variable. To run the experiment, the propellant is ignited with the pipe in motion and the pressure-time trace in the tube is used to give a value of the propellant response function. No measured values have been reported as yet, but it appears that determination of the acoustic losses in the pipe will be rather difficult.

B. Burning-Rate Effects

The experiments mentioned thus far deal with the effect of the test propellant on the acoustics of a cavity. Experiments have been carried out in which the burning of the test propellant was observed under oscillatory pressure conditions.

Diederichsen (222) (223) bases his investigation of the propellant on the behavior of the propellant flame during pressure changes generated by a loudspeaker. The object is to measure the instantaneous rate of energy release from a propellant strand burning under oscillating pressure. Diederichsen comments (222) that the regression rate of the condensed phase is not an accurate indication, because the amount of unburnt pyrolyzed products is probably varying during a cycle. As a result, he uses the variation of the light output from the reaction zone as an indicator of energy release. Some preliminary results have been reported (223). Errors arise from the connection of light output to reaction rate, the sensitivity to wavelength used, and obscuration of the reaction zone by the burnt gases.

A similar experiment was discussed by Schmidt and Wolfhard (224), who planned to measure infra-red radiation inside a chamber with oscillating pressure. By studying the radiation output vs. pressure, they hoped to be able to obtain any lags which might exist. No results have been reported to date.

Some experimenters have endeavored to measure the effect of oscillating pressure on instantaneous mass burning rate, but in a situation where no velocity-coupled erosive effects could interfere. As will be shown in the next Chapter, the experiment is almost doomed from the start by the accuracy required.

Nachbar (225) has attempted to measure the instantaneous burning rate of a propellant at one end of a T-burner type configuration (Fig.38), using optical techniques. Even with great care, he has been unable to obtain any but steady-state results when operating at frequencies near 1500 cps.

Watermeier (226) also tried to make optical measurements of burning rates for a propellant in an optical strand burner with a rotating exhaust valve furnishing the oscillating pressure. Once again, only average burning rates were obtained.

IV. Combustors with External Single-Pulse Wave

The experiments covered thus far have all been concerned with the response of the propellant to an oscillatory pressure, either self-excited or external in origin. From an experimental point of view, determination of a response function would be simplified if only a single pressure change were involved, such as from a shock or expansion wave. One major difficulty with this type of experiment lies in the fact that, as mentioned earlier, an amplitude change of about 1% upon reflection of a wave from a burning solid propellant is to be expected, which places rather stringent requirements on the accuracy of the recording equipment used. Some calculations to support this point will be given later.

The first to try the use of a single pulse was Landsbaum (227). He calculated the effect of a shock wave, represented by a pressure step,

on the burning rate of a solid propellant, assuming that the burning rate was controlled by temperature distribution in the solid, especially at the surface. It was found that any transient period in the burning rate would last less than 10^{-3} seconds, making experimental observation extremely difficult. Some attempts were made to obtain instantaneous burning rates using high-speed photography, but smoke, tube movement, and insufficient lighting defeated the experiment.

Agoston (228) investigated the effect of a weak pulse on the burning of solid propellant at atmospheric pressure, using an exploding wire as the source of the disturbance. He used a shadowgraph in an attempt to find any variations in gas behavior. No results were obtained.

Agoston then used the same concept of a small disturbance (peak pressure less than 1% of ambient) in an attempt to obtain a value of acoustic admittance (229). In this work, which was continued by Muller (230), the frequency spectrum of the incident and reflected pulse, as recorded by a pressure transducer, was analyzed by taking Fourier components. It was hoped that the admittance could be obtained from the wave analysis. However, most of the project was apparently involved with sorting out the effect of the sample from other termination effects, such as the mounting, and from tube losses. The tests run with a burning solid propellant as the end sample were failures, and led to the conclusion that the technique was impractical for measurement of solid-propellant acoustic admittance (231).

Lawhead has performed experiments using a shock tube as the source of the pressure pulse (232) (233). Very weak (pressure ratios less than 0.02) shocks were used, with mean pressures of the order of 450 psi. Once again, the pressure-time history would yield a transfer function which could be related to the acoustic admittance of the burning surface. However, it was found that the transfer function differed widely from the classical reflection coefficient for inert samples, so that calculating an admittance for a burning sample would have given a large error. The difference was ascribed to non-linear effects in the finite-amplitude (20-psi) disturbance. Despite this initial setback, work was continued to see if differences in pulses reflected from various burning-propellant surfaces could be detected. An interesting arrangement (shown in Fig. 39) using a wave-splitter technique was set up, so that pressure measurements could be made at the burning surface. Two transducers are used, one of which experiences only the incoming wave and a small reflected wave, since the tube termination in the lower section is sufficiently far downstream to allow the desired measurements to be made before the reflected pulse reaches the transducer. The difference in the signals from the two transducers is used to obtain the effect of the burning surface. The small piece of solid propellant which is burning downstream is designed to give similar hot-gas conditions in the two halves of the tube. Thus far, only qualitative results have been obtained, but claims are made that some difference in the response for an aluminized and a non-aluminized sample has been detected.

In closing this summary of the experimental studies of pressure-surface-flame coupling, it should be observed that many of the experiments

are on rather tenuous ground, since the accuracy required is greater than that attainable. In order to save time (and money), careful consideration should be given to the feasibility of an experiment before undertaking any construction of equipment, facilities, etc. Some consideration was given to a number of experimental techniques which might have been used here, and the results of this study are given in the next section, which forms Chapter VI of this report.

CHAPTER VI

CONSIDERATION OF POSSIBLE EXPERIMENTS TO MEASURE ACOUSTIC ADMITTANCE

I. Introduction

At the outset of the program on solid-propellant combustion instability at the Guggenheim Laboratories, some decisions had to be made as to the direction of experimental research. It was decided that the study of stability boundaries was not a profitable one and did not fit the facilities available. A direct study of the response function was chosen as the direction of research, and some different experiments were analyzed as to their feasibility. Among these were:

- (1) An "acoustic" method, especially the detuning of a resonant "organ-pipe" by burning a solid-propellant sample at one end wall.
- (2) Measurement of the modification of the pressure waveform of a shock wave reflected from the burning surface.
- (3) Measurement of the instantaneous thickness of a solid-propellant sample burning in an oscillatory manner.
- (4) Measurement of the outflow velocity with illuminated or self-luminous tracers.
- (5) Observation of the pulsation in stagnation temperature or composition of gas emitted under oscillatory pressure.

In this section, the experiments will be described, together with their respective advantages and limitations. The accuracy required for success will be discussed and compared with the accuracy attainable with equipment at the time of the study (Spring, 1961).

II. Acoustic Methods

The measurement of acoustic impedance or admittance is a long-standing experimental problem in the field of acoustics, dating back to 1919, when the impedance concept was introduced into the field. As a result, acousticians have evolved a number of measurement techniques, some of which are summarized by Beranek (234).

The techniques can be put into three main groups. In the first, data are taken at or near the surface of the sample in a sound field. In the second, data are taken at points in the sample container with a sound field present. In the third group, comparative measurements are taken between the effect of the sample and the effect of a material with known impedance on an acoustical circuit.

BLANK PAGE

The first group involves what could be called surface methods. In their simplest form, the pressure and particle velocity at a point are measured, giving impedance directly. However, this technique is never used in acoustics, because instruments small enough to avoid disturbing the sound field by their presence have not been built as yet. Another type of surface method is the Mawardi one (218), an adaptation of which was attempted at Thiokol, as previously mentioned (217).

The second group is based on what is referred to as the "acoustic transmission line," in analogy with electric circuits, and is based on the use of a smooth rigid-walled tube, with diameter small compared to the wavelength of sound involved. Losses at the walls are considered small, and some of the equations for this case have been developed in Appendix A. One experiment can be visualized as follows.

Consider a tube with a driver at $x = 0$ and a termination of unknown impedance at $x = \ell$, the other end of the tube. Denoting the position along the tube by a subscript, the impedance ratio of the unknown is $\Theta_\ell = Z_\ell / Z_0$ and the phase parameters are given by:

$$\Theta_\ell = k_\ell = \tanh [\pi (\alpha_\ell - i\beta_\ell)]. \quad (43)$$

Assuming no attenuation along the tube, $\alpha = \alpha_\ell$. However, β changes along the tube length since:

$$\beta = \beta_0 - 2x/\lambda = \beta_\ell + (2/\lambda) (\ell - x), \quad (44)$$

so that, at half-integral β , there is a maximum pressure fluctuation, while the fluctuation is minimum at integral values of β . Where the pressure amplitude is a minimum:

$$\begin{aligned} |p| &= 2P_+ e^{-\pi\alpha} \sinh(\pi\alpha_\ell) \\ (2/\lambda) (\ell - x) &= n - \beta_\ell, \end{aligned} \quad (45)$$

while at maxima:

$$\begin{aligned} |p| &= 2P_+ e^{-\pi\alpha} \cosh(\pi\alpha_\ell) \\ (2/\lambda) (\ell - x) &= n + 1/2 - \beta_\ell. \end{aligned} \quad (46)$$

The variation with pressure along the tube is shown in Fig. 40. A standard way of measuring impedance is based on measuring the sound pressure at points where p is a maximum or a minimum and measuring the distances from these points to the end of the tube ($x = \ell$) where the sample is located (235). An analysis of the experimental errors in the technique has been made by Scott (168), who used a travelling microphone probe as pressure detector.

In the case of solid propellant, information on the imaginary part of the impedance could be found by obtaining a new resonant frequency for the tube with burning propellant at one end and by comparing this frequency to the natural frequency of the tube containing gas with the same speed of sound as the hot propellant gases, but with a rigid wall at the $x = \ell$ end. Since a rigid wall has $\beta_\ell = 1/2$, the natural frequencies are

$$f_n = \frac{c}{4\ell} n \quad (n = 1, 3, 5, \dots)$$

For perfect reflection $\alpha = 0$, while for partial reflection $\alpha > 0$, causing imperfect cancellation and reinforcement.

Another transmission-line technique is suggested by Beranek (234), who keeps the pressure detector fixed at the source instead of moving, and varies the frequency of oscillation instead. It can be shown (by a lengthy derivation involving solution of the inhomogeneous wave equation by expansion in Fourier series and use of orthogonality conditions, based on the lack of transverse waves) that the sound-pressure variation at $x = 0$ with a frequency variation is given by:

$$|p|^2 = \frac{\frac{K \omega^2}{\ell^2}}{4\omega_m^2 k_1^2 + [\omega^2 - (\omega_m^2 - k_1^2)]^2} \quad (47)$$

where

K = constant of proportionality

ω = angular frequency

ω_m = normal angular frequency of longitudinal vibration for test conditions

ℓ = tube length

k_1 = total damping constant.

For maximum pressure,

$$\omega_m = \sqrt{\omega^2 - k_1^2} \quad (48)$$

The driver frequency is varied and the pressure at $x = 0$ is measured, giving the points where the square of the pressure at the source drops off to $1/w$ of the resonant value, giving:

$$\left(\frac{p_{\max}}{p} \right)^2 = \left(\frac{p_{\max}}{p} \right)^2 = w, \quad (49)$$

where the expected variation is shown in Fig. 41.

Assuming that the impedance remains constant, since the curve is obtained for a small frequency range, and assuming that the pressure drop on either side of the maximum is nearly symmetric:

$$k_1 \approx \pi \frac{(\gamma'' - \gamma')}{\sqrt{w - 1}} \quad (50)$$

Two pressure vs. frequency curves are traced, one with the test sample at the end $x = \ell$, the other with a blank wall at $x = \ell$. For the blank-wall case, a damping constant k_o and a resonant frequency γ_o are obtained, such that

$$\begin{aligned} k_m &= k_1 - k_o \\ \gamma_o &= 2\gamma_o \ell \end{aligned} \quad (51)$$

Write the impedance ratio of the test sample as

$$\begin{aligned} \left(\frac{z}{\rho c} \right) e^{-i \left(\phi + \tan^{-1} \frac{k_m}{\omega_m} \right)} &= \coth \left[(k_m + i \omega_m) \ell / c \right] \\ &= \coth \left[(k_1 - k_o) \frac{\ell}{c} + \frac{i \omega}{c} \left\{ \left(1 - \frac{k_1^2}{2 \omega^2} \right) \ell - \ell_o \right\} \right] \end{aligned} \quad (52)$$

Writing this in the form $\coth [C + iD]$, then

$$C = \frac{k \ell}{c}$$

$$D = -\frac{\omega}{c} \left\{ \ell_0 - \ell \left(1 - \frac{k_1^2}{2\omega^2} \right) \right\} \quad (53)$$

The curve-width method would be used for the determination of impedance as follows. With an oscillator tuned to vary the frequency output of a driver at the $x = 0$ end, the propellant, whose thickness is short compared to the tube length, is ignited. Burning takes place in the closed tube until such time as the test pressure is reached, at which time a relief valve, with area sufficient to choke the flow at the desired pressure, is opened automatically. While burning continues, a resonance curve is traced out. Immediately after burning ceases, the relief valve closes, and another resonance curve is traced out. The tube is then flushed clear of the hot gases.

Consider now some of the sources of error involved. Inquiries made to various electronic firms revealed that the least error available among transducers designed to operate near 100 psi was 1%, the value for the Massa M141A, which uses an ammonium di-hydrogen phosphate crystal as the sensing element. An Atlantic Research Corporation transducer, the LC-60, using lead zirconate as the sensing crystal, quotes $\pm 2\%$ to 100 psi. In both cases, there will be a variation in output due to the temperature change likely to occur in the microphone. The output could be measured with a logarithmic voltmeter, such as the Hewlett-Packard 400L, which has an accuracy of $\pm 1\%$ of full scale, or $\pm 2\%$ of reading, whichever is more accurate. The frequency error of the oscillator will be of the same order. There is likely to be a shift in sound speed due to the temperature gradients in the tube, and the relief valve will contribute an unknown impedance to the circuit when open, which is practically impossible to calculate, since the impedance of orifices is highly non-linear above 65db (236), (237). A propellant thickness of 1 centimeter would contribute a variation of 4% in the length for the tube needed to give resonance at 1000 cps, which is significant in the light of Beranek's observation (238) that a variation in tube length of less than 0.4% caused a five decibel dropoff in sound pressure. The temperature irregularities are serious in the light of Scott's observations on the conditions necessary to obtain 2% accuracy (168). The change in damping of the tube with and without burning, or even during burning, can be quite large, remembering Foner's results (213).

Some consideration must also be given to protecting the driver unit, both from the hot propellant gases and from the pressure. The pressure effect could be cancelled by having contact with the tube on both sides of the diaphragm or by allowing a regulated pressure on the

back face. On the front side, protection from the hot gases can be obtained by having a low-density, low-thermal-conductivity liquid with the fluid mass kept to a minimum, although sufficient fluid should be available to prevent boiling away of the insulator, with resultant damage to the phenolic diaphragm of the driver.

Typical of the third group of techniques, the comparison methods, is the "reaction on source" technique of Fay and White (239). In this technique, the unknown acoustic load is coupled to a transducer. Either the length of the tube connecting the transducer to the sample or the driving frequency is varied, and the electrical impedance of the transducer is measured. From these values of electrical impedance, a value of acoustic impedance for the sample can be obtained from the properties of the transducer diaphragm. This method, however, requires extreme temperature- and length-control.

To consider the feasibility of the "acoustic" methods, the magnitude of phase shifts to be expected must be calculated, which can be obtained by a purely physical argument or by using the Hart-McClure estimates of admittance.

From a physical standpoint, consider the magnitude of the change in gas efflux velocity caused by a pressure fluctuation. Assuming a sound pressure of 10 psi at 100 psi mean pressure, with a mean burning rate of 0.5 centimeters per second and a pressure index of 0.5, the pressure change would be expected to vary the burning rate by about 0.025 cm/sec. With a density ratio of 1000:1 between propellant and gas, this implies a change in gas efflux velocity of 25 cm/sec, which must be compared with the particle velocity present in the sound wave, as given by equation (A-13)

$$p = \rho c \left(\frac{\partial \xi}{\partial t} \right) \quad (A-13)$$

Taking $p = 7 \times 10^5$ dynes/cm²

$\rho = 0.001$ gm/cm³

$c = 10^5$ cm/sec,

a particle velocity of 7000 cm/sec results, so that the change in efflux velocity is only about 0.3% of the particle velocity, suggesting that little phase change will be caused.

The values estimated by Hart and McClure for admittance are of the order of 10^{-5} - 10^{-6} rayls, which has been confirmed by T-burner experiments (56). As a result, θ , the real part of the impedance, for zero phase angle is of the order of 10^5 . Expansion of the equation

$\theta - i\lambda = \tanh [\pi (\alpha - \beta i)]$ shows that values of the magnitude can only be obtained for β very close to 0.50, the blank-wall value, and α very close to 0, the blank-wall value.

It will be noted that all calculations have been made for 100 psi burning with 100 cps oscillations imposed. As the frequency increases, the length of the resonator tube decreases if a small number of modes are to be dealt with, making finite size effects more important, and cutting down on the attainable precision. However, McClure's model leads to the conclusion (85) that appreciable phase shifts occur only in the region above 10,000 cycles, the frequency of the fundamental mode in a 1-inch-length tube. In order to avoid transverse-mode effects, the diameter would have to be less than 5 millimeters (168). At higher pressures, greater power would be required to produce the same percent fluctuation in pressure as the mean pressure level increases. In addition, a smaller velocity perturbation results at higher pressure, since the burning rate increases with pressure to a power less than one, but the density increases directly with pressure.

In general, then, the "acoustic" methods and, more particularly, the "detuning" method do not appear applicable, largely because the propellant burning surface resembles a blank wall (acoustically) quite closely, especially at the point where information is most desired--in the region where the changeover occurs from a stable region to a possible unstable one. The acoustician would have great difficulty obtaining values of the expected magnitude under ideal conditions, and the effect of the severe thermal gradients and corrosive gases present in a "hot" experiment make the best techniques quite inapplicable.

III. Shock-Wave Reflection

The use of a single pulse in an attempt to measure a propellant response function, as applied by other experimenters, has been described earlier (227), (230), (233). It may be seen that little success has been attained, and some calculations will show why.

Consider a shock wave moving in a constant area duct with a velocity U (240), (241). Assume that the wave is a "discontinuity" and that the following gas properties before and after the shock are denoted by subscripts 1 and 2, respectively.

Then mass continuity is:

$$\rho_1(U-u_1) = \rho_2(U-u_2) \quad (54)$$

Momentum conservation is:

$$p_2 - p_1 = \rho_1 (U - u_1) (u_2 - u_1) \quad (55)$$

Eliminating, in turn, u_2 , u_1 , and U from (54) and (55),

$$U - u_1 = \left[\frac{p_2 - p_1}{(\rho_1/\rho_2) (\rho_2 - \rho_1)} \right]^{1/2} \quad (56)$$

$$U - u_2 = \left[\frac{p_2 - p_1}{(\rho_2/\rho_1) (\rho_2 - \rho_1)} \right]^{1/2} \quad (57)$$

and

$$u_2 - u_1 = \left[\frac{(p_2 - p_1) (\rho_2 - \rho_1)}{\rho_2 \rho_1} \right]^{1/2} \quad (58)$$

Energy conservation across the shock gives

$$e_2 - e_1 = \frac{(p_1 + p_2) (p_2 - p_1)}{2 \rho_1 \rho_2} \quad (59)$$

Assuming that

$$\frac{p}{\rho} = RT,$$

then, for ideal gases,

$$e = c_v T = \frac{c_v p}{R \rho} \quad (60)$$

Putting (60) into (59),

$$\frac{\rho_1}{\rho_2} = \frac{(\gamma + 1)p_1 + (\gamma - 1)p_2}{(\gamma - 1)p_1 + (\gamma + 1)p_2}$$

Defining $\sigma \equiv p_1/p_2$, then

$$M_1 = \frac{U - u_1}{c_1} = \left[\frac{(\gamma + 1)/\sigma + (\gamma - 1)}{2\gamma} \right]^{1/2} \quad (61)$$

$$\eta \equiv \frac{u - u_2}{c_2} = \left[\frac{(\gamma+1)\sigma + (\gamma-1)}{2\gamma} \right]^{1/2} \quad (62)$$

$$-\zeta \equiv \frac{u_2 - u_1}{c_2} = \frac{2(1 - \sigma)}{[2\gamma \{ (\gamma+1)\sigma + (\gamma-1) \}]} \quad (63)$$

where c is the speed of sound.

In addition, defining $\sigma' \equiv p_2/p_1$, then (62) and (63) become

$$\eta' \equiv \frac{u - u_1}{c_1} = \left[\frac{(\gamma+1)\sigma' + (\gamma-1)}{2\gamma} \right]^{1/2} \quad (64)$$

$$\zeta' \equiv \frac{u_2 - u_1}{c_1} = \frac{2(1 - \sigma')}{[2\gamma \{ (\gamma+1)\sigma' + (\gamma-1) \}]} \quad (65)$$

These variables are interrelated by

$$\zeta = \frac{2(\eta^2 - 1)}{(\gamma+1)\eta} \quad (66)$$

$$\zeta' = \frac{2(\eta'^2 - 1)}{(\gamma+1)\eta} \quad (67)$$

As a first step in the shock calculations, the pressure behind a shock wave reflected from a rigid end wall must be determined. Conditions before and after reflection are shown in Fig. 42.

Boundary conditions require the velocity at the wall to be zero before and after reflection, so that

$$-\zeta = \frac{u_2 - u_1}{c_2} = \frac{u_2}{c_2}, \text{ since } u_1 = 0$$

and

$$\zeta' = \frac{u_3 + u_2}{c_2} = \frac{u_2}{c_2}, \text{ since } u_3 = 0.$$

Therefore,

$$\zeta' = -\zeta \quad (68)$$

From (66) and (67), (68) then gives:

$$\gamma - \frac{1}{\gamma} = \frac{1}{\gamma'} - \gamma' \quad (69)$$

which has the non-trivial solution

$$\gamma' = \frac{1}{\gamma} \quad (70)$$

From (62) and (64), the pressure ratio p_3/p_2 is given by

$$\sigma' = \frac{(3\gamma - 1) - (\gamma - 1)\sigma}{(\gamma + 1)\sigma + (\gamma - 1)} \quad (71)$$

The same type of analysis can be used to predict the pressure waveform of the reflected shock for various propellant responses.

Consider a piece of propellant burning at 100 psi with a burning rate of 1 cm/sec. This sample is mounted on the end wall of a shock tube, down which a shock propagates, giving a pressure rise to 150 psi. First calculate the pressure behind the reflected shock for the case of a rigid, non-burning sample to give some idea of conditions to be encountered. Using $\gamma = 1.25$ and $\sigma = 0.667$, (71) gives $\sigma' = 1.46$ or $p_3 = 220$ psi.

Various shock velocities must be calculated before propellant effects can be incorporated. Assume that the gases are initially at 2500°K, and that the speed of sound in the gases is 1000 m/sec. The pressure ratio of 1.5 across the original shock implies a Mach number of 1.204 for the velocity of the gases flowing into the shock, from (61). The velocity of sound in the gases after the shock may be found from the temperature ratio:

$$\begin{aligned} \frac{T_2}{T_1} &= \frac{\left(1 + \frac{\gamma - 1}{2} M_1^2\right) \left(\frac{2\gamma}{\gamma + 1} M_1^2 - 1\right)}{\frac{(\gamma + 1)^2}{2(\gamma - 1)} M_1^2} \quad (72) \\ &= 2.58 \end{aligned}$$

Assuming no change in gas properties,

$$\begin{aligned} c_2 &\approx \sqrt{2.58} \quad c_1 \\ &= 605 \text{ m/sec.} \end{aligned} \quad (73)$$

If there is a burning rate of 1 cm/sec originally, and a density ratio of 1000:1 is assumed, then $u_1 = 10$ m/sec, flowing into the shock. From (61), $U = 1194$ m/sec.

From (63), $\sigma = 0.667$ gives

$$-\zeta = \frac{u_2 - u_1}{c_2} = 0.421$$

From (68),

$$u_2 - u_1 = 676 \text{ m/sec.}$$

so that

$$u_2 = 666 \text{ m/sec.}$$

Calculations can now be made as to the effect of varying the boundary condition after the reflection, i.e., of varying u_3 . If it is first assumed that $u_1 = u_3 = 10$ m/sec, some definite comparison with the non-burning case can be obtained. Equation (46) is used, as ζ' is first found, then σ' is obtained by expanding and solving the resulting quadratic equation. For $u_1 = u_3 = 10$ m/sec, the end-wall pressure rises to 249.8 psi. This case corresponds to a dynamic pressure index of 1, where it is assumed that the burning rate-pressure relation can still be written in the form $r = ap^n$ for rapid changes in pressure, although n may vary markedly from the steady-state value, at least momentarily.

The latter value of pressure may now be used as a representative one in calculating possible mass-burning-rate changes and resulting efflux-velocity changes. Various cases must be considered. For the case where $n = 0.5$, the propellant burning rate will rise to 1.58 cm/sec, with efflux velocity dropping to 632 cm/sec, since the density change is greater than the burning-rate change. An efflux velocity of 632 cm/sec gives an end-wall pressure of 249.2 psi, using the above-described calculation procedure.

The pressure resulting from 2 extreme cases may also be calculated. The first case is for a burning rate unchanged after reflection, so that the efflux velocity drops to 400 cm/sec, with a pressure of 248.8 psi resulting. The second case is for a dynamic index greater than 1, so that the propellant burning rate momentarily rises faster than the pressure. A calculation was made for a rise in efflux velocity of 2000 cm/sec, which represents a dynamic index of 1.75. The mass flow increase gives a resultant pressure of 251.6 psi.

At this point, it is helpful to tabulate the results of the foregoing calculations.

TABLE I

Pressure Behind Reflected Shock for $P_{\text{initial}} = 100 \text{ psi}$,

$P_{\text{shock}} = 150 \text{ psi}$, $r_b = 1 \text{ cm/sec}$

<u>Dynamic Index</u>	<u>Pressure (psi)</u>
$n = 0$	248.8
$n = 0.5$	249.2
$n = 1.0$	249.8
$n = 1.75$	251.6

As is readily seen, the wide range of response functions chosen has resulted in a narrow range of pressures - only a 1% variation. Moreover, the range from $n = 0$ to $n = 1$ is only 0.4%.

The calculations of this simple model are supported by the recent calculations of Agosta (242), who found very little change in reflected-shock strength or in reflected-wave velocity. The only effects of varying the dynamic index were to change the velocity of the contact surface and gas density behind the reflected wave.

The lack of pressure variation which is likely to be measurable makes it unlikely that a response function can be obtained with a shock wave and ordinary instrumentation, since the over-all effect is barely detectable and any hope of obtaining reaction kinetics and phase lags from a pressure-time history seems to be out of the question because of the times involved and the accuracy required. As a result, any thought of using a shock wave to obtain admittance was discarded.

IV. Instantaneous Thickness Measurement

The acoustic response of a burning solid propellant could be determined, without making measurements in the gas stream, by making a direct measurement of the thickness of a propellant sample as a function of time. Such a measurement, if performed with sufficient space and time resolution, would make possible a calculation of the mass burning rate at any instant, thereby giving exact information as to the response of the propellant to a pressure variation. It will be assumed that little mass is "stored" in the form of intermediate gaseous products. As will be seen, the only method which has any feasibility whatever would respond, in part, to any possible "stored" mass.

A large number of methods for measuring thickness is available, and industrial requirements have caused much interest in the improvement of thickness-measurement techniques. A typical problem is in steel-rolling mills, where automatic control may, for example, be effected by using load cells to signal any variations from a desired norm (243).

Two surveys of thickness-measurement techniques have been published, one by NBS (244), the other by ASTM (245). The ASTM publication is concerned with nondestructive techniques and lists over 250 patents and 500 references, while the NBS survey is more general and more recent, although only 229 references are listed.

The first consideration must, of course, be a determination of the precision and accuracy needed for a meaningful measurement of propellant response. Assume that the measurement is to be made at 100 psi, with pressure oscillations of 100 cps frequency and 10 psi amplitude, and that the propellant burns at 1 cm/sec under steady-state conditions. During one cycle, then, the propellant will burn 10^{-2} centimeters, or 100 microns. However, to obtain meaningful data, measurements should be taken ten times during a cycle. During the interval between measurements, the propellant will have regressed 10 microns under steady-state conditions, so that measurements to about 1 micron are needed to obtain the deviation from steady-state burning. The precision needed, then, corresponds to an accuracy of 0.01% of the total thickness for a 1-cm-thick sample, and an average accuracy of 0.02%. Measurements must be repeated at intervals of about 1 millisecond.

A. Optical Techniques

First consideration can, of course, be given to an optical method of determining instantaneous mass burning rate. However, the accuracy required, as shown above, makes this technique impractical, since the resolution and magnification required to attain the desired accuracy can be obtained only for conditions where a great deal of time is available and where no gas density gradients exist. Such considerations explain the previously-mentioned failures of Nachbar and Watermeier to obtain any but average regression rates.

B. Weighing Techniques

Another technique could be based on determining the weight of a burning propellant sample as a function of time, since the mass burning rate would be known directly. To see if this is feasible, assume a button of propellant 10 cm^2 in area, with a burning rate of 1 cm/sec. In one millisecond, the button would decrease in thickness by 10 microns, corresponding to a propellant consumption of about 2×10^{-2} grams. Therefore, a sensitivity of 2×10^{-4} grams would be needed in the weighing system to determine the response function for 1000 cps oscillations. Assuming that a strain gage system could be designed, the minimum readable deflection is of the order of 10^{-6} centimeters, using interferometric methods, requiring a wire of about 100-micron diameter to give this deflection. Moreover, since the weighing system would be a second-order system, it would have a natural frequency given by (3)

$$\omega_n = \frac{1}{2\pi} \left(\frac{k}{m} \right)^{1/2} \quad (74)$$

For a total system mass of 10 grams, which is close to a minimum, equation (74) gives a natural frequency of about 30 cps, which is obviously far too low to enable consideration to be given to weighing systems.

C. Ultrasonic Techniques

The use of ultrasonic waves to measure thickness is a recent advancement. Since the ultrasonic technique's popularity is partially based on the fact that access to only one surface of a test sample is required, the concept is a reasonable one for the desired experiment.

Two different techniques are used in ultrasonic thickness gaging - the resonance and the pulse-echo methods. In the resonance technique, continuous compressional waves are transmitted into the material from one side. The frequency is varied until a twice-reflected wave leaves the first material surface in phase with another incoming wave, resulting in standing waves being set up in the sample, with a concomitant increase in amplitude. The pulse-echo technique, on the other hand, uses discrete pulses of sound, and the thickness is determined by the time required for the pulse to be reflected from the other surface and received at the initial surface. Both techniques have their advocates, and accuracies of 1% are claimed (247), (248).

In order to estimate accuracies available, consider the various parameters involved in an ultrasonic thickness measurement. First of all, an operating frequency must be chosen. The Non-Destructive Testing Handbook recommends the following ranges for various applications (249):

gaging thick materials	.5 - 3 Mc.
gaging thin materials	3 - 25 Mc.
maximum accuracy	10 - 25 Mc.
gaging coarse structures	.5 - 3 Mc.

It is quickly seen that there is some contradiction for the case of a thin heterogeneous propellant sample. There is, however, a definite limitation placed on the frequency chosen, since, due to scattering losses in heterogeneous materials, the frequency cannot be too high or the penetration becomes too low (250). Some experiments with solid propellant for flaw-detection purposes encountered great difficulty transmitting a 2-Mc signal (251), and the range generally used for propellants by experimenters seems to be from 200 kc to 2.25 Mc (252).

The frequency chosen has an effect on the measurement for a number of reasons. First of all, the beam from the transducer will diverge with an angle which depends directly on the velocity of sound in the test sample and inversely on the transducer diameter and frequency used (253), so that small discontinuities cannot be resolved. Second, if the resonance technique is used, there will exist a minimum measurable thickness for a given frequency, since resonance cannot occur within less than a certain distance. Finally, the accuracy will be affected by the fact that the instrument must detect and display the small frequency change caused by a

thickness change. Under ideal conditions, and over a narrow range, a 2-kc change can be detected (254), which is 1% for a 200-kc signal.

There are a number of problems influencing the possible use of ultrasonics. One of the most important is the need for coupling between the transducer and the material under test. Variations in the speed of sound of the test medium due to crystalline structure (255) or changes in frequency (256) can also affect the accuracy. The lack of a clean signal, resulting from variations in composition or from irregular reflecting surfaces (257), makes accurate determinations of resonance points or times of arrival of an echo almost impossible.

In summation, the accuracy of ultrasonic thickness-gauging is limited by instrument resolution, calibration, variations in the velocity of sound in the medium, variations in the contact between the transducer and sample, scattering and dispersion in the sample, and spreading of the beam. All these effects tend to limit accuracies to the order of 1% at best. In the case of a burning solid-propellant sample, some resolution would be lost, since time to attain sharp tuning to resonance is not available. The irregular surface would cause a confusing reflection pattern, but the most serious problem would undoubtedly be the maintenance of a good contact between the propellant and the transducer throughout the test. It must be concluded, therefore, that the use of ultrasonic thickness-gauging is not applicable to the determination of the response of the burning of a solid propellant to a pressure change.

D. Radiation-Absorption Technique

The next technique to be considered for measuring thickness is probably the most popular non-contact method in use today. It involves the absorption of penetrating radiation or of beams of high-energy particles, such as X-rays, gamma rays, beta rays, etc. In general, the method is based on the exposure of the sample to a source of radiation, with the amount of radiation which penetrates the sample being recorded by a detector. The penetrating radiation is an inverse function of the weight per unit area of the intervening medium.

An up-to-date review of the field was given by Tenney at a 1957 ASTM symposium (258), and recent work in the field was studied through a use of the following sources: Physics Abstracts, Chem. Abstracts, Instrument Abstracts, Nuclear Science Abstracts, Nucleonics, Review of Scientific Instruments, Applied Science and Technology Index, and Applied Mechanics Review. Recent Russian scientific journals were also studied, but little information on thickness measurement was obtained.

The literature survey divulged a large number of recent references dealing with thickness measurement by absorption of radiation. Summaries of about 50 of these references, their accuracies, and the techniques involved are given in an earlier report (259).

Inquiries were also made to a number of companies as to the feas-

ibility of using their equipment or modifications thereof as a means of measuring propellant thicknesses to within 1 micron, with a measuring time of 1 millisecond. Some typical replies were:

- (i) Curtiss-Wright uses only ionization chambers to detect transmitted radiation, and the time constants involved are greater than $\frac{1}{2}$ second. From their experience, source irregularities and circuit noise will run to 1 - 2% of the signal (260).
- (ii) Industrial Nucleonics handles only ionization equipment, and the lower limit on time constants is 0.1 seconds at best (261).
- (iii) Radiation Counter Labs claims to be able to measure a 200-1000 mg/cm² thick sample in 0.2 seconds with 1% accuracy using β rays, if the sample thickness is constant during the measuring time. If γ rays are used, Geiger counters become feasible, with slightly shorter time constants possible. However, accuracies are only of the order of 1 - 10% with γ rays (262).

It is obvious that commercially-available equipment could not perform the desired experiment with the accuracy needed, so a consideration of the basic physics of the absorption technique is in order, so that possible designs might be evolved. The technique is outlined in Appendix C, together with a feasibility calculation for 100-psi operation with 100-cps oscillations superimposed.

The results of the calculations in Appendix C show that, although the art of measuring thickness has been developed to a high degree, high accuracy and rapid measuring times do not appear compatible, and the experimentalist wishing to make high-accuracy measurements rapidly is confronted by a situation such as would be encountered by a sailor who had found that Scylla and Charybdis had suddenly moved closer together, until no channel between them existed. The additional complication of high temperature and pressure, as well as relative inaccessability, make matters worse. It appears that the limitations of the system components are such that the thickness-measurement technique for determining response function is limited to possible use only at frequencies of the order of 100 cycles per second or lower, and that severe experimental difficulties are to be expected even at low frequencies.

V. Particle-Track Method

Observations of velocity profiles by means of luminous or illuminated particles have been used by a number of experimentalists to trace temperature profiles in laminar flames (263), (264), (265). The shapes of the flow pattern around various wings in low-speed wind tunnels have been studied with luminous tracers injected into the gas stream (266). Velocity profiles in liquid-propellant rocket motors have been studied by following solid particles in the combustion gases (267). The particle-tracking technique may be considered as a possible method of determining the response function of the burning solid-propellant surface.

The use of the track method consists of determining the velocity of the tracer as a function of time and position by either: (a) following individual particles through a number of frames from a movie film and determining velocity from the displacement-time history, (b) illuminating the flow field stroboscopically and determining the different velocities from the length of the lines which result on the film, or (c) following the progress of the tracer by a continuous-writing streak or strip camera, and determining velocities from measurements of the slope of the resulting curve (Fig. 43). In any one of the cases, a knowledge of the velocity and pressure as functions of time gives either the admittance directly or, together with the continuity-of-mass equation, gives a knowledge of the mass flow rate as a function of time. Hence, the reaction of the burning propellant to pressure fluctuations may be readily determined.

The setup shown in Fig. 44 is typical of the type which could be used. A flash bulb might be used because 25-milliseconds illumination (268) would allow recording of 10 periods at 500 cps, and would permit the following of 5 separate "families" of particles from the propellant surface through the viewing section. The use of a chopper to give periodic illumination makes velocity determinations far simpler, but steady light could be used to give a complete history of a particle, even though absolute measurements are harder. The focusing can be varied depending on the light requirements. In Fig. 44, a "pencil" of light is used, so that fewer particles will be under observation, leading to greater clarity in interpretation. Focusing on a point as opposed to a line might give better results.

The feasibility of using the particle-track method will depend upon the correctness to be expected from the results. To investigate the fidelity with which the particles follow the gas velocity, consider the classic Stokes equation for the motion of a spherical particle in a gas flowing with an imposed sinusoidal velocity variation (269).

$$\ddot{x} = \alpha(\bar{V} + \tilde{V} \sin \omega t - \dot{x}) \quad (75)$$

where \bar{V} = average gas velocity
 \tilde{V} = amplitude of gas-velocity variation
 $\alpha = 3\pi\mu D/m = 18\mu/\rho D^2$
 μ = gas viscosity
 D = particle diameter
 ρ = particle density

Equation (75) may be solved through the use of Laplace transformations, giving:

$$\dot{x} = \bar{V} (1 - e^{-\alpha t}) + \frac{\tilde{V}}{\sqrt{1 + \frac{\omega^2}{\alpha^2}}} \cos(\omega t - \phi) + \frac{\alpha \tilde{V} \omega e^{-\alpha t}}{\alpha^2 + \omega^2} \quad (76)$$

where $\phi = \tan^{-1} \left(\frac{\alpha}{\omega} \right)$.

The last term in equation (76) is small compared with the first two terms, since the magnitude of α is such that the exponential decays very rapidly and the preexponential term is less than unity.

Equation (76) indicates that three factors will affect the accuracy with which observed particle tracks will reflect the true gas-velocity history. In the first term of (76), the expression $(1 - e^{-\alpha t})$ represents the extent to which the particle attains the steady gas velocity. In the second term, the expression $(1 + \omega^2/\alpha^2)^{-1/2}$ represents the accuracy with which the particle track will indicate the amplitude of the gas-velocity oscillations, while ϕ represents the phase lag between the gas-velocity oscillation and the particle-velocity oscillation. The effects of these factors may be considered separately.

To study the error from the first term, the time and distance required for a particle to reach 95% of the gas velocity were calculated, using 500 cm/sec, $\rho = 2.8$ gm/cc (MgO), and $\mu = 0.063$ centipoise (an average viscosity based on calculated (270) gas composition and temperature). The results are as follows:

Table II

Time and Distance to Reach 95% of Gas Velocity

<u>Particle Diameter (microns)</u>	<u>t (msecs.)</u>	<u>x (cm.)</u>
5	0.24	0.08
10	0.95	0.32
20	3.79	1.30

It should be mentioned that the distances are large compared to the combustion-zone thickness, thereby justifying the use of a steady flow, rather than a rapidly-accelerating flow. The change in drag coefficient due to the acceleration is only important during the initial period (271).

To study the error from the second term, calculations were made to determine the magnitude of the phase lag, as well as the amplitude of \dot{x} compared to \dot{V} . Typical results are:

Table III

Particle in Oscillating Gas Flow

<u>D(microns)</u>	<u>Phase Lag</u>		<u>Relative Amplitude</u>	
	<u>100 cps</u>	<u>500 cps</u>	<u>100 cps</u>	<u>500 cps</u>
5	2.8°	13.9°	1.00	0.91
10	11.2°	44.7°	0.98	0.71
20	38.4°	75.9°	0.78	0.45

The use of 90% relative amplitude gives the criterion that $\omega/\alpha < 0.5$. This criterion leads to a 26° maximum limit in phase error, and also leads to the particle attaining 95% of the steady gas-flow velocity in less than $1/4$ period. Substituting, the criterion leads to the requirement that

$$\rho D^2 \omega < 8.8 \times 10^4 \text{ (D in microns),}$$

which is plotted in Fig. 45. The effect of the density of the particle should be noted. As a matter of interest, the imposition of a 95% relative-velocity amplitude leads to the criterion $\omega/\alpha < 0.1$, giving a phase error of about 6° , and equilibration times on the order of $1/20$ period. This criterion drops the maximum frequency for a given particle by a factor of 5.

As a check on the accuracy of these calculations, two previous results may be mentioned. Altman studied the effect of particle size on the accuracy of tracking a laminar flame (272), and found that a 2-micron particle would be needed to characterize an idealized laminar flame with a temperature plateau. Some photographs of 2-micron and 10-micron particles in a 2000-cps sound field revealed that the 10-micron particles did not respond at all, while particles which were 2 microns and smaller in diameter had varying degrees of response to the pressure fluctuations (273).

It is immediately obvious from Fig. 45 that very small particles must be made visible for the method to have any feasibility, even at low frequencies, so that good lighting and excellent optics are required. The minimum particle visible may be limited by film graininess, which is generally of the order of 20 microns or greater for the high-speed films needed for this experiment (274). Cinephoto-micrographic studies of aluminum-containing solid propellants were unable to resolve particles with diameters less than 20 microns (275). A program on spray distribution run under extremely well-controlled optical conditions has a lower resolution limit of 10 - 15 microns (276). Inadequate light plus loss of depth of field at higher magnification limit the possible degree of magnification. With 1X magnification, the depth of focus is likely to be about 0.02 inches (based on $f/2.8$), while at 4X magnification the depth of focus will drop to about 0.003 inches (277).

Other sources of error in the fidelity of the particles as tracers include the fact that the effective diameter of particles can increase when more than a few are used (278), varying drag due to non-spherical particles, and any turbulence will seriously affect observations. The variations in lag with diameter make correction techniques doubtful, even for spherical particles, since particle sizes will vary slightly on introduction to the propellant mix, will be changed in mixing and grinding, and may well be confused with dust particles and other foreign matter in the same size range. As a result, although the particle-track method has great usefulness in ordinary laminar flames, its application to the study of solid-propellant combustion instability is limited to low frequencies, and extremely small particles must be followed even at low frequencies.

VI. Composition-Wave Observation

When the survey of possible experimental methods was conducted, the observation of pulsations in temperature or composition of the gases emitted by a solid propellant burning under oscillating pressure was discarded as a possible technique for the determination of acoustic admittance because it was felt that not enough information could be obtained by using the method. Since that time, however, theoretical developments have been achieved which make the technique an attractive one. Basically, the advancement is connected with the fact that gas temperature is meaningful only if its variation is observed in coordination with the pressure variation, so it is preferable to report the combined effects of temperature and pressure as an entropy value. Moreover, as each element of combustion gas travels away from the flame zone, its temperature and pressure vary with time, but its entropy remains nearly constant (except for diffusional effects to be discussed in the next Chapter). The near-constancy of the entropy makes it the useful property to discuss theoretically and experimentally. Although the entropy of each element of burned gas changes slowly with time, the entropy values of successive elements are not, in general, the same. The variation of entropy from element to element shows up as an entropy wave train carried along with the gas stream.

The entropy wave system will show the same frequency as the acoustic wave system, but the entropy wave-length will be determined by the mass velocity (on the order of 2×10^2 centimeters/sec) while the acoustic wavelength will be determined by the velocity of sound (about 10^5 centimeters/sec), so that the two wave systems will have lengths in the ratio of the order of 5×10^2 to 1, as shown in Fig. 46. A characterization of the entropy wave system, as shown in the next Chapter, has the potentiality of not only determining the over-all acoustic admittance, but also of gaining a large amount of information about the steady-state processes of solid-propellant combustion.

CHAPTER VII

ACOUSTIC ADMITTANCE AND ENTROPY WAVES

I. The Acoustic Admittance Equation

The importance of the frequency-dependent acoustic admittance in describing the interaction between the oscillatory pressure at the burning surface and the emitted burned gas has been discussed in Chapter IV. It was shown there that

$$Y = - \frac{\bar{v}}{p} \left(\frac{\mu_1}{\epsilon} - \frac{\sigma_1}{\epsilon} \right) \quad (21)$$

In this derivation, derivatives were taken at a fixed location (in the Eulerian sense), the outer plane of the flame layer being the most appropriate place for the analysis of acoustic interaction, since that constitutes the interface between the reaction zone and the acoustic field.

When the variable quantities of mass flow, pressure, and density are inserted in the form of complex numbers which are exponential functions of time, the acoustic admittance Y divides into real and imaginary parts. A negative real part indicates that the velocity vector leads or lags the pressure by less than 90° , i.e., a component of the velocity is in phase with the pressure. As shown before, this situation leads to a flow of energy into the acoustic field and, hence, possible amplification.

As noted previously, equation (21) for the acoustic admittance is composed of two terms. The first is the variation of mass burning rate with pressure which, in steady-state measurements, would be equal to the conventional burning rate exponent n . Hart and McClure (85) have shown, however, that the variation, known as the response function, has a magnitude which is a function of frequency and, more important, has a non-zero phase with respect to pressure. It must be mentioned that, since the response function is of necessity defined at the flame zone-acoustic field boundary, measurements to determine acoustic admittance by studying the instantaneous burning rate of the solid cannot be expected to characterize the propellant's ability to amplify or attenuate sound, since both the magnitude and phase of the response will be determined not only by the gasification rate of the solid, but also by the rate of combustion of the pyrolyzed products. These two rates cannot be expected to respond similarly to disturbances over the range of frequencies and amplitudes of interest, so that the amount of pyrolyzed but unburned intermediate products oscillates with pressure, as in the variable time-lag theory. Moreover, the boundary itself oscillates relative to the solid surface.

II. Importance of σ/ϵ

The second term is the variation of density with pressure, as seen by an observer stationed at the outer edge of the flame zone. If the

burned gas is assumed to be ideal and polytropic, the density variation can be expressed in terms of the variation of the entropy of the burned gas with pressure. Thus, the second part of the acoustic admittance (equation 21) can be evaluated by measuring the amplitude and phase of the entropy variation at the station, since (21) becomes

$$Y = -\frac{\bar{v}}{\bar{p}} \left\{ \frac{\tilde{\mu}}{\tilde{\epsilon}} - \frac{1}{\gamma} + \frac{1}{c_p} \left(\frac{ds_f}{d \ln p} \right) \right\} \quad (77)$$

Equation (77) may be compared with the Hart-McClure revised form for Y, viz.

$$Y = -\frac{\bar{v}}{\bar{p}} \left\{ \frac{\tilde{\mu}}{\tilde{\epsilon}} - \frac{1}{\gamma} \left(1 + \frac{\tilde{\zeta}}{\tilde{\epsilon}} \right) \right\}$$

where $\tilde{\zeta} = \left(\frac{\gamma-1}{\gamma} \right) \frac{p_1}{\bar{p}} - \frac{(T - \bar{T})_1}{\bar{T}}$

As mentioned previously, $\tilde{\zeta}/\tilde{\epsilon}$ is the temperature response function, and expresses the extent to which conditions at $()_1$, the flame zone boundary,

are non-isentropic. Although the temperature response function can be calculated (as done by Hart and Cantrell), a measurement of the function would, when taken with the measured mass response function, give the complete experimental acoustic admittance for a propellant. It must, of course, be emphasized that the magnitude of variation of $\tilde{\sigma}/\tilde{\epsilon}$ is small compared to that of $\tilde{\mu}/\tilde{\epsilon}$, and that the variations in entropy are not sufficient to drive a rocket unstable by themselves, in contrast with the case for liquid-propellant rocket motors. However, a measurement of the entropy or temperature of the burnt gases from a sample burning under oscillating pressure will still give some information of the acoustic admittance function, and the variation of the temperature response function as a function of frequency and mean pressure can be related to the combustion processes of the solid propellant for both steady - and unsteady-state conditions.

III. Characteristics of the Zero-Frequency Regime

In the "zero-frequency" regime, it is assumed that steady-state processes prevail at all times. Accordingly, two simple cases may be conceived for the temperature response function. First, the entropy may be constant (as originally assumed by Hart and McClure) or, in other terms, the temperature response function is zero. Second, the flame temperature may be constant, which will lead to the generation of entropy waves (or visible temperature waves) by the burning propellant. These entropy waves, for this extreme case, will be 180° out of phase with the pressure. An explanation for this result, as well as a derivation of an analytical expression for the temperature field, follows.

For a polytropic gas:

$$s = s_o + c_p \ln \left(\frac{T}{T_o} \right) - R \ln \left(\frac{p}{p_o} \right), \quad (78)$$

where $()_o$ = some reference condition. As mentioned previously, the assumption is made that, in the zero-frequency regime, the flame temperature is constant, since the steady-state flame temperature is essentially independent of pressure. To simplify the expression further, it will also be assumed that s_o is invariant for successive elements of combustion products. This

assumption removes the necessity of estimating the contribution to the entropy of the several processes involved in the combustion of a heterogeneous propellant, such as mixing, crystalline phase changes, etc., and is an extension of the steady-state argument for the pressure-frequency regime in question. For these assumptions, then, the entropy at the edge of the flame zone becomes:

assumption removes the necessity of estimating the contribution to the entropy of the several processes involved in the combustion of a heterogeneous propellant, such as mixing, crystalline phase changes, etc., and is an extension of the steady-state argument for the pressure-frequency regime in question. For these assumptions, then, the entropy at the edge of the flame zone becomes:

$$s_f = \text{constant} - R \ln \left(\frac{p_f}{\bar{p}_f} \right) \quad (79)$$

where \bar{p}_f = mean pressure.

The pressure oscillation is described by:

$$p_f = \bar{p}_f (1 + \epsilon \sin \omega t), \quad (80)$$

so that (79) becomes:

$$s_f = \text{constant} - R \ln (1 + \epsilon \sin \omega t) \quad (81)$$

Since $\ln (1 + x) = x$ for $x \ll 1$

$$s_f = \text{constant} - R \epsilon \sin \omega t$$

$$\text{or} \quad s_f = \bar{s}_f + R \epsilon \sin (\omega t - \pi). \quad (82)$$

By (82), the pressure and entropy are expected to be 180° out of phase, so that an observer stationed at the edge of the flame zone sees the entropy of the emerging hot gas oscillate sinusoidally with time, with high-entropy waves emitted at pressure minima. The varying entropy of the gas particles is visualized as a temperature field, since the gas emitted by the flame at low pressure is compressed by subsequent pressure waves and

thereby raised to temperatures higher than the flame temperature. At the same time, gas emitted at high pressure is later cooled below the flame temperature by rarefaction, as shown in Figure 4/. In Figure 47, gas particle A is emitted at high pressure and low entropy, gas particle C is emitted at low pressure (high entropy), while gas particle B is emitted at an intermediate state.

Wood (193) has reported luminosity waves, seen by a streak camera, that are 180° out of phase with pressure for conditions of 200 cps and 800 psi. He also observed that going to higher frequency or lower pressure changed the phase of the luminosity wave, that is, the luminosity led the pressure by less than 180° . The results were only photographic, so that the character of the waves could not be determined. However, the occurrence of such waves was taken as an indication that non-isentropic conditions could, indeed, exist at the end of the flame zone.

The spatial distribution of entropy and pressure can be derived from equation (82). For a particle starting from the flame zone-acoustic field where $x = 0$, the entropy at time t at a distance x ,

$$s_f(x, t) = s_f(0, t - \frac{x}{\bar{u}}), \quad (83)$$

where \bar{u} is the average velocity of the burned gas. The time retardation is written as x/\bar{u} which is an approximation for the true value, which is

$$\int_0^x \frac{dx}{\bar{u} + \tilde{u} \sin \omega t}.$$

The approximation results in a slight distortion of the

spatial wave form, but other distortions will be more serious, as will be seen. Putting equation (82) into (83), and using the relation $R = \frac{\gamma-1}{\gamma} c_p$:

$$s_f(x, t) = \bar{s}_f + \epsilon \frac{\gamma-1}{\gamma} c_p \sin \left[\omega \left(t - \frac{x}{\bar{u}} \right) - \pi \right]. \quad (84)$$

Equation (84) is an entropy wave train moving from left to right.

To express (84) in terms of temperature, use (78), giving

$$c_p \ln \frac{T_x}{\bar{T}_f} - \frac{\gamma-1}{\gamma} c_p \epsilon \sin \omega t = \epsilon \frac{\gamma-1}{\gamma} c_p \sin \left[\omega \left(t - \frac{x}{\bar{u}} \right) - \pi \right]. \quad (85)$$

For small amplitudes, using $\ln(1+x) = x$,

$$\ln \frac{T_x}{\bar{T}_f} = \frac{T_x - \bar{T}_f}{\bar{T}_f},$$

so that (85) becomes:

$$\frac{T_x}{T_f} = 1 + \frac{\gamma-1}{\gamma} \in \left\{ \sin \left[\omega \left(t - \frac{x}{u} \right) - \pi \right] + \sin \omega t \right\} , \quad (86)$$

or, in a clearer form:

$$\frac{T_x}{T_f} = 1 + \frac{\gamma-1}{\gamma} \left\{ 2 \sin \frac{\omega x}{2u} \cos \left(\omega t - \frac{\omega x}{2u} \right) \right\} , \quad (87)$$

Equation (87) shows three significant features. First, at any instant t , there will be a sinusoidal variation of temperature along x , with amplitude $\frac{\gamma-1}{\gamma} \in$. Second, there will be points, given by $\frac{\omega x}{2u} = \left(n + \frac{1}{2} \right) \pi$, where the amplitude of the temperature fluctuation is twice that for the spatial wave. Third, there will be points, given by $\frac{\omega x}{2u} = n\pi$, where the temperature variation will be zero. The burning zone-gas field interface would be one such point. The burning zone-gas field interface is not strictly a fixed point in space relative to the solid surface, since it may be expected that the pressure fluctuations will change the flame stand-off distance. However, for the magnitudes of distance mentioned here for x , the use of the mean-surface approximation still appears valid.

The oscillating gas field can distort the appearance of the temperature distribution in two ways. First is the variation in flow velocity which results from the fact that the mass flux term in the equation of continuity is fluctuating owing to the effect of pressure variations on the regression rate. Wood (279) found that, for a pressure of 500 psi and a steady-state burning rate of 1.2 cm/sec, flow reversal occurred at about one centimeter from the surface for oscillations with an amplitude of 100 psi (200 psi peak-to-peak) and a frequency of 500 cycles per second. Second, and more important, is the distortion that the particle motion of the acoustic field can give. Consider a sample burning at 0.47 cm/sec at 400 psi steady pressure, with 250 cps oscillations imposing 100 psi amplitude (200 psi peak-to-peak) fluctuation on the pressure. From continuity, the gas efflux velocity will be about 250 cm/sec, giving a characteristic wave length for the entropy field of 1 centimeter. Associated with the sound field is a particle velocity which grows with increasing distance from the surface, as follows:

distance (mm)	velocity amplitude (cm/sec)
1	28
3	84
5	140
10	280

It can be seen that the temperature field will be grossly affected by the velocity fluctuations, and that measurements would have to be taken close to the surface. The waves would still be visible, but the simple nodal picture would no longer hold.

The amplitude of the temperature wave will also decay as a function of distance from the surface by dissipative processes. One of these is heat conduction, which limits the conditions under which observation can be made. Consider a stationary gas column with an initial temperature distribution, assumed sinusoidal, as seen by an observer riding with the gas stream. For simplicity, regard the displacement from the mean temperature as the quantity to be investigated. Assume pure one-dimensional heat conduction, so that:

$$\frac{\partial^2 T}{\partial x^2} = \frac{1}{\alpha} \frac{\partial T}{\partial t} \quad (88)$$

with boundary conditions

$$T(0, t) = T(\lambda, t) = 0$$

where λ is the entropy field wavelength and $T = T_{\max_i} \sin(2\pi x/\lambda)$ at $t = 0$.

The general solution of (88), is ():

$$T(x, t) = \frac{2}{\lambda} \sum_{n=1}^{\infty} \left[\int_0^{\lambda} f(z) \sin(2\pi x/\lambda) dz \right] \sin(n\pi x/\lambda) e^{-\left(\frac{n\pi}{\lambda}\right)^2 \alpha t} \quad (89)$$

where $f(z) = \sin \frac{2\pi x}{\lambda} T_{\max_i} e^{-(2\pi/\lambda)^2 \alpha t}$

Using the orthogonality of the sine function,

$$\begin{aligned} \int_0^{\lambda} \sin \frac{2\pi x}{\lambda} \frac{n\pi x}{\lambda} dx &= 0, \quad n \neq 2 \\ &= \frac{\lambda}{2}, \quad n = 2 \end{aligned} \quad (90)$$

Therefore, equation (89) becomes:

$$T(x, t) = \sin \frac{2\pi x}{\lambda} T_{\max_i} e^{-(2\pi/\lambda)^2 \alpha t} \quad (91)$$

To investigate the persistence of the entropy wave, it is necessary only to observe the decay of the exponential term. Solving for the time when the amplitude is T_{\max_i}/e :

$$\tau = \left(\frac{\lambda}{2\pi} \right)^2 \frac{1}{\alpha} \quad (92)$$

As an initial estimate, assume $\alpha = 1 \text{ cm}^2/\text{sec}$, which is obtained by an extrapolation, based on simple kinetic theory, from room temperature and pressure to $T = 2700^\circ\text{K}$ and $p = 25$ atmospheres.

For a particle wavelength of 1 centimeter, a $\tau = 25$ milliseconds results. For an average velocity of 250 centimeters/second, $x = 6.25$ centimeters. Since these values are for 400 cps oscillations, the persistence is over 6 times the wavelength and τ is 10 times the period.

Two factors will change the magnitude of the characteristic time: τ / λ , which is a measure of the frequency of oscillation, and α , which will vary with the pressure and temperature. As the frequency increases, the persistence decreases, both absolutely and relatively. The pressure effect is threefold: (i) gas diffusivity varies inversely with pressure, (ii) gas density varies directly with pressure, and (iii) burning rate varies with pressure to some power less than one, say $n = 0.5$. As can be seen from Table IV, there is a definite increase in the persistence of the temperature wave with increasing pressure.

Table IV

Persistence of Entropy Waves under Dissipation by Heat Conduction

pressure (atmospheres)	frequency (cps)	x(cm)	τ (msecs)
10	400	1.6	4
25	100	100	400
	400	6.25	25
	1000	1	4
50	400	9	50

In short, it is only at low pressures and high frequencies that temperature waves decay rapidly. Since these are not the conditions for which the zero-frequency case is likely to exist, heat conduction does not appear to be a serious dissipative factor.

Other dissipative processes which could smear out temperature waves include turbulent mixing, heat losses to the walls, spatial irregularities, and radiative heat transfer. However, it does appear that the effect of the acoustic particle velocity is the limiting criterion on the distance from the flame zone at which measurements can reasonably be made.

The tacit assumption has been made, in the consideration of the zero-frequency case, that the adiabatic flame temperature is independent of the pressure for steady-state conditions. It has been shown that the temperature constancy leads to the generation of entropy waves of a certain type. As mentioned before, Hart and McClure assumed that isentropic conditions existed at the end of the flame zone, which could exist, for instance, if the flame temperature varied with pressure by the proper amount, although variations in s_0 could also cause the same result. If it were assumed that

the temperature variation could be written $T_f = cp^m$ ($m < 1$) then $p = \text{const } p^{(1-m)}$

so that $\frac{\tilde{\sigma}_1}{\tilde{\epsilon}} = 1 - m$. For complete cancellation of entropy waves, the pressure-temperature relation would have to be the isentropic relation, i.e.,

$$\frac{p}{p_{\text{ref}}} = \left(\frac{T}{T_{\text{ref}}} \right)^{\frac{\gamma}{\gamma-1}} \quad (93)$$

For a $\gamma = 1.2$, and a pressure variation of 50%, the temperature variation would have to be 15% to give cancellation of entropy waves.

To test the possibility of large flame-temperature variations, calculations were made of the flame temperature versus pressure for two propellant systems - an 85% ammonium perchlorate - 15% polyurethane propellant, and a propellant containing 35% ammonium perchlorate and 65% plastisol binder. Only small variations of flame temperature with pressure resulted. In addition, the effect of adding 0.5% NaCl was studied, for reasons which will be explained, and the salt was found to lower the calculated flame temperature by only 8°K. Computational procedures and full results are given in Appendix D.

IV. Entropy Variation and Admittance

The determination of the temperature response has thus far been discussed for the extreme cases of the "zero-frequency" regime. However, the measurement of $\tilde{\sigma}/\tilde{\epsilon}$ for all pressure-frequency regimes is a significant task. For the two simple cases mentioned thus far, $\tilde{\sigma}/\tilde{\epsilon}$ has a particularly simple form. In the case originally assumed by Hart and McClure (85),

$$s = \text{constant} \quad (94)$$

so that

$$\frac{\partial s}{\partial(\ln p)} = 0 = \frac{\tilde{\sigma}}{\tilde{\epsilon}} \quad (95)$$

$$\frac{\tilde{\sigma}}{\tilde{\epsilon}} = \frac{1}{\gamma}$$

For the isothermal case in the "zero-frequency" regime,

$$\frac{\partial s}{\partial(\ln p)} = -R \quad (96)$$

$$\frac{\gamma}{\epsilon} = \gamma - 1$$

$$\frac{\gamma}{\epsilon} = 1$$

The general case of burned-gas entropy behavior is given by

$$s = F(t)$$

where $F(t)$ is some function, not necessarily a simple one, of time. It contains those changes in combustion-zone behavior which result from the effect of pressure variation on the combustion. The magnitude and type of change will, of course, depend on the mean pressure and the rate of change of pressure. As a result, a measurement of the temperature response function by an observation of the entropy of the gas field as a function of time and distance from the burning surface would yield information on the nature of the combustion zone for both steady-state and time-varying conditions. The behavior of the temperature response function as a function of frequency would give evidence of the characteristic times involved and of the relative importance of the different processes in combustion, and thus the physico-chemical nature of the solid-propellant combustion.

The broad general objective of the experimental program was, then, to obtain the variations of the temperature response function over a range of frequencies and pressures by an observation of the burnt-gas entropy in this range, and to relate the variations to the fundamental flame processes of solid propellants.

CHAPTER VIII

EXPERIMENTAL APPARATUS

I. Oscillator Selection

The first step in the study of the behavior of the burning of a solid propellant under oscillatory pressure conditions is the design and fabrication of an oscillator which will yield pressure oscillations of sizable amplitude and frequency, both of which can be controlled by a simple variation of the operating parameters of the oscillator. The amplitude should be of the order of at least 25 psi and the frequency range from 100 cps to about 2000 cps, since the large motors being designed today have natural frequencies in this range. In addition, by suitable variation in steady-state pressure, the different pressure-frequency regimes of acoustic interaction could be studied. The minimum desired amplitude implies an intensity over 170 decibels, with over 500 watts/cm² of acoustic power.

The types of generators available have been considered in reports dealing with effect of sound on the burning rate of solid propellants (281) (282). The type finally used in that study, an airjet whistle, is unsuitable for the frequency range of interest, since cavity sizes become too great for efficient operation (283). Mechanical methods of producing oscillations, such as pistons or rotating valves, are limited in frequency response by the finite mass to be moved, and chopper mechanisms where incoming gas flow is periodically interrupted involve gas dilution and severe temperature gradients. Electrical types would be hard put to produce the desired intensity, since the diaphragm would have to vibrate over 0.2 inches to produce the desired power at 100 cps (284). A barium titanate transducer to produce the necessary output would require a 10-foot-diameter crystal and 300 kev driving power (285). In both cases, elaborate cooling and pressure-equilization systems would be necessary, as discussed earlier.

II. T-Burner Design

As a result of these considerations, the oscillator design was built on the same principle as the T-burner used by other experimenters. The oscillator is, however, based on the original design of Price (99) in that internal-burning grains are used, rather than the end-burning ones used by Horton (197). The author made a flexible adaptation of the Price design while at Rohm & Haas, and a further adaptation was made for use at Princeton. The assembled motor is shown in Figure 48. Sections of the arms of the T contain cylindrical propellant grains, while the stem is composed of a plenum chamber and the exhaust nozzle. The lengths of the arms can be varied to give the frequency desired, since the motor tends to produce the fundamental longitudinal mode, with pressure antinodes at the ends of the arms and a pressure node at the exhaust section. The test propellant sample is mounted in the sample section at the end of one arm

BLANK PAGE

of the Γ , where a pressure gage and three view ports are located. Photographs of the assembly, the test section, and the sample holder (with a test specimen mounted) are shown in Figures 49, 50, and 51. In the original design, the test specimen was allowed to burn on the end only, so that pressure coupling alone would exist between the combustion and the oscillating gas field. The performance parameters of the oscillator are described in a latter section.

The oscillator is mounted on a thrust stand with the nozzle firing vertically. The thrust stand is composed of a 12-foot-long 6-inch Junior Channel mounted on three 4" Schedule 40 pipes. Cross bracing is provided by 6 gussets, made from 1/4" plate. As shown in Figure 49, the combustion products are exhausted to the atmosphere through an 18-inch duct. Figure 52 shows the exterior of the solid-propellant test cell which contains the oscillator and its associated instrumentation and controls. The test cell does not have the conventional opening to the outside, but is enclosed except for 2 of the 18-inch ducts, one in each compartment of the test cell. A floor plan is shown in Figure 52. Venting of the products is aided by a blower mounted on the roof, which delivers 15000 cubic feet per minute of air and gives a pressure inside the cell of 4 inches of H_2O above ambient pressure. As a result, there is a volume

flow rate of air which is well over 10 times the maximum combustion-gas production rate, so that all products are exhausted immediately. The walls of the test cell are 14-inch reinforced concrete, with Styrofoam blowout panels for pressure relief. Some of these panels are shown in the bottom of Figure 52. In addition, a number of small vent pipes are used to exhaust any lingering products. The net result is that experiments can be run under controllable temperature conditions and light-sensitive equipment can be handled without resorting to firing after dark.

III. Ignition and Controls

Ignition of the two "driver" grains is accomplished by a pair of 4-gram bag igniters, shown in Figure 53. The igniter material is propellant shavings, usually from an 85% ammonium perchlorate-15% polyurethane propellant. The igniter is made as shown in Figure 54 with an Atlas Match squib and a piece of polyethylene sheeting, and the shavings are contained by a rubber band around the bag. One of the bags is placed in each driver section and the igniter leads are passed through the nozzle, where they are clipped to the firing leads. Ignition has always been accomplished rapidly and reproducibly with this system, which does not appear to be brisant, and no igniter peaks have been obtained. No closuring is necessary.

The firing circuit, as well as the remainder of the control circuit, is shown in Figure 55. The 24-volt DC power is supplied by a Gates G30.30F power supply, which will give voltages to 32 volts and amperages to 30 amps. Two keys are necessary before power can go to the igniter, and both keys must be in the proper position, or else the igniter leads are shorted to ground. To assure that the keys remain in the cell while

anyone is working there, as an additional safety feature, the keys, when removed, actuate a pair of loud buzzer systems, an Edwards 1063 buzzer, so that no one can be in the cell without the keys inserted in the buzzer.

Firing is accomplished through a control panel (Figure 56), where the keys can also be seen. The fire switch used for the oscillator is in the lower left-hand corner of the panel, and is a guarded momentary switch, so that the firing circuit can not be left on. When the fire switch is actuated, the igniter receives power either immediately (manual control) or after a slight, pre-set delay. The delay is accomplished by a Model #RC-J2889 sequence timer of the Industrial Timer Corporation. This timer, when automatic control is desired, actuates relays which start recording equipment, the cameras, and signal marks used to correlate events recorded by two different sets of data-gathering equipment.

As an additional feature to avoid possible misfires, an igniter - tester circuit is installed in the control panel. This circuit utilizes a 1.4 V.D.C. mercury battery, which is not enough to actuate the squib, and a Simpson microammeter. It has been found that a steady current of 130 microamperes will flow through the test circuit when wiring conditions are normal. A falling current or a low current indicates either a voltage leak or a short circuit which might prevent actuation of the squib by the firing circuit. As a result, expensive film and recording equipment are not wasted by a bad squib or an open wire.

IV. Instrumentation

The pressure is sensed by Dynisco strain-gage pressure transducers. A Model PT 49 transducer, which is flush-mounted and water-cooled, is used when high frequency instrumentation is required, while a Model PT 76 transducer, which is connected to the chamber through a 1-1/2"-long 1/4" grease-filled line, is used when high-frequency data gathering is not required (Figure 57). It has been found that a 0.002-inch gold-plating protects the diaphragm of the PT 49 from the corrosive effects of the hot gases, while the grease is sufficient protection for the PT 76. The signals from the transducers are sent through a patch panel, which is on the right-hand side of the instrumentation panel shown in Figure 58. The signals go through Dana 2200 DC amplifiers, either into a Honeywell Model 8100 tape recorder or through Neff 106 DC amplifiers into a Model 906B Honeywell Visicorder, which is a direct-writing oscillograph. The oscillograph uses fluid-damped galvanometers, with the ones most often used having a flat frequency response of 0-2000 cps, and giving up to 6 inches deflection with $\pm 2\%$ linearity. The standard voltage for the strain-gage bridge of the transducers is furnished by a Video Instruments Corp. Model SR-200 EM power supply. The pressure-recording system is calibrated with an Amthor 0-5000 psi Dead-Weight Tester, and the deflection of the galvanometer is used to give a gain for the system. A time base is supplied by a Minneapolis-Honeywell Timing Unit, which is a multivibrator oscillator supplying sharp pulses at intervals of 0.01, 0.1, and 1.0 seconds. These pulses drive a pair of 2000 cps galvanometers so that full-width timing lines appear on the recording paper, which is either Kodak Linagraph Paper or duPont Linowrit 5 Direct Writing Paper.

The signal recorded on the tape recorder can be played back, through the patch panel, into either a Digitec D.C. Voltmeter, a Hewlett-Packard Voltmeter, a Tektronix Model 531 Oscilloscope, or, through the Neff amplifiers, the Visicorder. The Neff amplifiers are necessary to give the proper impedance match and to prevent a large current from reaching the galvanometer. A magnified time scale is obtained, since signals are recorded at 1-7/8, 3-3/4, 15 and 30 inches per second on the tape recorder and are played back at 1-7/8 and 3-3/4 inches per second.

V. Photographic Equipment

The appearance of the burning is recorded by high-speed cinematography, using a Wollensak Model WF-16 Fastax Camera, which is controlled by a Wollensak Goose Unit. Framing rates from 3000 to 8000 frames per second have been used, with most observations made at about 5000 frames per second. A 25-mm lens is used together with extension rings from 1/4" to 2", giving magnifications of 3/4 to 2. Most often, a 3/8" extension ring was used, giving a magnification of 1. Black and white film (duPont Rapid Reversal 931-A) is usually used, since it can be developed automatically in a Fairchild Model F316A Rapid Processor, allowing viewing of results within one-half hour after a test. When developed in this manner, a negative results, and the film rating is ASA80. When developed as a positive, the film speed is ASA160. For more definite viewing, Ektachrome reversal color film (ASA160) is used, which can be developed commercially or by hand, using the Kodak E-3 Process Kit.

The framing rate of the camera at any time is recorded on the film by use of a neon flasher bulb, which is focused on the edge of the film. The bulb is actuated at either 100 or 1000 cycles per second by a Wollensak Model WF311 Pulse Generator. Another internal camera timing light is used to provide synchronization between the camera film and the Visicorder record, with the sequence timer providing 3 switching pulses which are recorded on the Visicorder and also actuate the second timing bulb.

Other photographic evidence is obtained by streak photography, which gives evidence of the movement of the luminous bands expected from the entropy wave concept. A 1/32-inch slit, the length of one of the viewing windows, is focused on the ground glass of a Speed Graphic bellows camera by a lens system consisting of a 105-mm f/5.6 Schneider-Kreuznach lens, a 1-1/2" extension ring, and 2 Kodak 3 + Portra lenses, giving a magnification of approximately 4 1/2. The image of the slit is recorded by an ETC Scope Recording Camera, Model SM-100 on 35 mm Tri-X film, which moves at speeds up to 12000 in/min through the camera. Alternatively, a Kern-Surtar 50-mm f/1.8 lens was used with a 7-1/2" extension ring to give the same overall magnification on the recording film without the necessity for the ground glass.

VI. T-Motor Performance Parameters

The oscillator sections are made of 2-inch heavy-wall seamless stainless steel 304 tubing, and range in length from 3 inches to 5 feet.

They are bolted together, and to the center support section, through 5-inch diameter, 5/8"-thick flanges using case-hardened bolts. The center support section contains a blowout disc with a thrust neutralizer. The blowout used was a 1500-psi disc, and was protected from the hot gases by filling the extension between the plenum chamber and the disc with Fuller RL 3700 compound. This protection became necessary after some discs failed at low pressure, and, since that time, no blowout-disc ruptures have occurred.

The nozzle is a simple 1-inch-thick copper plate with the desired diameter hole drilled through. Only the inlet section is radiused, since exhaust conditions are of no concern for this program.

The choice of a driver propellant for the oscillator was first thought to be primarily dictated by the need for a high energy-release rate, since theory and experiment predicted that the greatest amplification of a reflected pulse would occur for rapid-burning "hot" propellants.

As a goal, the first attempt was to develop a propellant with a burning rate of at least 1 centimeter/second at 500 psi which could be readily prepared with suitable physical properties and castability. Some test propellants were fabricated in the processing facility of the Guggenheim Laboratories and their burning rates were determined in a strand burner. The first binder used was a polybutadiene-acrylic acid copolymer because of its mechanical and processing properties, its chemical properties, such as oxygen content, and the fact that moderately high rates had been obtained by Bastress (103) using this binder with ammonium perchlorate. High oxidizer loading was desired from the standpoint of both flame temperature and burning rate.

The first propellant tested contained 80% ammonium perchlorate, with a bimodal mixture, 70% unground and 30% fine (18μ), which was known to be castable in small rocket motors (286). However, the burning rate was below 1 cm/sec at 500 psi, the target rate. In an attempt to increase the burning rate, the coarse perchlorate was omitted, with the rates shown in Figure 59. The burning rate was satisfactory, but the mix was far too thick, giving poor casting properties. Next, tests were run with perchlorate ground at 8000 rpm rather than at 12000 rpm as previous, giving a mean diameter of 36μ . Although the burning rate was acceptable, there were air holes in the resulting propellant due to the high viscosity of the mix.

At this point, the use of a burning-rate accelerator was decided upon. The catalyst copper chromite was an obvious choice since this additive is a catalyst for ammonium perchlorate decomposition (287), and had previously been shown to affect a marked increase in the burning rate of ammonium perchlorate propellants (288). As a first test, 2% of the catalyst replaced the 36μ perchlorate with the result shown in Figure 59. It may be seen that a 50% increase in burning rate resulted. However, this mix was still too thick to be considered for motor use.

Due to the success of the copper chromite and the known castability of the bimodal-perchlorate propellant, the next propellant cast contained 2%

copper chromite added to the original 80% bimodal propellant. The resulting rates are shown in Figure 59. Once again, a 50% increase in burning rate at 500 psi resulted. The burning rate at 500 psi - 0.37 in/sec or 0.94 cm/sec - was considered close enough to the target rate to be a candidate for the driver propellant, especially since castability was good.

The first series of tests with this driver propellant was run using 1-foot extensions with 5-1/2-inch motor sections, giving a frequency near 430 cps. Some variations in propellant length showed that reproducible amplitudes were obtained with 5" propellant grains. These grains were inhibited with PBAA fuel on the end away from the nozzle. With inhibition on only one end, the grain shortened as the diameter increased, giving a relatively neutral pressure-time trace. Firings were made at pressures from 240 psig to 470 psig, with the results shown in Figure 60.

The frequency of the oscillations was varied by using 2-foot extensions, giving a 270 cycle per second natural frequency. The results for the two frequencies are compared in Figure 61. It should be noted that the pressure dropped off for the same K_n (burning surface - nozzle area ratio), probably because of heat-loss increase.

Difficulties to be described later forced the abandonment of the PBAA system as a driver, and the next system tested was an 80% bimodal ammonium perchlorate-20% LP-3 system. The LP-3 binder is a Thiokol Chemical Co. product, and is a polysulfide-type polymer. The propellant burned with rates shown in Figure 62. Although the rates are lower than those of the PBAA propellant, the LP-3 propellant gave comparable oscillations when used as a driver propellant, as shown in Figure 63.

The LP-3 propellant was still not completely satisfactory, so a polyurethane propellant was next tested. The polyurethane is based on toluenediisocyanate and polypropylene glycol. In order to increase oxidizer loading, a trimodal oxidizer distribution is used. This distribution contains 25% 350 μ , 50% 210 μ , and 25% 5 μ ammonium perchlorate, and a propellant containing 85% oxidizer can be cast into motors when this distribution is used. The burning rate of this propellant is shown in Figure 64. It can be seen that the rate is lower than that of the PBAA or the LP-3, and that the propellant appears to have some "plateau" behavior around 500 psig. The polyurethane propellant has been the one used most as driver, and frequencies generated range from 75 cycles per second (5-foot extensions plus 2-foot extensions) to 1600 cycles per second (3-inch motors only). The characteristics of the propellant as a driver at 430 cycles and 265 cycles are shown in Figure 65. A comparison with Figures 60 and 63 shows that the polyurethane is much less pressure-sensitive, both in P-K curve and in the amplitude of oscillation. In addition, the pressure-time curves are more neutral.

In every case, the inhibitor used was applied at the end away from the nozzle, and the material used was the binder material only, without the addition of an oxidizer.

One disadvantage with this type of oscillator - driver is related to the non-linear effect discussed by McClure (110). As the frequency decreases, the waveform tends to depart from purely sinusoidal, as some overtones appear. These overtones are most pronounced at higher pressures (above 500 psi). As the frequency is decreased further by the addition of longer extensions, the wave front steepens, until at 150 cps (4-foot extensions) the wave form approaches that of a shock, followed by a distorted sine wave. At still lower frequencies, the wave front becomes less steep, and the wave form begins to become sinusoidal again. Examples of these wave forms are shown in Figure 66. The changing form may be ascribed to erosive burning due to flow reversal (110) or to the effects of concentrated combustion (178), since, at low frequencies, the 5-inch-length driver becomes a small portion of the total motor length (up to 16 feet total), and becomes more of a concentrated heat source.

One method of improving the wave form involves the use of a spacer between the driver and the test section. The spacer was originally used to minimize the effect of back flow and possible turbulence caused by the proximity of the driver and the test sample. Both 3-inch and 7-inch spacers have been used. Although the amplitude of oscillation drops slightly (Figure 67), the waveform is closer to sinusoidal than for the same motor extensions (comparable frequency). One possible explanation is that the decrease in amplitude causes a decrease in erosive-burning effects.

In most of the tests mentioned above, a large amplitude was desired. However, the amplitude can be controlled through variations in propellant driver length, as shown in Figure 68 for the 430 and 265 cycles per second conditions (1-foot and 2-foot extensions).

The heat-loss effect mentioned earlier for the 2-foot extensions with the PBAA propellant has been encountered with even more severity at the longer extensions used with the polyurethane driver. Not only is the pressure lower for a given K, but the apparent speed of sound, obtained from the measured frequency and the motor length, also falls. A summary of this effect is given in the table below.

Table V

Effect of Heat Loss on T-Burner Operating Parameters

<u>Frequency</u>	<u>Extension</u>	<u>Apparent Speed of Sound</u>	<u>P</u>	<u>K</u>
430	1 foot	3200 ft/sec	360	165
265	2 foot	3050 ft/sec	330	165
190	3 foot	2950 ft/sec	300	165
150	4 foot	2900 ft/sec	300	185
105	5 foot	2500 ft/sec	290	200
77	7 foot	2400 ft/sec	450	260

The heat-loss effect could have been decreased by the use of insulating material, but it was not felt worthwhile for the purposes of the investigation.

VII. Window Design

The most difficult experimental problem to overcome was concerned with the actual viewing of the combustion products. The original test chamber is shown in Figure 69. The windows used were flat pieces of Vycor or quartz, leaving a recess in the test section. The thickness of the test-section walls was dictated by calculations of the yield of the test-section metal, and the desire to insure a good seal around the windows at high pressure. The window is held in by a stainless-steel plate, and sealing is accomplished by 1/16 inch Garlock-asbestos gaskets on either side of the window.

Initial firings, made without a test sample or a camera, showed that both Vycor and quartz windows could withstand the temperature and pressure without any untoward effects. Furthermore, both were quite clear after the shots, meaning that carbon deposition would apparently not present any problem.

Difficulties were, however, encountered when PBAA test samples of the same composition as the driver - 80% modal AP, 20% PBAA binder, and 2% copper chromite - were mounted in the test section. Soot built up shortly after ignition, obscuring the windows and preventing observation of the gas column.

Initial attempts to alleviate the difficulty were made without changing the ballistic properties of the burner. At first, a nitrogen purge was installed, designed to sweep across the viewing window. The purge system was operated under varying conditions, with flow rates up to 10% of the total mass flow in the T-burner, but no improvement was detected, even when preheated nitrogen was used. The recessing of the windows was thought to be a contributing factor, since it could lead to stagnant flow conditions at the window, with carbon deposition resulting. Thus, windows mounted flush with the chamber walls were installed, with the hope that the gas flow along the windows might sweep away the soot. Vycor and quartz were tried under these conditions, but with no success. Plexiglas was also used, since its ablation might carry away deposits. However, the windows were once again obscured by soot.

After these failures, the various components of the system were investigated as possible causes for the sooting. The igniter was first eliminated from consideration, as all of its various parts - the squib, the bag, and the igniter material itself - could be changed without affecting the observed behavior. A hot-wire ignition system was also tried. It was further observed that, when ignition delays occurred, the windows were clear until the propellant ignited. Finally, an igniter could be fired alone in the burner without obscuring the windows.

The next component of the system to be checked out was the inhibition of the test specimen. If the inhibitor did indeed burn, it would be a ready source of carbon. Different types of inhibitor were used and finally the inhibitor was completely eliminated, but no improvement in light transmission through the windows was observed.

Variation of the test specimen itself also failed to change the situation. Both the composition and the physical configuration of the test specimen were varied in this study. The basic idea was that the sample was emitting carbon, and that cutting down the test-specimen size might reduce deposition by reducing the source of carbon. Samples from 1/2 inch in diameter to nearly 2 inches (the I.D. of the test chamber) were used, but no difference in the deposition was observed. In addition, the smaller diameter samples gave flow patterns which were not one-dimensional, with a great deal of swirling and mixing. Finally, the test specimen was eliminated altogether but, contrary to the initial observations, soot still blanketed the window.

It now became apparent that the driver section of the system was causing the deposition. The next source of soot to be considered was the inhibition of the driver grains, which was not thought to be a likely source of trouble, since the inhibitor, a PEAA resin, was largely intact after firing. When the inhibition was eliminated the soot concentration was, if anything, increased. The operating pressure of the burner was varied from 200 to 700 psi to see if any combustion-product change would occur to improve the situation. However, no change in the degree of deposition was observed.

At about the time these latter tests were being made, a concomitant program was underway in the Solid Propellant Research Laboratory on steady-state burning of solid propellants (289). Part of this program involved the photographic observation of the burning surface of solid propellants in a window-type strand burner. When the PBAA driver propellant was burned in this apparatus at pressures above 50 psig, large amounts of luminescent carbon obscured the surface, and the inside of the bomb was coated with deposits, much as the windows of the oscillator's test section had been. This observation indicated that the source of the soot was the driver propellant. The generation of soot was mentioned in Chapter III in connection with particulate damping. In subsequent tests to solve the problem, attention was directed toward the modification of the driver propellant.

In the first tests on the driver, the PBAA binder was retained, but the formulation was changed slightly. Initially, the copper chromite, a possible source of solid deposits, was eliminated, but no improvement resulted. Next, the oxidizer level was increased to 84%, which, it was hoped, would cause complete combustion of the carbon in the binder. However, the same luminescence was observed in the window bomb, and the test-section windows were, once again, obscured by soot.

Since it seemed that the PBAA propellants were generating large amounts of carbon, the binder was changed. The next binder tested was

P-13, a polyester-styrene resin of the Rohm & Haas Chemical Company. Although the amount of soot produced was not as high as in the case of the PBAA propellants, an 80% AP-20% P-13 propellant caused obscuration of windows when fired in the burner.

Further improvement occurred with the use of another binder, the LP-3 binder mentioned earlier. Transmission increased to a large extent with LP-3 propellants.

The two next drivers tested here were graciously supplied by two outside agencies. One was a double-base propellant supplied by Picatinny Arsenal. This propellant was too "cool", however, and large amounts of soot were deposited on the windows. The other was a modified double-base propellant containing AP, a plastisol propellant, supplied by the Rohm & Haas Company, Redstone Arsenal Research Division. This propellant, when used as a driver, gave far cleaner windows. It was, however, too difficult to use extensively because the grain had to be cast by them, shipped, and then "potted" into the motor case.

Still more progress was accomplished with the 85% AP-15% polyurethane propellant described above. This propellant is cleaner-burning than any of the others mentioned, and, as a result, has been used as the driver propellant for the oscillator on all the photographic tests to be described later. The polyurethane propellants are difficult to make, as good quality control is required, but over 200 batches have been made in the solid propellant processing facilities, usually with good results. The propellant-manufacturing and motor-casting techniques are described in Appendix E.

Although the use of the compound windows to achieve flush mounting had not cured the soot-deposition difficulties, it was thought that flush-mounted windows would be preferable, especially when it became necessary to make entropy determinations. As a result, the test section was redesigned by relaxing the wall-thickness specification to take windows of a more complex shape, shown in Figure 70. These windows can be fabricated, although hand tooling is required, and are now used routinely.

Even with the improvements accomplished using the polyurethane drivers and the flush window, the test specimen still has a large effect on the test-section visibility. For instance, a PBAA test-specimen caused complete obscuration of the window almost immediately after ignition, and a P-13 sample caused a large amount of soot, as did a "cool" double-base propellant. The LP-3 and polyurethane propellants are cleaner burning, and a plastisol propellant without stabilizer and carbon black leaves no deposit at all. The inhibitor is still important, since it must vaporize to keep the surface visible, but not allow burning down the side or emit carbonaceous products to obscure the windows. The binders were not adequate, since they tended to leave a shell which obscured the surface. Test specimens were cast in Plexiglas tubes, then cut to the desired thickness. It was hoped that the Plexiglas would boil off, leaving the surface visible. However, the Plexiglas vapors apparently reacted with the propellant product gases,

causing smoke which obscured the sample. In the case of the polyurethanes, the best inhibitor found was VYLF, which is 5% polyvinyl chloride dissolved in methylene chloride. When the right amount was applied, the VYLF would vaporize cleanly, leaving clear windows. However, care had to be taken in the mixing and application of the inhibitor, since clumps of the polyvinyl chloride would land on the window and burn, leaving a deposit. Over-application of the inhibitor led to the same type of results. VYLF was incompatible with the plastisol propellant, so silicone vacuum grease was used on plastisol samples.

VIII. Temperature Measurements

With the window problem relieved, attention was turned to the experimental objective - the measurement of the entropy of the burned gas as a function of time and position. This is most easily accomplished by measuring the temperature-time history of the field. The history also leads to a value of $\tilde{\sigma} / \tilde{\epsilon}$ when combined with a simultaneous pressure-time record.

The measurement of temperature is a highly developed field, and many different physical principles have been invoked in designing experimental equipment. In the field of flames, methods such as thermocouples, compensated hot wires, or resistance thermometers are practically eliminated by material problems, i.e., the probe will probably melt in the hot gases, since temperatures near 3000°K are expected, especially with the increase caused by the compressive effect of the oscillations in the particular case under study. In addition, these techniques generally have some frequency-response limitation.

Optical techniques have a large advantage in the field of flame-gas-temperature measurement, since no disturbance of the flow or reactions occurs from probes inserted in the flow. Some of the techniques used have been the line-reversal method, the two-color method, the two-path method, brightness-emissivity methods, rotational-temperature methods, refractive-index methods, and X-ray methods. Critical surveys of these methods have been made by Penner (290) and by Gaydon and Wolfhard (291), and their applicability to solid propellants was considered by Sutherland (182) and Mahaffey (270). It is not appropriate to enter into a discussion of the various methods in this report.

Although different additives have been used to color flames for temperature measurement, the additive most commonly used in sodium, and the characteristic spectral lines used are the D-lines at 5890 and 5896

Angstroms, which result from $3^2\text{P}_{1/2} \longrightarrow 3^2\text{S}_{1/2}$ and $3^2\text{P}_{3/2} \longrightarrow 3^2\text{S}_{1/2}$

electronic transitions. These lines were used, for instance, by Sutherland to measure flame-temperature profiles near the burning surface (182) and by Bundy and Strong (292) to measure rocket-exhaust-temperature profiles.

The technique used in this experiment is a variation of the brightness-emissivity method, based on Kirchoff's law, which states that,

for thermal and radiative equilibrium, the flame absorptivity is equal to the emissivity for any given wavelength. The temperature sensitivity of the method can be optimized by suitable variation in gas emissivity, as shown by Sutherland. These variations can be obtained by changing the concentration of sodium atoms and the thickness of the flame, thus changing the number of radiators per unit area in the line of sight.

Errors could arise in the optical measurement of temperature with sodium-doped propellant from several different sources. The first of these is the effect on the flame temperature, which the calculations of Appendix D show is a small one. The second is the establishment of equilibrium conditions, but the radiative lifetime of an excited Na atom is of the order of 10^{-8} seconds (293), and the collision rates at the elevated temperatures and pressures of interest are far higher than this value. The third is the assumption that all sodium-containing molecules will be dissociated. The results of Minkowski (294) show that, at temperatures above about 2200°K , all NaCl molecules should be dissociated, although there is only 50% dissociation at temperatures near 2000°K . James and Sugden (295) found that, for hydrogen-air flames, sodium was completely dissociated at temperatures from 1650°K to 2250°K .

To obtain emissivity values, the degree of broadening must first be calculated for an optically "thin" flame. Then, the broadening of the line for a thicker flame must be obtained, starting from the value for the thin flame. A simplified calculational procedure is given in Appendix F, then a more sophisticated one which represents high-pressure conditions more closely.

The values of wavelength spread calculated in Appendix F show that, for many experimental conditions, the flame would have a black-body character when viewed through a standard interference filter. As a result, methods such as the brightness-emissivity method or the sodium reversal method would be impossible, since the background source required for comparison could not be seen through the flame. Instead, temperature would be measured directly by measuring the intensity of radiation emitted by the flame gas. Amplitudes to be expected in the zero-frequency regime are:

$$\text{observed pressure} = \frac{150 \text{ psi}}{400 \text{ psi}} = 40\%$$

Theoretical temperature $\frac{\gamma-1}{\gamma} \frac{\Delta p}{p} \approx 7\%$. This 7% variation leads to an amplitude variation of 29% of total radiation over the entire spectrum, assuming a uniform (grey body) emissivity. However, the variation of the radiation intensity using a "D" line filter, for the same 7% temperature change, is 76%, which should be measurable with precision.

However, the theory used in Appendix F is one which applies more strictly to an optically "thin" flame, that is, a flame with only a limited number of emitters in the line of sight. For an optically "thick" flame, however, the effect of self-absorption causes the radiation to grow with the

square root of the concentration of the emitters, rather than with the concentration directly, as in the "thin" flame region (296). Margenau (297) comments that the wings of a line rarely follow the Lorentz formula (Equation F-3), even though the center or core of the line does. This results from the inherent assumption of the Lorentz theory, i.e., the phase change in the emitted radiation resulting from a collision is much smaller than the period between collisions. Statistical theories are more successful in the "wings" of the line, since many interactions coincide to change the net energy of the radiator. Moreover, the transition from a "thin" to a "thick" flame is a complex one, depending on the relative degree of Doppler and pressure broadening for the "thin" flame (298), so that there is no general recipe for calculating spectral line shapes (299). Instead, the individual "curve of growth" must be measured. In addition, the calculations rely to some extent on the extrapolation of atmospheric-pressure results to elevated pressure, and the optical cross-section notion was originally introduced to hide inconsistencies between the Lorentz theory and experiment.

Two groups of experiments were performed. In one, the radiation from strands was studied, while in the other the full test section was used. The experimental setup for the strand tests is shown in Figure 71. The strands of propellant were burned in a modified Crawford bomb with quartz windows to permit viewing of combustion, which has been described in a report on another contract (300). The luminous output of the flame zone was focused on the entrance slit of a Bausch and Lomb 1.5-meter stigmatic grating spectrograph by a 155-mm condensing lens. The entrance slit width was set at 10 microns, and a Synchro-Compur shutter was used to allow light to fall on the entrance slit for 1/100 second. Royal X Pan 35 mm roll film was used, and was force-developed to at least ASA 1600 by using extended development - 8 minutes continuous agitation in DK50 at 68°F. The dispersion of the spectrograph is 15 Angstroms/mm, and the resulting line contours were mapped with a Leeds and Northrup recording microdensitometer, Cat. No. 6700 P-1.

The basic test propellant for the strand tests used an LP-3 binder, since polyurethane propellants containing sodium chloride are difficult to process. The base composition contained 75% bimodal AP (70% 45 μ and 30% 5 μ) and 25% LP-3. The small perchlorate was used to insure a relatively thin burning zone and a resulting spatial uniformity in the spectra. The following amounts of NaCl were added to the base composition: 0.01%, 0.1%, 0.5%, and 1.0%. Analysis indicated that close to 0.01% NaCl might be expected as an impurity. Strand thicknesses of 1/4" and 1/2" were used. The upper limit was set by the bomb dimensions, while the lower one was chosen to minimize edge effects and to insure even burning.

In the analysis of the data from the densitometer, a transmission value of 50% of the peak value for the line was taken as the measuring point, because of the varying shapes of lines which resulted. Because of the low contrast of the film when used in this range of exposure, this transmission implies an exposure change of about 10%, but accurate readings at higher transmissions were not possible, because of film imperfections and recording noise of the microdensitometer.

The following data resulted.

Table VI

Measured Spectral Line Widths for LP-3 Strands

<u>% NaCl</u>	<u>Thickness (in.)</u>	<u>Pressure (psi)</u>	<u>$\Delta\lambda$ (Angstrom Units)</u>
0.5	1/4	100	11.8
0.5	1/2	100	14.2
0.5	1/4	300	21.4
0.5	1/2	300	31.9
0.1	1/4	100	2.4*
0.1	1/2	100	4.1*
0.1	1/4	300	11.2
0.1	1/2	300	12.4*
0.01	1/4	100	1.3*
0.01	1/2	100	1.9*
0.01	1/4	300	2.9*
0.01	1/2	300	9.4

In the case of the data points marked by (*), the two lines were separated, while in the other cases, they were not. Nearly all data points represent at least 3, and usually 4, different firings. Reproducibility was quite good. The values for the samples containing 1.0% NaCl are not given since the luminosity profiles, as monitored by a photocell, indicated that the strands burned irregularly. One interesting - and predictable - result which was noted was the occurrence of self-reversal of the "D" lines, which was caused by the absorption of some of the radiation emitted by the sodium excited by the hot flame gases. The absorption occurred in the gases near the edge of the strand, which were cooled by the nitrogen purge flowing by the strand to prevent burning down the sides.

The measured line widths were, naturally, smaller than the values calculated by the method outlined in Appendix F. The values for the lower pressure and salt concentrations were close, but the disparity rapidly increased as the flame became "thicker." It may be observed, in Table VI, that something on the order of a square-root dependence on the optical flame "thickness" may be applied to the higher salt concentrations.

The second set of experiments was performed using the full width of the test section as the flame thickness, i.e., the same as motor firing conditions. The experimental set-up is shown in Figure 72. An f/3.5 quartz lens with a focal length of 132 mm was used to focus the flame image on the slit, with a magnification of 1.15. Once again, a slit width of 10 microns was used, but the shutter was set at 1/50 second, since the window transmission caused a dropoff in exposure, especially for the propellants containing less salt. The samples were end-burning discs inhibited with Dow-Corning silicone vacuum grease, and pressure regulation was accomplished by a nozzle.

The base composition used was the plastisol type, containing 43.26% triethylene glycol dinitrate, 21.49% Olin-Mathieson Ball Powder "A", and 35.25% AP(70% 45 μ - 30% 5 μ). More on this type propellant will be given in the next section, and processing techniques are given in Appendix G. The plastisol was used rather than the LP-3 because of the plastisol's "cleaner" burning. The salt concentrations used were those thought likely to be used in actual motor firings, namely 0.05%, 0.1% and 0.5% NaCl. In addition, higher pressures than those possible in the optical strand burner were used, again because of the probable range for motor firings.

general, reproducibility was not good, because of non-even burning, some window dirtying by vacuum-grease combustion, and the wide spectral curves which resulted. Once again, a 50% transmissivity was used for band-width measurements. The following data resulted.

Table VII

Measured Line Widths for Plastisol Test Specimens

<u>% NaCl</u>	<u>Average Pressure (psi)</u>	<u>$\Delta\lambda$ (Angstrom Units)</u>
0.05	325	55
0.05	740	75
0.1	380	180
0.1	700	240
0.5	400	*
0.5	730	*

In the case of the 0.5% NaCl firings, the curves were so broad that other combustion spectral features overlapped, so that good readings could not be obtained.

A comparative test was also made to obtain the band width of the standard interference filter used, a Bausch and Lomb second-order filter number 33-79-58, with a peak transmittance of 34% and a half-width of 100 Angstroms. A spectrum of the output of a tungsten lamp after passage through the filter was obtained, and the 50%-transmissivity criterion resulted in a band width of 210 Angstroms. By comparison, then, the line shapes were broader than the filter-transmission shape for a salt concentration of 0.1% and pressures above 700 psi and for all pressures likely to be used for a salt concentration of 0.5% (Figure 73).

A simple experiment to corroborate these findings was performed during actual test firings with the oscillator. A molybdenum rod was placed inside the test section and viewed through a sodium filter with the Fastax movie camera, so that the rod was being viewed through slightly less than a 1-inch-thick flame. With unsalted samples, the rod was visible

throughout a firing. With 0.1% salt, the road was barely visible at high pressure and became invisible for 0.2% salt at high pressures, while the rod quickly disappeared in firings with samples containing 0.5% salt, showing that radiation from less than a 1-inch thickness of the flame gas was passing through the filter. These observations correlate well with the spectral-line-width experiments.

IX. Photomultiplier Design and Calibration

A schematic drawing of the apparatus used for simultaneous measurement of luminosity and pressure is shown in Figure 74. In addition to the direct recording of the two signals, the outputs are also recorded on the tape recorder mentioned above for more detailed analysis. Since the slit is fixed and the sample surface regresses, the phototube records the luminosity at a continuously increasing distance from the surface.

At first, a 1P42 photocell was used as the sensing element, with the collimating slits set at 1 millimeter, so that radiation from a 1-millimeter-wide-cross-section of gas was incident on the receiving element. The absolute magnitude of signals received was well within an order of magnitude of that predicted, indicating that the emissivity was, indeed, close to unity. However, the signal-to-noise ratio was too low to permit accurate recording.

As a result, a 6217 photomultiplier replaced the photocell as the sensing element. The circuit used is shown in Figure 75. The driving voltage was supplied by a Keithley Model 242 Regulated High Voltage Supply, which delivers up to 3500 volts with 0.005% regulation. With highly salted samples, 750 volts excitation provided signal levels near 1 volt, even though the collimating slit width was decreased to 0.5 millimeters, thereby increasing the resolution of the experiment. The photomultiplier has the additional advantage that the signal can be increased greatly by increasing the power-supply voltage as needed, as for example when a small salt concentration is used.

A series of calibration runs was performed with the photomultiplier system to test for linearity and any possible hysteresis. A G. E. tungsten-filament lamp, Model Number 18A/T10/2P-6V, with an SR-6A filament was used as the source, with a sodium filter interposed between the lamp and the phototube system. The temperature of the source was taken with a Leeds and Northrup optical pyrometer, and tests were run with the lamp inside and outside of the test section, and with and without a window in the test section. An excitation voltage of 750 volts was used, and the slits were set at 0.5 mm width. The data are given in Tables VIII, IX, and X, and are plotted in Figures 76 through 80. The effects of enclosing the lamp in the test section and on the window transmissivity can be clearly seen. It is also apparent that the photomultiplier is linear and has no hysteresis.

An additional check was obtained with the aid of a set of optical neutral-density filters with densities from 0.1 to 1.0 (transmissivity from 0.795 to 0.10). The output of the photomultiplier fell linearly as the transmissivity of the filter decreased, showing that the phototube radiometric system was linear.

Table VIII

Photomultiplier Calibration for Lamp Out of Test Section

<u>Current (amps)</u>	<u>T_b (°K)</u>	<u>T_b⁻¹ (10⁻⁶°K⁻¹)</u>	<u>Photomultiplier Output (Volts)</u>
14	2333	429	0.070
16	2508	399	0.182
18	2653	377	0.378
20	2813	355	0.775
22	2983	335	1.35
24	3083	324	2.06
22	2953	339	1.32
20	2818	355	0.815
18	2663	376	0.401
16	2523	396	0.195
14	2333	429	0.070

Table IX

Photomultiplier Calibration for Lamp in Test Section

<u>Current (amps)</u>	<u>T_b (°K)</u>	(with windows)	<u>Photomultiplier Output (Volts)</u>
		<u>T_b⁻¹ (10⁻⁶°K⁻¹)</u>	
16	2418	414	0.163
18	2573	389	0.380
20	2718	368	0.705
22	2853	351	1.18
24	2963	337	1.96
14	2293	436	0.072
16	2433	411	0.163
18	2603	384	0.383
20	2723	367	0.700
22	2863	349	1.22
24	2983	335	1.92

Table X

Photomultiplier Calibration for Lamp in Test Section

<u>Current (amps)</u>	(without windows)		<u>Photomultiplier Output (Volts)</u>
	<u>T_b(°K)</u>	<u>T_b⁻¹(10⁻⁶°K⁻¹)</u>	
14	2373	421	0.065
16	2533	395	0.182
18	2703	370	0.398
20	2858	350	0.845
22	2973	336	1.41
24	3123	320	2.25
22	2993	334	1.40
20	2863	349	0.810
18	2713	369	0.415
16	2548	392	0.182
14	2383	420	0.070

CHAPTER IX

EXPERIMENTAL RESULTS

The experimental results to be reported are essentially negative, since the expected strong thermal waves were not found. However, some explanation for the type waves reported by Wood (193) has been obtained.

The techniques used to observe and characterize the expected waves were discussed in the preceding section. They fall into two main categories, radiometric and photographic, although the photography can be further subdivided into cinematography and streak photography. The radiometric technique, based on the addition of a sodium salt to the test sample and the recording of the emission from the spectral region near the D-lines, was outlined previously in Chapter VIII. Cinematography with the Fastax used black-and-white film most often, with color film being employed for more definitive viewing. Black-and-white film was used in conjunction with a sodium filter for the photography of the combustion of salted samples. In the streak-camera work, only Tri-X black-and-white film was used, both with and without a sodium filter.

Preliminary test firings, all at 430 cps, were made with the LP-3 binder system, as mentioned earlier. A sample containing 80% bimodal AP (70% $210\ \mu$ - 30% $25\ \mu$) seemed to emit some bands at 300 psig with oscillations of 100 psig amplitude, but not at 600 psig with 170 psig amplitude. In addition, the same basic composition, but with a $45\ \mu$ - $5\ \mu$ oxidizer distribution, did not emit any thermal waves at either 350 psig or 650 psig. In an attempt to make the waves more visible, 0.1% NaCl was added to the LP-3 propellants, but no evidence of waves was obtained.

The first propellant system to be studied extensively under oscillating pressure conditions was the polyurethane system. Observations were made at frequencies from 77 cycles per second to 950 cycles per second.

The photographic (color) results for end-burning samples containing 85% trimodal ammonium perchlorate are shown in Table XI on the following page.

Table XI

Observation of Luminosity Waves from Polyurethane Propellant

Containing 85% Ammonium Perchlorate

<u>Frequency (cps)</u>	<u>Pressure (psig)</u>	<u>Amplitude (psig)</u>	<u>Remarks</u>
950	600	15	No Waves
430	430	150	Narrow faint band emitted from surface about 90° after a pressure minimum.
265	330	85	Wide faint band emitted from surface near pressure minimum.
190	270	80	
150	310	50	
105	290	90	
77	455	80	

In no cases were these waves as distinct as had been expected, and determination of phase relations was quite difficult.

The effect of oxidizer particle size was studied by using a finer perchlorate blend, (70% 45 μ - 30% 5 μ), which would lead to a thinner combustion zone. Because of the higher viscosity resulting from the finer particles, the oxidizer content was lowered to 80%. The photographic (color) results for the 80% - 20% propellant are given in Table XII below.

Table XII

Observation of Luminosity Waves from Polyurethane Propellant

Containing 80% Ammonium Perchlorate

<u>Frequency (cps)</u>	<u>Pressure (psig)</u>	<u>Amplitude (psig)</u>	<u>Remarks</u>
950	600	15	No Waves
430	720	120	
	400	180	
	310	150	
265	1150	90	
	850	95	
265	330	105	Wide faint bands, becoming more diffuse as frequency dropped.
190	450	55	
150	340	75	

No particular difference in behavior was observed for the different oxidizer sizes, although the bimodal grind samples did seem to emit slightly clearer waves. As a result, propellant based on the bimodal perchlorate was chosen as the base propellant for addition of 0.1% salt, both to intensify the waves for photographic observation and to enable the use of the luminosity equipment. Tests were made for the conditions in Table XIII.

Table XIII

Conditions for Observation of Luminosity Waves from Polyurethane

Propellant with 0.1% Salt

<u>Frequency</u> <u>(cps)</u>	<u>Pressure</u> <u>(psig)</u>	<u>Amplitude</u> <u>(psig)</u>
950	600	10
430	{ 510	55
	{ 430	150
	{ 340	140
265	{ 840	75
	{ 570	65
	{ 330	105
190	1060	125
	250	85

Neither the phototube radiometer nor the film record (black-and-white through a Na filter) showed any entropy variation. The fluctuation of luminosity recorded by the phototube was exactly in phase with the pressure, and the film record showed that the entire visible field had a uniform emissive power, although varying sinusoidally with time (Figure 95).

Various explanations for the lack of distinct thermal waves were advanced. The first concerned the possibility that one driver grain was too close to the sample surface, and was interfering with the gas flow from the sample surface, probably through turbulence, or was "poisoning" the entropy waves through backflow and resulting cancellation of wave effects. To correct this, a 4" spacer assembly was added, giving a distance of 6" between the inhibited end of the driver grain and the sample surface. A series of runs was made using polyurethane samples, with the results shown in Table XIV.

Table XIV

Conditions for Testing Standoff Effect with Polyurethane Samples

<u>Frequency (cps)</u>	<u>Pressure (psig)</u>	<u>Amplitude (psig)</u>	<u>% AP</u>	<u>Remarks</u>
400	350	95	85	Narrow faint band emitted from surface about 90° after pressure minimum.
255	700	75	80	} Diffuse bands about 45° after minimum.
	560	80		
	480	70		
115	620	70	80	} Diffuse bands, too weak to obtain phase.
	560	70	85	

Comparison of the results in Table XIV with those of Tables XI and XII indicates that driver proximity had no effect on the lack of emission of thermal waves. In fact, no difference in the appearance of the gas zone in the sample chamber could be detected, indicating that the amount of backflow and turbulence from the driver grain was minimal.

Another possibility was based on the fact that the sodium added to the propellant to bring out the thermal waves might, in fact, be smearing them out by some chemical means. The possibility of some concentration effects causing an obscuration of all but boundary-layer effects was also considered. To test these possibilities, the salt concentration was varied from 0.02% to 0.5% NaCl and photographs and radiometric traces were taken for a wide range of pressures and frequencies. Color movies were taken for the lower concentrations, and black-and-white movies were taken through a sodium filter for the higher concentrations. In no case were thermal waves observed.

The method of adding the sodium to the test sample was also considered. To make sure that bunching of NaCl particles was not occurring, the salt was ground in a grinder at 12000 RPM, screened, and kept dry in an oven until placed in the mixer hopper. Microscopic observation of the propellant surface did not show any salt particles larger than 10 - 20 μ . One difficulty was never overcome, however. The sodium was always added as a salt which was insoluble in the polyurethane binder. Attempts to use sodium compounds which would dissolve in the polyurethane were unsuccessful, since all compounds tried affected the polymerization of the fuel adversely.

Considerations with sodium seemed minor, however, considering the fact that Wood (193) had photographed clear luminous waves emitted from the surface of an ammonium perchlorate-containing plastisol nitrocellulose type of propellant. At a pressure of 800 psi and a frequency of 200 cps, streak

photographs indicated that the release of luminous bands from the surface preceded the pressure maxima by somewhere between 90° and 180° (Figure 81). At lower pressures (400 psi) and higher frequencies (500 cps), the waves were more diffuse and the phase lead was less. In these tests, Wood did not have to add sodium to the propellants to obtain waves which were visible, both in colored movies and in black-and-white streak photographs.

As a result, next consideration was given to possible differences in combustion characteristics for the plastisol system used by Wood and the pure composite systems used in the original (although exhaustive) tests performed here. At about the same time, facilities for making plastisol-type propellants had been set up in the Solid Propellant Processing Laboratory of the Guggenheim Labs (see Appendix G) through the kind assistance of personnel at the Rohm & Haas Company's Redstone Arsenal Research Division, who had developed the processing techniques and cast the propellants used by Wood. The burning rate of a typical plastisol propellant as a function of pressure is given in Figure 82.

A series of tests followed with plastisol propellants. Full compositional details are given in Appendix G, so only distinguishing characteristics will be given. Test conditions were as given in Table XV.

Table XV

Test Conditions for Plastisol Propellant Samples

<u>Frequency (cps)</u>	<u>Pressure (psig)</u>	<u>Amplitude (psig)</u>	<u>Propellant</u>
255	650	70	P-4
	620	90	P-6
	700	60	
	600	55	P-7
	700	50	
	680	40	P-8
	550	50	
	570	60	P-9
180	850	45	9a-67
	900	50	
	700	40	
	910	45	P-7
	700	40	
175	700	50	9a-67

It should be noted that the runs were generally at higher pressures than for the polyurethane. Spacers were used in every case, both to insure no backflow and to give amplitudes comparable with those used by Wood, which

were of the order of 75 psi for the 800-psi firings. The distinguishing characteristics of the plastisols made here, all designated with a P-No., are as follows. All contained 35% AP, which was 70% 45 μ - 30% 5 μ , except for P-6, which contained all 5 μ perchlorate. Batch P-6 also contained 0.2% NaCl, while P-8 was identical to P-4 plus 0.2% NaCl. Batches P-4 and P-7 were identical, as were P-8 and P-9. The 9a-67 propellant was furnished by Rohm & Haas, and was the same type as that used by Wood in some tests.

The results of the firings were quite bewildering, since no waves of the type reported by Wood were observed, either photographically from movies or streak photographs or radiometrically. In every case, more than one run was made for a set of test conditions. The same statement can be made for the different tests reported with the polyurethanes, where duplicate runs were made, first with black-and-white film, to establish proper exposure, then with color film.

A search for minor compositional differences between propellants used at Princeton and those used at Rohm & Haas was carried out. Although exact formulations were classified, it was found that a slightly different ball powder (containing no carbon black) was used, no stabilizing agent was added, and that the anticaking agent used on the ammonium perchlorate was magnesium oxide, rather than the tricalcium phosphate present on the oxidizer as received at Princeton. Successive batches made here eliminated the stabilizer (P-10), changed the ball powder (P-15), and changed the oxidizer particle size (P-16). Firings were made over a range of pressures at oscillation frequencies of 180 and 255 cycles per second, but no waves were photographed at all.

The next avenue investigated was the configuration of the test sample. A phone call to Wood (301) revealed that the thickness was 0.25 inches, while the sample diameter was 1.50 inches in a chamber having a 1.85-inch diameter. It was further revealed that waves had been observed only in tests where the sample had been left uninhibited to insure that the windows were not dirtied, and that a few inhibited firings, late in his test program, had shown no waves. The lack of observable waves was ascribed to experimental difficulties.

As a result of this communication, a series of firings was conducted. Duplicate conditions were used, except that the sample was uninhibited in one firing and inhibited in the other. To insure window clarity and even burning, the inhibited samples were cast into steel cups and cured. Although the surface was blocked from view, the observations of interest were away from the surface, so the cup technique was felt to be a good one for this series. The sets of conditions given in Table XVI were used.

Table XVI

Test Conditions for Comparing Inhibited and Uninhibited Test Samples

<u>Frequency (cps)</u>	<u>Pressure (psig)</u>	<u>Amplitude (psig)</u>	<u>Propellant</u>
255	760	45 }	P-11
	850	30 }	
	1040	40 }	
175	880	55	P-11
	700	40	9a-67
	780	40 }	P-15
	640	35 }	
	770	40 }	P-16
	650	35 }	
	770	40	
	650	35 }	85% trimodal AP, 15% polyurethane
	790	35 }	
			80% bimodal AP, 20% polyurethane

In every one of these twelve sets of firing conditions, luminous waves were emitted from the propellant when the sample was uninhibited, while the inhibited samples gave no waves, indicating that the luminous waves previously observed by Wood (5) did not arise from a one-dimensional situation. The waves were observed both by colored movies and by black-and-white streak photographs (Figures 83, 84). Sample diameters of 1.50" and 1.75" were used in the Princeton test chamber, which has a diameter of 1.938", and 0.25-inch-thick samples were used. No definite statement can be made as to the comparative strength of the waves for the different sample diameters used here.

Possible explanations for the nonoccurrence of entropy waves in a one-dimensional situation will be considered in following sections. Some preliminary tests were performed to characterize the waves found at Princeton for the uninhibited (non-one-dimensional) case. These tests involved the addition of salt to the test sample to see if the waves were strictly temperature waves. However, streak pictures taken through a sodium filter indicated very little wave behavior, especially after equilibrium pressure (600 psig) had been reached. In addition, simultaneous radiometric traces, also through a sodium filter, revealed that the luminosity fluctuation was again in phase with the pressure. Both of these results indicated that one-dimensional entropy waves still did not exist.

The most logical explanation for the generation of waves from the uninhibited, side-burning test specimen is involved with wall effects, owing to the large heat sink represented by the cooler walls. The pressure fluctuations lead to periodic cooling, resulting in the liberation of temperature

waves as follows. When the pressure rises, the gas velocity falls, while the efflux velocity rises in the decreasing part of the pressure cycle, so that the gases around the side of the propellant can be released into the gas stream. As a result, the gases effectively have an oscillatory stay time, which leads to an oscillatory cooling or heat-loss effect, so that the temperature of the gases emitted from the sample sides will fluctuate with time. Therefore, these waves are a type of entropy wave, but they result from an oscillatory cooling effect.

This mechanism of wave generation also explains the failure to observe the waves with salted propellant. The dominant radiation from the salted test specimen comes from the center of the specimen, and would overwhelm any variations in luminosity from the edge. In the case of the unsalted propellants, however, the gases emitted from the edges would be clearly visible. Systematic tests with varying sample diameter, and with salt only in the outer portion of the test specimen, should help to reveal the magnitude of any such periodic cooling effects.

CHAPTER X

DAMPING MECHANISM STUDIES

The failure to observe the predicted entropy waves leads to a study of possible mechanisms through which the waves can be damped out or reduced in magnitude. First thought was given to the possibility of an error in estimation of the proper boundaries of the pressure-frequency map of acoustic interaction (Fig. 21).

The region of most interest was the "low-frequency" one, since experiments here had been conducted in the "zero-frequency" and "low-frequency" regimes, as drawn in Fig. 21. The "low-frequency" regime is characterized by the assumption that the reactions in the flame zone are quasi-steady, but the temperature distribution in the solid deviates from the steady-state.

Consider the following very simplified model of a solid-propellant flame:

(1) There are no exothermic reactions in the solid. The time-dependent heat-transfer equation in the solid becomes:

$$k \frac{\partial^2 T}{\partial x^2} - mc \frac{\partial T}{\partial x} = \rho c \frac{\partial T}{\partial t} \quad (98)$$

For steady-state, integrating once,

$$k \frac{dT}{dx} - mc (T - T_0) = 0 \quad (99)$$

where T_0 = initial temperature of the solid

c = heat capacity

(2) The solid decomposition reaction near the surface is assumed to occur in such a narrow zone that this region can be considered as a surface with a unique temperature (varying only with time) and with negligible heat content. The heat equation for this zone can be written

$$k \left(\frac{dT}{dx} \right)_{s^+} - mcT_s = k \left(\frac{dT}{dx} \right)_{s^-} - mcT_s + m \Delta H_v \quad (100)$$

where T_s = temperature at the surface, s^+ refers to the gas-phase side of the surface, and s^- refers to the solid-phase side of the surface. Defining

$$\Delta H_v = cT_o = h \quad (101)$$

equation (100) becomes, for steady-state,

$$k \left(\frac{dT}{dx} \right)_{s^+} = \bar{m} (c\bar{T}_s + h) \quad (102)$$

(3) The solid decomposition reaction is pressure-independent and a function of temperature only. It is further assumed that this dependence is described by an Arrhenius equation, i.e.

$$m = Ae^{-E/RT_s} \quad (103)$$

Under these conditions, the heat flux from the gas phase into the solid becomes, from (102):

$$\begin{aligned} \frac{d}{d\bar{p}} k \left(\frac{dT}{dx} \right)_{s^+} &= \frac{d}{d\bar{p}} [\bar{m}(c\bar{T}_s + h)] = (c\bar{T}_s + h) \frac{d\bar{m}}{d\bar{p}} \\ &+ \bar{m} \frac{d}{d\bar{p}} (c\bar{T}_s + h) \end{aligned} \quad (104)$$

Assuming that

$$m = ap^n \quad (105)$$

$$\frac{d\bar{m}}{d\bar{p}} = \frac{n \bar{m}}{\bar{p}} \quad (106)$$

If it is further assumed that h is independent of pressure, then (104) becomes

$$\frac{d}{d\bar{p}} k \left(\frac{dT}{dx} \right)_{s^+} = \left(c\bar{T}_s + h + \bar{m}c \frac{d\bar{T}_s}{d\bar{m}} \right) \frac{n \bar{m}}{\bar{p}} \quad (107)$$

At this point, it is well to reiterate that (104) and (107) are for steady-state conditions or slow changes from steady-state.

(4) The flame zone near the surface is thin enough that its heat capacity can be neglected. The heat equation across this zone is then:

$$k \left(\frac{dT}{dx} \right)_{x=x_F} - mcT_F = k \left(\frac{dT}{dx} \right)_s - mcT_s + m \Delta H_F \quad (108)$$

For steady-state,

$$c(T_F - T_s) + \Delta H_F = -(cT_s + h) \quad (109)$$

since

$$k \left(\frac{dT}{dx} \right)_{x=x_F} = 0$$

These four statements, equations (98), (100), (103), and (108), define the model.

Consider now a small sinusoidal pressure perturbation with angular frequency ω . In complex notation,

$$p = \bar{p} + \tilde{p} e^{i\omega t} \quad (110)$$

where

$$\left| \frac{\tilde{p}}{\bar{p}} \right| \ll 1$$

If the flame is stable to the pressure perturbation, then the temperature and mass flow will also vary sinusoidally (to first order) with the same frequency. As a result,

$$T_s = \bar{T}_s + \tilde{\Theta}_s e^{i\omega t} \quad (111a)$$

$$T_F = \bar{T}_F + \tilde{\Theta}_F e^{i\omega t} \quad (111b)$$

$$\frac{dT}{dx} = \left(\frac{dT}{dx} \right) + \frac{d\tilde{\Theta}}{dx} e^{i\omega t} \quad (111c)$$

$$m = \bar{m} + \tilde{m} e^{i\omega t} = \bar{m} + \frac{\tilde{\mu}}{RT_s} \bar{m} \tilde{\Theta}_s e^{i\omega t}$$

or, defining $\beta = \frac{\bar{m} E}{RT_s^2}$,

$$m = \bar{m} + \beta \tilde{\Theta}_s \quad (111d)$$

In this form, partial derivatives become ratios, e.g.

$$\frac{\partial \mu}{\partial \Theta} = \frac{\tilde{\mu}}{\tilde{\Theta}}$$

Equation (100) can now be written:

$$\begin{aligned} k \left(\frac{d\tilde{\Theta}}{dx} \right)_s + -mc \tilde{\Theta} - \bar{T}_s c \beta \tilde{\Theta} - \beta \tilde{\Theta}_s h = \\ k \left(\frac{d\tilde{\Theta}}{dx} \right)_s - -mc \tilde{\Theta}_s - \beta \tilde{\Theta}_s c (\bar{T}_s - \bar{T}_0) \end{aligned} \quad (112)$$

By solving the heat conduction equation in the solid for a cyclic temperature perturbation

$$k \frac{d^2 \tilde{\Theta}}{dx^2} - \bar{m} c \frac{d\tilde{\Theta}}{dx} - \left(\tilde{\Theta}_s \frac{d\bar{T}}{dx} - i\omega \tilde{\Theta} \right) = 0 \quad (113)$$

under the boundary conditions

$$x = 0, \quad \tilde{\Theta} = \tilde{\Theta}_s$$

$$x = -\infty, \quad \tilde{\Theta} = \tilde{\Theta}_0$$

(see Hart and McClure (85), Akiba and Tanno (87), or Shinnar and Dishon (82)); the following equation is obtained

$$\begin{aligned} k \left(\frac{\partial \tilde{\Theta}}{\partial x} \right)_s = \frac{\tilde{\Theta}_s \bar{T}_s \bar{m} c}{2} [1 + (1 + 4i\omega \tau_s)^{\frac{1}{2}}] + \frac{\beta \tilde{\Theta}_s c (\bar{T}_s - T_0)}{2i\omega \tau_s} \\ [(1 + 4i\omega \tau_s)^{\frac{1}{2}} - 1] \end{aligned} \quad (114)$$

where

$$\gamma_s = \frac{k \rho}{c \bar{m}} \quad (115)$$

The characteristic time γ_s is a measure of the response time of the solid to a temperature change at the boundary.

Inserting (114) into (112):

$$k \left(\frac{d\tilde{\Theta}}{dx} \right)_{s+} - \tilde{\Theta}_s (mc + \beta T_s c + \beta h) = \beta \tilde{\Theta}_s Q(\omega) \quad (116)$$

where

$$Q(\omega) \equiv c(\bar{T}_s - \bar{T}_0) \left[\frac{(1 + 4i\omega\gamma_s)^{\frac{1}{2}} - 1}{2i\omega\gamma_s} - 1 \right] + \frac{1}{2} \frac{cm}{\beta} [(1 + 4i\omega\gamma_s)^{\frac{1}{2}} - 1] \quad (117)$$

and

$$\tilde{\Theta}_s = k \left(\frac{d\tilde{\Theta}}{dx} \right)_{s+} \frac{1}{(cm + \beta c T_s + \beta h) + \beta Q(\omega)} \quad (118)$$

In the same way, equation (108) becomes

$$c\bar{m} (\tilde{\Theta}_F - \tilde{\Theta}_s) + c\beta \tilde{\Theta}_s (\bar{T}_F - \bar{T}_s) = -k \left(\frac{d\tilde{\Theta}}{dx} \right)_{s+} - \beta \tilde{\Theta}_s \Delta H_F \quad (119)$$

or, using (109):

$$c\bar{m} \tilde{\Theta}_F = -k \left(\frac{d\tilde{\Theta}}{dx} \right)_{s+} + \tilde{\Theta}_s [\beta (c\bar{T}_s + h) + \bar{m}c] \quad (120)$$

Combining (118) and (120):

$$c\bar{m} \tilde{\Theta}_F = -k \left(\frac{d\tilde{\Theta}}{dx} \right)_{s+} \left(-1 + \frac{\beta (c\bar{T}_s + h) + \bar{m}c}{\beta (c\bar{T}_s + h) + \bar{m}c + \beta Q(\omega)} \right) \quad (121)$$

Equation (121) gives a relation between $\hat{\Theta}_F$ and $\left(\frac{d\hat{\Theta}}{dx}\right)_{s+}$, assuming that the gas-phase reactions are very fast and that there are no delays in the burning zone. If one further assumes that equation (104) also applies to the "low-frequency" range then

$$\frac{k \left(\frac{d\hat{\Theta}}{dx} \right)_{s+}}{\hat{\phi}} = \frac{\bar{m}}{\bar{p}} \left(c\bar{T}_s + h + \frac{\bar{m}c}{\beta} \right) \quad (122)$$

One can now compute the relative magnitude of the flame-temperature oscillations as compared to the pressure oscillations:

$$\frac{\hat{\Theta}_F \bar{p}}{\bar{T}_F \hat{\phi}} = \frac{(c\bar{T}_s + h + \frac{\bar{m}c}{\beta}) n}{c\bar{T}_F} \left[\frac{-Q(\omega)}{c\bar{T}_s + h + \frac{\bar{m}c}{\beta} + Q(\omega)} \right] \quad (123)$$

In addition, the acoustic admittance for the "low-frequency" region can also be derived and compared to the value for the isothermal case. Since the flame reactions are immediate, the acoustic admittance can be written:

$$Y_F' = - \left(\frac{dv}{dp} \right)_{x=x_F} = - \frac{d(m/\rho)}{dp} = - \left(\frac{1}{\rho} \frac{dm}{dp} + m \frac{d(1/\rho)}{dp} \right) \quad (124)$$

But

$$\frac{d(1/\rho)}{dp} = \frac{d \left(\frac{RT}{p} \right)}{dp} = - \frac{RT}{p^2} + \frac{1}{p} \frac{d(RT)}{dp} \quad (125)$$

so that

$$\begin{aligned} Y_F' &= - \left(\frac{1}{\rho} \frac{dm}{dp} - \frac{mRT}{p^2} + \frac{mR}{p} \frac{dT}{dp} \right) \\ &= - \frac{mRT}{p^2} \left(\frac{p^2}{mRT\rho} \frac{dm}{dp} - 1 + \frac{p}{T} \frac{dT}{dp} \right) \\ &= - \frac{m}{\rho p} \left(- \frac{p}{\rho m} \frac{dm}{dp} - 1 + \frac{p}{T} \frac{dT}{dp} \right) \end{aligned} \quad (126)$$

For small perturbations, (126) can be written:

$$Y_F' = - \frac{\bar{m}}{\bar{\rho} \bar{p}} \left(\frac{\bar{p} \tilde{\mu}_F}{\tilde{\rho} \bar{m}} - 1 + \frac{\bar{p} \tilde{\Theta}_F}{\bar{T} \tilde{\rho}} \right) \quad (127)$$

At $x = x_F$, $T = T_F$, $\mu_F = \mu_s = \beta \Theta_s$, so that (127) becomes:

$$Y_F' = - \frac{\bar{V}}{\bar{p}} \left(\frac{\bar{p} \beta \tilde{\Theta}_s}{\bar{m} \tilde{\rho}} - 1 + \frac{\bar{p} \tilde{\Theta}_F}{\bar{T}_F \tilde{\rho}} \right) \quad (128)$$

Of the terms in parentheses, $\bar{p} \tilde{\Theta}_F / \bar{T}_F \tilde{\rho}$ is given by (123), and $\bar{p} \beta \tilde{\Theta}_s / \bar{m} \tilde{\rho}$ can be found by combining (118) and (122), giving

$$\frac{\bar{p} \beta \tilde{\Theta}_s}{\bar{m} \tilde{\rho}} = \frac{\beta n (c \bar{T}_s + h + \frac{\bar{m} c}{\beta})}{\beta (c \bar{T}_s + h + \frac{\bar{m} c}{\beta}) + Q(\omega)} \quad (129)$$

If $\left(\frac{\bar{p} \beta \tilde{\Theta}_s}{\bar{m} \tilde{\rho}} - 1 + \frac{\bar{p} \tilde{\Theta}_F}{\bar{T}_F \tilde{\rho}} \right)$ has a real positive part, the propellant

is unstable. As a check, it can be seen that, as $\omega \rightarrow 0$, equation (123) $\rightarrow 0$

and $Q(\omega) \rightarrow 0$, so that the admittance becomes $Y = \frac{-\bar{V}}{\bar{p}} (n-1)$, the value predicted for the "zero-frequency" case, which is the only truly isothermal case.

Actually, Y_F' should be replaced by Y_F , the value in the isentropic region far from the surface. For low frequencies, however, with their long wavelengths, there should be very little difference between Y_F' and Y_F and there is, therefore, little justification to compute the far more complicated Y_F .

In order to determine the effect of the several physical parameters involved, the temperature variation was calculated for a range of reasonable values of these parameters. Trends were investigated by using extreme values. The ranges used are shown in Table XVII. Figures 85-92 demonstrate some typical results. The result of most interest here is the real part of the relative temperature variation $(\tilde{\Theta}_F \bar{p} / \bar{T}_F \tilde{\rho})$, which is plotted

against frequency for various conditions in Figures 85, 89, 90, 91, 92. The specific acoustic admittance for one case is shown in Fig. 86, while Figs. 87 and 88 demonstrate the factors which make up the real part of $(\hat{\Theta}_F \bar{p} / \bar{T}_F \hat{\phi})$, i.e., the magnitude of the relative temperature fluctuation and the phase angle between the fluctuation and the pressure disturbance causing it.

Figure 85 shows the effect of a variation in the heat of surface reaction, as exemplified by $H = \Delta H_v - c_s T_o$. As H becomes less negative, the temperature fluctuation, originally out of phase with the pressure, goes into phase with the pressure. The phase angle plot in Fig. 87 shows why the real part of $(\hat{\Theta}_F \bar{p} / \bar{T}_F \hat{\phi})$ goes from negative to positive.

Table XVII

Numerical Values of Parameters Used in Calculations

H	= -200, -150, -100, +100 cal/gm
T_{surface}	= 600, 700, 900 °K
m	= 0.2, 0.5, 1.0, 2.0 gm cm ⁻² sec ⁻¹
E	= 10,000, 40,000, cal/mole (1 and 10 ⁻⁶ cal/mole for extreme cases)
k	= 5 x 10 ⁻⁴ , 10 x 10 ⁻⁴ , 15 x 10 ⁻⁴ cal cm ⁻¹ °C ⁻¹ sec ⁻¹
ρ	= 1.6 gm cm ⁻³
c	= 0.3 cal gm ⁻¹ °C ⁻¹
T_o	= 300 °K
T_F	= 2500 °K

It should be noted at this point that the in-phase temperature variation would tend to diminish the magnitude of entropy waves. Since the value of the temperature fluctuation is of the order of $\frac{\delta - 1}{\gamma}$ of the pressure fluctuation for isentropic compression, the burning would be ef-

fectively isentropic for $\text{Re} \left(\frac{\hat{\Theta}_F \bar{p}}{\bar{T}_F \hat{\phi}} \right) \approx 0.16$, and only small local temper-

ature oscillations would be expected for $\text{Re} \left(\frac{\hat{\Theta}_F \bar{p}}{\bar{T}_F \hat{\phi}} \right) > 0.08$, say. For

the conditions in Fig. 85, it can be seen that entropy waves would be obscured above 100 cycles for $H = -100$ cal/gm. The frequency range in which

this effect is appreciable will be discussed in later figures.

Figure 86 shows the specific acoustic admittance for the same parameters. It can be seen that, although the admittance is usually negative, acoustic instability is occasionally possible with this model at relatively low frequencies; less than 200 cycles per second in one case plotted, and less than 10 cycles per second in some cases.

Figure 88 shows the magnitude of the relative temperature fluctuations for different values of the heat of the surface reaction. For all the cases studied, the maximum magnitude is greater than about 10%, indicating that no single physical parameter can be adjusted to diminish the temperature variations to a point where isothermal conditions can be assured.

In Figs. 89 and 90, the importance of the characteristic time τ_s , defined by equation (115), is demonstrated. A small τ_s implies that a quasi-steady analysis can be used to higher frequencies than for a large τ_s . In the case under study, Fig. 90 shows that entropy waves would not be expected at frequencies above only 10 cycles per second for a mass flow rate of $0.2 \text{ gm cm}^{-2} \text{ sec}^{-1}$, while if the same propellant's burning rate were increased by a factor of 10, an isothermal analysis could be used up to 500 cycles per second. The burning rate affects the magnitude of the fluctuation only slightly. The main effect of burning rate variations is to modify the characteristic time and, thus, to displace the frequency scale. The thermal conductivity of the propellant affects τ_s only, and the uncertainties in the measured values of k could shift the frequencies plotted. The other factors in τ_s , ρ and c_s , are less likely to vary.

Figure 91 shows that a variation in the activation energy of the surface decomposition reaction can bring about a wide change in $\text{Re} \left(\frac{\tilde{\Theta}_F \bar{p}}{\bar{T}_F \tilde{\phi}} \right)$.

For an exothermic surface reaction, a change in the activation energy can bring about a sign change, leading to a temperature variation which is out of phase with pressure. This sign reversal with different values of E and H can occur even for very high values of activation energy.

Figure 92 shows that a decrease in surface temperature can lead to a minimization of the relative temperature fluctuations. It should be noted that the flame temperature affects only the absolute magnitude of the temperature variation, and not the relative fluctuation. The same holds true for the acoustic admittance.

The immediate result which is apparent from those calculations is that the frequency range where an isothermal analysis can be used is consistent with that proposed in Fig. 21, that is, the model used gives numerical results to support the boundary drawn on the basis of physical intuition. The boundary between the "zero-frequency" and "low-frequency" regimes rests on the criterion that the period is ten times the solid-phase heat-up time.

These calculations show that this is an accurate criterion, since the solid heat-up zone can cause quite sizable temperature fluctuations. This fact in itself shows the limits of the model, since the quasi-steady assumption becomes somewhat tenuous when the effect of the increase in gas-phase temperature on heat transfer to the solid is considered. As a result, the model undoubtedly begins to break down quantitatively when the temperature fluctuations exceed some magnitude. However, the main result - that strong flame-temperature fluctuations are possible for relatively low frequencies - should remain correct as long as the basic model of the combustion process is correct.

There exists one slight difference between the model used here and that used by Hart and McClure for the solid heat-up zone (85). In their calculations, they considered that perturbations in mass burning rate resulted from perturbations in the temperature gradient at the surface, as well as the surface temperature. This was expressed by

$$\frac{dm}{m} = \beta' \left(\frac{dT_s}{T_s} \right) + \alpha \left(\frac{dG_o}{G_o} \right) \quad (130)$$

where $G_o = dT/dx$ at the surface. For a zero-order reaction, they estimated

$$\beta' \sim \frac{E}{RT_s}, \quad \alpha \sim -1 \quad (131)$$

It can be seen that the model used here corresponds to $\alpha = 0$.

As a result of taking the gradient into account, a different form results for $Q(\omega)$ (Equation 117). The Hart-McClure form is:

$$Q(\omega) = c(\bar{T}_s - T_o) \left[\frac{(1 + 4i\omega\tau_s)^{\frac{1}{2}} - 1}{2i\omega\tau_s} - 1 \right] \quad (132)$$

$$+ \frac{1}{2} c\bar{T}_s [(1 + 4i\omega\tau_s)^{\frac{1}{2}} - 1] \times \left\{ 1 - \alpha - \frac{\alpha c_p(\bar{T}_s - T_c)}{c\bar{T}_s + h} \left[\frac{(1 + 4i\omega\tau_s)^{\frac{1}{2}} - 1}{2i\omega\tau_s} + 1 \right] \right\}$$

$$\left(\beta' + \frac{1}{2} \alpha \left[\frac{2c_p\bar{T}_s + c\bar{T}_s [(1 + 4i\omega\tau_s)^{\frac{1}{2}} - 1]}{c_p\bar{T}_s + h} \right] \right)$$

which reduces to (117) for $\alpha = 0$. The value $\alpha = -1$ was used for all their calculations. However, Hart and Cantrell (192) used values of $\alpha = -1$ and $\alpha = -0.5$ for the calculation of two different curves (Figs. 2 and 3 of Ref.

192) of temperature fluctuation, and obtained very different results. Since a number of other parameters were also changed, it was difficult to estimate the effect of α , although some qualitative remarks could be made. As a result, calculations were performed here using Equation (132) for $Q(\omega)$, rather than Equation (117). Values from -1 to 0 for α were used, with the results shown in Figs. 93 and 94. It can be seen that the larger absolute values of α tend to wash out the frequency effects on the real part of the flame-temperature fluctuation. However, the effect is slight for values of $\omega \tau < 10$, say, which is the region of most interest, so that the difference between the two models is not serious in this regard.

Other factors which could affect the interaction regime would be those which led to a thickening of the combustion zone and a subsequent increase in the transit time of a particle through the combustion zone. In the drawing of Fig. 21, a non-reactive composite solid with a thin one-stage reaction zone was assumed. Deviations from this simple model are possible in both the solid and gas phases.

A parallel program under way in the Solid Propellant Research Laboratory at the Guggenheim Laboratories is concerned with the steady-state combustion of solid propellants at low (subatmospheric) pressures (302). Under conditions where heat loss causes extinction of the gas-phase flame ($1\frac{1}{2}$ " of Hg), combustion is observed to continue for some time. Thermocouple records of the temperature in the solid indicate that reactions are occurring at relatively low temperatures ($\sim 206^\circ\text{C}$). A parallel program dealing with the propellant surface temperature during ignition has also found some evidence of heat release in the solid, but the amount of energy involved is quite small - no more than that involved in exothermic pyrolysis - and should not be important in steady-state burning at pressures of the order of 500 psi (303). Further research is underway at Princeton on the magnitude of these subsurface reactions, which might interact in a different manner with a pressure fluctuation than the gaseous flame zone. Additional work in the same field is being carried out at United Technology Center (304), but no quantitative results are available.

A more likely cause for a possible error in estimating transit times through the reaction zone is the structure of the gaseous phase of the flame zone. For a heat- and mass-transfer balance to exist in steady-state combustion, there must be a steep temperature gradient immediately adjacent to the surface. This gradient could be caused by the occurrence of the bulk of combustion in a thin zone (of the order of 100 microns) near the surface. However, it is quite possible that this concentrated combustion zone is followed by a rather diffuse after-burning zone where the combustion reactions go to completion. Such an after-burning zone would modify the pressure-flame interaction in two ways. First, the transit time could be affected, and second, (although a corollary), the thermochemistry could be affected. If, for instance, pressure-sensitive reactions were involved in the completion of combustion, the energy release could fluctuate as a function of time at the edge of the flame zone.

The determination of the thickness of the flame zone is not a simple matter. Ordinary photographs do not suffice. Some qualitative experiments

conducted here indicate, however, that the flame-zone thickness may be of the order of 1 - 2 millimeters, rather than 100 microns, as reported by Sutherland (182). Sabadell (131) observed that thermocouple traces levelled off in the gas phase of the flame for 2 millimeters or more at pressures as high as 1000 psig before rising a second time, which shows that, for some propellants, the gaseous reactions may occur in two stages.

Another set of experiments concerned the spectral distribution of the flame zone. For this work, two spectrographs were used - the Bausch and Lomb Stigmatic Grating Spectrograph mentioned earlier and a Hilger and Watts Intermediate Quartz Spectrograph. The experimental layout used is the same as that for the "D" line contour tests shown in Fig. 72. Once again, Royal-X Pan 35 mm roll film was used with the Bausch and Lomb, and Kodak Super Pan-chro-Press 5 x 7 Plates were used in the Hilger and Watts instrument. For identification of emitting spectra, exposures of 1 second were used. The recording microdensitometer was used with the Bausch and Lomb, for species identification, together with the compendium of Gaydon and Pearse (305). A comparison of these with the results of Sutherland show a number of disparities. First, a number of emitters characteristic of impurities are present. These result from the presence of calcium, and the CaCl red and orange systems ($A^2\Pi \rightarrow X^2\Sigma$ and $B^2\Sigma \rightarrow X^2\Sigma$) are nearly as strong as the sodium lines. In addition, the 5570-5530 CaOH band is present, as is the Ca line at 4227 Angstrom units. The calcium is present as tricalcium phosphate, which is used as an anticaking agent for the ammonium perchlorate oxidizer. In addition, a number of CuCl bands ($D^1\Pi \rightarrow X^1\Sigma$, $E^1\Sigma \rightarrow X^1\Sigma$) were observed. These resulted from the igniter lead wires, even though the shutter was not opened until some time after the ignition. The use of a Nichrome hot wire to ignite the propellant shavings in the igniter bag eliminated the copper-impurity emitters.

A more significant difference lies in the spectra due to emitters characteristic of hydrocarbon flames. For instance, no evidence of C_2 bands at 5165 and 4730 Å was ever obtained. In addition, the CH band at 4315 was quite weak. The CN band at 3883 was present, however, as were the OH band. Polyurethane propellants give some evidence of bands which might be ascribed to CHO near 3377, 3359, and 3299 Å.

The difference in emitters can be due to the fact that Sutherland's results are for a different binder - P - 13 - and are for strands burning in air at ambient pressure, while these spectra are for propellants at elevated pressures (20-50 atmospheres) in actual rocket-firing conditions. The effect of the surrounding atmosphere has been reported (in his sub-atmospheric work) by Most (306), who noted that a blue layer was definitely present in the gas-phase combustion of composites based on LP-3 and PBAA binders when the propellant was burned in nitrogen, while the blue layer disappeared for burning in atmospheres containing air for the same operating-pressure level. The presence of oxygen external to the binder might modify the relative importance of reactions, especially at low pressures where diffusion times are shortest. The effect of the binder is less important, since the same general differences apply between Sutherland's spectra and the ones

reported here. Since Sutherland did not state his oxidizer loading, no definite comparison on mixture ratio can be made. A difference in mixture ratio could be quite important since, as pointed out by Gaydon (307), the absolute and relative intensity of the various band systems varies considerably with mixture strength. However, Sutherland's propellants were probably more fuel-rich than those used here, a condition which would cause the C_2 and CH bands to be stronger.

Some qualitative observations on flame-zone thickness have been made. These were based on exposures of 1/10 second and viewing the relative strength of spectral lines at different heights above the surface, since the burning surface was perpendicular to the slit in these tests. During this time, the burning surface would move about 1 millimeter, depending on the burning rate. Another source of error was the finite thickness of the burning sample, since the cone subtended by the quartz lens used to focus the flame on the spectrograph slit had a height of nearly 1 millimeter at the edge of the sample. Adding these to the aberrations of the simple lens system and the viewing windows, it is difficult to say how exact quantitative measurements can be made with this particular experimental arrangement. It was observed, however, that a mercury arc used for backlighting showed a fairly sharp cutoff at the surface. The observation that the CN bands were not confined to the surface region, but extended, in some cases, over more than 3 millimeters from the surface, indicates the possibility of a reaction zone with a thickness of 1 - 2 millimeters at the pressures used (up to 30 atmospheres).

More exact tests are being carried out by Povinelli (308) and Selzer (309), who are determining quantitative distribution of emitters through the reaction zone. Their results indicate that appreciable emission takes place up to at least 2 millimeters from the surface, although both are working at atmospheric pressure. The results of Watermeier (310) indicate a reaction zone thickness of .8 - 3 millimeters at pressures from 250 to 750 psi, and Tourin (311) found, using infrared techniques, that the flame temperature was not attained until at least 1 millimeter from the surface at a pressure of 800 psi. In no case was a narrow cut of oxidizer used, so that some of the uncertainty could have resulted from different crystal sizes. In addition, the effect of pressure on apparent reaction-zone thickness has not, as yet, been carefully studied.

The effect of these experiments is, however, to cast substantial doubt on the thickness originally assumed (50μ) for the gas-phase reaction zone, and to give strong indications that a more diffuse region may exist which could be affected in a number of different ways by fluctuating pressure. One experiment proposed to delineate the effect of pressure variation on solid-propellant combustion is discussed in Appendix H.

CHAPTER XI

CONCLUSIONS AND FUTURE EXPERIMENTS

This thesis reports on an investigation of the interaction between a pressure variation and solid-propellant regression rate. The interaction is significant in the problem of combustion instability of solid-propellant rockets, some aspects of which have been described. The problem of proper classification has been shown to be important in analyzing combustion instability, and the morphological approach was used to separate the different components of the over-all phenomenon of instability in order to make a meaningful review of past and present theoretical and experimental investigations into the phenomenon. The necessity of making a proper analysis of a proposed experiment to investigate the pressure-burning rate interaction has been demonstrated, since some of the experiments performed could not possibly have succeeded owing to inherent errors greater than the effects they have tried to measure. The review also brought out the usefulness of the concept of acoustic admittance in analyzing a solid-propellant rocket as a potential amplifier of small perturbations into high-amplitude pressure and/or velocity disturbances. The acoustic admittance of a burning solid propellant was analyzed here, and found to be made up of two parts. The first of these, the dynamic burning-rate function, has been the major subject of most experimental and theoretical attacks on combustion instability. A theoretical analysis made here, based on a model which had been successful in predicting steady-state regression-rate behavior, showed that equally valuable information could be gained by investigating the second part of the admittance function, viz., the dynamic flame-temperature function. This latter function is important, not only because of its effect on the admittance, but mainly because it gives an insight into the character of the burning rate-pressure interaction as a function of frequency, steady-state pressure, and burning rate. The theoretical analysis predicted that the interaction could be investigated by a measurement, as a function of time, of the entropy of the gas emerging from the flame zone of a solid propellant burning under varying pressure. It was further predicted that, for a wide range of experimental conditions, entropy waves would be emitted from the surface of a sample burning under oscillating pressure. These waves would be visible as cyclic variations in gas temperature, so an experimental program was carried out to measure the temperature and, since the pressure was known, the entropy of the gases in a duct where a solid propellant was burned under oscillating pressure. A 2-inch-diameter T-tube combustor was found to be an excellent source of fluctuating pressure, giving oscillations from 75 to 1600 cycles/second with amplitudes adjustable up to 50% of the mean pressure level, which was as high as 1200 psi. The acoustic interaction, as represented by the gas-temperature behavior, was observed by optical techniques, including high-speed (5000 frames per second) cinematography, streak photography, and spectral radiometry with sodium-doped samples.

None of the experimental techniques employed detected the thermal waves whose existence had been predicted by the above-mentioned theoretical analysis. Four different propellant systems based on ammonium perchlorate

BLANK PAGE

were studied. Three were of the inert-fuel binder type, using a polybutadiene-acrylic acid binder, a polysulfide binder, or a polyurethane binder, while the fourth used a plastisol-nitrocellulose binder. In no case were entropy waves observed to be emitted from a sample burning in a one-dimensional manner. Since waves appearing to have some of the properties expected of entropy waves had previously been observed photographically by another investigator, an attempt was made to duplicate the experimental conditions under which the waves had been observed. In the study made here, it was found that the observed waves were generated only by an uninhibited, side-burning test specimen, which allowed effects other than the one-dimensional ones considered in the theoretical analysis. One possible explanation for the generation of these waves, based on periodic cooling by the test-section walls, was hypothesized.

From the experimental results, it must be concluded that some facet of the model used in the theoretical analysis of the problem is in error. Although the basic principles may be correct enough to predict steady-state effects, there may be some weakness in the model for the treatment of unsteady phenomena. Calculations were made for the fluctuations in flame temperature resulting from heat-conduction lag in the solid phase. Although these calculations showed that the original estimation, based on a simple model, of the regimes of pressure and frequency for the most observable interaction was correct, the calculations did show that large temperature fluctuations are possible for relatively low frequencies, meaning that the combustion reactions may follow quasi-steady behavior over a limited range of pressure variation with time. In addition, some evidence exists that some reaction, albeit low-energy, may occur in the solid phase, contrary to the original model. The most likely cause for the failure to detect entropy waves, however, is some variation of the gas phase from the original model, which assumed a thin ($\sim 100\mu$), one-stage reaction zone. One modification of this model, which would retain the model's validity for steady-state burning and possibly explain the unsteady-state behavior observed, is to allow, (in addition to a thin zone where most of the combustion occurs), a diffuse after-burning zone where the reactions go to completion. The existence of such an after-burning zone would allow for the presence of pressure-sensitive reactions which would smear out any waves which might have been generated close to the burning surface and which would alter the transit times used in estimating the frequency range over which the pressure-burning rate interaction could be assumed quasi-steady. Some preliminary observations on the spatial distribution of flame spectral emitters indicated the possibility of an extended reaction zone for propellants burning under steady-state conditions, and the kinetics of this zone could change markedly for different conditions of frequency and steady-state pressure.

The experimental results indicate that further work in steady-state combustion mechanisms would be profitable in the study of pressure-burning rate interactions for non-steady conditions. The role of possible reactions in the solid phase must be determined, and the structure of the gaseous-phase reaction zone must be mapped out with care.

The range of pressure variations with time between that employed in this study and steady-state conditions must be investigated. An experiment to cover this range and to determine the rate of pressure change at which quasi-steady behavior can no longer be assumed is outlined in Appendix H. Such a determination would help delineate the effects of possible sub-surface reactions and a diffuse after-burning zone on the pressure-burning rate interaction, and might well feed back to a steady-state regression model.

In addition, further experiments in unsteady combustion should be performed. The nature of the waves which are observed for a side-burning sample should be determined to verify the proposed hypothesis or their generation. Tests over a wider amplitude range should be performed at some of the lower frequencies. In addition, the use of the particle-track technique should be investigated to determine the lower limit of particle diameter at which the particle can be tracked. In this way, the present apparatus could be used for direct measurement of the acoustic-admittance function, which would serve to check the accuracy of the values measured with the T-burner technique. It would be possible to test for possible effects of amplitude on the admittance, and would also allow the extension of the range of testing to low frequencies, where the ordinary T-burner loses accuracy because of increased heat losses.

In summary, although the experimental results reported in this thesis appear to be negative in nature, the results do point out some different experiments in both steady-state and unsteady combustion which would advance the state of knowledge of solid-propellant combustion mechanisms.

APPENDIX A

Acoustic Admittance

Consider a smooth, rigid-walled tube, with diameter small compared to wavelength. The one-dimensional wave equation is (A-1):

$$\rho \frac{\partial^2 \xi}{\partial t^2} = \rho \frac{\partial u}{\partial t} = - \frac{\partial p}{\partial x} \quad (\text{A-1})$$

where (x, t) = average displacement of a particle due to sound wave,

$u = \frac{d\xi}{dt}$ = average velocity of the plane in the x-direction,
taken as the particle velocity

p = excess pressure

Using mass continuity, the density change, δ , occurring between the equilibrium pressure and the actual pressure, can be written

$\delta = \frac{\partial \rho}{\partial x}$ for those sound waves where density and displacement are small.

For most sound waves, the compression will be adiabatic, so that

$$c_p \left(\frac{dV}{V} \right) = -c_v \left(\frac{dp}{p} \right) \quad (\text{A-2})$$

where c_p = heat capacity at constant pressure

c_v = heat capacity at constant volume

Then, defining S as the cross-sectional area of the tube, the gas volume between $x + dx$ is Sdx . Therefore, the volume change will be given by $Sdx \frac{d\xi}{dx}$, so that

$$c_p \left(\frac{\partial \xi}{\partial x} \right) = -c_v \left(\frac{p}{P_0} \right) \quad (\text{A-3})$$

where P_0 is the equilibrium pressure.

Therefore,

$$p = -\delta P_0 \left(\frac{\partial \xi}{\partial x} \right) = \delta P_0 \delta \quad (\text{A-4})$$

where $\gamma = c_p/c_v$

Then, the following relations can be derived for a plane sound wave:

$$\frac{\partial^2 \xi}{\partial x^2} = \frac{1}{c^2} \frac{\partial^2 p}{\partial t^2}, \quad \frac{\partial^2 p}{\partial x^2} = \frac{1}{c^2} \frac{\partial^2 p}{\partial t^2}, \quad \frac{\partial^2 \rho}{\partial x^2} = \frac{1}{c^2} \frac{\partial^2 \rho}{\partial t^2}, \quad (A-5)$$

$$\text{where } c = \sqrt{\frac{P_0 \gamma}{\rho}}, \quad (A-6)$$

the speed of sound in the medium.

$$\text{Also, } p = P_0 \gamma \xi = -\rho c^2 \frac{\partial \xi}{\partial x} \quad (A-7)$$

It can be seen that displacement, density, and pressure obey the equation for propagation of waves with the characteristic velocity c . The three quantities are interrelated.

Next, consider a simple harmonic plane wave going to the right with pressure amplitude P_+ . Then the following equations can be written:

$$p_+ = P_+ e^{ik(x-ct)} \quad (A-8)$$

$$\text{where } k = \frac{2\pi f}{c} \quad (A-9)$$

and f = frequency of the wave,

$$\xi_+ = A_+ e^{ik(x-ct)} \quad (A-10)$$

$$\text{where } A_+ = -\left(\frac{P_+}{2\pi i \rho c}\right), \quad (A-11)$$

$$\text{and } \frac{\partial \xi_+}{\partial t} = U_+ e^{ik(x-ct)}$$

$$\text{where } U_+ = \frac{P_+}{\rho c} \quad (A-12)$$

$$\text{In addition } P_+ = \rho c \left(\frac{\partial \xi_+}{\partial t} \right) \quad (A-13)$$

The same can be written for a wave going to the left, except that the equations become, for example:

$$p_- = P_- e^{-ik(x+ct)} \quad (A-14)$$

If the tube is closed, then both incident and reflected waves will be present near an end wall. Adding (A-8) and (A-14),

$$p = P_+ e^{ik(x-ct)} + P_- e^{-ik(x+ct)} \quad (A-15)$$

and

$$\frac{2f}{2t} = \frac{1}{\rho c} \left\{ P_+ e^{ik(x-ct)} - P_- e^{-ik(x+ct)} \right\} \quad (A-16)$$

The various amplitude ratios can be expressed as exponentials:

$$- \left(\frac{P_-}{P_+} \right) = \left(\frac{A_-}{A_+} \right) = \left(\frac{U_-}{U_+} \right) = e^{-2\psi} \quad (A-17)$$

where $\psi = \pi\alpha - i\pi\beta$ (A-18)

The two components of ψ give the magnitude and phase between the two waves. The amplitude ratio is given by $e^{-2\pi\alpha}$, while the phase angle at $x = 0$ is given by $-2\pi\beta$.

In terms of ψ , the pressure and particle velocity become:

$$p(x) = P_+ e^{-\psi - 2\pi i \eta t} \left(e^{\psi + i k x} - e^{-\psi - i k x} \right) = 2P_+ e^{-\psi - 2\pi i \eta t} \sinh \left(\psi + \frac{2\pi i \eta x}{c} \right) \quad (A-19)$$

$$u(x) = \frac{2P_+ e^{-\psi - 2\pi i \eta t}}{\rho c} \cosh \left(\psi + \frac{2\pi i \eta x}{c} \right) \quad (A-20)$$

Dividing (A-19) by (A-20) gives:

$$z(x) = \left(\frac{P}{2f/2t} \right) = \rho c \tanh \left(\psi + \frac{2\pi i \eta x}{c} \right) \quad (A-21)$$

The quantity $z(x)$, which is the ratio between pressure and particle velocity in the gas, is called the specific acoustic impedance. It

must be noted that velocity is defined in the direction opposite to that in equation 17. Non-dimensionalizing, $\mathcal{Z} = \frac{z}{\rho c}$ is the acoustic impedance ratio while its inverse $\eta = 1/\mathcal{Z}$ is the admittance ratio, and is a measure of the impedance mismatch at a boundary between two media. \mathcal{Z} is also complex, and can be written

$$\mathcal{Z} = \frac{z}{\rho c} = \Theta - i\chi = \tanh [\eta (\alpha - i\beta)] \quad (\text{A-22})$$

The importance of the acoustic admittance is that it gives an indication as to whether a wave incident on a surface will be reflected with increased or decreased amplitude. The real part of the admittance is the important quantity, as can be seen from a consideration of the incident and reflected waves.

For a wave which strikes a wall perpendicularly from the right and is reflected, the pressure distribution is

$$p = P_i e^{-ik(x+ct)} - P_r e^{-ik(x-ct)} \quad (\text{A-23})$$

The ratio between incident and reflected pressure is

$$\frac{P_r}{P_i} = e^{-2\pi(\alpha - i\beta)} \quad (\text{A-24})$$

as given by equation (A-17).

In terms of the acoustic impedance directly,

$$\frac{z}{\rho c} = \frac{P_i - P_r}{P_i + P_r} \quad (\text{A-25})$$

The ratio of the energies is given by the square of the pressure ratio, namely:

$$\left| \frac{P_r}{P_i} \right|^2 = \left| \frac{1 - \frac{z}{\rho c}}{1 + \frac{z}{\rho c}} \right|^2 \quad (\text{A-26})$$

In order to have amplification,

$$\left| \frac{P_r}{P_i} \right|^2 > 1 \quad (\text{A-27})$$

$$\text{or } \frac{1 - (\theta - i\chi)^2}{1 + (\theta - i\chi)^2} = 1 \quad (\text{A-28})$$

As a result,

$$(1 - \theta)^2 + \chi^2 = (1 + \theta)^2 + \chi^2 \quad (\text{A-29})$$

$$\text{or } \theta < 0. \quad (\text{A-30})$$

In other words, the real part must be negative for amplification, which is what was to be shown.

In terms of the admittance,

$$\left| \frac{P_r}{P_i} \right|^2 = \left| \frac{1 - \frac{1}{\gamma}}{1 + \frac{1}{\gamma}} \right|^2 = \left| \frac{\gamma - 1}{\gamma + 1} \right|^2 = \left| \frac{K - i\sigma - 1}{K + i\sigma + 1} \right|^2 \quad (\text{A-31})$$

$$= 1 - \frac{4}{(K + 1)^2 + \sigma^2} \quad (\text{A-32})$$

Once again, $K < 0$ for amplification.

APPENDIX B

Cavity Acoustics

The acoustic modes of a cylindrical cavity may be obtained as follows (B-1, B-2). The wave equation in cylindrical coordinates r , ϕ , and z is (B-3).

$$\frac{1}{c^2} \frac{\partial^2 p}{\partial t^2} = \frac{\partial^2 p}{\partial r^2} + \frac{1}{r} \frac{\partial p}{\partial r} + \frac{1}{r^2} \frac{\partial^2 p}{\partial \phi^2} + \frac{\partial^2 p}{\partial z^2} \quad (\text{B-1})$$

where c is the velocity of sound in the medium and p is the pressure disturbance. If we assume that we are dealing with a cylindrical cavity of length L and radius R , closed at both ends and with rigid walls, the solution to the wave equation is

$$p = \sin(m\phi) \cos\left(\frac{\omega_z z}{c}\right) J_m\left(\frac{\omega_r r}{c}\right)$$

and
$$\omega = \frac{1}{2\pi} \sqrt{\omega_z^2 + \omega_r^2} \quad (\text{B-2})$$

where the J_m 's are the integral Bessel functions, ω is the characteristic frequency, and ω is the circular frequency. From a consideration of the boundary conditions, i.e., the z component of the particle velocity is zero at $z = 0, L$ and the radial particle velocity is zero at $r = R$, we find that the characteristic values are

$$\omega_z = \left(\frac{n_z c}{L}\right) \quad (n_z = 0, 1, 2, \dots)$$

$$\omega_r = \left(\frac{\pi \alpha_{mn} c}{R}\right)$$

$$\omega = \frac{c}{2} \sqrt{\left(\frac{n_z}{L}\right)^2 + \left(\frac{\alpha_{mn}}{R}\right)^2} \quad (\text{B-3})$$

where α_{mn} is the n th root of the equation

$$\frac{dJ_m(\pi x)}{dx} = 0$$

with values

TABLE I

m/n	0	1	2	3	4
0	0.000	1.220	2.233	3.238	4.241
1	0.586	1.697	2.714	3.726	4.731
2	0.972	2.135	3.173	4.192	5.204
3	1.337	2.551	3.612	4.643	5.662
4	1.693	2.955	4.037	5.082	6.110

The wave numbers m , n , and n_z characterize the particular mode of oscillation. For pure modes, only one wave number is non-zero. The "axial" or "longitudinal" mode occurs for $m = n = 0$. These are the familiar "organ-pipe" modes where the motion is parallel to the z -axis. The other two classes are generally referred to as "transverse" modes. For these modes, particle velocity and wave motion are functions of r . For $n_z = n = 0$, the waves are called "tangential." Tangential modes are of two types, "standing" and "spinning," which are differentiated by the non-movement and movement, respectively, of the nodal points. Cross-sectional views of these modes are shown in Figure B-1. It should be noted that the maximum pressure variation is found at $r = R$ for the tangential mode. The other type of transverse mode occurs for $n_z = m = 0$. These are the "radial" modes, in which the motion is parallel to the r -coordinate and in which the pressure disturbance is focused along the cylindrical axis. Wave patterns for these modes are shown in Figure B-2.

It may seem surprising that an isentropic analysis based on a closed cylinder is used,* but experimental evidence shows that the frequencies found in acoustic instability correspond to those predicted by equation (B-3), even at large amplitudes (B-4, B-5, B-6). In fact, the cylindrical cavity analysis can be extended to more complex shapes. It has been found that, for some star geometries, tangential modes can exist in the star points (B-7, B-8). Wave analysis of the oscillation has been used extensively and has disclosed the existence of harmonics up to the sixth, at least (B-9, B-10, B-11).

The frequencies correspond well because of two counterbalancing factors. The effect of flow is to decrease the characteristic frequency (B-6), but a finite amplitude pressure disturbance will move with a Mach number slightly greater than 1 (B-4). The result is that frequencies will be within 5% of those for a closed cavity, so that the thermodynamic uncertainties existing in a rocket motor practically eliminate any possibility of distinguishing between experiment and the simple theory outlined above.

* This applies for transverse modes and for axial modes when the motor length is much greater than effective nozzle length (the usual case for Solid Propellant Rockets).

APPENDIX C

Thickness Measurement with X-Rays and Photomultiplier

The transmission of absorbed radiation may be expressed (C-1):

$$I_x = I_o e^{-\mu x} \quad (C-1)$$

where

I_x = intensity after passage through material of thickness x

I_o = initial intensity

μ = absorption coefficient

The fact that μ varies with the wavelength of the penetrating radiation makes it possible to optimize the resolution through choice of wavelength. To minimize meter error, the value of μ should be $2/x$ (C-2), (C-3). For X-rays, a general rule is that the voltage should be selected so that the sample thickness to be penetrated is five half-value layers (C-4). In general, though, to increase the change in transmitted intensity with a change in thickness, a large value of μ is desirable, implying "soft" X-rays (long wavelengths).

A calculation of the absorption coefficient of the materials involved in a propellant thickness measurement is the first step. Assuming a value of 0.6 \AA wavelength rays (21 kev X-rays), the element's mass absorptions are first obtained (C-5). The attenuation coefficient of a compound or mixture is then determined by the average of the coefficients weighted with respect to the composition (C-6). On this basis, the absorption coefficient for NH_4ClO_4 is found to be 5.23 cm^{-1} at 0.6 \AA , while a representative polymeric binder, $\text{C}_4\text{H}_8\text{O}$, has a calculated coefficient of $.40^{-1}$. For a 75% NH_4ClO_4 propellant, then, the absorption coefficient is 4 cm^{-1} , which would minimize the meter error for a $\frac{1}{2}$ centimeter thick sample, based on the $2/x$ relation mentioned above.

The absorption coefficients of iron and aluminum are also important since the propellant will be burning in a pressurized chamber, and the X-ray source could not be placed in the combustion chamber because of the high temperatures existing there and because of the effect of the physically large source on the flow field. For 21 kev X-rays, iron has a linear coefficient of 189 cm^{-1} , while the coefficient for aluminum is only 9 cm^{-1} , since the absorption coefficient varies approximately as the fifth power of the atomic number in this frequency range (C-7). The obvious ad-

vantage of using an aluminum window is apparent, although the absorption is still large compared to that for propellant.

The next consideration involves the beam strength necessary, which is related to the accuracy, as may be seen in the following manner. First, examine the absorption equation in its differential form,

$$\frac{dI}{I} = -\mu dx \quad (C-2)$$

Since 1 micron increments in x are to be measured, and the absorption coefficient has been found to be 4 cm^{-1} , a fractional change in intensity, $\frac{dI}{I}$, of 4×10^{-4} must be measured.

Since the measurement of radiation effectively involves the counting of the number of incident particles, the beam strength is effectively determined by particle statistics as follows. The probable error in statistics is related to the number of events, and, for this case (C-8), (C-9),

$$\frac{dI}{I} = \left(\frac{1}{\text{number of counts}} \right)^{\frac{1}{2}} \quad (C-3)$$

which can be derived from the statistics of counting (C-10).

As will be seen, with the number of counts needed to obtain data, the normal distribution which is theoretically obtained for an infinite number of samples is approached. This is given by

$$P(x)dx = \frac{1}{\sqrt{2\pi}\sigma} e^{-\frac{(x-M)^2}{2\sigma^2}} dx \quad (-\infty < x < \infty) \quad (C-4)$$

where $P(x)$ = the distribution

M = the mean representing the true value of the quantity measured

σ = the standard deviation, which is related to the probable error.

Then, the probability P_0 that a single experimental result is in the range $M \pm n\sigma$ is given by the area under $P(x)$ from $M - n\sigma$ to $M + n\sigma$.

$$P_0 = \frac{1}{\sqrt{2\pi}\sigma} \int_{M-n\sigma}^{M+n\sigma} e^{-\frac{(x-M)^2}{2\sigma^2}} dx \quad (C-5)$$

$$\text{or } \rho_0 = \frac{1}{\sqrt{2\pi}} \int_{-n}^n e^{-y^2/2} dy \quad (\text{C-6})$$

$$\text{where } y = \frac{(x - M)}{\sigma}$$

Nuclear counting results generally follow the Poisson distribution

$$P(x) = \frac{e^{-M} M^x}{x!} \quad (\text{C-7})$$

where $M = ct$
 $c =$ counting rate
 $t =$ counting time
 $x =$ number of counts recorded in t .

The Poisson distribution has a mean of M and a standard deviation $M^{1/2}$. Moreover, for $M > 100$, the Poisson and normal distributions closely coincide.

Then the error can be estimated as follows. If the normal distribution holds, but M and σ are not related (as would be the case for a thickness measurement), the confidence limits for M derived from n measurements are

$$\pm \frac{ts}{\sqrt{n}}$$

where $s^2 = \sum_i \frac{(x_i - x_{ave})^2}{n - 1}$, the variance, and t is the

variable in the Student's t distribution (C-11), which is based on the sample standard deviation, rather than on the population standard deviation, thereby overcoming the lack of knowledge of the true standard which exists in most practical problems. For a large ($n > 30$) sample, $t = 1$ gives a confidence level of 68%, which corresponds to a 1σ limit.

The same result can be obtained in another way (C-12), assuming Poisson's law (equation C-7) holds. The standard deviation is defined as

$$\sigma = \left[\sum_0^{\infty} (x_i - x_{ave})^2 P(x) \right]^{1/2} \quad (\text{C-8})$$

Upon substituting the Poisson value for $P(x)$, using Sterling's approximation for $x!$, and replacing summation by integration,

$$\sigma \approx \sqrt{x} \quad (\text{C-9})$$

The relative deviation is given by

$$\frac{\sigma}{x} \approx \frac{1}{\sqrt{x}} \quad , \quad (C-10)$$

which is the same relation as C-3, since $x (= ct)$ is the number of counts recorded in time t .

Based on C-3, then, it is found that, for $dI/I = 4 \times 10^{-4}$, a total of 7×10^6 counts is needed in one millisecond measuring interval, implying a counting rate of 7×10^9 counts/sec at the detector.

Statistical considerations also dictate the minimum diameter of the sample. It has been assumed thus far that the regressing propellant surface is flat, or that sufficient surface is involved to average out the fluctuations which do exist due to the heterogeneous nature of the propellant. In fact, one advantage of the radiation absorption technique over an optical technique is that an average regression rate is automatically obtained. The pictures taken by Bastress (C-13) indicate that the fluctuations will vary in magnitude with the particle size of the ammonium perchlorate and the pressure level. To obtain some idea of the sample diameter needed, assume that large perchlorate is being used at low burning pressures, with a resultant surface irregularity of 100 microns, which will give a conservative estimate for the sample size needed.

The statistical theorem to be used is: "If x is normally distributed with mean M and standard deviation σ and a random sample of size n is drawn, then the sample mean \bar{x} will be normally distributed with mean M and standard deviation σ/\sqrt{n} " (C-14). If a 5 square centimeter sample diameter is used, then 3×10^4 of the 100 micron samples will be in the area tested, giving a standard deviation of

$$\frac{\sigma}{\sqrt{n}} = \frac{100 \text{ microns}}{\sqrt{3 \times 10^4}} = 0.6 \text{ microns} \quad (C-11)$$

For a 95% confidence level, a 2σ limit is required, or about 1 micron. When smaller irregularities are present, then the area needed will decrease directly with the size of the irregularity. Since a 2.5 centimeter diameter sample is sufficient to give only 1 micron of "noise" for a large irregularity, it would seem that the use of a 1 inch diameter propellant sample would eliminate error caused by the surface irregularities, unless a higher precision of measurement is desired.

The next factor to consider in the design of a system which measures thickness by radiation absorption is the source, the energy, and the radiation. A figure of 20 kev was chosen earlier to give an absorption coefficient of 4 cm^{-1} , as explained above. Lower energies are hard

to obtain, and higher energies would result in a decrease in sensitivity due to the rapid drop in μ with increasing energy. The type of the radiation is partially dictated by penetrating power, since α particles and β rays are both short range in character. Gamma ray sources in use seem to have a minimum average energy of about 350 kev (C-15) and a survey of the nuclides shows that all nuclides emitting γ rays with energies anywhere near 20 kev have many other characteristic radiations, and that the decay schemes for the low energies are not well known (C-16).

As to the source selection, the following comparisons can be made between X-ray sources and radioactive isotopes:

- (1) Maintenance costs for isotopes are generally lower than for X-ray sources.
- (2) Isotopes are less complex and more reliable than X-ray generators.
- (3) X-ray sources have less potential hazard, since they may be turned off completely.
- (4) X-rays may be obtained at the energy desired for sensitivity, accuracy, or stability.

The overriding problem for the present is, however, the source strength requirement. Nearly 10^{10} counts/sec are needed at the detector to give the required accuracy. The radiation transmitted by a 1 cm thick propellant sample would be about 2% of the incident radiation, and 1/16" thick aluminum windows (200 psi design) would allow transmission of about 1×10^{-4} of the incident radiation. Geometrical considerations are important, since only those events happening in a small solid angle are being detected. For an area of 5 cm^2 at a distance of 5 centimeters from the source, a geometric factor of nearly 100 results. The combined result of all these losses is that a source strength near 10^{18} disintegrations per second, well over a megacurie of radioactive material, which would be highly impractical, is required, so that the use of X-rays is dictated as the source. The power level can be estimated from (C-17).

$$\frac{\text{photons/sec}}{\text{watt input}} = 10^{10} Z, \quad (\text{C-12})$$

which gives a power input of slightly over a megawatt, which could be attained by pulsing. The design formula (C-12) used for estimation of actual power input required in practice corresponds to an efficiency of 0.3%, which at first seems quite low. However, Compton (C-18) gives a formula for the efficiency of X-ray generation which is based on both theory and experiment, i.e., $\epsilon \approx 1 \times 10^{-9} ZV$. For $Z = 74$, and assuming that the tube is operated near 20 kv, an efficiency of 0.15% is readily calculated.

The next factor in the thickness measurement experiment is the detector, which must measure transmitted radiation in order to determine the type and amount of energy loss. Three general classes may be considered: (i) solid-state radiation detectors, (ii) ionization chambers, Geiger-Muller counters, or proportional counters, and (iii) scintillator-photomultiplier combinations. Solid-state detectors, which utilize photoconductive crystals, can be eliminated immediately because of a finite rise time, high temperature sensitivity, and slow response (C-19), (C-20). The applicability of the other two classes to detect 5 to 50 kv X-rays has been considered in a critical survey (C-21) where it was found that the scintillation counter was best for the range, since Geiger counters have long dead times, are non-linear, and proportional counters have a low quantum counting efficiency ($\sim 1\%$) and limited lifetimes ($10^3 - 10^9$ counts). A review of other references (C-22) on the subject also supports the belief that an ionization-chamber type of device is unsuitable for measuring high counting rates with accuracy needed in this problem.

The scintillation counter is a relatively new instrument, having come into use in the last ten to fifteen years, and has been of invaluable use in the high-energy field, since the short resolving times possible under certain circumstances make it an invaluable tool for the detection and energy measurement of particles. Two reviews and summaries of scintillation counters are available in book form (C-23), (C-24).

The scintillation counter has two elements in addition to recording equipment; these are the phosphor crystal and a secondary emission multiplier. The phosphor crystal has the property of emitting fluorescent radiation when traversed by an ionizing particle, and it appears that sodium iodide activated with thallium is the most suitable phosphor for the energy range of interest. Errors can arise from the decay time of the radiation, which can lead to noise buildup for high counting rates, due to overlapping of pulses (C-25), and errors can also occur due to the high temperature coefficient of the phosphor output - about $-0.5\%/^{\circ}\text{C}$ (C-26).

The absolute accuracy of the photomultiplier output is limited by a number of problems. The gain varies with source intensity and recent counting history (C-27), fatigue plays a large role in determining the gain of a photomultiplier (C-28), and the gain varies with temperature, depending on the individual tube, and sensitivities of $-1\%/^{\circ}\text{C}$ have been encountered (C-29). The photomultiplier gain is, however, most sensitive to voltage, varying with the supply voltage to as high as the tenth power, so that the stabilization of voltage to 0.01% would still permit a gain change of 0.1%.

Other sources of error exist in the proposed experiment, such as the variation of X-ray intensity with voltage (a cubic relation (C-30)) and the variation in the absorption coefficient with wavelength changes in the emitted X-radiation, which is a third power relation. The location of the source and detector leads to another source of error, since the radiation must traverse the propellant gas. The assumed 5 centimeters of gas at 100 psi and 2700°K is equivalent to about 3.5 centimeters of air

at standard conditions. Assuming that the absorption coefficient varies only with density (no changes in atomic number), 3.5 centimeters of air will absorb as much radiation as 27 microns of propellant, which seems negligible, but the 10% pressure variation gives a "noise" level equivalent to 3 microns of propellant, compared to the 1 micron accuracy required.

The use of a non-burning reference sample of propellant as the basis for a comparative measurement technique would help to circumvent partially some of the sources of error. If the same X-ray beam were detected after passage through the burning and non-burning sample, then the effect of the varying pressure of the combustion gases could be eliminated by difference techniques. Moreover, voltage variations in the X-ray source could be detected from the known thickness of the non-burning sample, as could possible drifts in phosphor output and photomultiplier response due to temperature changes. However, the magnitude of the drifts would probably be dissimilar, since temperature coefficients vary from tube to tube and from phosphor to phosphor. Drifts in gain due to supply voltage variation would be detected if a common source were used for the two photomultipliers, but possible changes in gain as a result of fatigue or past usage would still be characteristics of individual tubes. Filtering would ease the problem of designing an amplifier with the desired accuracy (0.02%), although the amplifier would still have to change gain or bias by a factor of 100 through the shot, due to increased transmission of X-rays as the propellant sample becomes thinner. The stringent conditions are, however, ameliorated by two factors: first, the quantity of main interest is the oscillating component of the burning rate; and, second, there will probably be at least 20 cycles over which information can be obtained, assuming a one second burning time and 100 cycle per second oscillations. (Figure C-1)

These calculations have been made for 100 cycles per second oscillations imposed on 100 psi steady pressure. If the frequency of oscillation is increased, experimental difficulties are doubly magnified, both by the shorter measuring time and by the smaller amount of regression due to the shorter time. As the steady-state pressure is increased, the density of the intervening gases increases, as does the aluminum "window" thickness needed, both of which increase extraneous absorption effects. Although a higher burning rate results, the fact that the increase is a function of pressure to a power less than one means that the benefit of the increase will be outweighed by the extraneous absorption. As a result, the case for which calculations were made represents an optimum one.

APPENDIX D

Flame Temperature Calculations

The methods of calculation of the combustion reaction products and resulting flame temperature from a given solid propellant composition have been reviewed, together with the thermochemical considerations involved, by Brinkley (D-1). The technique used here was originated by Zeleznik and Gordon (D-2), and is based on the simultaneous solution of the equilibrium equations for the several species involved in the combustion reactions. Since 40 species were taken into account, numerical iteration techniques became advisable. In the technique used, the equilibrium composition is obtained by the Newton-Raphson iteration method (D-3), using a modification of the Huff iteration equations (D-4), which have the advantage that the iteration equations can be written in a form which is independent of the choice of the components involved. A reproduction of the FORTRAN program for the calculation forms the concluding portion of this Appendix.

The assumptions involved were: (1) zero gas velocity in the combustion chamber, (2) perfect gas law, (3) homogeneous mixing, and (4) complete, adiabatic combustion.

The following species were considered: CO, CO₂, Cl, Cl₂, ClO, H, H₂, HClO, HCl, H₂O, N₂, NO, O, O₂, and OH. In addition, the following species were considered, but were found to have mole fractions less than 0.005% for all conditions calculated: C, C₂, C₃, CCl, CCl₄, CH, CH₂, CH₃, CH₄, C₂H₂, C₂H₄, CN, C₂N₂, COCl₂, ClCN, ClO₂, Cl₂O, HCN, NH, NH₃, N₂O, N₂O₄, NO₂, and C (solid). Atomic nitrogen was at first included, but found to be quite unimportant at the resulting temperatures for the pressures considered, so was omitted in later calculations. It should be noted that the program permits calculation of the expansion products for both equilibrium and frozen flow considerations, but only the flame temperature is important in this report.

Results of the calculations are given in Tables D-2 through D-6. D-2, D-3, and D-4 are for the plastisol system, and show the effects of ball powder types and of adding stabilizer to the propellant. Compositions are given in Table D-1.

Table D-1Plastisol Compositions Considered in Thermochemical Calculations

	<u>Table D-2</u> <u>Plastisol "A"</u>	<u>Table D-3</u> <u>Plastisol "B"</u>	<u>Table D-4</u> <u>Plastisol "C"</u>
NH ₄ ClO ₄	35.25	35.25	34.89
TEGDN	43.26	43.26	42.83
Ball Powder "A"	21.49	-----	-----
Ball Powder "B"	-----	21.49	21.28
Stabilizer R-1	-----	-----	1.00

From Table D-2, it can be seen that the temperature varies only 1½% over the pressure range most often used, 300-1000 psia. By way of contrast, isentropic compression would cause a temperature increase of 22%, assuming $\gamma = 1.20$. The propellant of Table D-2 is the plastisol composition most often used, owing to its cleaner-burning characteristics, compared to the other two.

Tables D-4 and D-5 show the effects of pressure and of the addition of 0.5% salt on the flame temperature of the polyurethane propellant system. From D-5, it can be seen that, over the pressure range 300-700 psia, the temperature varies about 2%, while isentropic compression would cause a 15% increase. In addition, comparison of Tables D-4 and D-5 shows that the replacement of 0.5% of the oxidizer by inert salt only drops the calculated flame temperature by 8°K.

Table D-2Effect of Pressure on Flame Temperature of Plastisol Propellant "A"

<u>Pressure (psia)</u>	<u>T_f (°K)</u>
30	2631
150	2689
300	2707
600	2721
1000	2730
1500	2735

Table D-3Effect of Pressure on Flame Temperature of Plastisol "B"

<u>Pressure (psia)</u>	<u>T_f(°K)</u>
300	2745
400	2753
500	2758
550	2760
600	2762
700	2765

Table D-4Effect of Pressure on Flame Temperature of Plastisol "C"

<u>Pressure (psia)</u>	<u>T_f(°K)</u>
400	2702
500	2706
550	2708
600	2709
700	2712
800	2714

Table D-5Effect of Pressure on Flame Temperature of Propellant
Containing 85% AP, 15% Polyurethane

<u>Pressure (psia)</u>	<u>T_f(°K)</u>
450	2910
500	2917
550	2924
600	2930
650	2935

Table D-6

Effect of Pressure on Flame Temperature of Propellant Containing
84.5% AP, 0.5% NaCl, 15% Polyurethane

<u>Pressure (psia)</u>	<u>T_f (°K)</u>
300	2874
400	2894
500	2909
550	2916
600	2922
700	2932

APPENDIX E

Polyurethane Processing and Motor Casting Procedure

As the first step in the manufacture of polyurethane propellants, a premixed fuel, consisting of a polyether diol, a polyether triol, and a polymer degradation additive, and a catalyst, was prepared a day prior to the mixing of propellant. The ammonium perchlorate oxidizer (25% 350 μ , 50% 210 μ , and 25% 5 μ) was dried at 240°F for 24 hours prior to mixing.

The propellant mixing was carried out in a Day Co. (nominal four kilogram capacity) horizontal mixer with double nobben blades. The required amount of fuel was weighed out and placed in the mixer, whose temperature was set at 85°F. The desired amount of oxidizer was placed in the Syntron vibrator feeder. The mixer was started by remote control, and the oxidizer was then fed in by remote control, with the addition rate being monitored by closed circuit television. After the oxidizer was added, the mixer was covered, and the components were mixed for 30 minutes at a vacuum of 5 mm Hg. The cross-linking agent (toluene diisocyanate) was then added, and mixing was continued for an additional 15 minutes under the same vacuum.

The propellant was then removed from the mixer, placed in a heated funnel and cast through a 1/16" slit into the motors. A vacuum of 6 mm Hg. was applied during casting to accomplish deaeration and to aid propellant flow. A sample of the mix was withdrawn and the viscosity obtained using a Brookfield viscosimeter mounted in a "Helipath" stand.

A mandrel was next inserted into each motor. This mandrel is made from a 1" diameter Teflon rod, which is turned at the end to fit the base plate of the casting fixture. A guide piece was used during insertion to insure centering and alignment, after which the top of the casting fixture was positioned on the motor.

The motor was then cured for two days at 80°C. After removal from the oven, the motor ends were trimmed, then a 1/16" layer of inhibitor consisting of polyurethane (premixed fuel and cross-linker) was placed on one end of each motor grain. The motor was then returned to the 80°C oven for another 24 hours. Upon removal from the oven, the propellant was machined to the desired length and an I. D. of 1.5 inches. The ends of the motor were covered with aluminum foil, and then the motor was sealed in a plastic bag and placed in storage until needed.

APPENDIX F

"D" Line Contour Calculations

There are three factors which cause the originally monochromatic radiation of excited sodium atoms from a thin wafer of flame to be broadened to some contour. These are natural line broadening, Doppler broadening, and collision or Lorentz broadening (F-1), (F-2), (F-3).

Natural line broadening occurs as a result of the Heisenberg Uncertainty Principle (F-3). The half width resulting from this factor is only about 10^{-4} Å, and is small compared to that from other factors (F-1). Doppler broadening results from the thermal motion of the emitting atoms. As a result of this motion, the frequency of the emitted radiation is shifted by a factor containing the velocity divided by the speed of light. The velocity distribution is given by the Maxwell-Boltzmann law, giving rise to a Gaussian distribution for the line. The resulting half-width is: (F-1)

$$(W_o)_{\text{dopp}} = 1.386 \left(\frac{RT}{m} \right)^{\frac{1}{2}} \frac{\lambda}{c} \quad (\text{F-1})$$

where R is the gas constant, T the absolute temperature, λ the wavelength, c the velocity of light, and m the gram atomic mass of the emitting atoms. For the sodium D-line, this gives:

$$(W_o)_{\text{dopp}} = 4.48 \times 10^{-12} T^{\frac{1}{2}} \text{ cm.} \quad (\text{F-2})$$

Collision broadening results from collisions between emitting sodium atoms and other species in the flame gas. As a result, the wavelength of the radiation band is spread, and a contour having the shape of a damped resonance curve results. From the Lorentz electron theory, it is found that the resulting half-width is (F-1)

$$(W_o)_{\text{Coll}} = \frac{2\lambda^2}{c} N_{\text{opt}}^2 p (\pi \mu RT)^{-\frac{1}{2}} \quad (\text{F-3})$$

where N is Avogadro's No., p is the absolute pressure, μ is the reduced mass of a sodium atom and a flame gas molecule, and σ_{opt} is the optical collision diameter of the sodium atom, which is not necessarily equal or

close to the collision diameter determined from transport properties. For the D-line,

$$(W_o)_{\text{Coll}} = 5.18 \times 10^6 \sigma_{\text{opt}}^2 T^{-\frac{1}{2}} \text{ cm/atm} \quad (\text{F-4})$$

Some measurements have been made of σ_{opt} at low temperature in inert gases, and optical-collision diameters two or three times greater than kinetic theory diameters result (F-4). Based on experiment, Bundy and Strong (F-1) give a value of 6 \AA for sodium atoms with flame gases, which will be the value used, although both Hinnov (F-5) and James and Sugden (F-6) obtained values near 8 \AA . The latter two are based on experiments with atmospheric-pressure flames, while the work quoted by Bundy and Strong was carried out at high pressures, which is closer to the test conditions here than the low-pressure flame work.

As a result,

$$\begin{aligned} (W_o)_{\text{Coll}} &= 1.87 T^{-\frac{1}{2}} \text{ \AA/atm} \\ &= 0.47 \text{ \AA at 200 psi} \\ &= 0.94 \text{ \AA at 400 psi} \end{aligned} \quad (\text{F-5})$$

for a temperature of 3000°K . Since the Doppler broadening for this temperature is 0.02 \AA , the contour for a thin layer of emitting sodium atoms is almost purely the dispersive type resulting from collision broadening.

The width of the contour will be further increased by absorption broadening resulting from the non-zero optical depth of the flame. Absorption broadening results from the passage of the radiation from a thin zone through successive layers of absorbing and emitting atoms. As this radiation goes through the flame, the radiation is selectively absorbed, since the initial radiation will be strongly absorbed at the center and more weakly at the edges of the line. In addition, other parts add their own radiation in the passage through successive zones. As a result, the spectral line emissivity of the gas increases at the center, ultimately reaching the black body emissivity. As the line continues to broaden as more absorption and emission take place, successive regions achieve the black body emissivity. The resulting emissivity is given by

$$\epsilon_\lambda = 1 - e^{-\tau_\lambda} \quad (\text{F-6})$$

where $z = 1$ is defined as the concentration of Na atoms per unit area which gives the optical depth sufficient to decrease the intensity of radiation at the wavelength of the center of the sodium D-line to e^{-1} of its initial value and s is the "shape factor" for the sodium line contour. For a dispersion-type contour, such as is encountered in collision broadening, this shape factor is

$$s = \frac{W_o^2}{W_o^2 + \Delta\lambda^2} \quad (F-7)$$

where W_o is the initial half-width before absorption broadening occurs, and has been calculated for this case as 0.47 \AA at 200 psi and 0.94 \AA at 400 psi. Using various values of z , emission contours can be drawn for different concentrations of salt in the test propellant, different pressures, and different sample diameters.

The parameter z was determined as follows. First, the concentration of sodium atoms under various operating conditions was calculated. For 200 psi operation, assuming a 500:1 density ratio between gas and propellant, a propellant density of 1.6 gm/cc , and 0.1% NaCl in the propellant, there are

$$\frac{1 \times 10^{-3}}{500} \times 1.6 = 3.2 \times 10^{-6} \frac{\text{gm NaCl}}{\text{cc gas}} \quad (F-8)$$

Since the molecular weight of NaCl is 58.5, there are

$$\frac{3.2 \times 10^{-6}}{58.5} = 5.5 \times 10^{-8} \frac{\text{moles Na Cl}}{\text{cc gas}} \quad (F-9)$$

Using Avogadro's No., $6.02 \times 10^{23} \frac{\text{atoms}}{\text{mole}}$, there are $3.3 \times 10^{16} \frac{\text{atoms Na}}{\text{cc gas}}$.

The number of Na atoms/cm² in the line of sight for different thicknesses of flame may then be calculated. Sample thicknesses of 1 cm, 2.5 cm, and 5 cm were used, since the test section is approximately 2 inches in diameter. The following concentrations of Na atoms/cm² result:

Flame Thickness (Transverse)	200 psi	400 psi
1 cm	3.3×10^{16}	6.6×10^{16}
2.5 cm	8.3×10^{16}	1.65×10^{17}
5 cm	1.65×10^{17}	3.3×10^{17}

Bundy and Strong found that $z = 1$ for 6.6×10^{12} Na atoms/cm² in the line of sight. The concentrations calculated above give the following values of z . In addition, " z " factors are calculated for a concentration of .01% NaCl in the sample propellant.

0.1% NaCl

Thickness (cm)	200 psi	400 psi
1	5×10^3	10^4
2.5	1.25×10^4	2.5×10^4
5	2.5×10^4	5×10^4

0.01% NaCl

1	5×10^2	10^3
2.5	1.25×10^3	2.5×10^3
5	2.5×10^3	5×10^3

As the number of sodium atoms in the optical path is changed, by changes in pressure, in the amount of added sodium, and in the sample thickness, the wavelength range over which the gas acts as a black body ($\epsilon = 1$) is also changed. This range is shown for various conditions in the table below.

p (psi)	%NaCl	Diameter (cm)	$\Delta\lambda$ (Å)
200	0.01	1	10
200	0.01	2.5	16
200	0.01	5	22
400	0.01	1	30
400	0.01	2.5	50
400	0.01	5	70
200	0.1	1	28
200	0.1	2.5	44
200	0.1	5	62
400	0.1	1	88
400	0.1	2.5	140
400	0.1	5	220

The $\Delta\lambda$ values are those for which $\epsilon > 0.99$ for an isolated "D" line. Curves of emissivity vs wavelength are shown in Figs. F-1 through F-4 for these conditions. The presence of the second "D" line would, of course, result in a broader wavelength band.

APPENDIX G

Plastisol Processing Procedure

Castable plastisol propellants were made using triethylene glycol dinitrate and nitrocellulose as the binder with ammonium perchlorate oxidizer. The nitrocellulose was obtained in the form of "Fluid Ball" Type "A" casting powder manufactured by the Olin Mathieson Chemical Corporation, with a mean particle size (d_{50}) of 55μ .

The processing procedure was as follows: first, the nitrated glycol was poured into a vertical mixer, and the ammonium perchlorate and ball powder were placed in the proper hoppers. By remote control, ball powder in the amount of 2% (by weight) TEGDN was added to the mixer. Mixing started, with the rotation speed brought to 300 RPM and the temperature raised to 70°C . This so-called "pre-gelling" mixing lasted for 5 minutes, after which the temperature was dropped to 20°C . The pre-gelling was done to increase the viscosity of the glycol to a level at which no settling of the oxidizer would occur during curing. While mixing continued at 300 RPM, the ball powder was added remotely, followed by the ammonium perchlorate and other additives, e.g., NaCl. After all ingredients were added, mixing continued for 20 minutes at 600 RPM.

At the end of mixing, the propellant was pulled into a casting can through narrow (0.060-in) slits to accomplish deaeration of the propellant. The propellant was poured from the casting can into molds, which were placed in a container submerged in an 80°C water bath and cured for 24 hours.

APPENDIX H

dp/dt Experiment

One explanation for the failure to observe strong entropy waves is that the flame temperature adjusts to give an isentropic variation with pressure, rather than remaining relatively constant, as expected from steady-state conditions. The only way to determine the existence of this possibility is to go to lower rates of pressure changes than those used in the T-burner experiments.

The lowest dp/dt values used to date have been about 20,000 psi/sec (77 cps, 80 psi amplitude) and 32,000 psi/sec (115 cps, 70 psi amplitude). Although the amplitude could be lowered, observation of temperature changes would be more difficult, so that lowering the frequency is preferable. Unfortunately, the frequency range of the T-burner is limited by the size of the test cell and by practical considerations such as heat loss, so some other means of varying the pressure must be used.

One possible technique would use the chamber-filling pressure rise which occurs in a rocket motor. By varying the nozzle size and the chamber volume independently, the pressure curves shown in Fig. H-1 would result. During the period of pressure rise, the luminosity of the flame gases, in the spectral region of the NaD lines, would be measured at a position near the burning surface.

For an optically "thin" flame, the luminous output should be proportional to pressure if the temperature remains constant. As a result, a cross-plot of the pressure vs. luminosity for a test would have the appearance shown in Fig. H-2, giving the flame-temperature behavior shown in Fig. H-3. The variation of temperature with pressure at the higher dp/dt values would show the effect of the energy released in a diffuse after-burning reaction zone.

Since this experiment calls for a smooth rapid ignition with no lingering luminosity from the igniter, another technique to vary the pressure might be to change the nozzle size after equilibrium conditions had been attained in the chamber. Either increases or decreases in pressure could be studied in this manner. No matter which technique was employed, the same observable - luminosity - variation would be used to determine the dp/dt at which the steady-state assumption can no longer be made.

Table G-1
Plastisol Propellant Compositions

	<u>P-4, P-7</u>	<u>P-6</u>	<u>P-8</u>	<u>P-9</u>	<u>P-10, P-11</u>	<u>P-12</u>
TEGDN	42.7	42.5	42.7	42.7	43.2	43.2
Ball Powder "B"	21.3	21.3	21.3	21.3	21.5	21.5
Ball Powder "A"	----	----	----	----	----	----
AP (5 μ)	11.7	35.0	11.7	11.7	11.8	11.8
AP (45 μ)	23.3	----	23.3	23.3	23.5	23.5
Stabilizer R-1	1.0	1.0	1.0	1.0	----	----
NaCl	----	0.2	0.2 (added)	0.5 (added)	----	----
MgO	----	----	----	----	----	0.2 (added)

	<u>P-14</u>	<u>P-15</u>	<u>P-16</u>	<u>P-17</u>	<u>P-18</u>	<u>P-19</u>
TEGDN	43.2	43.2	43.2	43.2	43.2	43.2
Ball Powder "B"	----	----	----	----	----	----
Ball Powder "A"	21.5	21.5	21.5	21.5	21.5	21.5
AP (5 μ)	11.8	35.3	----	11.8	11.8	11.8
AP (45 μ)	23.5	----	35.3	23.5	23.5	23.5
Stabilizer R-1	----	----	----	----	----	----
NaCl	----	----	----	0.5 (added)	0.1 (added)	0.05 (added)
MgO	----	----	----	----	----	----

APPENDIX I

LIST OF EQUIPMENT

<u>ITEM</u>	<u>PURPOSE</u>	<u>MANUFACTURER</u>
Quartz blanks	view window material	O&S Research, 1912 Bernard St. Riverton, New Jersey
Vycor blanks	view window material	Corning Glass Works, Corning, New York
Garlock asbestos	gaskets for window	Garlock Packing Co., Philadelphia, Pa.
1/2" stainless steel rupture discs	motor protection	Black, Sivalls & Bryson, Inc. Wayne, Penna.
Blow-out assembly 1/2" safety head assy.	motor protection	Black, Sivalls & Bryson, Inc. Wayne, Penna.
Filler RL-3700 potting compound	blow-out disc protection	W. P. Fuller & Co., P. O. Box 3727 Terminal Annex, Los Angeles 54, Calif.
Edwards 1063 buzzer	safety warning	Edwards, Norwalk, Conn.
Wollensak Model WF-16 Fastax camera	high speed movies	Wollensak, Rochester 21, New York
Wollensak "Goose"	camera control	Wollensak, Rochester 21, New York
Tripod	camera support	Quickset, Inc., 8121 N. Central Park Ave. Skokie, Illinois
Photocell, G.E. 1P42	photodetection	Federated Purchaser, 1021 U.S. Route 22 Mountainside, New Jersey
Photomultiplier, RCA 6217	photodetection	Federated Purchaser, Mountainside, N.J.
Gates power supply, G3030F	igniter current	Gates Electronics Corp, New York, N.Y.
Keithley power supply	photomultiplier power	Keithley Inst. Inc., 12415 Euclid Ave., Cleveland 6, Ohio

APPENDIX I

ITEM

PURPOSE

MANUFACTURER

Microdensitometer Cat. No. 6700 P-1

interpret spectra

Leeds & Northrup, 4907 Stenton Ave.,
Philadelphia 44, Pa.

Pyrometer

lamp calibration

Leeds & Northrup, Philadelphia, Pa.

Tungsten lamp, GE Model No. 18A/T10/2P-6V

photodetector calibration

Princeton University Store, Princeton, N.J.

Amthor 0-5000 deadweight tester

transducer calibration

Amthor Inst. Testing Co., Brooklyn, N. Y.

Wollensak Model WF311 pulse generator

timing light actuator

Electronic Counters, Syosset, L.I., New York

Vacuum tube voltmeter model 400 HR

calibration of equipment

Hewlett-Packard Co., 395 Page Mill Road,
Palo Alto, California

Wide range oscillator, 200CDR

calibration of equipment

Hewlett-Packard Co., Palo Alto, Calif.

Bantam Micropulverizer, Type SH

oxidizer grinding

Metals Disintegrating Co., Chatham Road,
Summit, New Jersey

Z-blade laboratory mixer, Model 35LP

propellant mixing

Atlantic Research Corp., Alexandria, Va.

Read Co. overlapping arm lab. mixer
One quart capacity

propellant mixing

Read Standard Corp., York, Pa.

Day mixer, Model 1 AH 1-1/2 JUS

propellant mixing

J. H. Day Co., 480 Lexington Avenue
New York 17, N. Y.

One gallon cap. Double hobbin blades

APPENDIX I

<u>ITEM</u>	<u>PURPOSE</u>	<u>MANUFACTURER</u>
Oscilloscope camera, ETC Model SM-100	strip films	Electronic Tube Corp., 1200 E. Mermaid Lane Philadelphia, Pa. 19118
Adjustable slit	photodetector	Edmund Scientific, Barrington, N. J.
Kodak TriX 35 MM film, Type TX 417	scope camera	Eastman Kodak Co., Rochester, N. Y.
DuPont 931-A 16 mm film	movies	E. I. DuPont Co., 380 Allwood Road, Clifton, N. J.
Kodak ER 16 mm film	movies	Eastman Kodak Co. Rochester, N. Y.
Royal-X Pan 35 mm film	spectra	Eastman Kodak Co. Rochester, N. Y.
Super-Panchro Press 5 x 7 plates	spectra	Eastman Kodak Co. Rochester, N. Y.
Bausch & Lomb 1.5 meter stigmatic grating spectrograph	spectra	Bausch & Lomb, Inc., 62662 Lomb Park, Rochester 2, N. Y.
Hilger & Watts intermediate quartz spectrograph	spectra	Adam Hilger, London, England
Synchro-compur shutter	exposure time for spectra	Ilex Co., Rochester, New York
132 mm f/3.5 quartz condensing lens	spectra optics	Bausch & Lomb, 62662 Lomb Park, Rochester, N. Y.
105mm f/5.6 Schneider-Kreuznach lens	streak camera optics	Electronic Tube Corp., 1200 E. Mermaid Lane Philadelphia, Pa.
Kern-Surtar 50 mm f/1.8 lens	streak camera optics	"
Fairchild Model F316A rapid processor	develop 16 mm film	Fairchild Camera Corp., 221 Fairfield Ave., Plainview, New York

APPENDIX I

<u>ITEM</u>	<u>PURPOSE</u>	<u>MANUFACTURER</u>
Dana amplifiers, D.C. 2200 & 2200A	amplification of input signals to tape & oscillograph	Dana Laboratories, Inc., 630 Young St., Santa Anna, California
Neff amplifiers, 10G D.C.	tape playback	Neff Inst. Corp., 1088 E. Hamilton Road, Duarte, California
SR-300 EM power supply	transducer voltage	Video Instrument Co., Santa Monica, Calif.
Tektronix scope Model 531	systems monitor	Tektronix, Inc., Portland 7, Oregon
D.C. voltmeter, digital	calibrations & systems monitor	United Systems Corp., 918 Woodley Road Dayton 3, Ohio
Simpson microammeter	ignition circuit tester	Simpson Elec. Co., 5200 W. Kinzie St., Chicago 44, Illinois
Tape recorder, Honeywell Model 8100	data recording	Honeywell, 4800 E. Dry Creek Road, Denver, Colorado 80217
Visicorder, Honeywell Model 906B	data recording	Honeywell, Denver, Colorado.
Visicorder timing unit	visicorder timing lines	Honeywell, Denver, Colorado.
DuPont linowrit 5 paper	visicorder paper	E. I. DuPont Co., 380 Allwood Road, Clifton, N. J.
Sequence timer, Model RC-J2889	equipment control	Industrial Timer Corp., State Electronics 36 Route 10, Hanover, N. J.
Water pump assy. Model 2L pump 1/3 H.P. motor	water pressure for transducer	Labawco Pump Company, Bellemead, N. J.
Pressure Transducer, PT-49-1M	pressure measurement	Dynisco Inst. Co., Cambridge, Mass.
Pressure Transducer, PT-76	pressure measurement	Dynisco, Cambridge, Mass.

APPENDIX J

LIST OF CHEMICALS

<u>ITEM</u>	<u>PURPOSE</u>	<u>MANUFACTURER</u>
<u>Ammonium Perchlorate</u>	oxidizer	American Potash & Chemical Corp. 3000 W. Sixth Street, Los Angeles, Calif.
(A) standard AMS-C66F	non-spherical std.	
(B) rounded class I 2-10% + 50 mesh 91-99% + 200 mesh	spherical std.	"
(C) 5 micron nominal at 50% point	spherical fine 5 μ	"
(D) -10 + 35 mesh	coarse spherical	"
(E) 45 micron at 50% point	spherical 45 μ	"
<u>PBAA Propellant</u>		
PBAA Polymer	fuel binder	American Synthetic Rubber Corp. P O. Box 360 Louisville 1, Kentucky
Epoxy resin (shell) (EPON 828)	fuel binder	Miller-Stephenson Chem. Co., Phila. 8, Pa.
Copper chromite	propellant additive (burning rate modifier)	Harshaw Chemical Company, Cleveland, Ohio
Ferric oxide	propellant additive (burning rate modifier)	Baker Chemical Company, Phillipsburg, N. J.
<u>LP-3 Propellant</u>		
LP-3 polymer	fuel binder	Thiokol Chem. Corp. Trenton, N. J.
GMF (P-Quinonedioxime)	propellant curing agent	Naugatuck Chem. Co., 152 Elm St., Naugatuck, Connecticut
Sulfur, sublimed (sulfur flowers)	propellant curing agent	Fischer Scientific Co., Fairlawn, N. J.
<u>P-13 Propellant</u>		
Polyester resin, Type P-13	fuel binder	Rohm & Haas Co., Philadelphia, Pa.

APPENDIX J

<u>ITEM</u>	<u>PURPOSE</u>	<u>MANUFACTURER</u>
Nuodex cobalt, accelerator	propellant curing agent	Nuodex Products Co., New York, N. Y.
Lecithin B-60, vegetable, technical	propellant wetting agent	Fischer Scientific Co., Fairlawn, N. J.
Lupersol DDM	propellant curing agent	Wallace & Tiernan, Buffalo, N. Y.
<u>Polyurethane Propellant</u> for AUP 85T		
Voranol P-2000 [PFG, polypropylene glycol] (note: P-1850 no longer available. Using P-2000 OH# 56.1 approx.)	resin	Dow Chemical Co., 217 Atlantic Avenue Camden, N. J.
Trimethylolpropane (TMP)	resin	Celanese Chem. Co., 522 Fifth Ave., New York 36, N. Y.
Ferric Acetylacetonate (FeAA)	catalyst	Aceto Chem. Co., 40-40 Lawrence St., Flushing 54, New York
N-phenyl 2-naphthylamine	antioxidant	Matheson Coleman & Bell, East Rutherford, N. J.
Calcium stearate, powdered	anticaking agent	Fischer Scientific Co., Fairlawn, N. J.
TDI (toluene 2-4 diisocyanate) Hylene T	crosslinking agent	E. I. DuPont, Wilmington, Delaware
Stannous octoate	catalyst	K & K Laboratories, Plainview, N. Y.
<u>Plastisol Propellant</u>		
Triacetin		Matheson Coleman & Bell East Rutherford, N. J. (Scientific Glass)

APPENDIX J

<u>ITEM</u>	<u>PURPOSE</u>	<u>MANUFACTURER</u>
Fluid Ball Powder Type "A" Type "B"	propellant	Associated Products Operation, Olin Matheson Chem. Co., East Alton, Illinois
TEGDN	propellant	Propellex, Div. of Chromalloy Corp. P. O. Box 187, Edwardsville, Ill.
TMETN	propellant	"
ALCOA aluminum, atomized powder No. 123 200 Mesh, granular (Av. part. dia. 18 μ)	propellant additive BR modifier	Aluminum Co. of America, 1501 Alcoa Bldg., Pittsburgh 19, Penna.
Sodium chloride, reagent, crystals (note: powdered 1 pass in Bantam Pulverizer at 12,000 RPM)	propellant additive	Scientific Glass & Apparatus Co., Bloomfield, N. J.
Sodium stearate, powdered (stearic acid sodium salt)	propellant additive	Scientific Glass & Apparatus Co., Bloomfield, N. J.
Magnesium oxide (U.S.P.)	propellant additive	Fisher Scientific Co., Fairlawn, New Jersey
VYLF plastic	inhibitor	Union Carbide Plastics Co., 30 E. 42nd St., New York 17, N. Y.
High vacuum grease (silicone lubricant)	mold release agent	Dow Corning Corp., Midland, Michigan (obtainable at Fischer Scientific Co., 633 Greenwich St., New York, N. Y.)
Aluminum powder MD105	propellant additive	Metal Disintegrating, Elizabeth, N. J.

REFERENCES

1. Boys, S. F. and Schofield, A., "Investigations on Secondary Peaks", Advisory Council on Scientific Research and Technical Development (Great Britain) Report No. A. C. 5649/Rep./20/43, 1943.
2. Green, L., "Observations on the Irregular Reaction of Solid Propellant Charges", Jet Propulsion 26, 1956, p. 655.
3. Wimpers, R. N., "Internal Ballistics of Solid-Fuel Rockets", McGraw-Hill, New York, 1950), Chapt. 9.
4. Anderson, A. B. C. and Hunt, D. M., "Operational Characteristics of the Dyna-Gage in Investigations of Pressures in Statically Fired Rockets", NAVORD Report 1031 (NOTS 150), 1948.
5. Manson, C. D., "Resonance Burning in Rocket Grains," NOTS TM 439, 1951.
6. Smith, R. P. and Sprenger, D. F., "Combustion Instability in Solid Propellant Rockets", 4th Symp. on Combustion (Williams and Wilkins, Baltimore, 1953), p. 893.
7. Schultz, R., Green, L., and Penner, S. S., "Studies of the Decomposition Mechanism, Erosive Burning, Sonance, and Resonance for Solid Composite Rockets", Combustion and Propulsion, 3rd AGARD Colloquium (Pergamon Press, New York, 1958), p. 401.
8. Waesche, R. H. W., Rohm & Haas Co. Ballistics Section Progress Report No. 78, January, 1959.
9. Green, L., "Studies on the Reaction Stability of Solid Propellant Charges", Aerojet-General TN 1077, 1956.
10. Green, L., "Some Effects of Oxidizer Concentration and Particle Size on Resonance Burning of Composite Solid Propellants", ARS Journal 28, 1958, p. 159.
11. Geckler, R. D., "The Mechanism of Combustion of Solid Propellants", Selected Combustion Problems (Butterworths Scientific Publications, London, 1954), p. 289.
12. Geckler, R. D., "Unsolved Problems in Solid Propellant Combustion", 5th Symp. on Combustion (Reinhold Publishing, New York, 1955), p. 29.
13. Price, E. W., "Combustion Instability in Solid Propellant Rocket Motors", Astronautica Acta 5, 1959, p. 63.
14. Wall, R. H., "Resonant Burning of Solid Propellants: Review of Causes, Cures, and Effects", Progress in Astronautics and Rocketry: Solid Propellant Rocket Research (Academic Press, Inc., New York, 1960), Vol. I, p. 603.

15. Osborn, J. R., "Unstable Burning in Solid and Liquid Propellant Rocket Motors," *Raketentechnik und Raumfahrtforschung* 2, 1963, p. 47.
16. Shuey, H. M., AIAA Research Award Citation, January, 1964.
17. McClure, F. T., et al., "A General Review of Our State of Knowledge", First Report of the Working Group on Solid Propellant Combustion Instability, APL/JHU TG 371-1, 1960.
18. Epstein, P. S. and Carhart, R. R., "The Absorption of Sound in Emulsions and Suspensions, I. Water Fog in Air", *J. Acous. Soc. Am.* 25, 1953, p. 553.
19. Zink, J. W. and Delsasso, L. P., "Attenuation and Dispersion of Sound by Solid Particles Suspended in a Gas", *J. Acous. Soc. Am.* 30, 1958, p. 765.
20. Price, E. W., "Combustion Instability in Solid Propellant Rocket Motors", *ARS Journal* 30, 1960, p. 574.
21. McClure, F. T., Hart, R. W. and Bird, J. F., "Acoustic Instability in Solid Fuel Rockets", *ARS Journal* 30, 1960, p. 908.
22. Horton, M. D., "Acoustic Admittance of a Burning Solid Propellant Surface", *ARS Journal* 32, 1962, p. 644.
23. Waesche, R. H. W., Rohm & Haas Co. Internal Report, 1957.
24. Landsbaum, E. M. and Spaid, F. W., "Experimental Studies of Unstable Combustion in Solid Propellant Rocket Motors," JPL/CIT Technical Report No. 32-146, 1961.
25. Waesche, R. H. W., Wenograd, J. and Summerfield, M., "Entropy Wave Observations in Oscillatory Combustion of Solid Propellants: A Progress Report", AIAA Preprint 64-154, January 1964.
26. McClure, F. T., Bird, J. F. and Hart, R. W., "Erosion Mechanism for Nonlinear Instability in the Axial Modes of Solid Propellant Rocket Motors", *ARS Journal* 32, 1962, p. 374.
27. Brownlee, W. G., "Nonlinear Axial Combustion Instability in Solid Propellant Motors", *AIAA Journal* 2, p. 275.
28. Price, E. W., "Axial Mode, Intermediate Frequency Combustion Instability in Solid Propellant Rocket Motors", AIAA Preprint 64-146, January 1964.
29. Purdy, K. R., Jackson, T. W. and Gorton, C. W., "Viscous Fluid Flow Under the Influence of a Resonant Acoustic Field", ASME Paper No. 62-WA-116, November, 1962.
30. Moore, F. K. and Maslen, S. H., "Transverse Oscillations in a Cylindrical Combustion Chamber", NACA TN 3152, October, 1954.

III

31. Vandenbergkhove, J., "Erosive Burning of a Colloidal Solid Propellant", Jet Propulsion 28, 1958, p. 599.
32. Crump, J. E. and Price, E. W., "Effect of Acoustic Environment on the Burning Rate of Double-base Solid Propellants", ARS Journal 31, 1961, p. 1026.
33. Crump, J. E. and Price, E. W., "Effect of Acoustic Environment on the Burning Rate of Solid Propellants", AIAA Journal 2, 1964, p. 1274.
34. Crump, J. E. and Price, E. W., "Catastrophic Changes in Burning Rate of Solid Propellants During Combustion Instability", ARS Journal 30, 1960, p. 705.
35. Eisel, J. L., "The Effect of Acoustic Pressure on the Burning Rates of Solid Rocket Propellants", Pyrodynamics 1, 1964, p. 61.
36. Nadaud, L., and Gicquel, M., "Influence des Ondes Sonores sur la Vitesse de Combustion des Propergols Solides", la Recherche Aeronautique 88, 1962, p. 59.
37. Watermeier, L. A., "Experimental Study of Combustion Instability in Solid Rocket Propellants", ARS Journal 31, 1961, p. 564.
38. Yamazaki, K., Hayashi, M., and Iwama, A., "The Effect of Sound Waves on the Burning Velocity of a Solid Propellant", Int. Chem. Eng. 5, 1965, p. 186.
39. Watermeier, L. A., Aungst, W. P., and Strittmater, R. C., "Experimental Study of Acoustic Erosivity Effects on Solid Propellant Burning Rates", First ICRPG Combustion Instability Conference, CPIA Publ. No. 68, p. 413.
40. Flandro, G. A., "Roll Torque and Normal Force Generation in Acoustically Unstable Rocket Motors", AIAA Journal 2, 1964, p. 1303.
41. Westervelt, P. J., "The Theory of Steady Rotational Flow Generated by a Sound Field", J. Acous. Soc. Am. 25, 1953, p. 60.
42. Green, L., "Some Effects of Charge Configuration in Solid Propellant Combustion", Jet Propulsion 28, 1958, p. 483.
43. Waesche, R. H. W., Rohm & Haas Co. Ballistics Section Report No. 69, January, 1958.
44. Green, L., "Unstable Burning of Solid Propellants", Jet Propulsion 24, 1954, p. 252.
45. Sotter, G., "Investigation of Combustion Instability in Solid Propellant Rocket Motors", Progress Report No. 3, Department of Fuel Technology and Chemical Engineering, University of Sheffield, January, 1963.

46. Swithenbank, J. and Sotter, G., "Vortices in Solid Propellant Rocket Motors", AIAA Journal 1, 1963, p. 1682.
47. Swithenbank, J. and Sotter, G., "Vortex Generation in Solid Propellant Rockets", AIAA Journal 2, 1964, p. 1297.
48. Mager, A., "Approximate Solution of Isentropic Swirling Flow Through a Nozzle", ARS Journal 31, 1961, p. 1140.
49. Price, E. W., Mathes, H. B., Crump, J. E., and McGie, M. R., "Experimental Research in Combustion Instability of Solid Propellants", Combustion and Flame 5, 1961, p. 149.
50. McClure, F. T., Contribution to panel discussion "Unstable Combustion in Solid-Fuel Rocket Engines", 8th Symp. on Combustion (Williams & Wilkins, Baltimore, 1962), p. 931.
51. Price, E. W., "Review of Experimental Research on Combustion Instability of Solid Propellants", Progress in Astronautics and Rocketry: Solid Propellant Rocket Research (Academic Press, Inc., New York, 1960), Vol. 1, p. 561-602.
52. Angelus, T. A., "Unstable Burning Phenomenon in Double-Base Propellants", Progress in Astronautics and Rocketry: Solid Propellant Rocket Research (Academic Press, Inc., New York, 1960), Vol. 1, pp. 527-561.
53. Brownlee, W. S. and Marble, F. E., "An Experimental Investigation of Unstable Combustion in Solid Propellant Rocket Motors", Progress in Astronautics and Rocketry: Solid Propellant Rocket Research (Academic Press, Inc., New York, 1960), Vol. 1, pp. 455-494.
54. Zwicky, F., "Morphology of Aerial Propulsion", Helvetica Physica Acta 21, 1948, p. 299.
55. Hart, R. W. and Bird, J. F., "Scaling Problems Associated with Unstable Burning in Solid Propellant Rockets", 9th Symp. on Combustion (Academic Press, New York, 1963), pp. 993-1104.
56. Hart, R. W. and McClure, F. T., "Theory of Acoustic Instability in Solid-Propellant Rocket Combustion", 10th Symp. on Combustion (The Combustion Institute, Pittsburgh, 1965), p. 1047.
57. Summerfield, M., et al., "Burning Mechanism of Ammonium Perchlorate Propellants", ARS Preprint No. 737-58, November 1958.
58. Summerfield, M., "Remarks to Ad Hoc Committee on Solid Propellant Combustion Instability", June 8, 1960, Alexandria, Va.
59. Robinson, C. N., "Measurement of the Complex Dynamic Shear Compliance of Composite Solid Propellant", Proceedings of the Third Meeting, Technical Panel on Solid Propellant Combustion Instability, APL/JHU TG 371-5, p. 127.

60. Lighthill, M. J., "On Sound Generated Aerodynamically, I. General Theory", Proceedings of the Royal Society of London, Series A 211, 1952, p. 564.
61. Price, E. W., "Experimental Solid Rocket Combustion Instability", 10th Symp. on Combustion (The Combustion Institute, Pittsburgh, 1965), p. 1067.
62. Huggett, C. M., "Combustion Processes", High Speed Aerodynamics and Jet Propulsion (Princeton University Press, Princeton, 1956), Vol. II, p. 516.
63. Summerfield, M., "A Theory of Unstable Combustion in Liquid Propellant Rocket Systems", ARS Journal 21, 1951, p. 108.
64. McClure, F. T., Hart, R. W., and Bird, J. F., "Solid Propellant Rocket Motors as Acoustic Oscillators", Progress in Astronautics and Rocketry: Solid Propellant Rocket Research (Academic Press, Inc., New York, 1960), Vol. 1, pp. 295-358.
65. Higgins, B., Nicholson's Journal 1, 1802, p. 130.
66. Wood, A. B., "A Text Book of Sound", (Macmillan Co., New York, 1955), p. 211.
67. Putnam, A. A. and Dennis, W. R., "Survey of Organ-Pipe Oscillations in Combustion Systems", J. Acous. Soc. Am. 28, 1956, p. 246.
68. Roginskii, O. G., "Oscillatory Combustion", Soviet Physics-Acoustics 7, 1961, p. 107.
69. Mallard, E., and Le Chatelier, H., Ann. Mines 8, Series 4, 1883, p. 274.
70. Howland, A. H. and Simmonds, W. A., "Combustion Inside Refractory Tubes", 4th Symp. on Combustion (Williams & Wilkins, Baltimore, 1953), pp. 592-602.
71. Fenn, J. B., Forney, H. B. and Garmon, R. C., "Burners for Supersonic Ramjets", Ind. Eng. Chem. 43, 1951, p. 1663.
72. Bortzmeyer, H. G., and Crocco, L., "Analysis of Longitudinal High Frequency Combustion Instability in a Gas Fueled Rocket Motor", Aeronautical Engineering Report No. 587, Princeton University, 1961.
73. Zucrow, M. J., and Osborn, R. J., "An Experimental Study of High-Frequency Combustion Pressure Oscillations", ARS Journal 28, 1958, p. 654.
74. Gaydon, A. G. and Wolfhard, H. G., "Flames", 2nd ed., (MacMillan Company, New York, 1960), p. 167 et seq.
75. Jones, A. T., J. Acous. Soc. Am. 16, 1945, p. 254.

76. Rayleigh, G. W. S., "The Theory of Sound", Vol. II, (Dover Publications, New York, 1945), p. 226.
77. Rijke, P. L., Phil. Mag. 17, 1859, p. 419.
78. Rayleigh, G. W. S., op cit., p. 233.
79. Diederichsen, J., and Gould, R. D., "Combustion Instability: Radiation from Premixed Flames of Variable Burning Velocity", Comb. Flame 9, 1965, p. 25.
80. Grad, H., "Resonance Burning in Rocket Motors", Comm. Pure Appl. Math. 2, 1949, p. 79.
81. Cheng, S. I., "High-Frequency Combustion Instability in Solid Propellant Rockets", Jet Propulsion 24, 1954, p. 27 and p. 102.
82. Price, E. W., Mathes, H. B., Crump, J. E. and McGie, M. R., "Experimental Research in Combustion Instability of Solid Propellants", Combustion and Flame 5, 1961, p. 157.
83. Schultz, R., Green, L., Penner, S. S., "Studies of the Decomposition Mechanism, Erosive Burning, Sonance, and Resonance for Solid Composite Rockets", Combustion and Propulsion, 3rd AGARD Colloquium (Pergamon Press, New York, 1958), p. 407.
84. Cheng, S. I., "On Unstable Burning of Solid Propellants", Jet Propulsion 25, 1955, p. 79.
85. Hart, R. W. and McClure, F. T., "Combustion Instability: Acoustic Interaction with a Burning Surface", J. Chem. Phys. 30, 1959, p. 1501.
86. Williams, F. A., "Response of a Burning Solid to Small-Amplitude Pressure Oscillations", J. Appl. Phys. 33, 1962, p. 3153.
87. Akiba, R. and Tanno, M., "Low Frequency Instability in Solid Propellant Rocket Motors", 1st Symp. (Int'l.) on Rockets and Astronautics, Tokyo, 1959, p. 74.
88. Sehgal, R. and Strand, L., "A Theory of Low Frequency Combustion Instability in Solid Rocket Motors", Jet Propulsion Lab., CIT, TN-33-130.
89. Price, E. W., "L* Combustion Instability", 3rd Meeting of the Technical Panel on Solid Propellant Combustion Instability, JHU/APL TG 371-5 (1963), p. 153.
90. Smith, A. G., "A Theory of Oscillatory Burning of Solid Propellants Assuming a Constant Surface Temperature", Progress in Astronautics and Rocketry: Solid Propellant Rocket Research (Academic Press, Inc., New York, 1960), Vol. 1, pp. 375-392.

91. Dennison, M. R. and Baum, E., "A Simplified Model of Unstable Burning in Solid Propellants", ARS Journal 31, 1961, p. 1112.
92. Cheng, S. I., "Closure by Sin - I. - Cheng", op. cit.
93. Lewis, B. and von Elbe, C., "Combustion, Flames, and Explosions of Gases", (Academic Press, New York, 1951), p. 612.
94. Green, L., "Some Properties of a Simplified Model of Solid Propellant Burning", Jet Propulsion 28, 1958, p. 386.
95. Nachbar, W. and Green, L., "Analysis of a Simplified Model of Solid Propellant Resonant Burning", J. Aero/Space Sci. 26, 1959, p. 518.
96. Schultz, R., Green, L., and Penner, S. S., op. cit., p. 416.
97. Cheng, S. I., "Unstable Combustion in Solid Propellant Rocket Motors", 8th Symp. on Combustion (Williams & Wilkins, Baltimore, 1962), p. 84.
98. Price, E. W., "Combustion Instability in Solid Propellant Rockets", ARS Preprint No. 1492-60, December, 1960, p. 21.
99. Price, E. W. and Sofferis, J. W., "Combustion Instability in Solid Propellant Rocket Motors", Jet Propulsion 28, 1958, p. 190.
100. Green, L. and Nachbar, W., "Comment on 'Combustion Instability in Solid Propellant Rocket Motors'", Jet Propulsion 28, 1958, p. 769.
101. "Closure by W. Nachbar and L. Green, Jr.," ARS Journal 30, 1960, p. 576.
102. Barrere, M. and Bernard, J. J., "Combustion Instability of Solid Propellant with Time Delay Distribution (Theoretical Study)", 8th Symp. on Combustion (Williams & Wilkins, Baltimore, 1962), p. 886.
103. Bastress, E. K., "Modification of the Burning Rates of Ammonium Perchlorate Solid Propellants by Particle Size Control", Ph.D. Thesis, Department of Aeronautical Engineering, Princeton University, January, 1961.
104. Kling, R. and Brulard, J., "Etude de la Combustion des Poudres Composites par la Microphotographie Ultra-Rapide", la Recherche Aeronautique 80, 1961, p. 3.
105. Barrere, M., "Les Instabilites de Combustion du Type Acoustique dans les Fusees a Propergol Solide", la Recherche Aeronautique 80, 1961, p. 17.
106. Vandenkerckhove, J., "Tentative Explanation of Irregular Burning in Solid Propellant Rockets", ARS Journal 31, 1961, p. 1466.
107. Landsbaum, E. M., Kuley, W. C., and Spaid, F. W., "Experimental Investigations of Unstable Burning in Solid Propellant Rocket Motors", Progress in Astronautics and Rocketry: Solid Propellant Rocket Research (Academic Press, Inc., New York, 1960), Vol. 1, pp. 495-526.

108. Shinnar, R. and Dishon, M., "Heat Transfer Stability Analysis of Solid Propellant Rocket Motors", Progress in Astronautics and Rocketry: Solid Propellant Rocket Research (Academic Press, Inc., New York, 1960), Vol. 1, pp. 359-374.
109. McClure, F. T., Bird, J. F. and Hart, R. W., "An Erosion Mechanism for Non-Linear Instability in the Axial Modes of Solid Propellant Rocket Motors", ARS Journal 32, 1962, p. 374.
110. Hart, R. W., Bird, J. F., Cantrell, R. W. and McClure, F. T., "Nonlinear Effects in Instability of Solid Propellant Rocket Motors", AIAA Journal 2, 1964, p. 1270.
111. Dickinson, L. A., "Command Initiation of Finite Wave Axial Combustion Instability in Solid Propellant Rocket Motors", ARS Journal 32, 1962, p. 643.
112. Morris, E. P., "A Pulse Technique for the Evaluation of Combustion Instability in Solid Propellant Motors," CARDE T.R. 487/64, May 1964.
113. Brownlee, W. G., "Nonlinear Axial Combustion Instability in Solid Propellant Motors", AIAA Journal 2, 1964, p. 275.
114. Jackson, F., Brownlee, W. G. and Roberts, A. K., "Influence of Axial Combustion Instability on the Development of a 23KS-20,000 Motor", 4th Meeting of the Technical Panel on Solid Propellant Combustion Instability, JHU/APL TG 371-7 (1964), p. 77.
115. Horton, M. D. and McGie, M. R., "Particulate Damping of Oscillatory Combustion", AIAA Journal 1, 1963, p. 1319.
116. Horton, M. D. and Rice, D. W., "The Effect of Compositional Variables Upon Oscillatory Combustion of Solid Rocket Propellants", Comb. Flame 8, 1964, p. 21.
117. Horton, M. D., "Testing the Dynamic Stability of Solid Propellants: Techniques and Data", NOTS TP 3610, August, 1964.
118. Dickinson, L. A., Brownlee, W. G. and Jackson, F., "CARDE Investigations of Finite Wave Axial Combustion Instability", 2nd Meeting of the Technical Panel on Solid Propellant Combustion Instability, JHU/APL TG 371-4B (1962), p. 59.
119. Brownlee, W. G., "CARDE Experiments on Nonlinear Axial Combustion Instability", 3rd Meeting of the Technical Panel on Solid Propellant Combustion Instability, JHU/APL TG 371-5 (1963), p. 63.
120. Dickinson, L. A., Muller, G., and Capener, E. L., "Influence of Compositional Factors on Axial Instability", 4th Meeting of the Technical Panel on Solid Propellant Combustion Instability, JHU/APL TG 371-7, (1964), p. 75.

121. Dickinson, L. A. and Capener, E. L., "A Study of Combustion Instability and Its Dependence on Propellant Combustion Characteristics", Stanford Research Institute Final Report on Contract No. AF 49(638)-565, 1964.
122. Yount, R. A. and Angelus, T. A., "Chuffing and Nonacoustic Instability Phenomena in Solid Propellant Rockets", AIAA Journal 2, 1964, p. 1307.
123. "Rocket Fundamentals", OSRD 3711, 1944.
124. Angelus, T. A., Contribution to panel discussion on "Unstable Combustion in Solid-Fuel Rocket Engines", 8th Symp. on Combustion (Williams & Wilkins, Baltimore, 1962), p. 921.
125. Huffington, J. D., "The Unsteady Burning of Cordite", Transactions of the Faraday Society 50, 1954, p. 942.
126. Huffington, J. D., "The Burning and Structure of Cordite", Transactions of the Faraday Society 47, 1951, p. 864.
127. Frank-Kamenetskii, A. D., J. Physic. Chem. Soc. Rus. 18, 1939, p. 738.
128. Clemmow, D. M. and Huffington, J. D., "An Extension of the Theory of Thermal Explosion and Its Application to the Unsteady Burning of Explosives", Transactions of the Faraday Society 52, 1956, p. 385.
129. Huggett, C. M., "Combustion Processes", High Speed Aerodynamics and Jet Propulsion (Princeton University Press, Princeton, 1956), Vol. II, Sec. 4, p. 550.
130. Mellor, A. M. and Glassman, I., "A Physical Criterion for Metal Ignition", Laboratory Report No. 698, Department of Aerospace and Mechanical Sciences, Princeton University, 1964.
131. Sabadell, A. J., "The Measurement of the Temperature Profiles of Burning Solid Propellants by Microthermocouples", M.S.E. Thesis, Princeton University, 1963.
132. Inami, T. H. and Shanfield, H., "Nonacoustic Combustion Pulsations of Ammonium Perchlorate Containing Aluminum", AIAA Journal 2, 1964, p. 1314.
133. Eisel, J. L., Horton, M. D., Price, E. W. and Rice, D. W., "Preferred Frequency Oscillatory Combustion of Solid Propellants", AIAA Journal 2, 1964, p. 1319.
134. Price, E. W., Rice, D. W. and Crump, J. E., "Low-Frequency Combustion Instability of Solid Rocket Propellants", NOTS TP 3524, July 1964.
135. Cheng, S. I., "Combustion Instability in Solid Rockets Using Propellants with Reactive Additives", Progress in Astronautics and Rocketry: Solid Propellant Rocket Research (Academic Press, Inc., New York, 1960), Vol. 1, pp. 393-422.

136. Ellis, H., Odgers, I., Stosick, A. J., van de Verg, N., and Wick, R. S., "Experimental Investigation of Combustion Instability in Rocket Motors", 4th Symp. on Combustion (Williams & Wilkins, Baltimore, 1953), p. 880.
137. Morse, P. M., "Vibration and Sound", (McGraw-Hill, New York, 1948), Sect. 23.
138. Tsien, H. S., "The Transfer Functions of Rocket Nozzles", Journal of the ARS 22, 1952, p. 139.
139. Crocco, L., "Supercritical Gaseous Discharge with High Frequency Oscillations", L'Aerotecnica 33, 1953, p. 46.
140. Crocco, L., and Cheng, S. I., "High Frequency Combustion Instability in Rockets with Distributed Combustion", 4th Symp. on Combustion (Williams and Wilkins, Baltimore, 1953), p. 865.
141. Cheng, S. I., "Low-Frequency Combustion Stability of Liquid Rocket Motors with Different Nozzles", Jet Propulsion 25, 1955, p. 163.
142. Crocco, L., Grey, J. and Harrje, D. T., "Theory of Liquid Propellant Rocket Combustion Instability and Its Experimental Verification", ARS Journal 30, 1960, p. 159.
143. Lambiris, S., "Experimental Verification of Nozzle Admittance Theory in a Simulated Rocket Chamber", Princeton University Dept. of Aero. Eng. Report No. 401, September 1947.
144. Crocco, L., Monti, R. and Grey, J., "Verification of Nozzle Admittance Theory by Direct Measurement of the Admittance Parameter", ARS Journal 31, 1961, p. 771.
145. Scala, S., "Transverse Wave and Entropy Wave Combustion Instability in Liquid Propellant Rockets", Ph.D. Thesis, App. A., Princeton University Dept. of Aero. Eng. Report No. 380, April 1957.
146. Crocco, L., "The Transverse Admittance of a deLaval Nozzle", Appendix to Princeton University Dept. of Aero. Eng. Report No. 216-dd, Dec. 1959.
147. Reardon, F. H., "An Investigation of Transverse Mode Combustion Instability in Liquid Propellant Rocket Motors", Ph.D. Thesis, App. C., Princeton University Dept. of Aero. Eng. Report No. 550, June 1961.
148. Crocco, L., Harrje, D. T. and Reardon, F. H., "Transverse Combustion Instability in Liquid Propellant Rocket Motors", ARS Journal 32, 1962, p. 366.
149. Reardon, F. H., Crocco, L., and Harrje, D. T., "Velocity Effects in Transverse Mode Liquid Propellant Rocket Combustion Instability", AIAA Journal 2, 1964, p. 1631.

150. Culick, F. E. C., "Stability of High-Frequency Pressure Oscillations in Rocket Combustion Chambers", AIAA Journal 1, 1963, p. 1097.
151. Culick, F. E. C., MIT Technical Report 480, June, 1961.
152. Bird, J. F., McClure, F. T., and Hart, R. W., "Acoustic Instability in the Transverse Modes of Solid Propellant Rockets", XIIth Int'l. Astronautical Congress (Academic Press, Inc., New York, 1963), p. 459.
153. Bird, J. F., Haer, L., Hart, R. W., and McClure, F. T., "Effect of Solid Propellant Compressibility on Combustion Instability", J. Chem. Phys. 32, 1960, p. 1423.
154. McClure, F. T., Hart, R. W. and Bird, J. F., "Acoustic Resonance in Solid Propellant Rockets", J. Appl. Phys. 31, 1960, p. 884.
155. Bird, J. F., Hart, R. W. and McClure, F. T., "Vibrations of Thick-Walled Hollow Cylinders - Exact Numerical Solutions", J. Acoust. Soc. Am. 32, 1960, p. 1404.
156. Bird, J. F., "Vibrations of Thick-Walled Hollow Cylinders - Approximate Theory", J. Acous. Soc. Am. 32, 1960, p. 1413.
157. Deters, O. J., "Effects of Gas Phase and Solid Phase Damping on Instability of Low Frequency Modes in Solid Propellant Rockets", ARS Journal 32, 1962, p. 378.
158. Ryan, N. W., Contribution to panel discussion on "Unstable Combustion in Solid-Fuel Rocket Engines", 8th Symp. on Combustion (Williams & Wilkins, Baltimore, 1962), p. 925.
159. Nall, B. H., "Acoustic Attenuation in a Solid Propellant", AIAA Journal 1, 1963, p. 76.
160. Ryan, N. W. and Coates, R. L., "Acoustic Instability: Influence of and on the Solid Phase", AIAA Journal 2, 1964, p. 1130.
161. Lambert, R. F., "A Study of the Factors Influencing the Damping of an Acoustical Cavity Resonator", J. Acous. Soc. Am. 25, 1953, p. 1068.
162. Cantrell, R. H., McClure, F. T. and Hart, R. W., "Acoustic Damping in Cavities with Mean Velocity and Thermal Boundary Layers", J. Acous. Soc. Am. 35, 1963, p. 500.
163. Strittmater, R., Watermeier, L. A. and Pfaff, S. P., "Virtual Specific Acoustic Admittance Measurements of Burning Solid Propellant Surfaces by a Resonant Tube Technique", 9th Symp. on Combustion (Academic Press, Inc., New York, 1963), p. 311.
164. Watermeier, L. A., et al., "A Summary of Recent Combustion Instability Research in Solid Rocket Propellants at the BRL", BRL Memorandum Rpt. No. 1489, July, 1963.

165. MacFarlane, J. J., Holderness, F. H. and Whitcher, F. S. E., "Soot Formation Rates in Premixed C₅ and C₆ Hydrocarbon-Air Flames at Pressures up to 20 Atmospheres", Comb. Flame 8, 1964, p. 215.
166. Chow, J. C. F., "The Attenuation of Acoustic Waves in a Two-Phase Medium", Div. of Engineering, Brown Univ., Report ABL/X96, May, 1963.
167. Dobbins, R. A. and Temkin, S., "Measurements of Particulate Acoustic Attenuation", AIAA Journal 2, 1964, p. 1106.
168. Scott, R. A., "An Apparatus for Accurate Measurement of the Acoustic Impedance of Sound-Absorbing Materials", Proc. Phys. Soc. 58, 1946, p. 253.
169. Altman, D., "Acoustical Damping of Aluminized Propellants", 1st Meeting of the Technical Panel on Solid Propellant Combustion Instability, JHU/APL TG 371-3, p. 145.
170. Blair, D. W., "Particle Damping of a Plane Wave by Solid Particles Suspended in a Gas", AIAA Journal 1, 1963, p. 2625.
171. Sehgal, R., "An Experimental Investigation of a Gas-Particle System", JPL Rept. 32-238, March 1962.
172. Dobbins, R. A., "Combustion Instability and Particulate Attenuation of Light and Sound", 1st ICRPG Combustion Instability Conference, Orlando, Fla., November, 1964.
173. Ribnick, A. and Calcote, H. F., "Acoustic Absorption Coefficients of the Combustion Products of Aluminized Propellants", 4th Meeting of the Technical Panel on Solid Propellant Combustion Instability, JHU/APL TG 371-7 (1964), p. 52.
174. Parker, J. G., "Effect of Several Light Molecules on the Vibrational Relaxation Time of Oxygen", J. Chem. Phys. 34, 1961, p. 1763.
175. Lukasik, S. J. and Young, J. E., "Vibrational Relaxation Times in Nitrogen", J. Chem. Phys. 27, 1957, p. 1149.
176. Young, J. E. and Mawardi, O. K., "Molecular Absorption of Sound in Gases at High Temperatures", J. Chem. Phys. 24, 1956, p. 1109.
177. Lang, J. J., et al., Illinois Inst. Technology Final Report on Contract No. AF49(638)-1094, July, 1963.
178. Sirignano, W. A., "A Theoretical Study of Nonlinear Combustion Instability: Longitudinal Mode", Ph.D. Thesis, Princeton University, 1964.
179. Weiner, S. D., "The Acoustics of Solid Propellant Combustion Instability," Bolt Beranek and Newman Rpt. No. 1164, December, 1964.

180. Cheng, S. I., "Unstable Combustion in Solid Propellant Rocket Motors", 8th Symp. on Combustion (Williams & Wilkins, Baltimore, 1962), p. 88.
181. Summerfield, M., et al., "Burning Mechanism of Ammonium Perchlorate Propellants", Progress in Astronautics and Rocketry: Solid Propellant Rocket Research (Academic Press, Inc., New York, 1960), pp. 141-182.
182. Sutherland, G. S., "Mechanism of Combustion of an Ammonium Perchlorate-Polyester Resin Composite Solid Propellant", Ph.D. Thesis, Princeton University, 1956.
183. Bircumshaw, L. L. and Newman, B. H., "The Thermal Decomposition of Ammonium Perchlorate", Proc. Roy. Soc. A 227, 1955, p. 228.
184. Friedman, R., Nugent, R. G., Rumbel, K. E. and Scurlock, A. C., "Deflagration of Ammonium Perchlorate", 6th Symp. on Combustion (Reinhold Publishing, New York, 1958), p. 612.
185. Arden, E. A., Powling, J. and Smith, W. A. W., "Observations on the Burning of Ammonium Perchlorate", Comb. Flame 6, 1962, p. 21.
186. Irwin, O. R., Salzman, P. K. and Anderson, W. H., "Deflagration Characteristics of Ammonium Perchlorate at High Pressures", 9th Symp. on Combustion (Academic Press, Inc., New York, 1963), pp. 358-365.
187. Cantrell, R. H., Hart, R. W. and McClure, F. T., "Linear Acoustic Gains and Losses in Solid Propellant Rocket Motors", AIAA Journal 2, 1964, p. 1100.
188. Crocco, L. and Cheng, S. I., "Theory of Combustion Instability in Liquid Propellant Rocket Motors", AGARDograph No. 8 (Butterworths, London, 1956).
189. Cheng, S. I., "Unstable Combustion in Solid Propellant Rocket Motors", 8th Symp. on Combustion (Williams & Wilkins, Baltimore, 1962), p. 89.
190. Trubridge, G. F. P., "Expanded Versions of Applied Physics Laboratory Reports on Solid Propellant Instability of Combustion", Summerfield Research Station, Imperial Metal Industries (Kynoch) Limited, Kidderminster, Worcestershire, July, 1963.
191. Summerfield, M., Private Communication to F. T. McClure, January 8, 1962.
192. Hart, R. W. and Cantrell, R. H., "Amplification and Attenuation of Sound by Burning Propellants", AIAA Journal 1, 1963, p. 398.
193. Wood, W. A., "Oscillatory Burning of Solid Composite Propellants", 9th Symp. on Combustion (Academic Press, Inc., New York, 1963), pp. 335-344.

194. Johnson, W. E. and Nachbar, W., "Deflagration Limits in the Steady Linear Burning of a Monopropellant with Application to Ammonium Perchlorate", 8th Symp. on Combustion (Williams & Wilkins, Baltimore, 1962), p. 678.
195. vonKarman, T., "The Present Status of the Theory of Laminar Flame Propagation", 6th Symp. on Combustion (Reinhold, New York, 1957), p. 4.
196. Price, E. W., "Analysis of Results of Combustion Instability Research on Solid Propellants", ARS Preprint No. 1068-60, January, 1960.
197. Horton, M. D., "One-Dimensional Solid Propellant Oscillatory Burner", ARS Journal 31, 1961, p. 1596.
198. Price, E. W., Mathes, H. B., Crump, J. E. and McGie, M. R., "Experimental Research in Combustion Instability of Solid Propellants", Comb. Flame 5, 1961, p. 156.
199. Horton, M. D., "Oscillatory Burning of Solid Rocket Propellants", Ph.D. Thesis, University of Utah, May 1961.
200. McClure, F. T., Hart, R. W., and Cantrell, R. H., "Interaction Between Sound and Flow: Stability of T-Burners", AIAA Journal 1, 1963, p. 586.
201. Cantrell, R. H. and Hart, R. W., "Interaction Between Sound and Flow in Acoustic Cavities: Mass, Momentum and Energy Considerations", J. Acous. Soc. Am. 36, 1964, p. 697.
202. Dyer, I., "The Effect of Flow on Burning Instability", 3rd Meeting of the Technical Panel on Solid Propellant Combustion Instability, JHU/APL TG 371-5 (1963), p. 147.
203. Westervelt, P. J., Quarterly Progress Report No. 2 on "The Acoustics of Solid Propellant Combustion Instability", Bolt Beranek and Newman, Inc., April, 1963.
204. Starr, E. A., Quarterly Tech. Progress Report No. 3 on "The Acoustics of Solid Propellant Combustion Instability", Bolt Beranek and Newman, Inc., August, 1963.
205. Gordon, C. G. and Smith, P. W., "Acoustic Losses in a Resonator with Steady Gas Flow", Bolt Beranek and Newman, Inc., Rpt. No. 1142, June 1964.
206. Hart, R. W. and Cantrell, R. H., "Acoustic Radiation from Pressure-Antisymmetric Modes of a Centrally Vented Cylindrical Cavity", J. Acous. Soc. Am. 35, 1963, p. 18.
207. Smith, P. W., "The Acoustics of T-Burners", Bolt Beranek and Newman, Inc., Report No. 1077, November, 1963.
208. Horton, M. D., "Use of the One-Dimensional T-Burner to Study Oscillatory Combustion", AIAA Journal 2, 1964, p. 1112.

209. Coates, R. L., Horton, M. D. and Ryan, N. W., "T-Burner Method of Determining the Acoustic Admittance of Burning Propellants", AIAA Journal 2, 1964, p. 1119.
210. Cantrell, R. H., "Acoustic Wall Loss Theory", 3rd Meeting of the Technical Panel on Solid Propellant Combustion Instability, JHU/APL TG 371-5 (1963), p. 21.
211. Westervelt, P. J., Quarterly Progress Report No. 7 on "The Acoustics of Solid Propellant Combustion Instability", Bolt Beranek and Newman, Inc., August, 1964.
212. Horton, M. D. and Price, E. W., "Dynamic Characteristics of Solid Propellant Combustion", 9th Symp. on Combustion (Academic Press, Inc., New York, 1963), p. 303.
213. Foner, S. N., Hudson, R. L., and Nall, B. H., "Acoustic Measurements of Solid Propellants by an Acoustic Oscillator Technique", AIAA Journal 2, 1964, p. 1123.
214. Ryan, N. W., Coates, R. L., and Baer, A. D., "Participation of the Solid Phase in the Oscillatory Burning of Solid Rocket Propellants", 9th Symp. on Combustion (Academic Press, Inc., New York, 1963), p. 311.
215. Horton, M. D., General Discussion in 9th Symp. on Combustion (Academic Press, Inc., New York, 1963), p. 333.
216. Strittmater, R., Watermeier, L., and Pfaff, S., "The Experiment at BRL on Acoustic Admittance Measurements of Burning Propellant Surface", 3rd Meeting of the Technical Panel on Solid Propellant Combustion Instability, JHU/APL TG 371-5, p. 29.
217. Leader, G. R., "Experiments for the Measurement of the Acoustic Impedance of a Burning Solid Propellant", Thiokol Chem. Corp. (Elkton) Report E104-63, June, 1963.
218. Mawardi, O. K., "Measurement of Acoustic Impedance", J. Acous. Soc. Am. 21, 1949, p. 84.
219. Blair, D. W., "Acoustic Admittance Measurements on Burning Propellants", 2nd Meeting of the Technical Panel on Solid Propellant Combustion Instability, APL/JHU TG 371-4B (1962), p. 21.
220. Blair, D. W., "Acoustic Wave-Burning Zone Interaction in Solid Propellants", Aerochem Research Laboratories TP-49, 1962.
221. Converse, A. O., "An Experimental Study of Solid Propellant Combustion Instability in a Standing Wave Tube", 4th Meeting of the Technical Panel on Solid Propellant Combustion Instability, JHU/APL TG 371-7 (1964), p. 25.
222. Diederichsen, J., "Stability Grading of Solid Propellants by the Oscillatory Strand Burner Test", 2nd Meeting of the Technical Panel on Solid Propellant Combustion Instability, JHU/APL TG 371-4B (1962), p. 40.

223. Diederichsen, J., "Further Development of 'Stability Grading of Solid Propellants by the Oscillatory Strand Burner Test'", 4th Meeting of the Technical Panel on Solid Propellant Combustion Instability, JHU/APL TG 371-7 (1964), p. 56.
224. Schmidt, D. J. and Wolfhard, H. G., "The Observation and Modulation of Infrared Radiation as a Possible Means of Investigating Rocket Engine Instability", 2nd Meeting of the Technical Panel on Solid Propellant Combustion Instability, JHU/APL TG 371-4B (1962), p. 105.
225. Engler, J. F., and Nachbar, W., "Experiments with a Solid Propellant Acoustic Oscillator", AIAA Journal 2, 1964, p. 1279.
226. Watermeier, L., "An Experimental Study of Combustion Instability in Solid Rocket Propellants - Part II", BRL Rpt. No. 1116, Sept., 1960.
227. Landsbaum, E. M., "The Effect of a Shock Wave on a Burning Solid Propellant", 2nd IAS Congress, 1960.
228. Agoston, G. A., "The Study of the Origin and Propagation of Disturbances in the Burning of Solid Propellants", Summary Rpt. AFOSR TN 60-336, 1960.
229. Muller, G. M., and Agoston, G. A., "Acoustic Admittance of Burning Solid Propellant Surface", 2nd Meeting of the Technical Panel on Solid Propellant Combustion Instability, JHU/APL TG 371-4B (1962), p. 27.
230. Muller, G. M., "Acoustic Admittance Measurements: Reflected-Pulse Method", 3rd Meeting of the Technical Panel on Solid Propellant Combustion Instability, JHU/APL TG 371-5 (1963), p. 47.
231. Muller, G. M., "The Study of the Origin and Propagation of Disturbances in the Burning of Solid Propellants - Phase I: The Measurement of Acoustic Admittance", Final Report, Stanford Research Institute, May 1964.
232. Lawhead, R. B. and Carlson, L. W., "Physical Processes of Solid Propellant Combustion", 3rd Meeting of the Technical Panel on Solid Propellant Combustion Instability, JHU/APL TG 371-5 (1963), p. 43.
233. Carlson, L. W. and Lawhead, R. B., "Basic Physical Processes of Solid Propellant Combustion", 4th Meeting of the Technical Panel on Solid Propellant Combustion Instability, JHU/APL TG 371-7 (1964), p. 30.
234. Beranek, L. L., "Acoustic Measurements", (John Wiley and Sons, Inc., New York, 1949), Chapt. 7.
235. Wente, E. C. and Bedell, E. H., "The Measurement of Acoustic Impedance and the Absorption Coefficient of Porous Materials", Bell System Tech. Journal 7, 1928, p.1.

236. Ingard, U. and Labate, S., "Acoustic Circulation Effects and the Non-linear Impedance of Orifices", J. Acous. Soc. Am. 22, 1950, p. 221.
237. London, A., "The Determination of Reverberant Sound Absorption Coefficients from Acoustic Impedance Measurements", J. Acous. Soc. Am. 22, 1950, p. 263.
238. Beranek, L. L., "Precision Measurement of Acoustic Impedance", J. Acous. Soc. Am. 12, 1940, p. 3.
239. Fay, R. and White, J., "Acoustic Impedance from Motional Impedance Diagrams", J. Acous. Soc. Am. 20, 1948, p. 98.
240. Hayes, W. D., "The Fundamentals of Gas Dynamics", High Speed Aerodynamics and Jet Propulsion (Princeton University Press, Princeton, 1958), Vol. III, Section D.
241. Landau, L. D. and Lifshitz, E. M., "Fluid Mechanics" (Addison-Wesley, Reading, Mass., 1959), Chapt. X.
242. Agosta, V. D., "Shock Wave-Burning Solid Propellant Interaction", 4th Meeting of the Technical Panel on Solid Propellant Combustion Instability, JHU/APL TG 371-7 (1964), p. 36.
243. Ringger, L. E. and Koss, G. S., "Automatic Thickness Control", Iron and Steel Eng., February 1960, p. 110.
244. Keinath, G., "The Measurement of Thickness", NBS Circular 585, Jan., 1958.
245. McMaster, R. C. and Wenk, S. A., "A Basic Guide for Management's Choice of Non-Destructive Test", ASTM Spec. Publ. No. 112, June, 1950, p. 3.
246. Constant, F. W., "Theoretical Physics-Mechanics", (Addison-Wesley, Cambridge, 1954).
247. Anonymous, "A Portable Ultrasonic Gage", Marine Eng./Log. 64, 1959, p. 102.
248. Evans, D. J., "Ultrasonic Measurement of Tank Ship Corrosion Losses", Corrosion 15, 1959, p. 21.
249. McMaster, R. C., ed., "Non-Destructive Testing Handbook" (Ronald Press, New York, 1959), p. 50-1.
250. Mason, W. P., "Physical Acoustics and the Properties of Solids", (D. van Nostrand Co., Princeton, 1958), Chapt. 8.
251. Anonymous, "Ultrasonics for Detection of Flaws", Rich-Roth Labs. MPR-PA 14-18, 1956.

252. Non-Destructive Testing Handbook, op. cit., p. 48-1.
253. Non-Destructive Testing Handbook, op. cit., p. 50-11.
254. Non-Destructive Testing Handbook, op. cit., p. 50-18.
255. Mason, W. P., op. cit., p. 397.
256. Evans, D. J., op. cit., p. 23.
257. Non-Destructive Testing Handbook, op. cit., p. 50-32.
258. Tenney, G. H., "Survey of Radiation Techniques", Symposium on Non-destructive Tests in the Field of Nuclear Energy, ASTM 223, April, 1957, p. 44.
259. Waesche, R. H. W., Report to M. Summerfield on "Thickness Measurement", April, 1961.
260. Letter, Dec. 29, 1960; Phone Call to Dr. N. E. Walters.
261. Letter, Dec. 17, 1960; Phone Call to Mr. J. C. Clement.
262. Letter, Jan. 6, 1961; Phone Call to Mr. M.J. Seavy.
263. von Elbe, G. and Lewis, B., "Stability and Structure of Bunsen Flames", J. Chem. Phys. 11, 1943, p. 75.
264. Anderson, J. W. and Fein, R. S., "Measurements of Normal Burning Velocities and Flame Temperatures of Bunsen Flames", J. Chem. Phys. 17, 1949, p. 1268.
265. Fristrom, R. M., Avery, W. H., Prescott, R., and Mattuck, A., "Flame Zone Studies by the Particle Track Technique. I. Apparatus and Technique", J. Chem. Phys. 22, 1954, p. 106.
266. Bourot, J. M., "Chronophotographie des Champs Aerodynamiques", Scientific and Technical Publications of Air Ministry of France, No. 226, 1949.
267. Lambiris, S. and Combs, L. P., "Steady-State Combustion Measurements in a LOX/RP-1 Rocket Chamber and Related Spray Burning Analysis", IAS-ARS Preprint No. 61-132-1826, June, 1961.
268. "Flash Technique", Eastman Kodak Co. Pamphlet C-2, 1956.
269. Lamb, H., "Hydrodynamics" (Dover Press, New York, 1945).
270. Mahaffey, D. A., "Experimental Determination of Combustion Temperatures of Ammonium Perchlorate Rocket Propellants", M.S.E. Thesis, Princeton University, 1955.
271. Hughes, R. R. and Gilliland, E. R., "The Mechanics of Drops", Chem. Eng. Progress 48, 1952, p. 497.

272. Gilbert, M., Davis, L., and Altman, D., "Velocity Lag of Particles in Linearly Accelerated Combustion Gases", *Jet Propulsion* 25, 1955, p. 26.
273. Hueter, T. F. and Bolt, R. H., "Sorics" (John Wiley and Sons, New York, 1955), p. 12.
274. "Kodak Plates and Films for Science and Industry", Eastman Kodak Co. Pamphlet No. P-9, 1962.
275. Wood, W. A., "Metal Combustion in Deflagrating Propellants", *Progress in Astronautics and Rocketry: Solid Propellant Rocket Research* (Adademic Press, Inc., New York, 1960), pp. 287-291.
276. Bredfeldt, H. R., "Evaluation of a Light Scattering Technique for Determining the Spray Characteristics of Impinging Liquid Jets", M.S.E. Thesis, Princeton University, 1964.
277. Brown, E. B., "Optical Instruments", (Chemical Publishing Co., Brooklyn, 1945), pp. 496-499.
278. Hawkesley, P. G. W., "Survey of the Relative Motions of Particles and Fluids", Suppl. No. 3, *Brit. J. Appl. Phys.*, 1954, p. S1.
279. Wood, W. A., Private Communication, Dec. 1963 (available in Rohm & Haas internal memoranda).
280. Miller, K. S., "Partial Differential Equations in Engineering Problems", (Prentice-Hall, New York, 1953).
281. Bastress, E. K., Hall, K. P. and Summerfield, M., "Research on Burning Rate Control Factors in Solid Propellants", Princeton University Dept. of Aeronautical Engineering Report No. 446a, April, 1959, p. 9.
282. Summerfield, M., "Control of Solid Propellant Burning Rate by Acoustic Energy", *ARS Journal* 29, 1959, p. 791.
283. Crawford, A. A., "Ultrasonic Engineering" (Butterworths, London, 1955), p. 113.
284. Hueter, T. F. and Bolt, R. H., op. cit., p. 52.
285. Lupfer, M., Gulton Industries, Private Communication, August 22, 1960.
286. Lancaster, R. W., "Experimental Investigation of the Ignition Process of Solid Propellants in a Practical Motor Configuration", M.S.E. Thesis, Princeton University, 1961.
287. Hermoni, A. and Salmon, A., "The Catalytic Decomposition of Ammonium Perchlorate", 8th Symp. on Combustion (Williams & Wilkins, Baltimore, 1962, pp. 656-662.
288. Taback, H. J., "The Effects of Several Composition Factors on the Burning Rate of an Ammonium Perchlorate Solid Propellant", M.S.E. Thesis, Princeton University, 1958.

289. Hall, K. P., Wenograd, J., Cole, R. B. and Summerfield, M., "Burning Rate Control Factors in Solid Propellants", Princeton University Dept. of Aeronautical Engineering Report No. 446m, July, 1962.
290. Dyne, P. J., and Penner, S. S., "Optical Methods for the Determination of Combustion Temperatures", Journal of the American Rocket Society 23, 1953, p. 165.
291. Gaydon, A. G., and Wolfhard, H. G., op. cit., pp. 234-282.
292. Strong, H. M., Bundy, F. P. and Larson, D. A., Temperature Measurements on Complex Flames by Sodium Line Reversal and Sodium D Line Intensity Contour Studies", 3rd Symp. on Combustion (Williams & Wilkins, Baltimore, 1949) p. 641.
293. Penner, S. S., "Quantitative Molecular Spectroscopy and Gas Emissivities", (Addison-Wesley, Reading, Mass., 1959), p. 24.
294. Minkowski, R., Muller, H. G. and Weber-Schafer, M., "Transition Probability for the D-Lines of Sodium from Absolute Intensity Measurements, Dissociation of Sodium Salts, and Half-Width of the D-Lines in the Air-Coal Gas Flame", Zeits. fur Phys. 94, 1935, p. 145.
295. James, C. G. and Sugden, T. M., "Photometric Investigations of Alkali Metals in Hydrogen Flame Gases. I. A General Survey of the Use of Resonance Radiation in the Measurement of Atomic Concentrations", Proc. Roy. Soc. 227, 1955, p. 312.
296. Unsold, A., "Physik der Sternatmospheren" (Springer-Verlag, Berlin, 1955), p. 292.
297. Margenau, H. and Lewis, M., "Structure of Spectral Lines from Plasmas", Rev. Mod. Phys. 31, 1959, p. 574.
298. Penner, S. S. and Kavanagh, R. W., "Radiation from Isolated Spectral Lines with Combined Doppler and Lorentz Broadening", J. Opt. Soc. Am. 43, 1953, p. 385.
299. von Roos, O., "General Theory of Collision Broadening of Spectral Lines", Proc. of 5th Intern. Conf. Ionization Phenomena in Gases, Munich, 1961, p. 913.
300. Cole, R. B., Wenograd, J. and Summerfield, M., "Solid Propellant Combustion Mechanism Studies", Princeton University Dept. of Aeronautical Engineering Report No. 446n, January 1963.
301. Wood, W. A., Private Communication, June, 1964.
302. Most, W. J., BSE Thesis, Princeton University, to be published.

303. Kosdon, F. J., "The Measurement of the Temperature of Solid Propellant Surfaces During Ignition Transients by Infrared Radiometry", M.S.E. Thesis, Princeton University Dept. of Aerospace and Mechanical Sciences, June, 1965.
304. Anderson, R. and Brown, R. S., "Structure of the Combustion Zone in Composite Propellant Burning", 1st ICRPG Combustion Instability Conference, Orlando, Fla., November 1964.
305. Pearse, R. W. B. and Gaydon, A. G., "The Identification of Molecular Spectra" (Chapman and Hall, London, 1963).
306. Most, W. J., Private Communication, August, 1964.
307. Gaydon, A. G., "The Spectroscopy of Flames", (John Wiley & Sons, New York, 1957), p. 123.
308. Povinelli, L. A., "Study of Composite Solid-Propellant Flame Structure Using a Spectral Radiation Shadowgraph Technique", NASA TM X-52071, 1964.
309. Selzer, H., Private Communication to R. H. W. Waesche, December 1964.
310. Watermeier, L. A., Aungst, W. P. and Pfaff, S. P., "An Experimental Study of the Aluminum Additive Role in Unstable Combustion of Solid Rocket Propellants", 9th Symp. on Combustion (Academic Press, New York, 1963), pp. 316-326.
311. Penzias, G. J., Discussion in 9th Symp. on Combustion (Academic Press, New York, 1963), p. 327.

REFERENCES

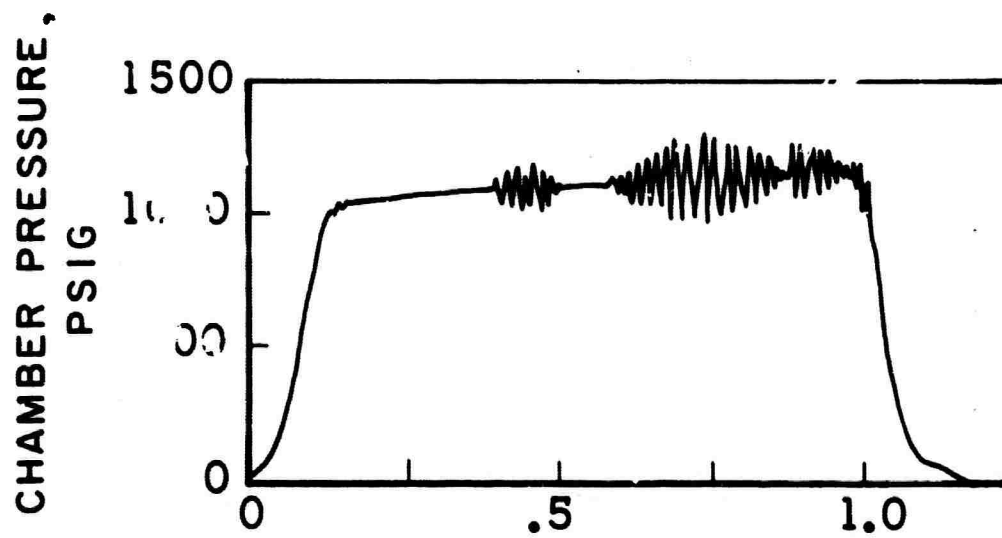
- A-1 Morse, P. M., "Vibration and Sound", 2nd ed. (McGraw-Hill, New York 1948), Chapt. VI.
- B-1 Rayleigh, J. W. S., "The Theory of Sound", Vol. II, (Dover Publications, New York City, 1945).
- B-2 Morse, P. M., "Vibration and Sound", 2nd Edition (McGraw-Hill, New York City, 1948).
- B-3 Constant, F. W., "Theoretical Physics-Mechanics", (Addison-Wesley, Cambridge, 1954).
- B-4 Ross, C. C. and Datner, P. P., "Combustion Instability in Liquid Propellant Rocket Motors", Selected Combustion Problems I (Butterworths Scientific Publications, London, 1954), p. 352.
- B-5 Elias, I. and Gordon, R., "Longitudinal Vibrations of Gas at Ambient Pressure in a Rocket Thrust Chamber", Journal of the American Rocket Society 22, 1952, p. 263.
- B-6 Hart, R. W. and McClure, F. T., "Theory of Acoustic Instability in Solid-Propellant Rocket Combustion", 10th Symp. on Combustion (The Combustion Institute, Pittsburgh, 1965), p. 1047.
- B-7 Green, L., "Some Effects of Charge Configuration in Solid Propellant Combustion", Jet Propulsion 28, 1958, p. 483.
- B-8 Waesche, R. H. W., Rohm & Haas Co. Ballistics Section Report No. 69, January, 1958.
- B-9 Crump, J. E. and Price, E. W., "Catastrophic Changes in Burning Rate of Solid Propellants During Combustion Instability", ARS Journal 30, 1960, p. 705.
- R-10 Angelus, T. A., "Unstable Burning Phenomenon in Double-Base Propellants", Progress in Astronautics and Rocketry: Solid Propellant Rocket Research (Academic Press, Inc., New York, 1960), Vol. 1, pp. 527-561.
- B-11 Brownlee, W. S. and Marble, F. E., "An Experimental Investigation of Unstable Combustion in Solid Propellant Rocket Motors", Progress in Astronautics and Rocketry: Solid Propellant Rocket Research (Academic Press, Inc., New York, 1960), Vol. 1, pp. 455-494.
- C-1 Clark, G. L., "Applied X-Rays" (McGraw-Hill, New York, 1955), p. 161.
- C-2 Non-Destructive Testing Handbook, op. cit., p. 18-17.
- C-3 Zumwalt, L. R., "The Best Performance from Beta Gages", Nucleonics 12, 1954, p. 55.

- C-4 Non-Destructive Testing Handbook, op. cit., p. 19-46.
- C-5 Non-Destructive Testing Handbook, op. cit., p. 18-32, et seq.
- C-6 Non-Destructive Testing Handbook, op. cit., p. 13-23.
- C-7 Non-Destructive Testing Handbook, op. cit., p. 18-2.
- C-8 Glasstone, S., "Principles of Nuclear Reactor Engineering" (D. van Nostrand, Princeton, 1955), p. 307.
- C-9 Riedel, O., "Statistical Purity in Nuclear Counting", Nucleonics 12, 1954, p. 64.
- C-10 Taffey, A. H., "Statistical Tests for Accuracy of Counting", Nucleonics 10, 1960, p. 180.
- C-11 Hoel, P. G., "Introduction to Mathematical Statistics", (J. Wiley & Sons, New York, 1954), p. 223.
- C-12 Glasstone, S., op. cit., p. 306.
- C-13 Bastress, E. K., "Modification of the Burning Rates of Ammonium Perchlorate Solid Propellants by Particle Size Control", Ph.D. Thesis, Princeton University Department of Aeronautical Engineering, January, 1961.
- C-14 Hoel, P. G., op. cit., p. 103.
- C-15 Non-Destructive Testing Handbook, op. cit., p. 18-1.
- C-16 "Chart of the Nuclides", Knolls Atomic Power Laboratory, 1957.
- C-17 Hansen, C. W., Tracerlab, Private Communication, March, 1961.
- C-18 Compton, A. H. and Allison, S. K., "X-Rays in Theory and Experiment" (D. van Nostrand, New York, 1949), p. 90, 106.
- C-19 Jacobs, J. E., "The Electrical Conductivity of Cadmium Sulphide When Exposed to Pulsation X-Radiation", Elec. Eng. 70, 1951, p. 667.
- C-20 Jacobs, J. E., "The Use of Semi-Conductors as Detectors of X-Radiation", Proc. Nat. Elec. Conf. 7, p. 331.
- C-21 Perrish, W. and Kohler, T. R., "Use of Counter Tubes in X-Ray Analysis", Rev. Sci. Inst. 27, 1956, p. 795.
- C-22 Waesche, R. H. W., Report to M. Summerfield on "Thickness Measurement", April, 1961.
- C-23 Morton, G. A., "The Scintillation Counter", Advances in Electronics (Academic Press, Inc., New York, 1953), Vol. IV. p. 69.

- C-24 Staub, H., "Detection Methods", Experimental Nuclear Physics (J. Wiley and Sons, New York, 1953), Vol. I, p. 50.
- C-25 Gillespie, A. B., "Signal, Noise and Resolution in Nuclear Counter Amplifiers" (Pergamon Press, New York, 1953), p. 123.
- C-26 Ball, W. P., Booth, R. and MacGregor, M., "Temperature Coefficients of Scintillating Systems", Nuclear Instrum. 1, 1957, p. 71.
- C-27 Caldwell, R. L. and Turner, S. E., "Gain Variation of Photomultiplier Tubes", Nucleonics 12, 1954, p. 47.
- C-28 Cathey, L., "Fatigue in Photomultipliers", Proceedings of the 6th Scintillation Counter Symposium, Trans. IRE NS-5, 1958, p. 109.
- C-29 Kinard, F. E., "Temperature Dependences of Photomultiplier Gain", Nucleonics 15, 1957, p. 92.
- C-30 Howell, J. T., "High Speed Inspection of Canned and Packaged Products Using Solid X-Ray Detectors", Proc. Natl. Elec. Conf. 7, p. 337.
- D-1 Brinkley, S. R., "Combustion Processes", High Speed Aerodynamics and Jet Propulsion (Princeton University Press, Princeton, 1956), Vol. II, Section C.
- D-2 Zeleznik, F. J. and Gordon, S., "A General IBM 704 or 7090 Computer Program for Computation of Chemical Equilibrium Compositions, Rocket Performance and Chapman-Jouget Detonations", NASA TN D-1454, October 1962.
- D-3 Scarborough, J. B., "Numerical Mathematical Analysis" (Johns Hopkins University Press, 1930), p. 178.
- D-4 Gordon, S., Zeleznik, F. J. and Huff, V. N., "A General Method for Automatic Computation of Equilibrium Compositions and Theoretical Rocket Performance of Propellants", NASA TN D-132, 1959.
- F-1 Bundy, F. P., and Strong, H. M., "The Theoretical Shapes and Intensities of Sodium Lines from Flames of Complex Structures", General Electric Report No. 55275, September 1948.
- F-2 Bundy, F. P. and Strong, H. M., "Physical Measurements in Gas Dynamics and Combustion", High Speed Aerodynamics and Jet Propulsion (Princeton University Press, Princeton, 1954), Vol. IX. Section I.
- F-3 Penner, S. S., op. cit., Chap. 3.
- F-4 Margenau, H., and Watson, W. W., "Pressure Effects of Foreign Gases on the Sodium D-Lines", Phys. Rev. 44, 1933, p. 92.
- F-5 Hinnov, E., "A Method of Determining Optical Cross Sections", J. Opt. Soc. Am. 47, 1957, p. 151.

- F-6 James, C. G. and Sugden, T. M., "Photometric Investigations of Alkali Metals in Hydrogen Flame Cases I. A General Survey of the Use of Resonance Radiation in the Measurement of Atomic Concentrations", Proc. Roy. Soc. 227, 1955, p. 312.

OSCILLATORY BURNING



UNSTABLE BURNING

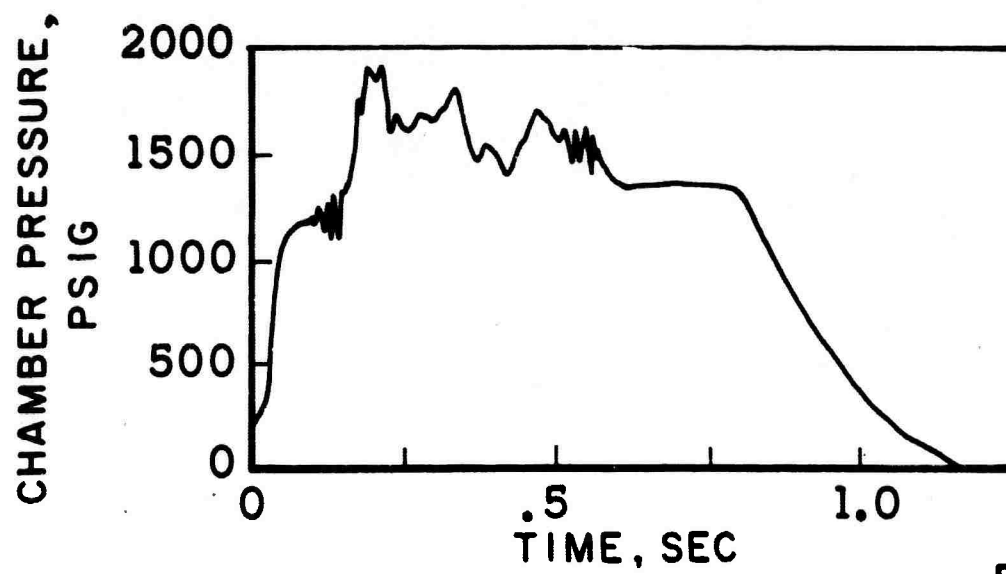


FIGURE 1

PRESSURE-TIME CURVES FOR TUBULAR
JPN BALLISTITE GRAIN
(WIMPRESS, REF. 3)

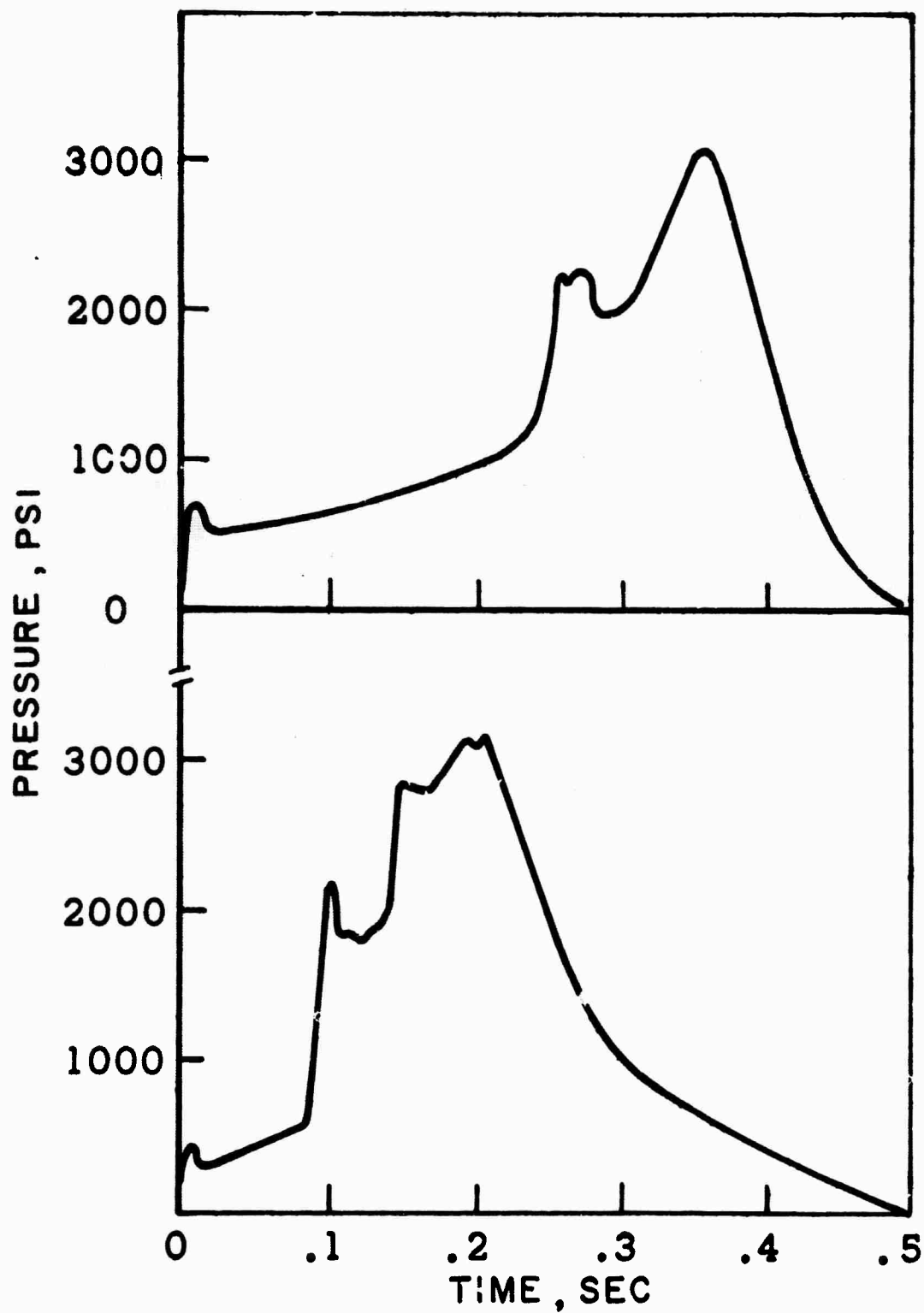


FIGURE 2

PRESSURE CHANGE
DUE TO OSCILLATORY BURNING
(PRICE, REF. 20)

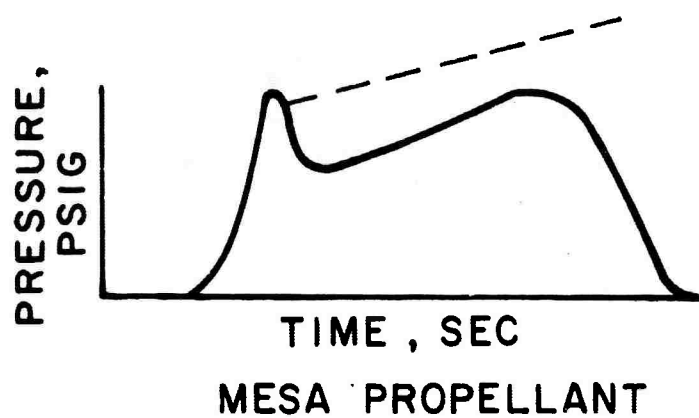
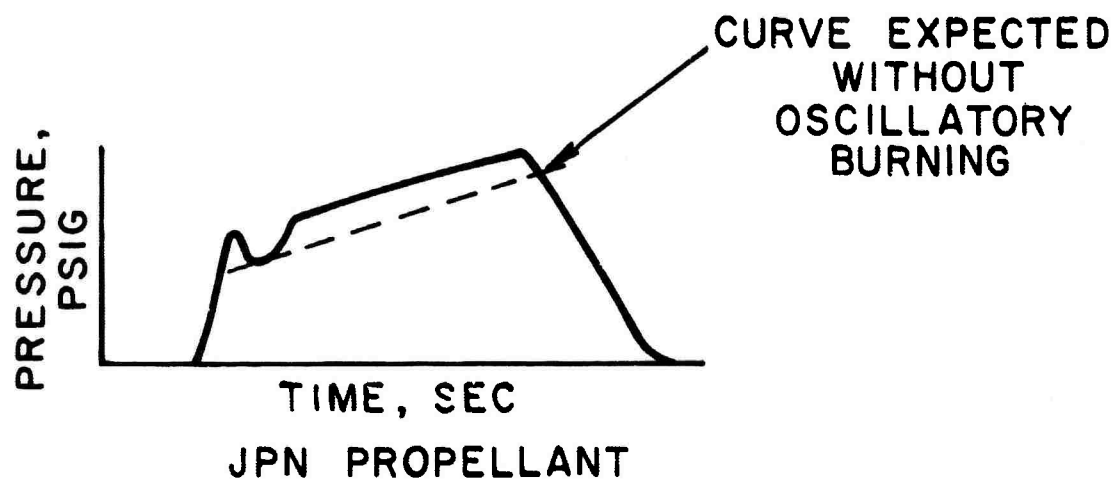


FIGURE 3

APPARATUS USED BY PRICE
TO OBTAIN THE EFFECT OF OSCILLATORY BURNING ON
PROPELLANT BURNING RATE

(REF. 33)

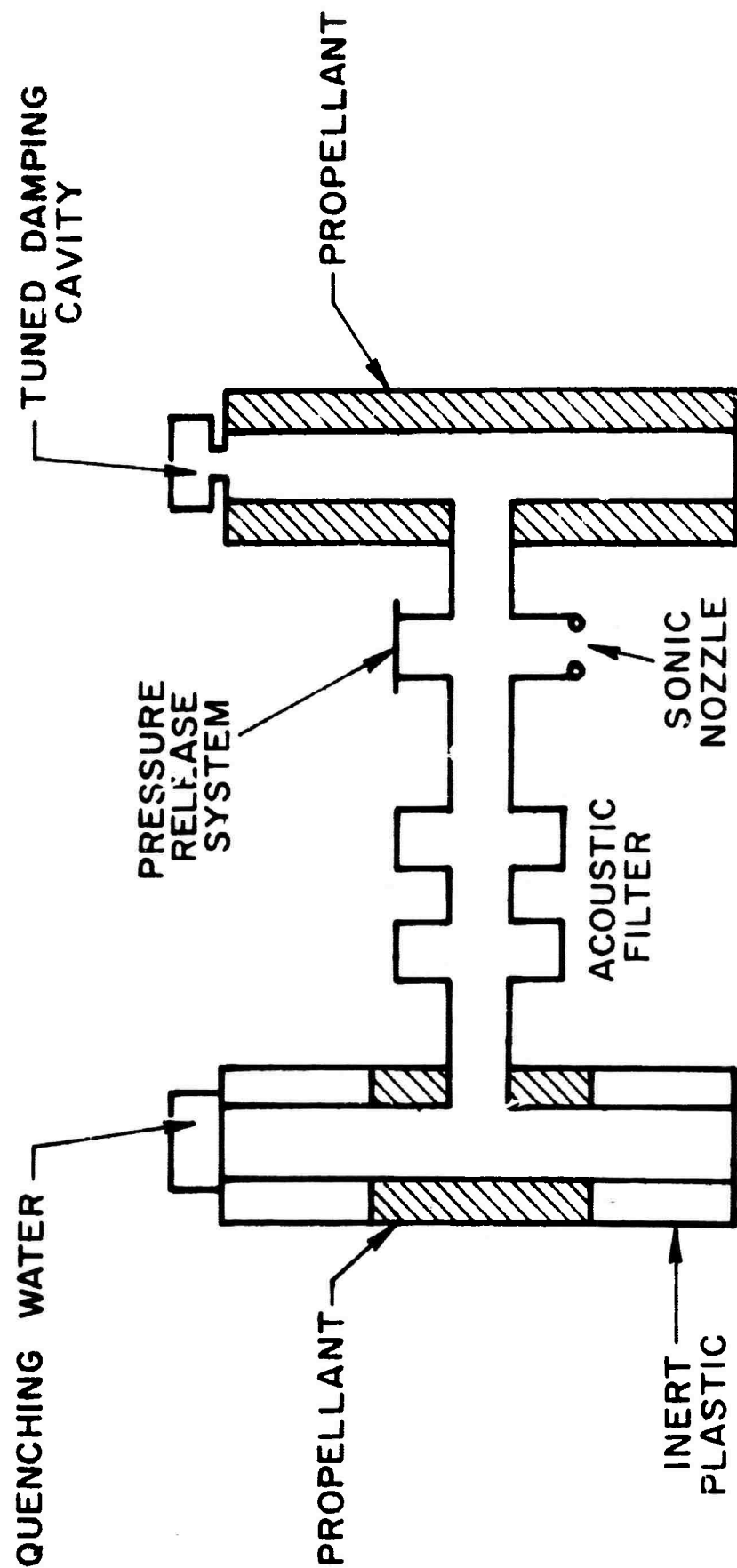


FIGURE 4

CHANGE IN BURNING RATE AS A FUNCTION OF ACOUSTIC
ENVIRONMENT FOR COMBUSTION OSCILLATIONS AT 4200 cps
FOR FOUR DOUBLE-BASE PROPELLANTS

(PRICE, REF. 33)

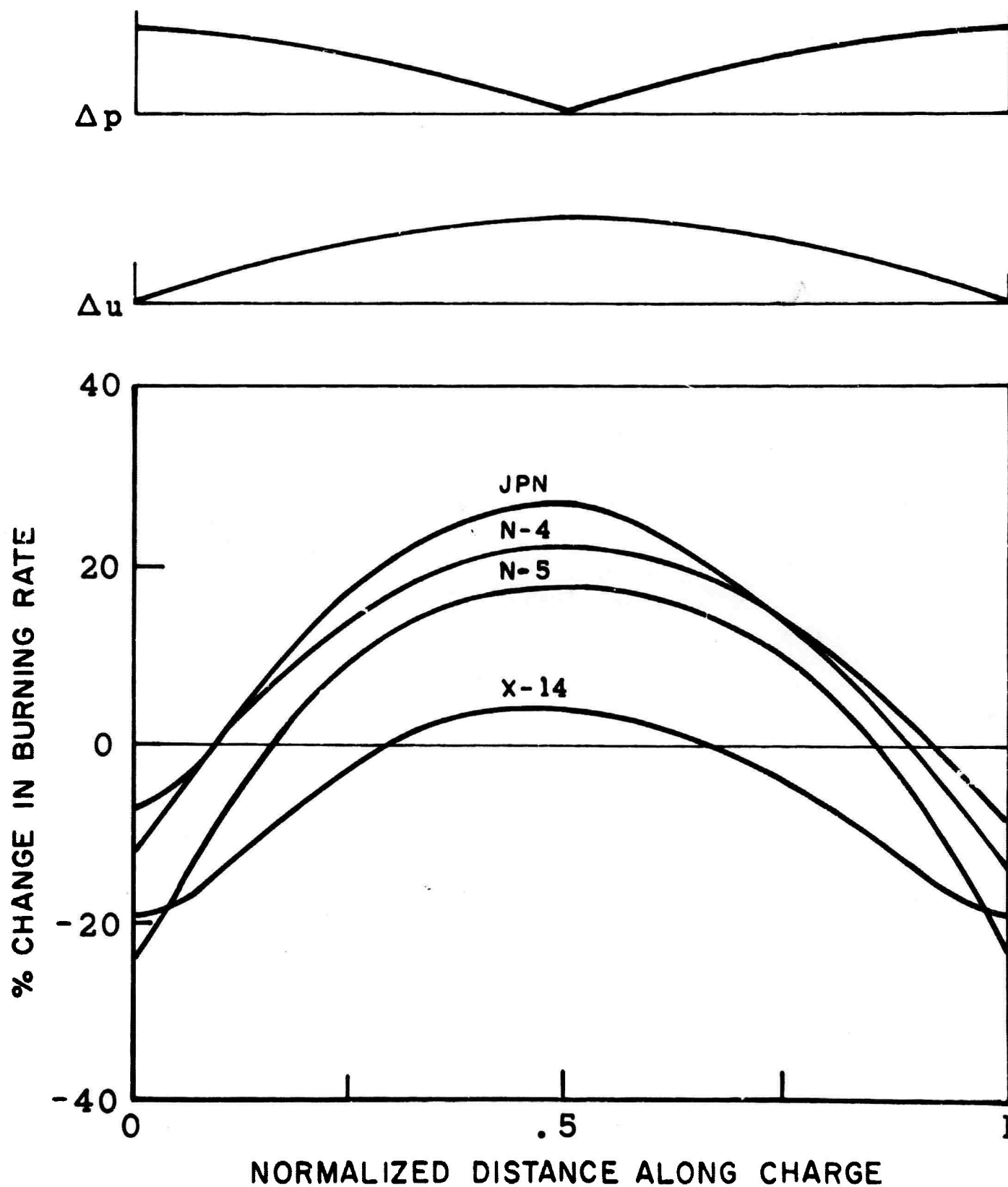


FIGURE 5

CHANGE IN BURNING RATE AS A FUNCTION OF ACOUSTIC
ENVIRONMENT FOR COMBUSTION OSCILLATIONS AT 4200 cps
AP-PBAA COMPOSITE PROPELLANT

(PRICE, REF. 35)

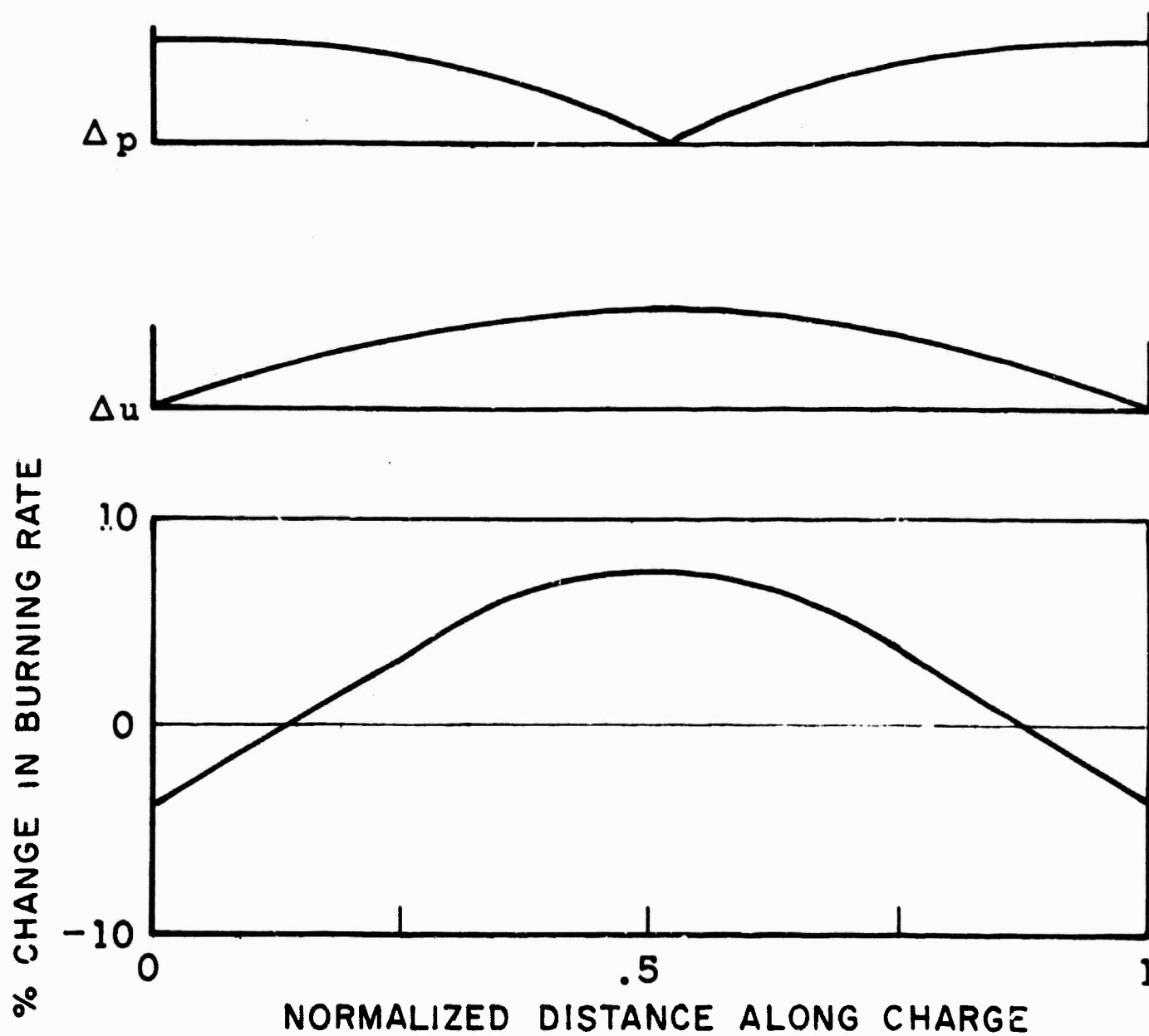


FIGURE 6

RATIO OF BURNING RATE UNDER OSCILLATORY CONDITIONS
TO THE STEADY-STATE BURNING RATE AS A FUNCTION
OF FREQUENCY

(NADAUD REF. 36)

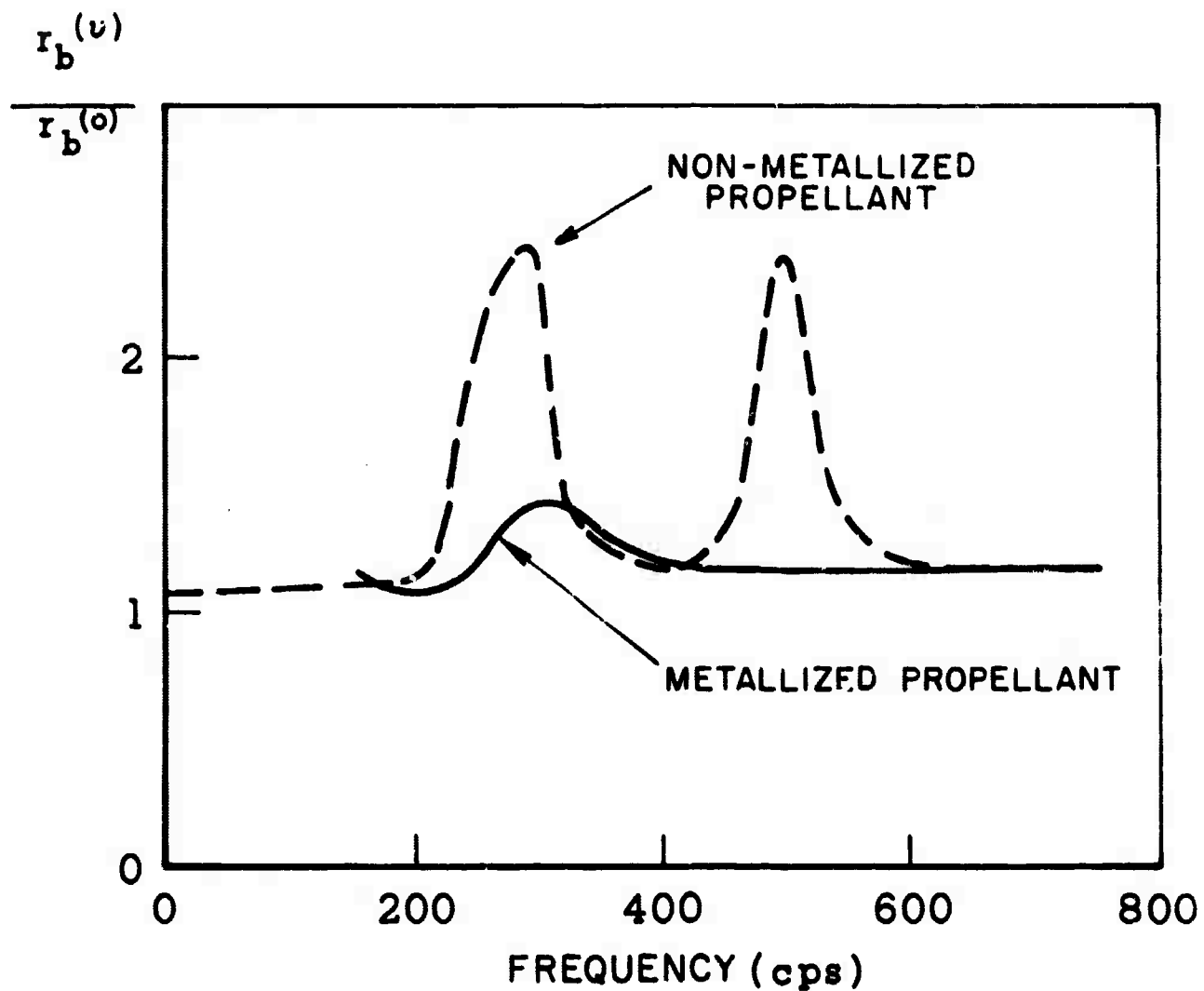


FIGURE 7

APPARATUS USED BY WATERMEIER TO DETERMINE EFFECT OF OSCILLATIONS ON BURNING RATE

(REF. 39)

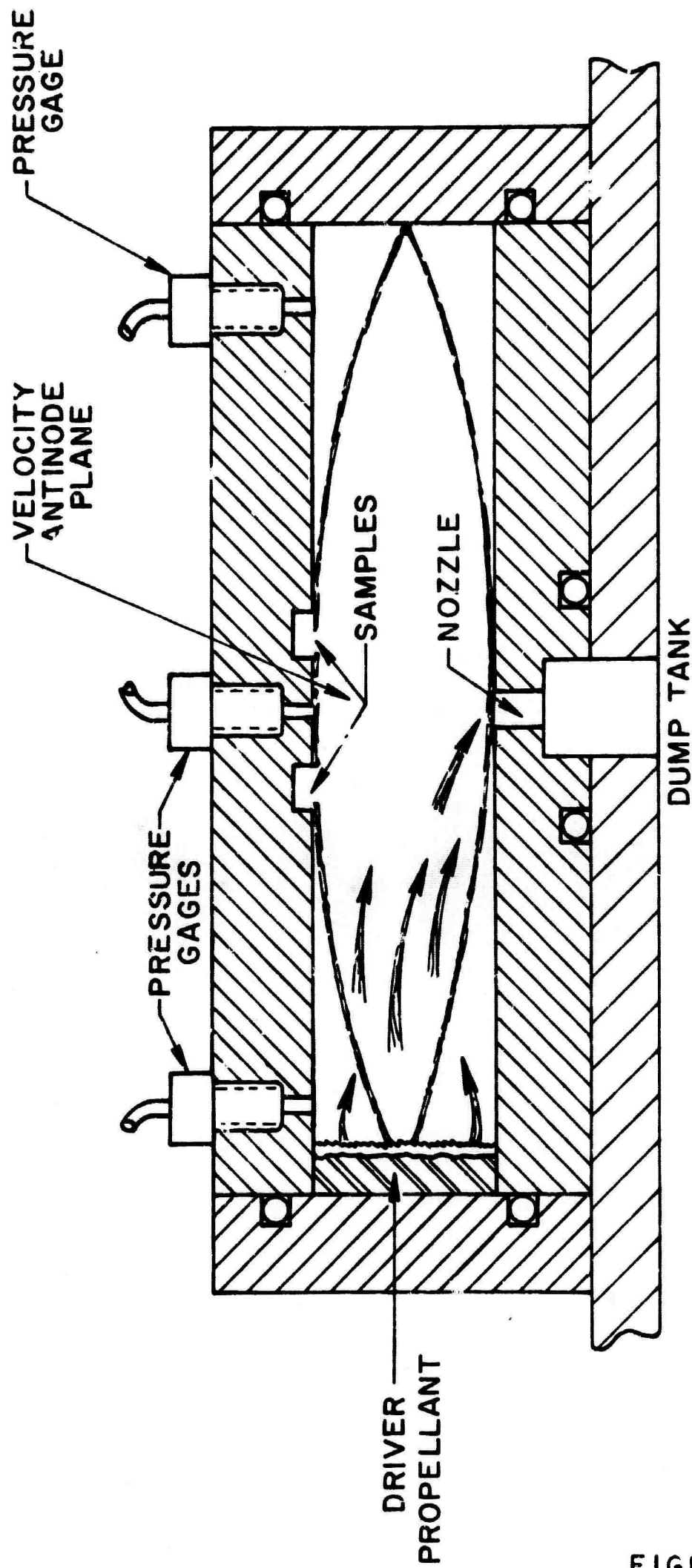


FIGURE 8

STAR GRAIN GEOMETRY WITH ROTATING TANGENTIAL MODE
(WAESCHE, REF. 34)

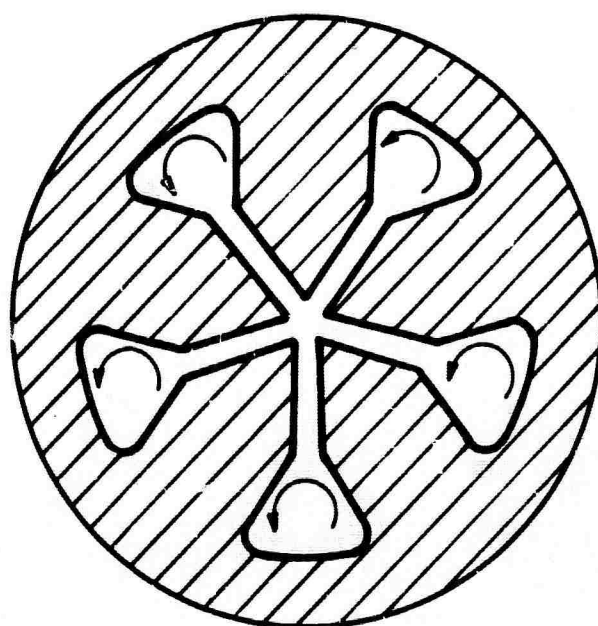


FIGURE 9

ACOUSTIC SOURCES AND SINKS IN A SOLID PROPELLANT ROCKET MOTOR

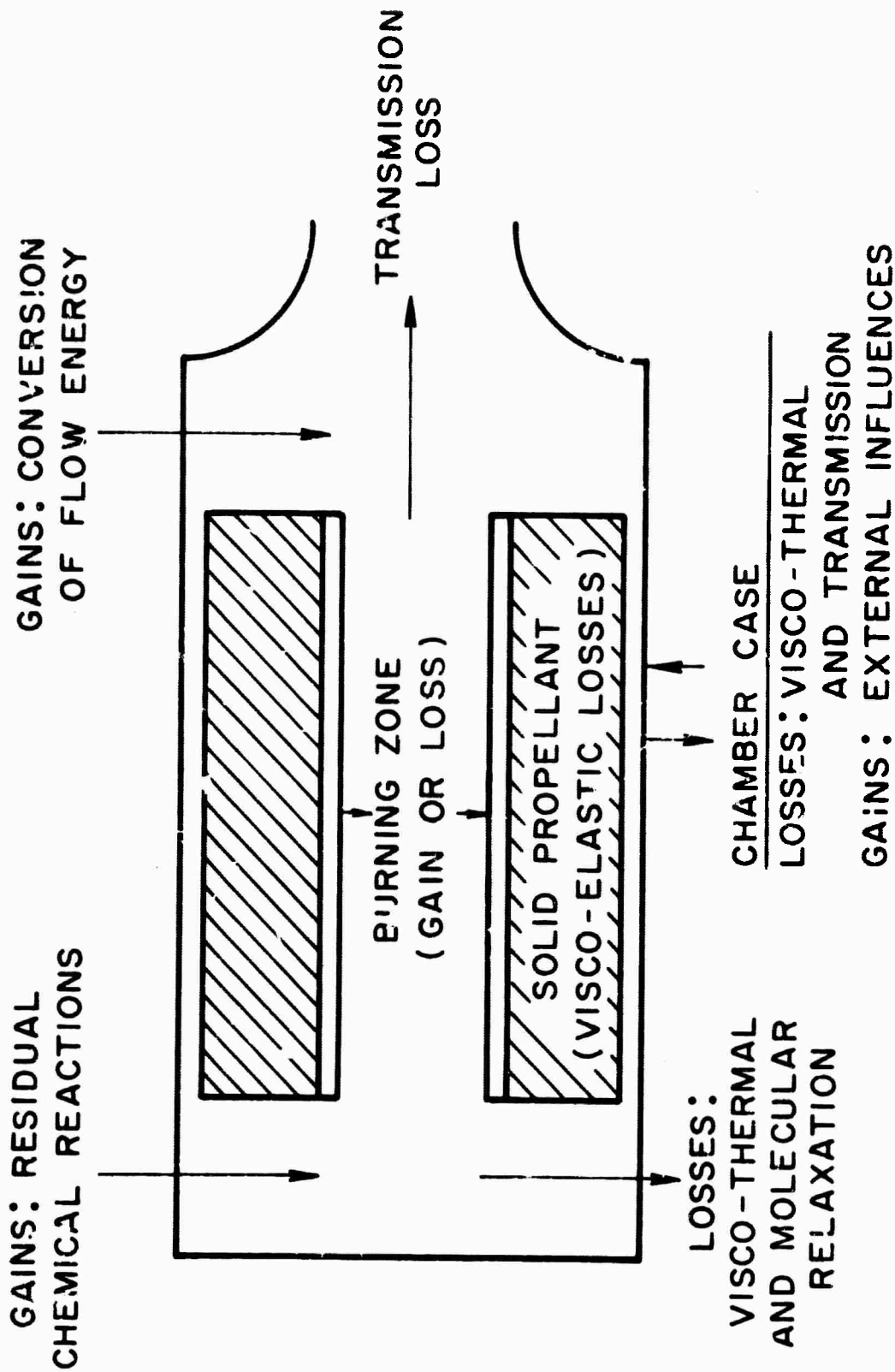


FIGURE 10

HISTORY OF PRESSURE PULSE FOR CONDITIONS OF AMPLIFICATION

(PRICE, REF.13)

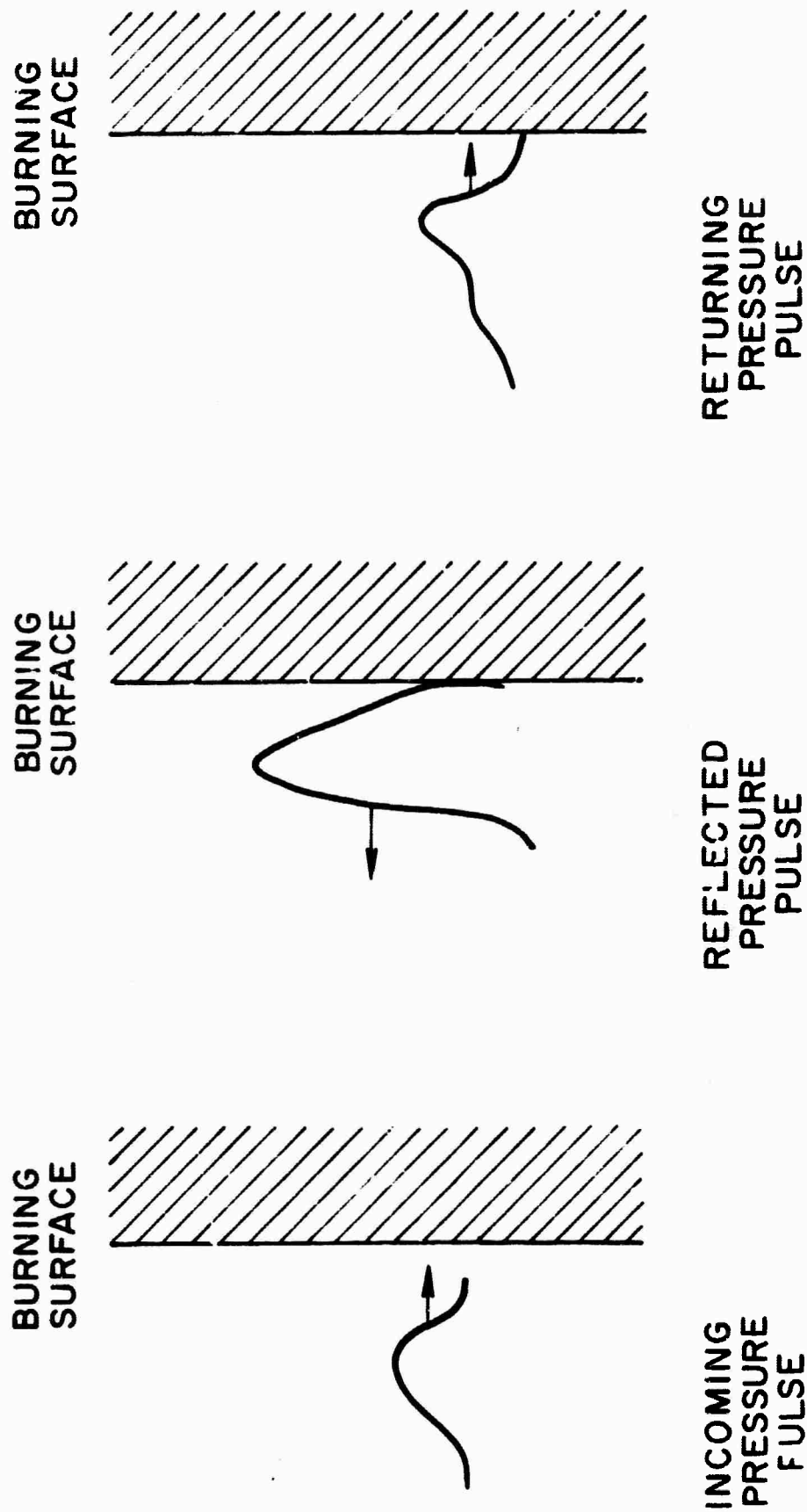
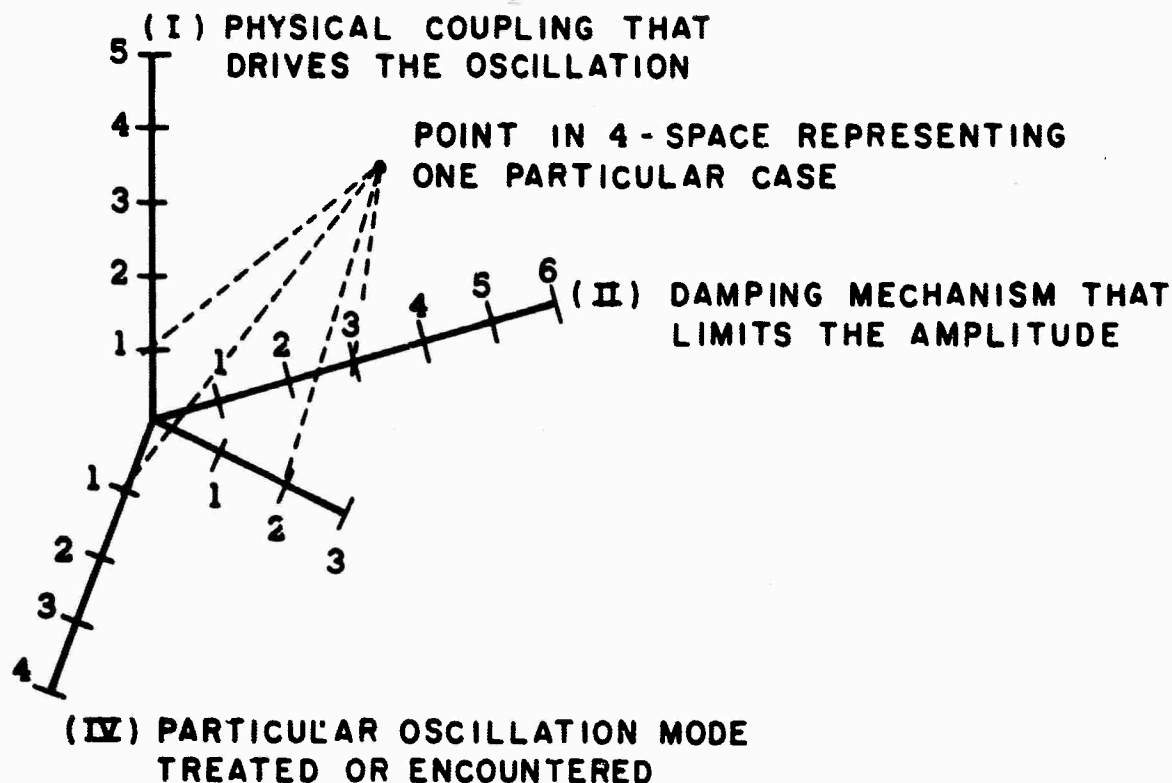


FIGURE 11

MORPHOLOGICAL LATTICE SPACE OF COMBUSTION OSCILLATIONS



COMPONENTS OF AXES

(I)	(II)	(III)	(IV)
1 - PRESSURE - SURFACE FLAME	1 - NOZZLE LOSSES	1 - LINEAR DISTURBANCES (SMALL AMPLITUDES)	1 - AXIAL
2 - VELOCITY - SURFACE FLAME	2 - SOLID PROPELLANT VISCOELASTIC LOSSES	2 - NON - LINEAR DISTURBANCES (LARGE AMPLITUDES)	2 - STANDING TRANSVERSE
3 - RADIATION - SURFACE FLAME	3 - VISCOUS DISSIPATION BY INERT COMPONENTS		3 - SPINNING TANGENTIAL
4 - STRESS COUPLING	4 - HEAT LOSSES TO INERT COMPONENTS		4 - CAPACITIVE
5 - PRESSURE - DISTRIBUTED FLAME	5 - RELAXATION LOSSES TO GASES		
	6 - VISCOUS DISSIPATION BY CONDENSED PARTICLES IN THE GAS		

FIGURE 12

MODEL USED BY GREEN

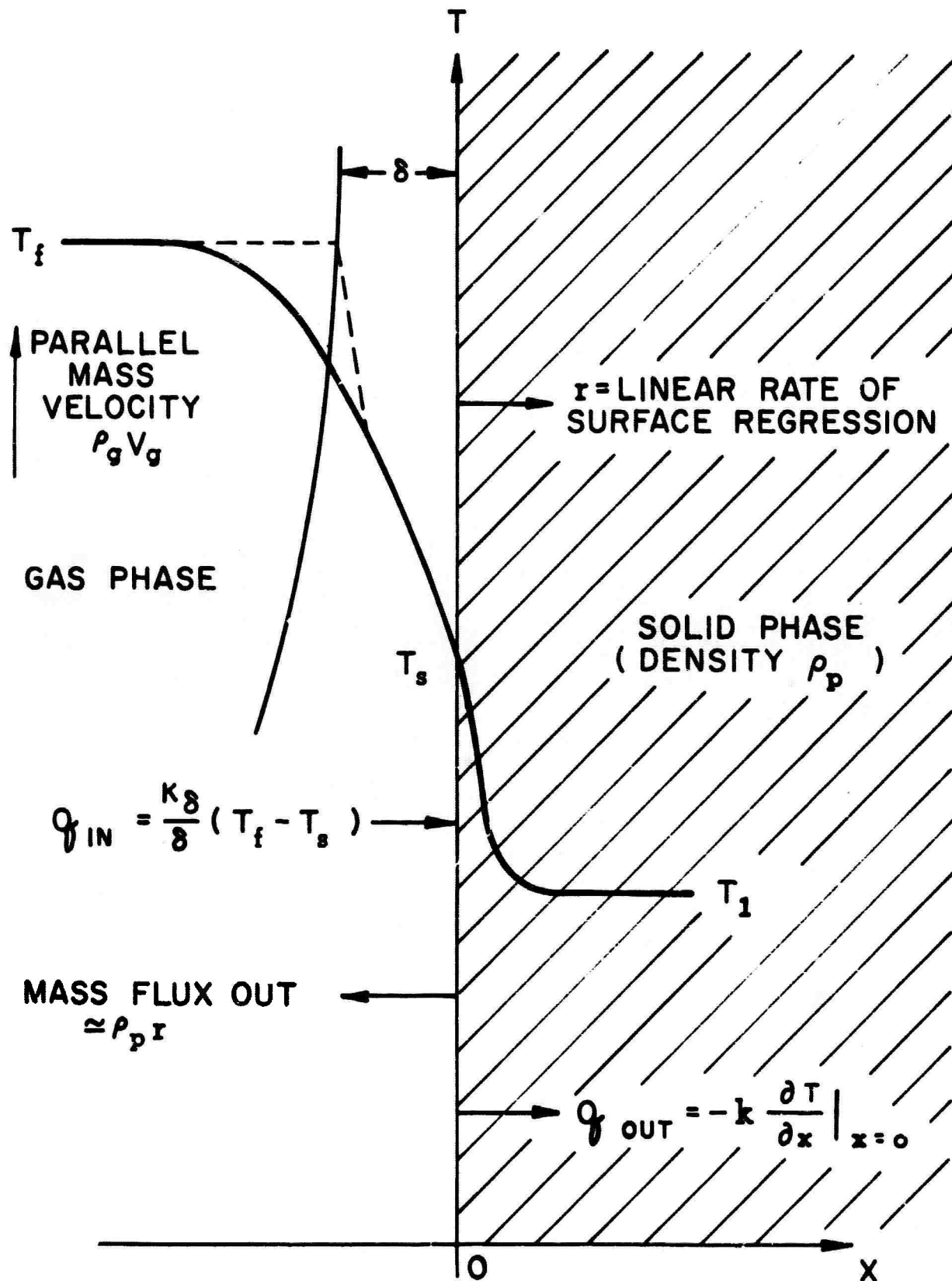


FIGURE 13

RESULTS OF GREEN THEORY FOR RESONANCE
AND NEAR-RESONANCE CONDITIONS

(REF. 94)

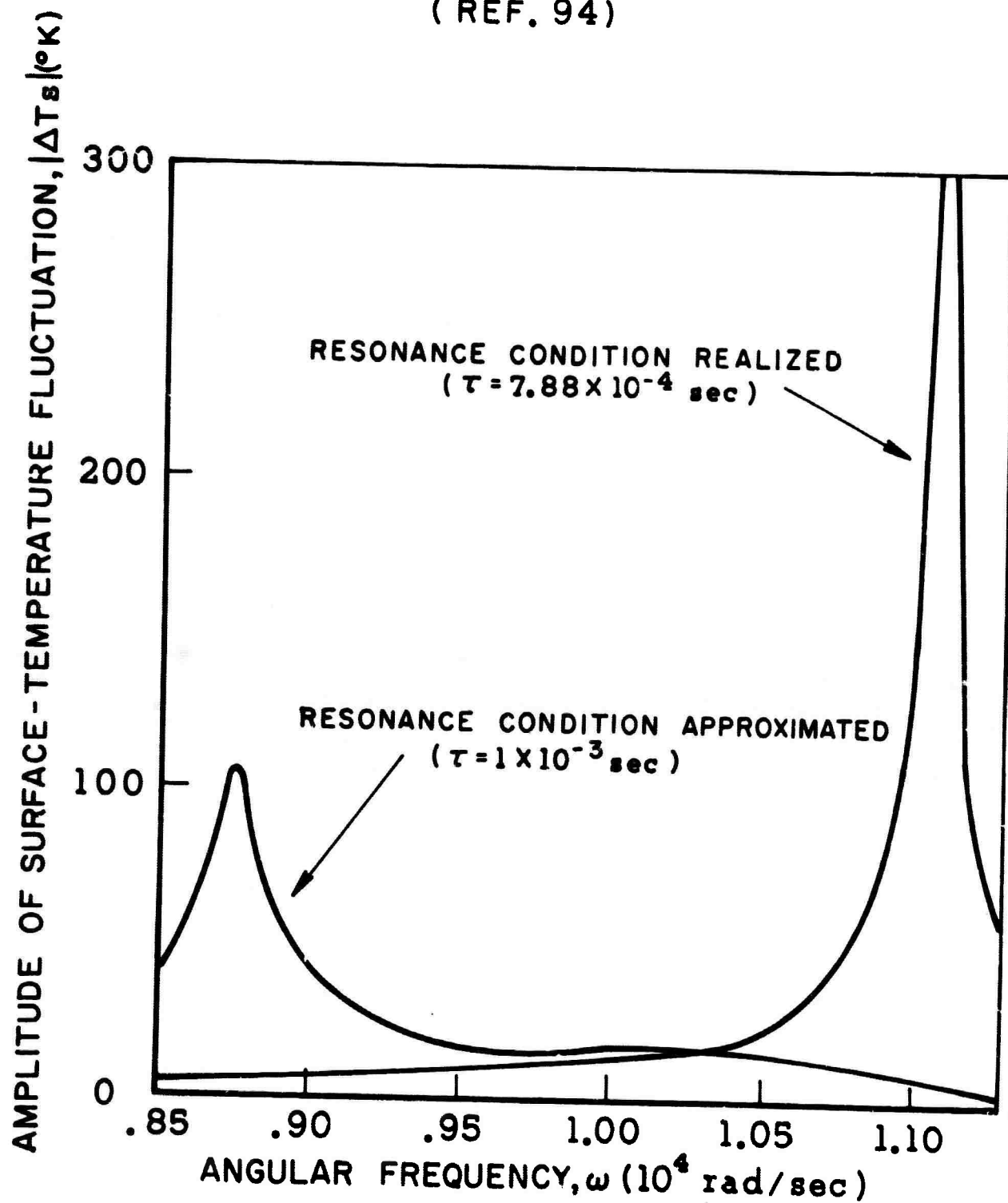


FIGURE 14

DEPENDENCE OF SEVERITY OF IRREGULAR BURNING ON PRESSURE
(LANDSBAUM, REF.107)

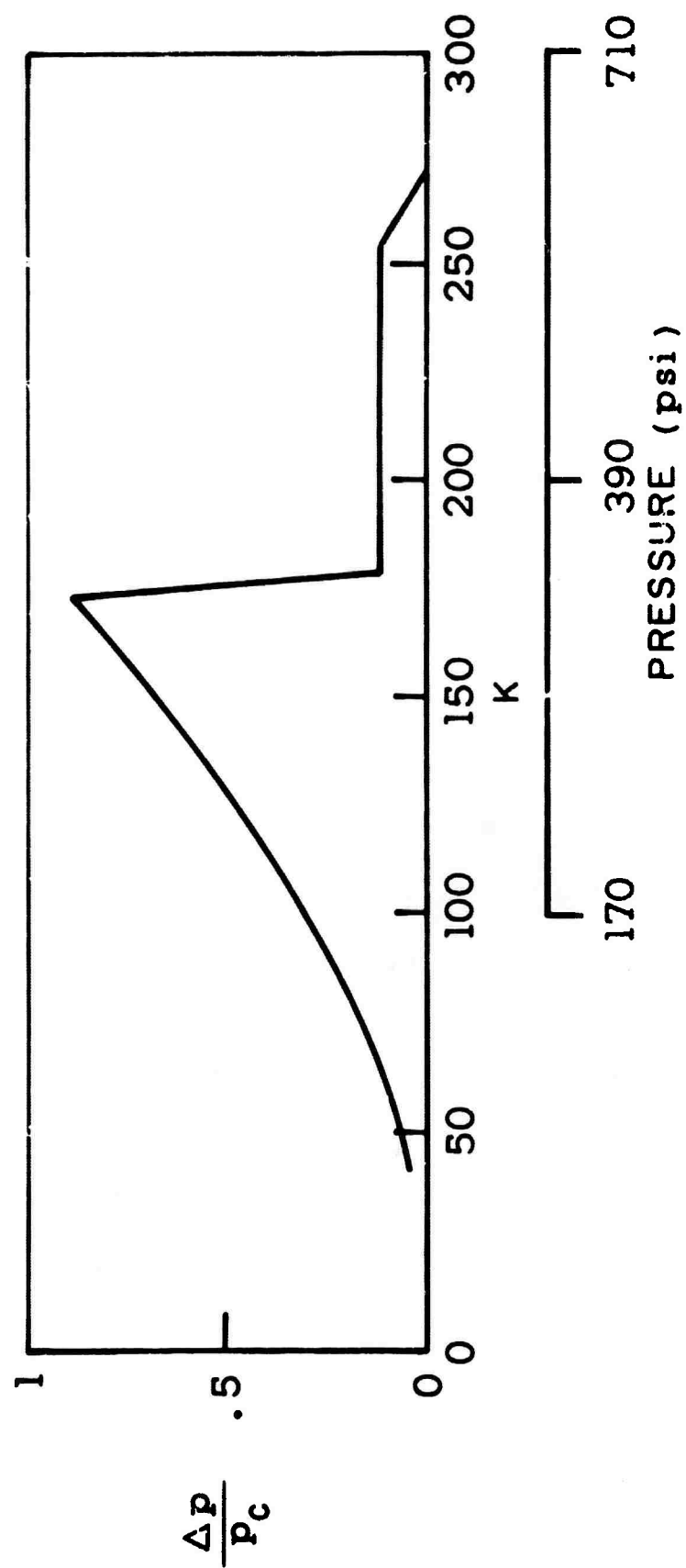
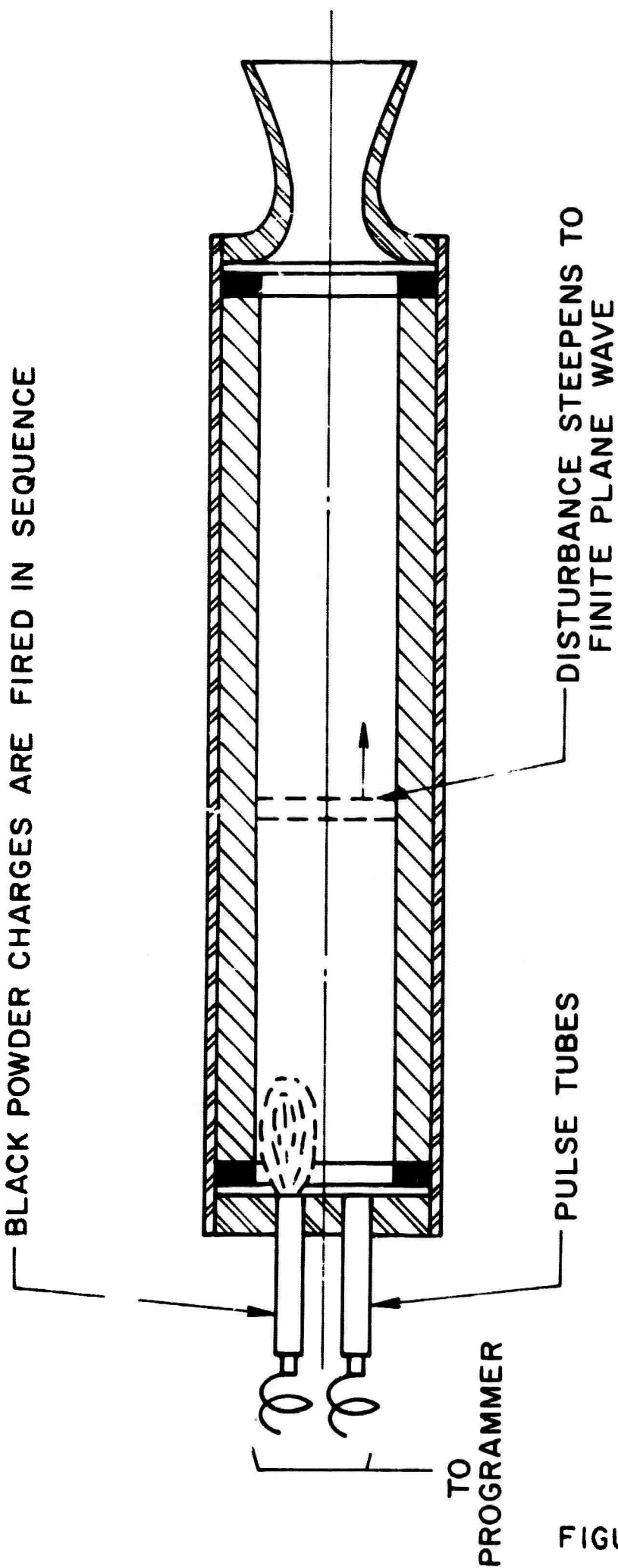


FIGURE 15

DEMONSTRATION OF NON-LINEAR INSTABILITY

(CARDE, REF. 111)

BLACK POWDER CHARGES ARE FIRED IN SEQUENCE



PULSE TUBES

TO
PROGRAMMER

DISTURBANCE STEEPENS TO
FINITE PLANE WAVE

FIGURE 16

NON-LINEAR INSTABILITY TESTS IN STABLE
AND UNSTABLE REGIMES

(CARDE, REF.111)

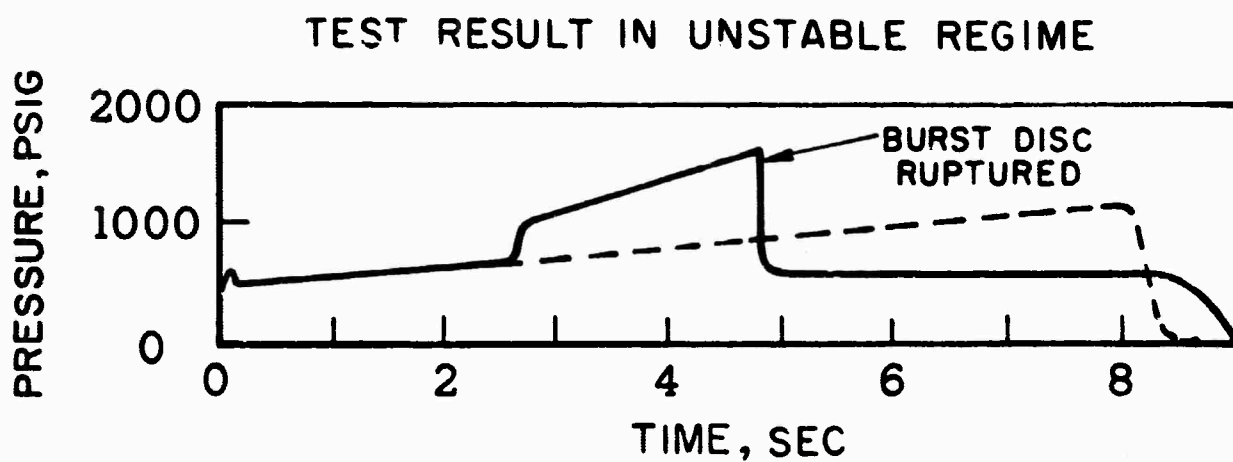
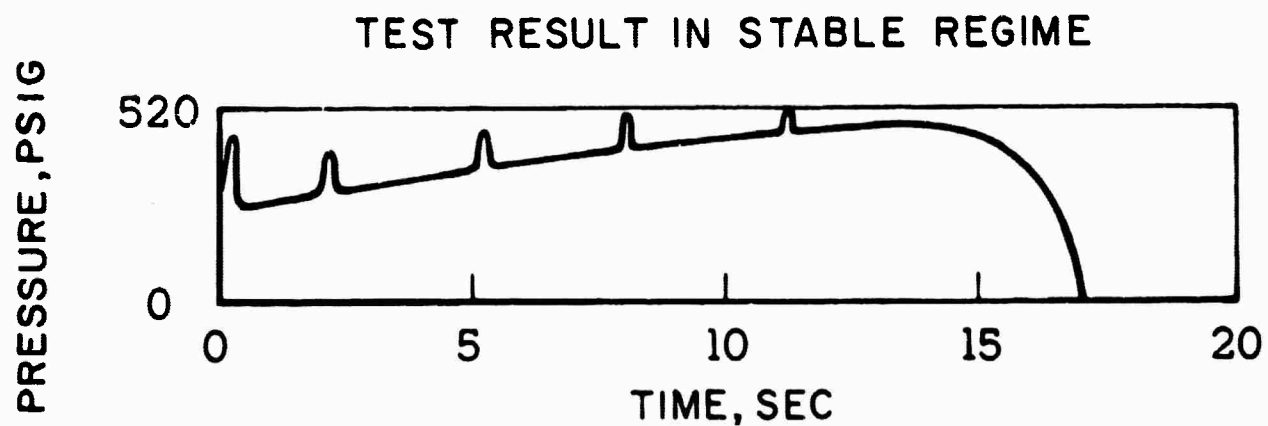


FIGURE 17

NON - ACOUSTIC INSTABILITY
(NOTE FREQUENCY DEPENDENCE ON PRESSURE)

(ANGELUS, REF.122)

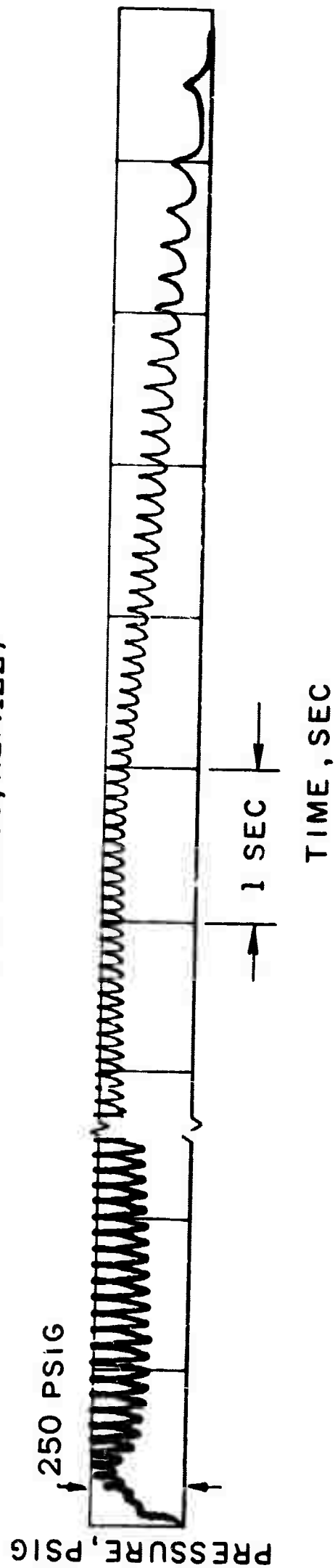


FIGURE 18

CHUFFING

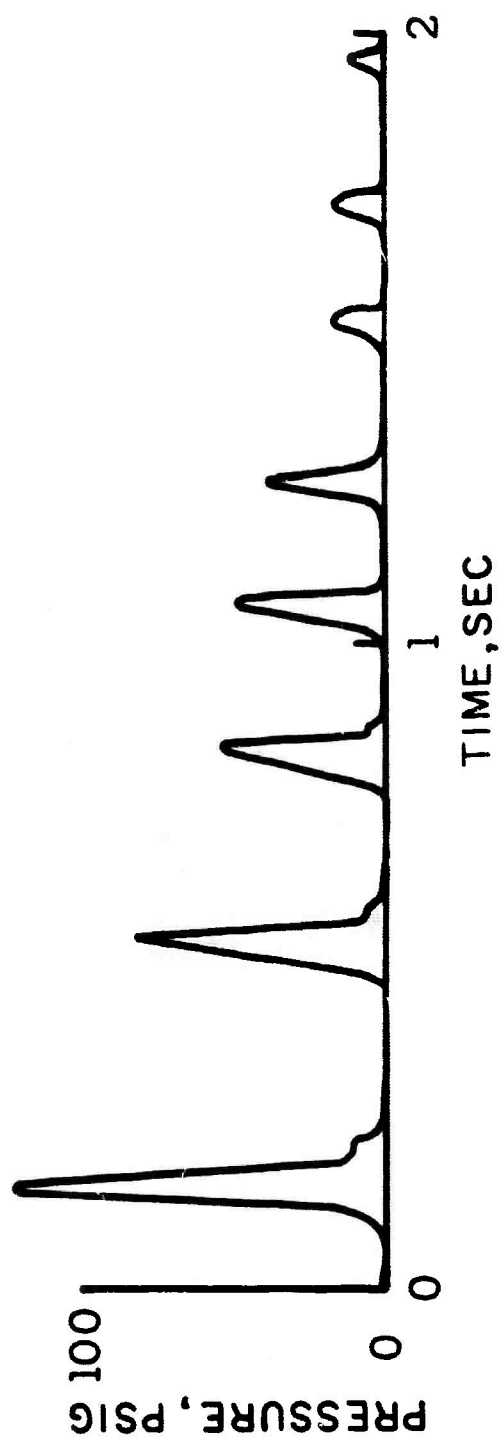


FIGURE 19

EFFECT OF PROPELLANT COMPRESSIBILITY ON
RESPONSE FUNCTION

(MC CLURE, REF. 152)

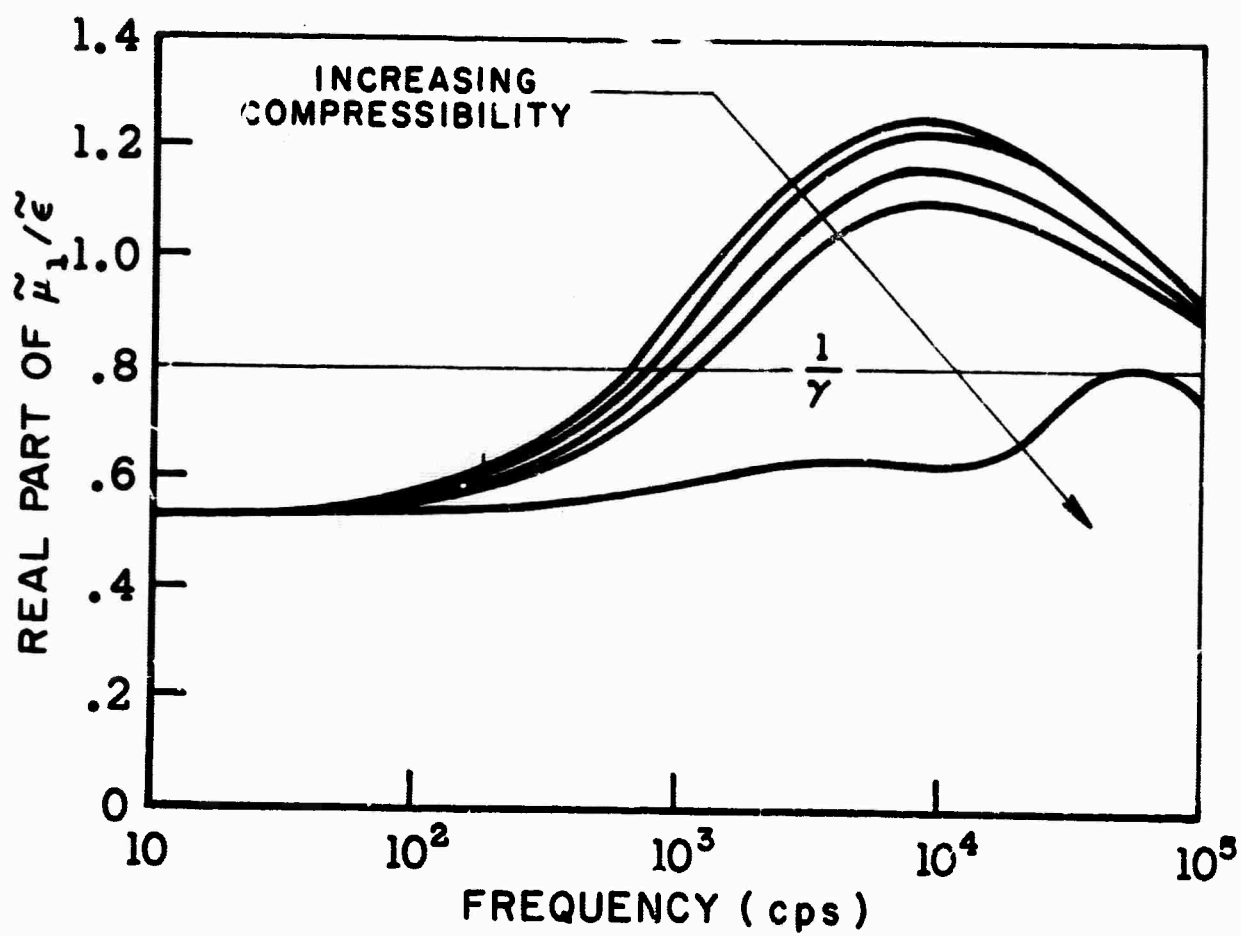


FIGURE 20

PRESSURE-FREQUENCY REGIMES OF ACOUSTIC INTERACTION WITH COMBUSTION ZONE

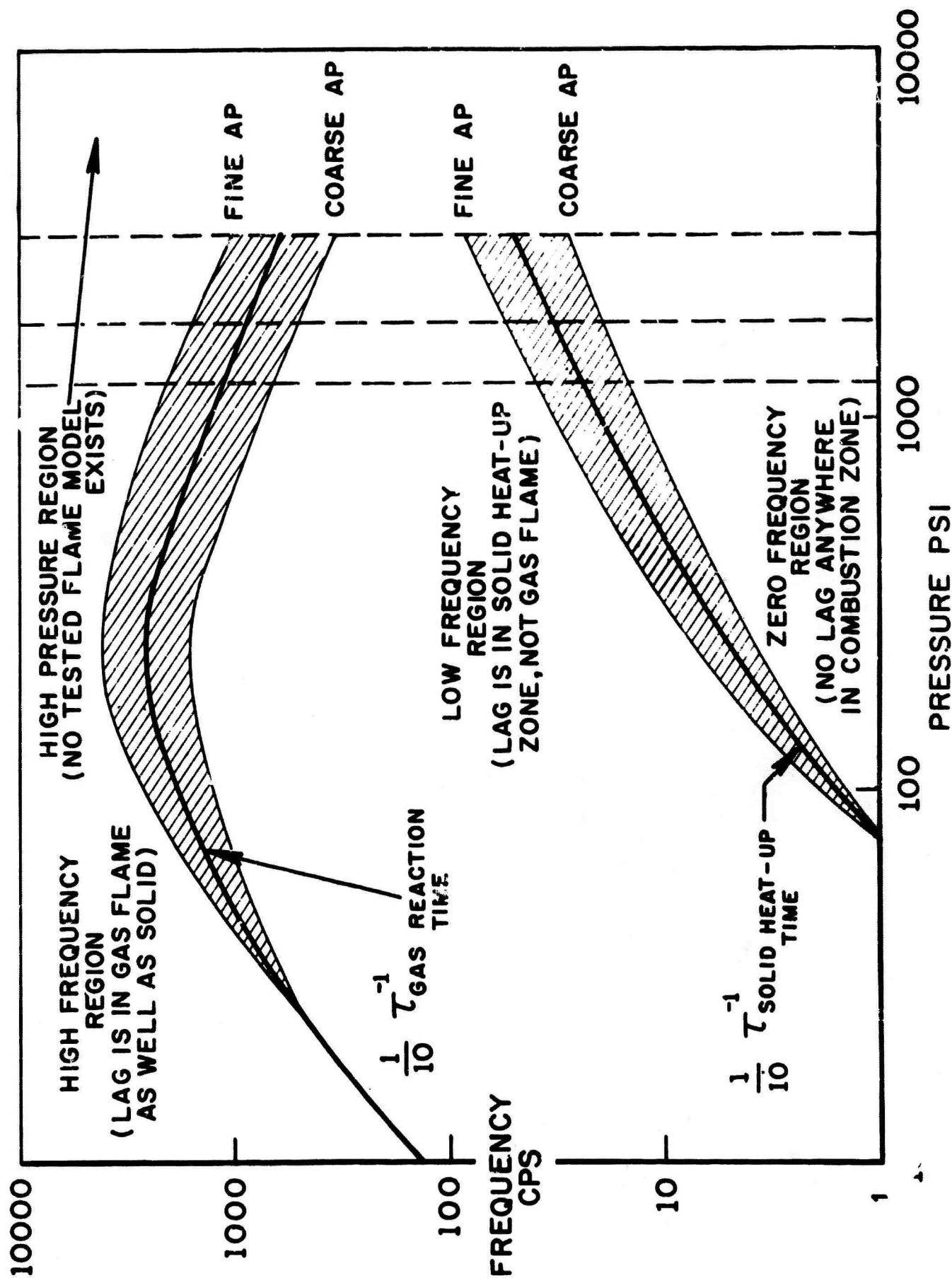


FIGURE 21

RESPONSE FUNCTIONS OBTAINED BY HART-Mc CLURE AND BY CHENG
WITH FIXED AND VARIABLE TIME LAG

(REF.189)

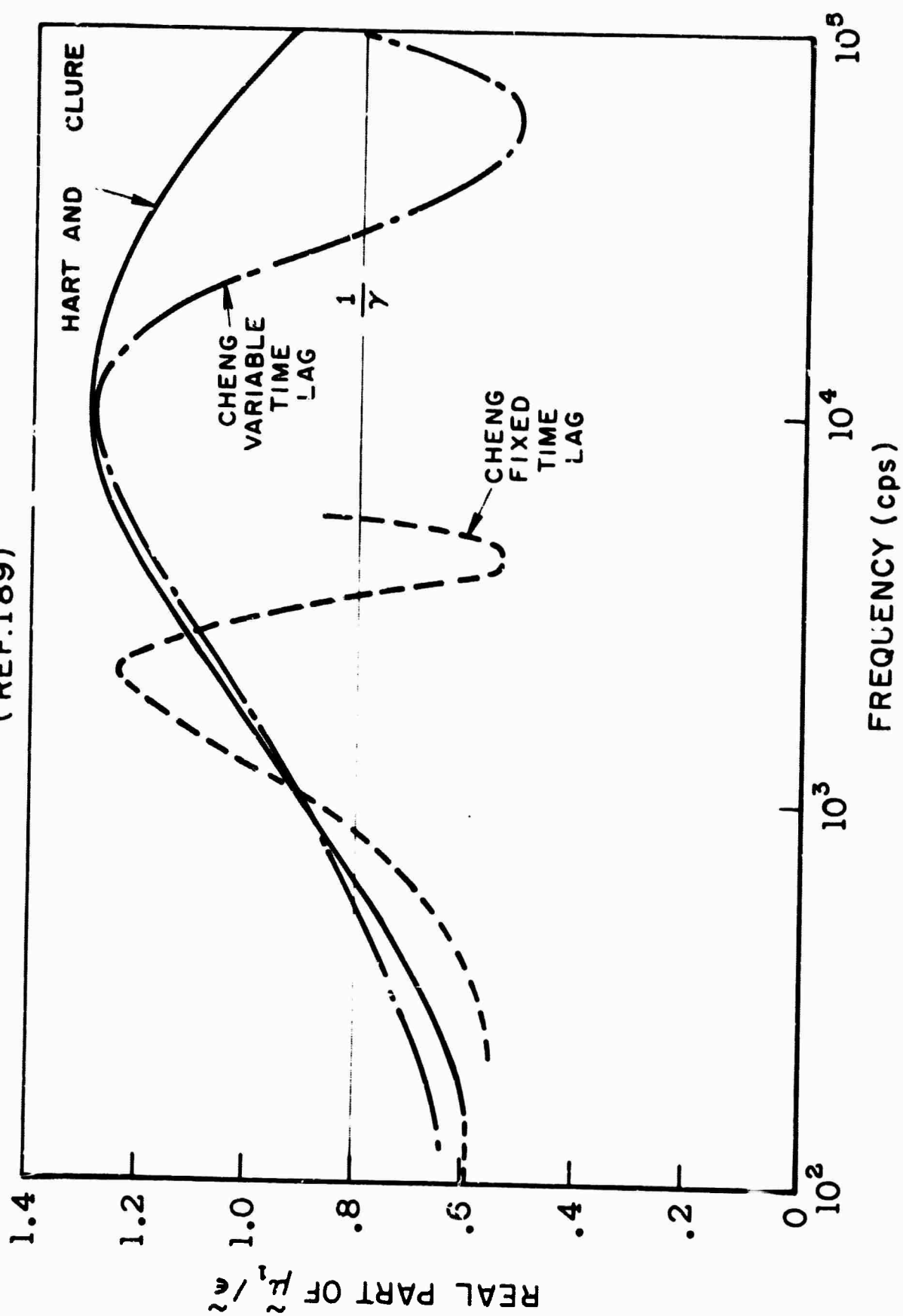


FIGURE 22

COMBUSTION ZONE MODEL USED BY HART & MCCLURE

(REF. 85)

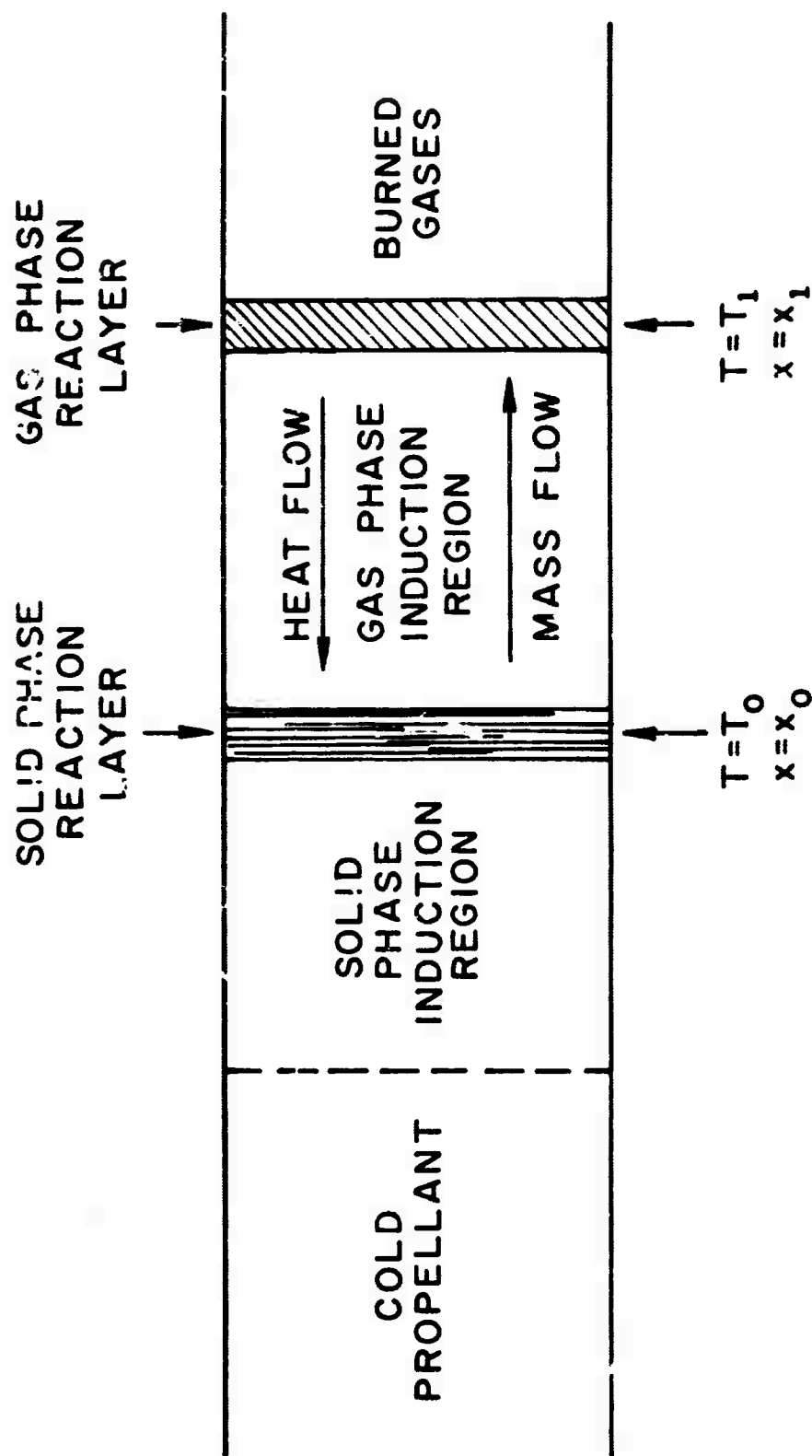


FIGURE 23

A TYPICAL RESPONSE VS FREQUENCY CURVE CALCULATED
BY HART & MCCLURE (AMPLIFICATION IN SHADED AREA)

(REF. 85)

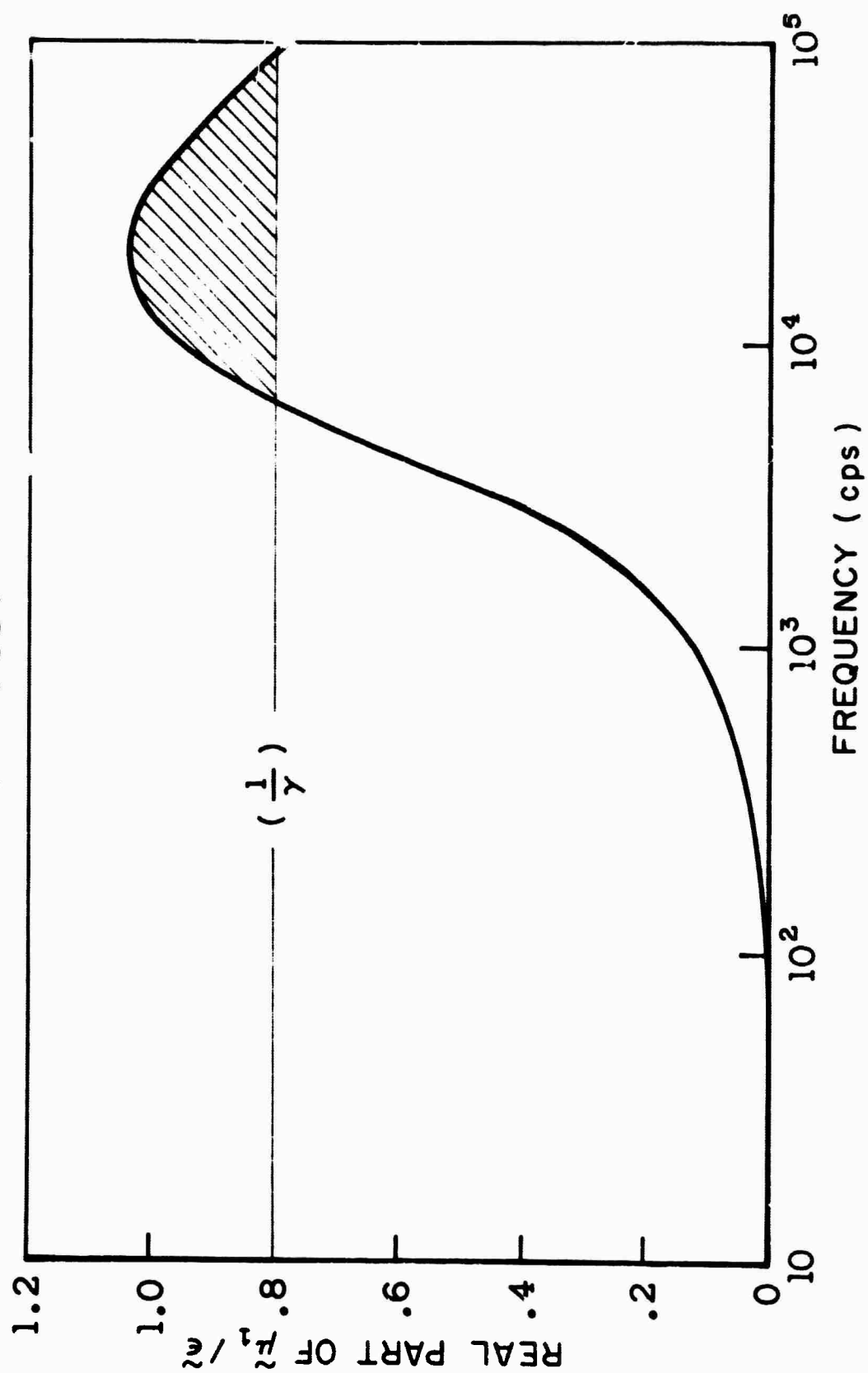


FIGURE 24

EFFECT OF TEMPERATURE SENSITIVITY ON RESPONSE FUNCTION
(MC CLURE, REF. 85)

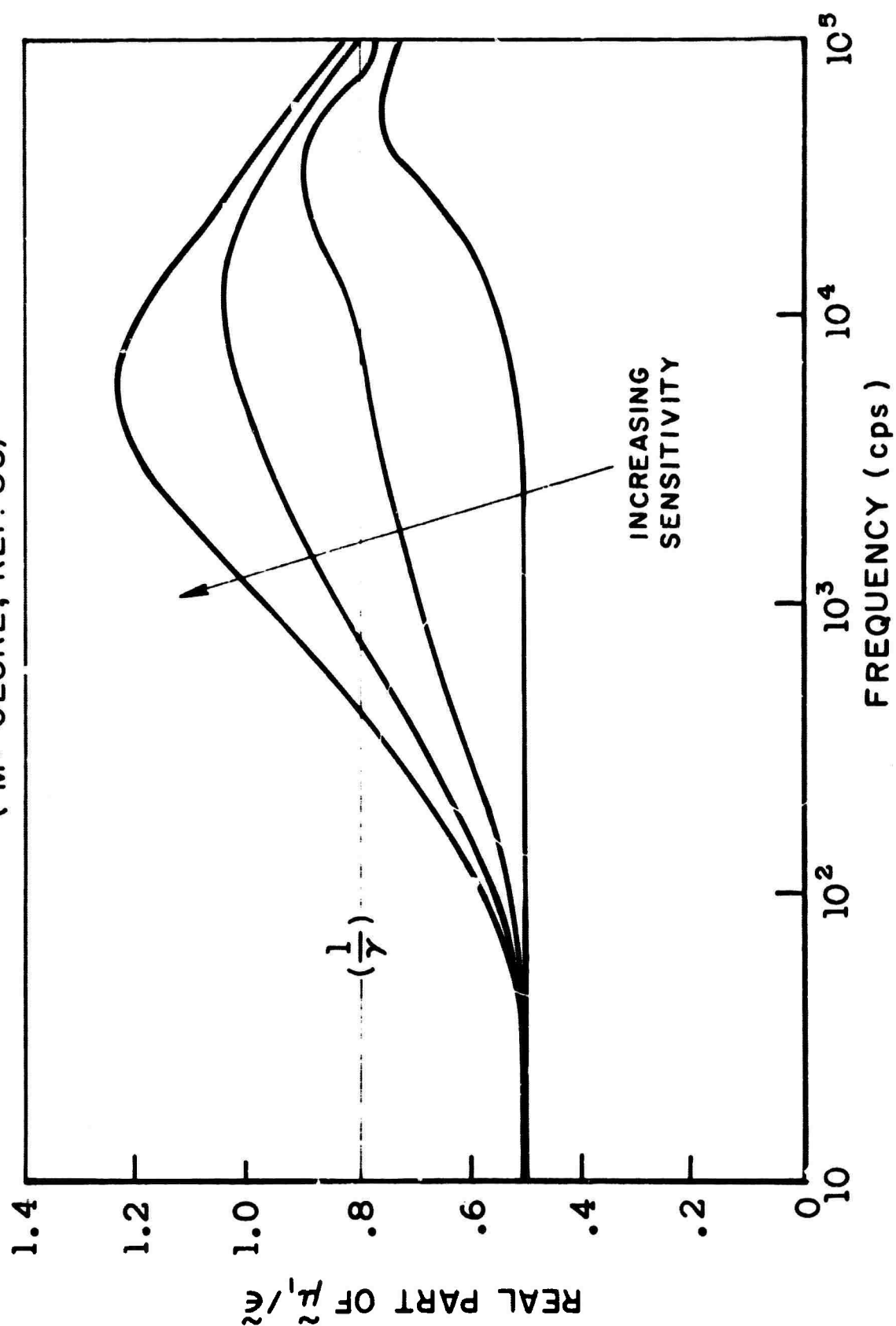


FIGURE 25

DOMAINS OF STABILITY & INSTABILITY

(DENNISON & BAUM, REF. 91)

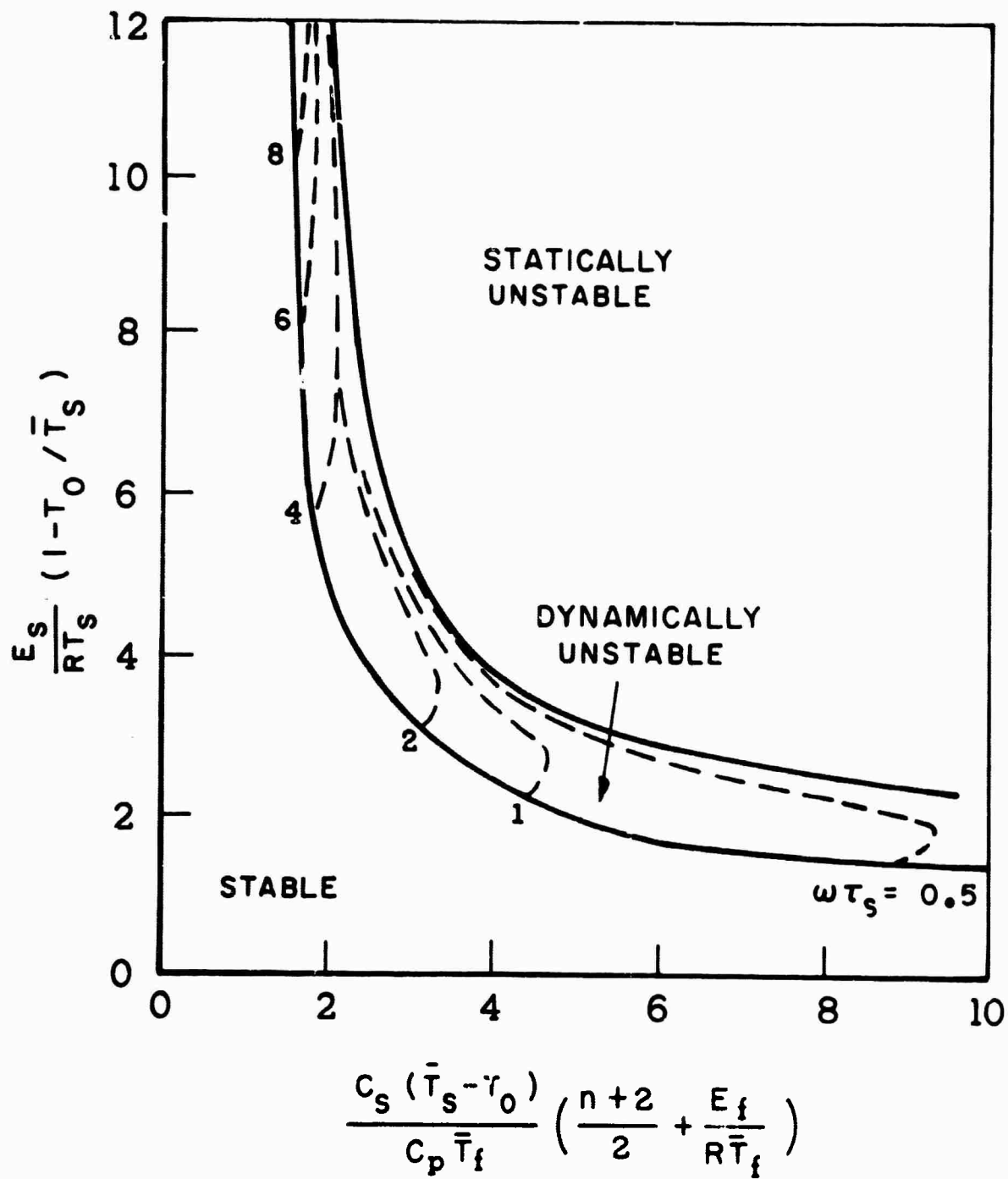


FIGURE 26

T-BURNER USED BY PRICE

(REF. 99)

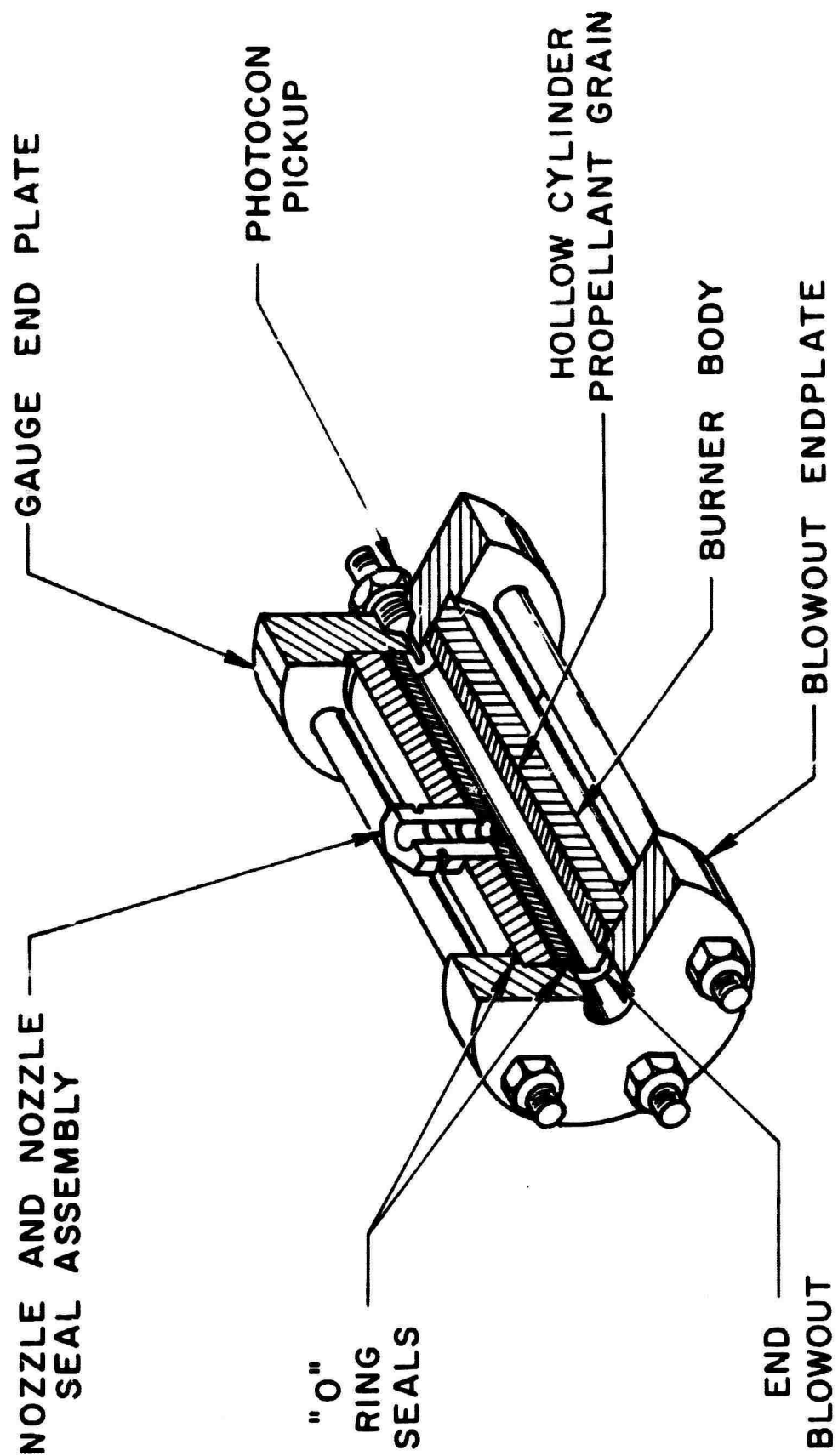


FIGURE 27

T-BURNER FOR OSCILLATORY BURNING EXPERIMENTS

(HORTON, NOTS, REF.197)

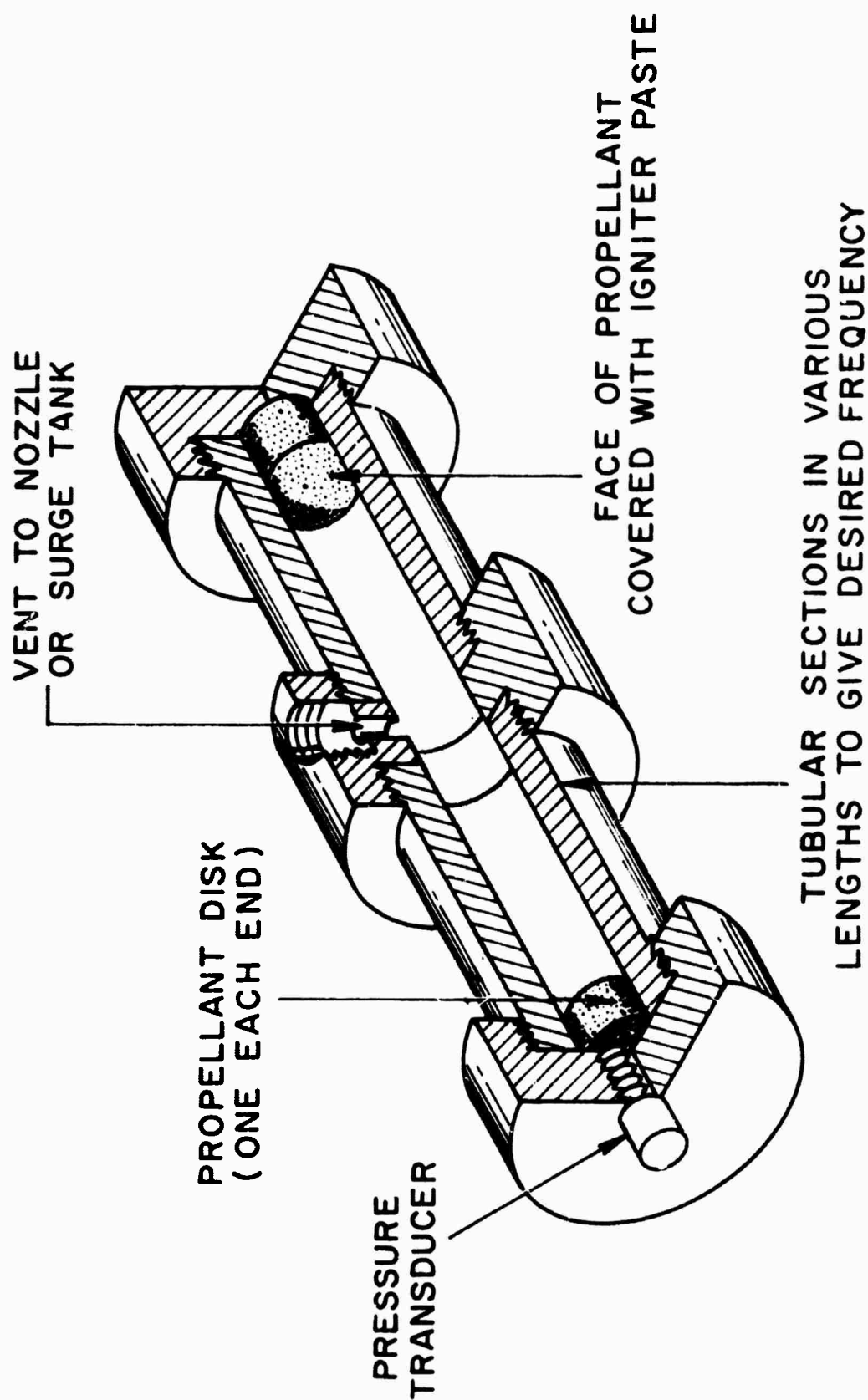


FIGURE 28

RESPONSE FUNCTIONS FOR TWO PROPELLANTS AS MEASURED BY DIFFERENT LABORATORIES

(REF. 215)

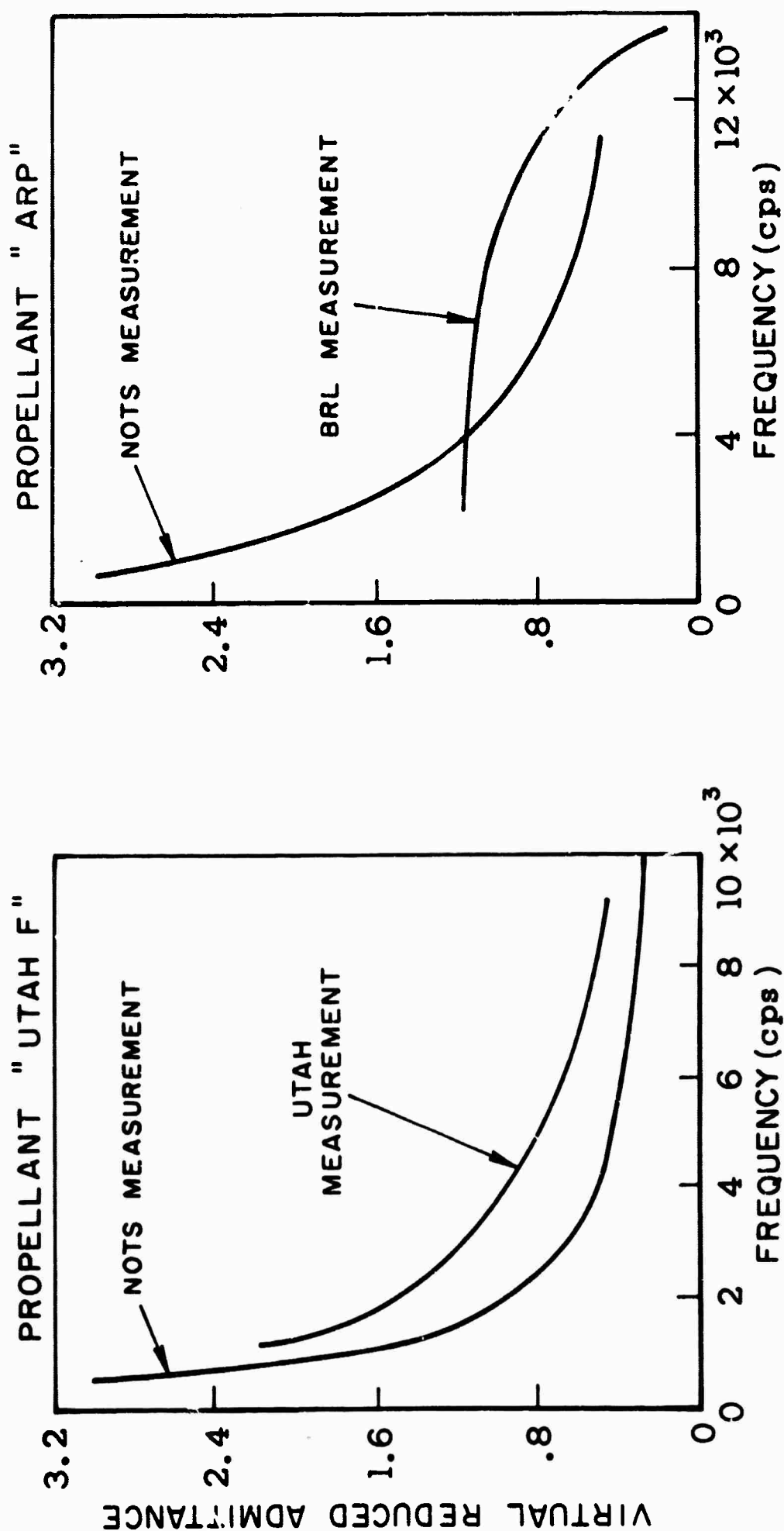


FIGURE 29

FOUR-NOZZLE RESONANT CHAMBER USED BY WATERMEIER

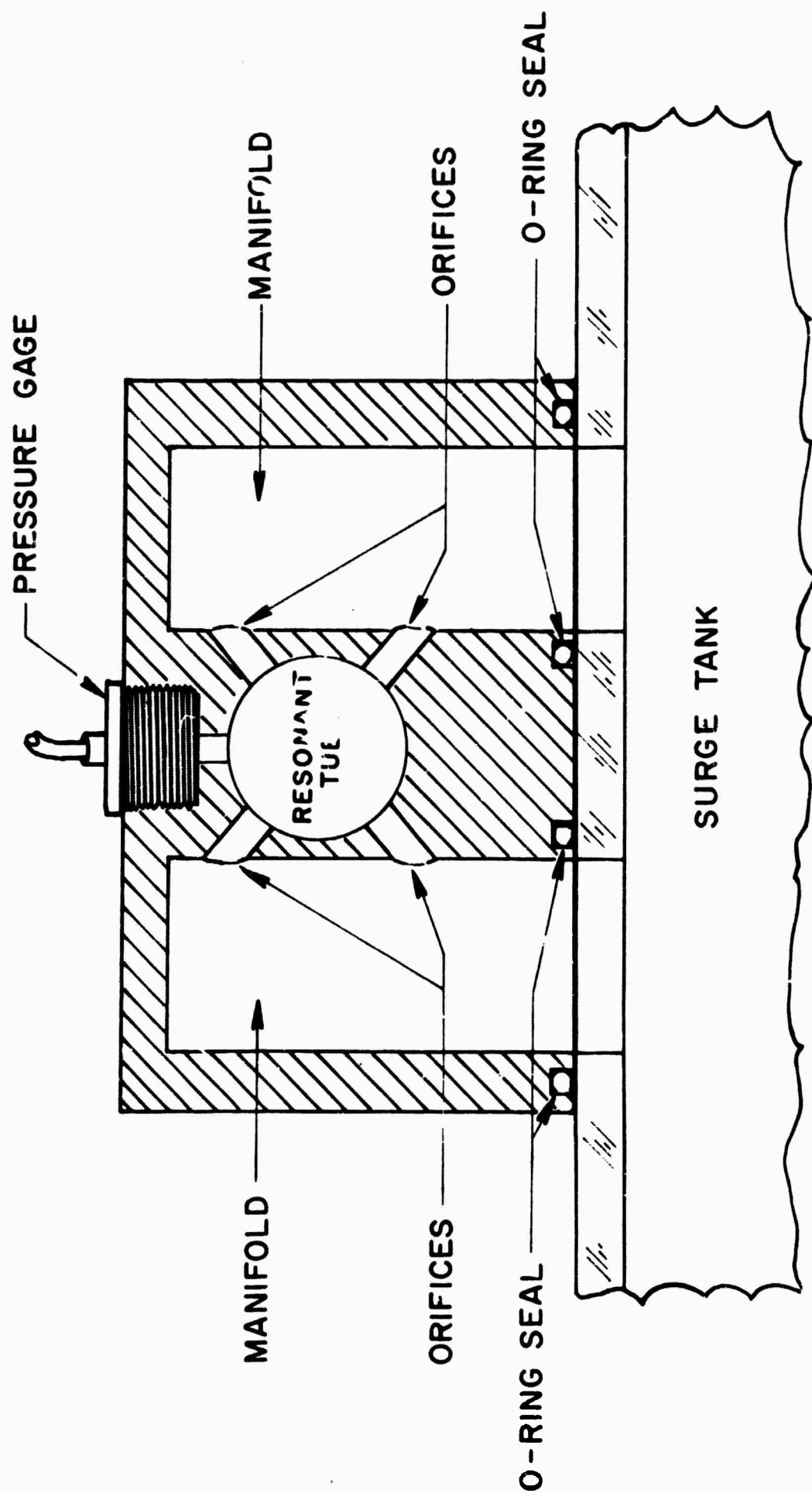


FIGURE 30

THE EFFECT OF BINDER COMPOSITION UPON THE
RESPONSE FUNCTION OF A PROPELLANT
(HORTON, REF.116)

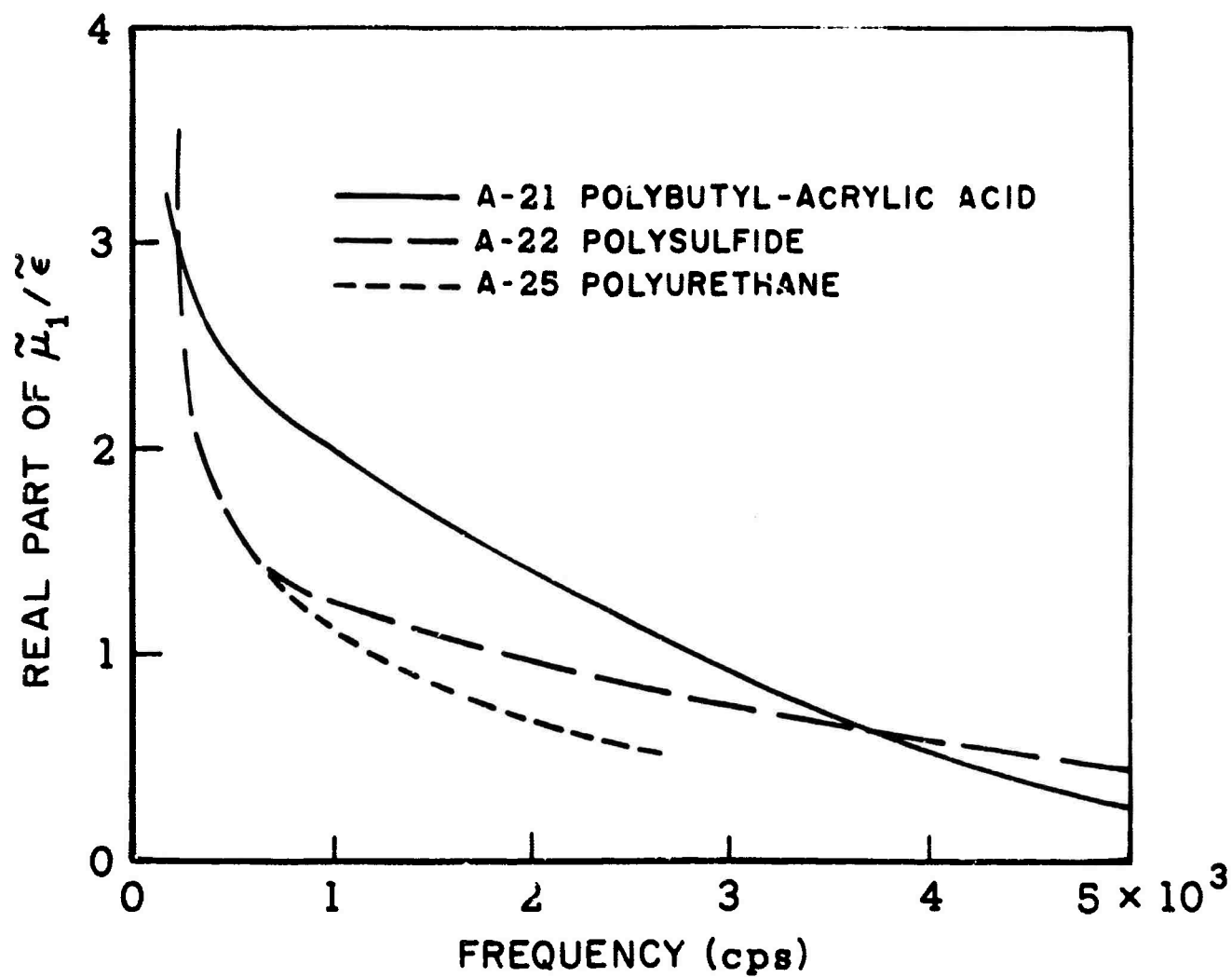


FIGURE 31

THE EFFECT OF BURNING RATE MODIFIERS UPON
THE RESPONSE FUNCTION
(HORTON, REF.116)

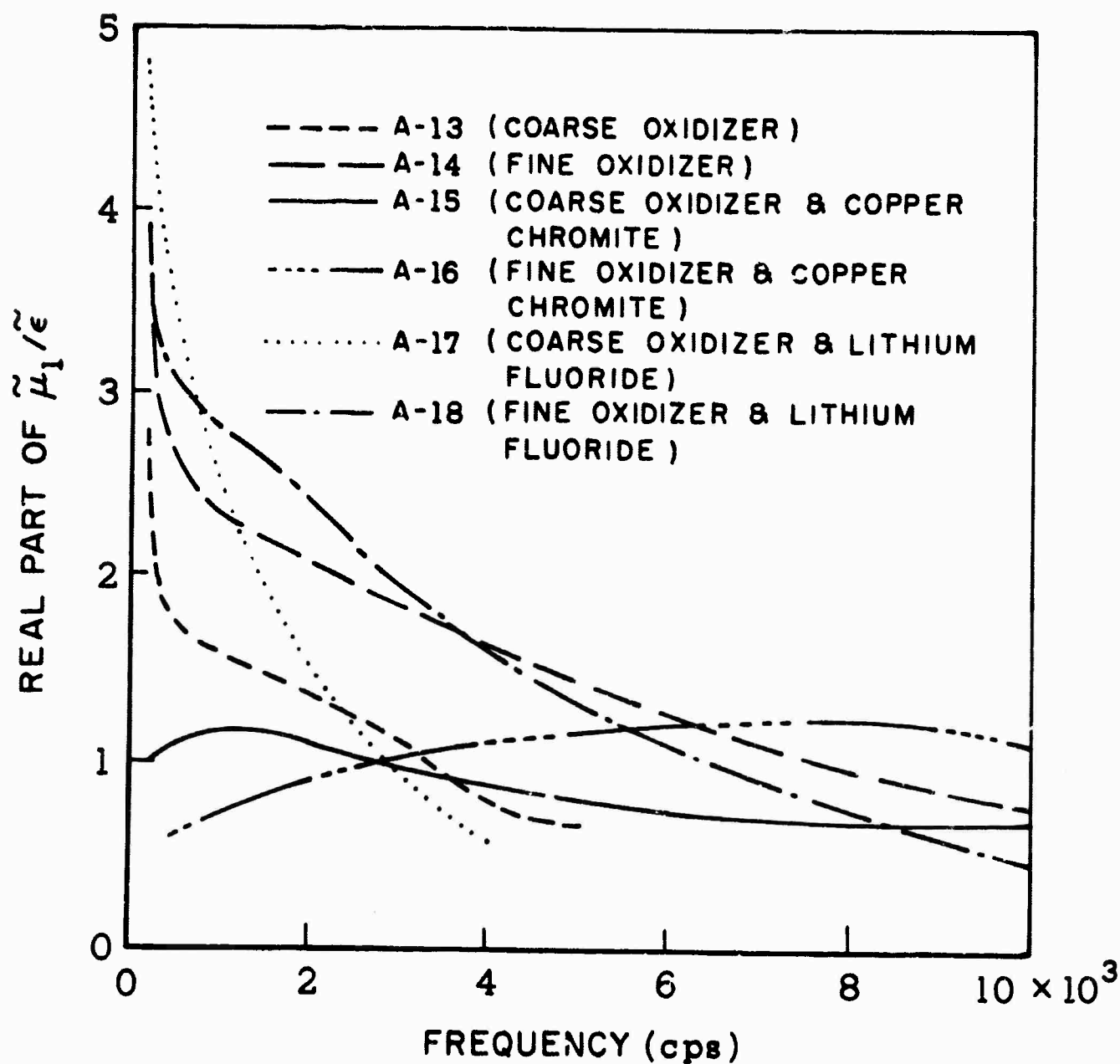


FIGURE 32

PROPELLANT RESPONSE FUNCTION PLOTTED AGAINST FREQUENCY
AND AGAINST FREQUENCY DIVIDED BY THE SQUARE OF THE BURNING RATE

(REF.116)

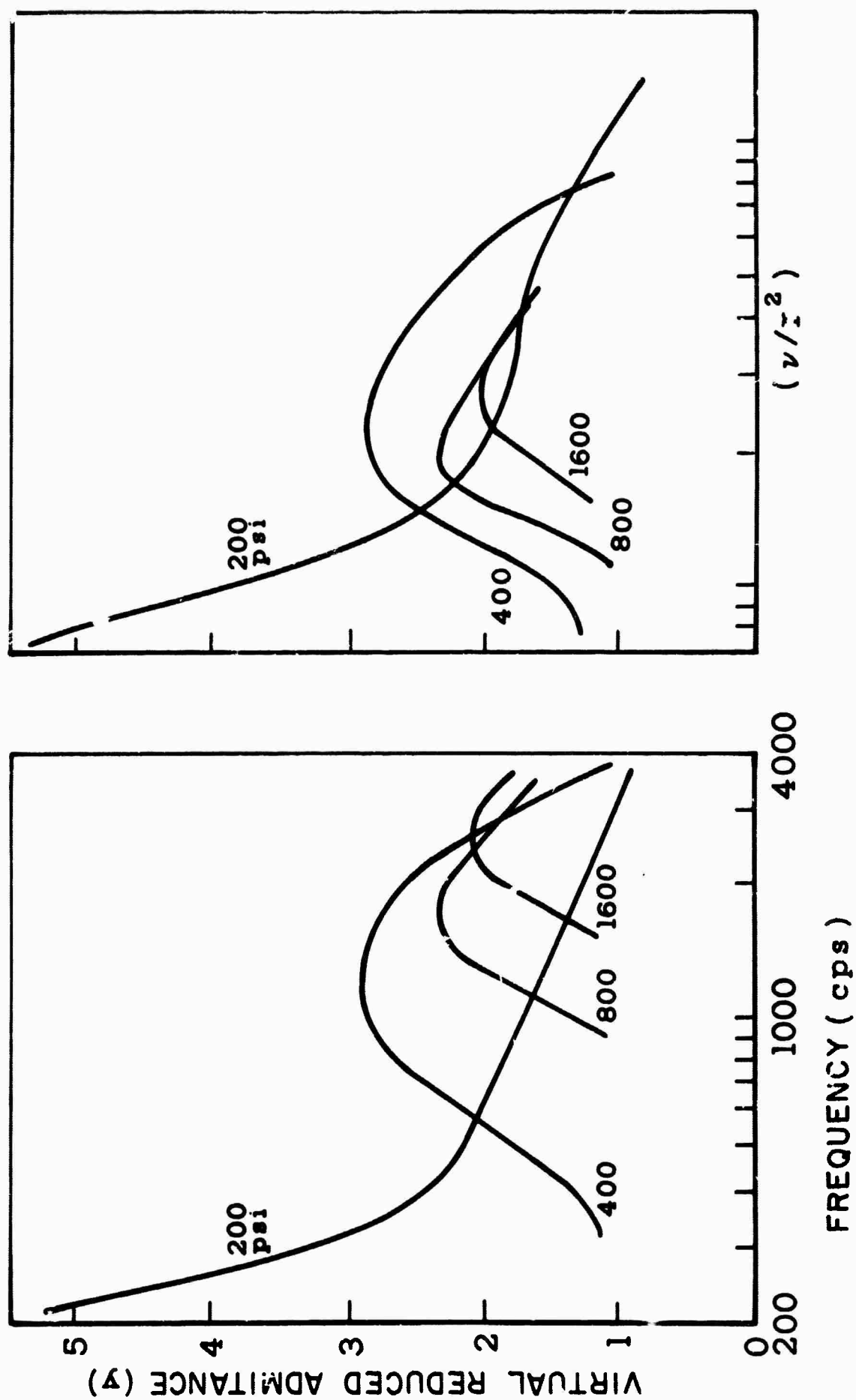


FIGURE 33

COMPARISON OF ADMITTANCE DATA FOR THREE METHODS
 USED BY RYAN
 (REF. 209)

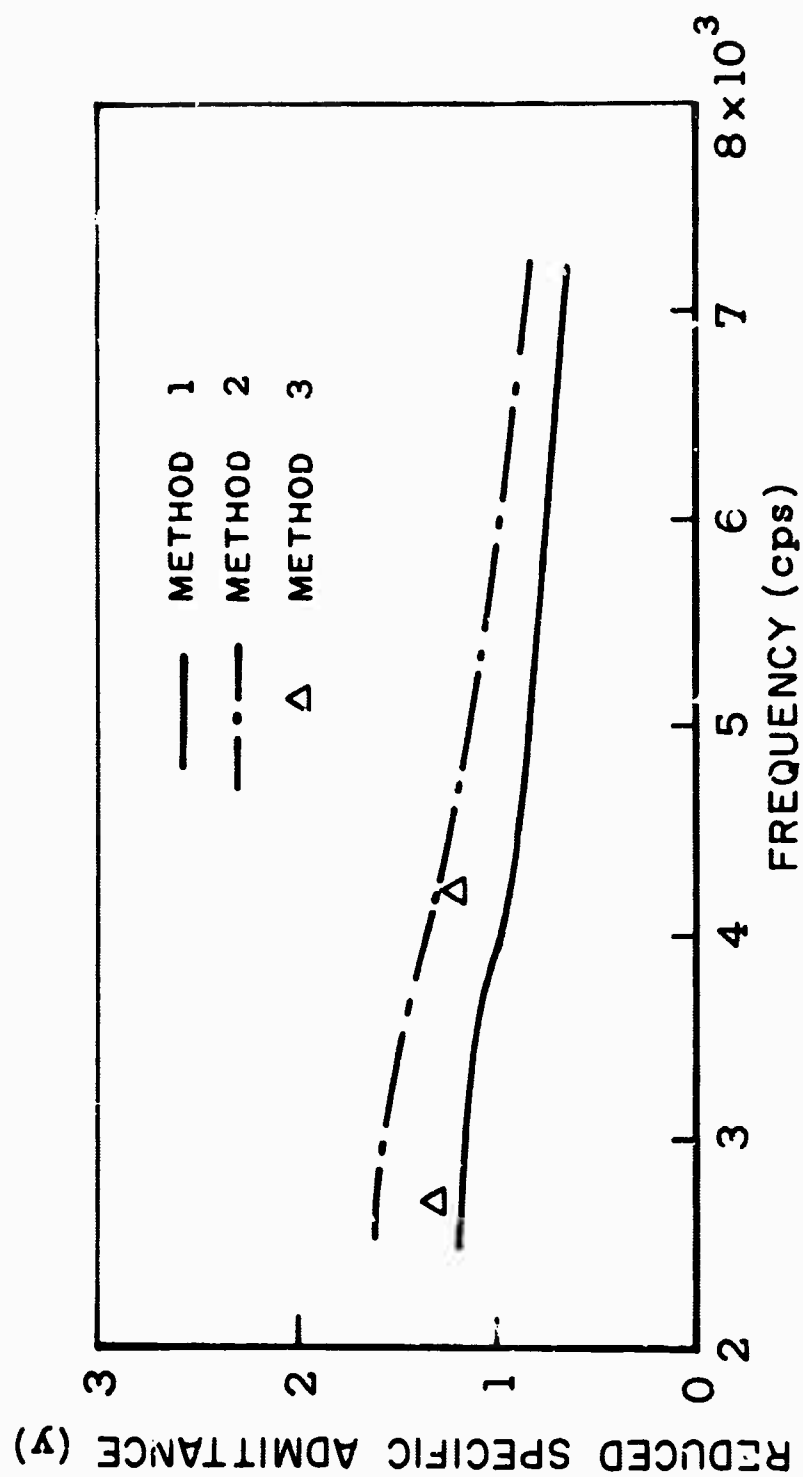


FIGURE 34

TECHNIQUE USED TO INCREASE THE PROPELLANT BURNING SURFACE AREA

(UTAH, REF. 209)

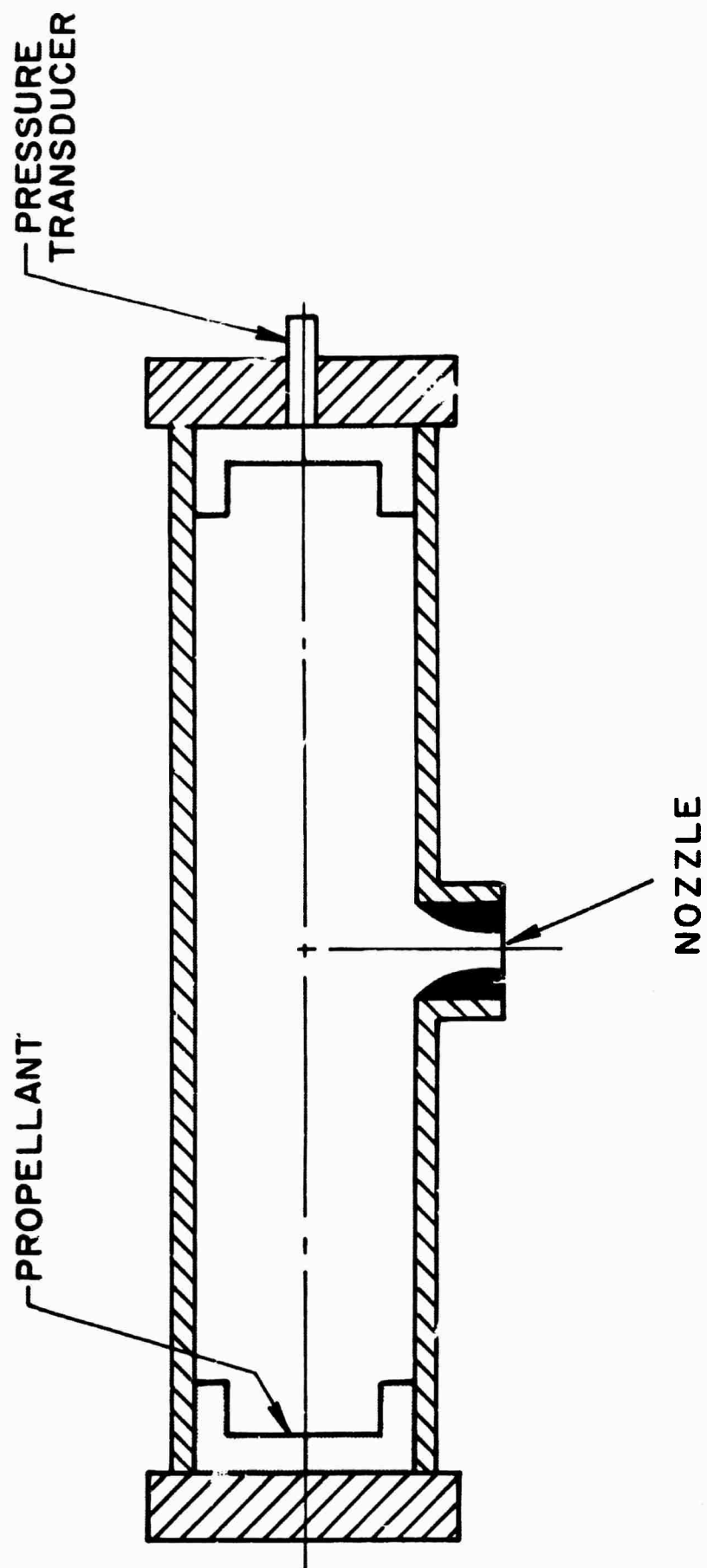


FIGURE 35

OSCILLATOR USED BY FONER FOR MEASURING
SOLID PROPELLANT RESPONSE

(REF. 213)

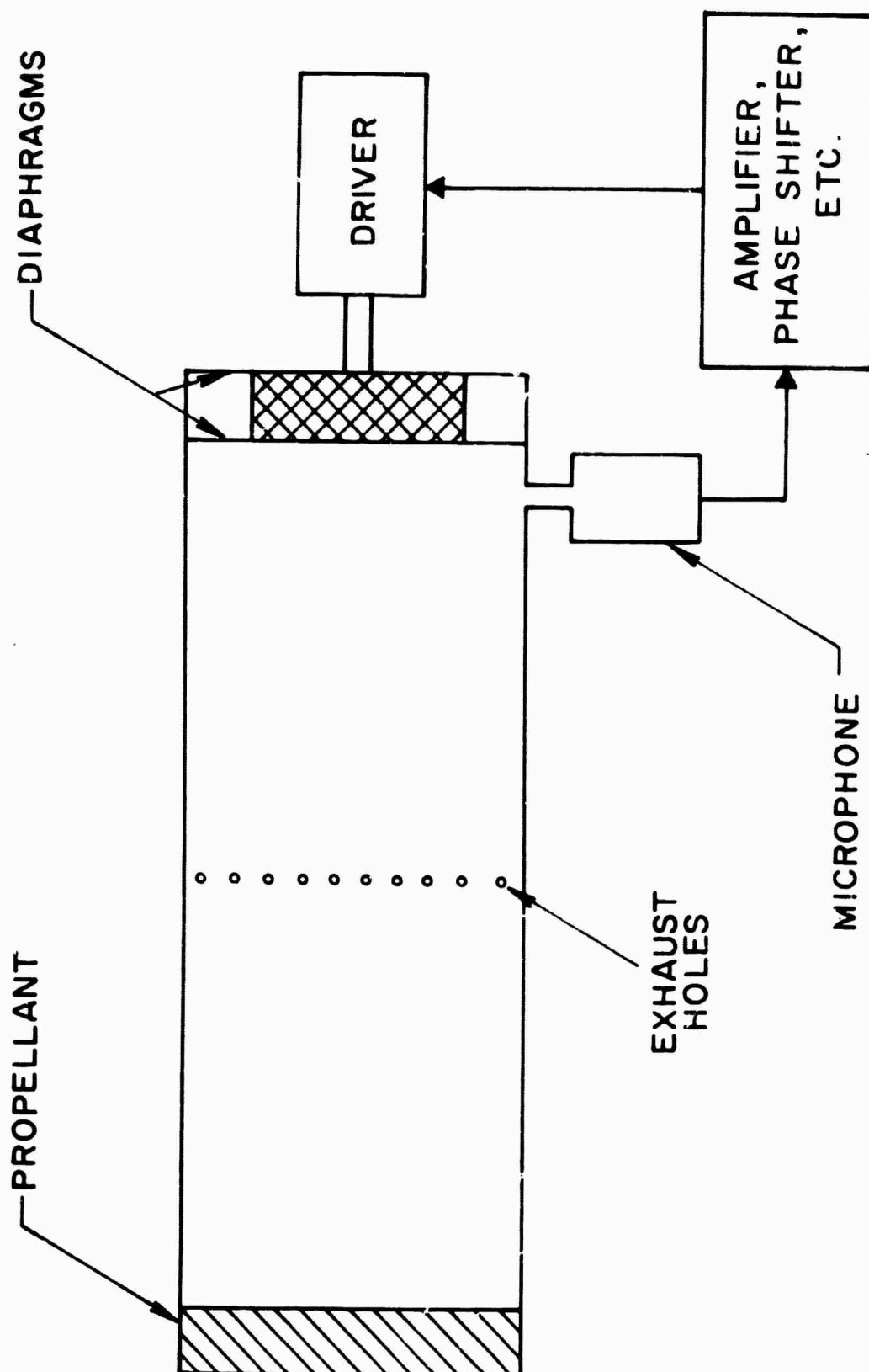


FIGURE 36

MODIFIED MAWARDI IMPEDANCE MEASUREMENT
(THIOKOL CHEM. CORP, ELKTON DIV., REF. 217)

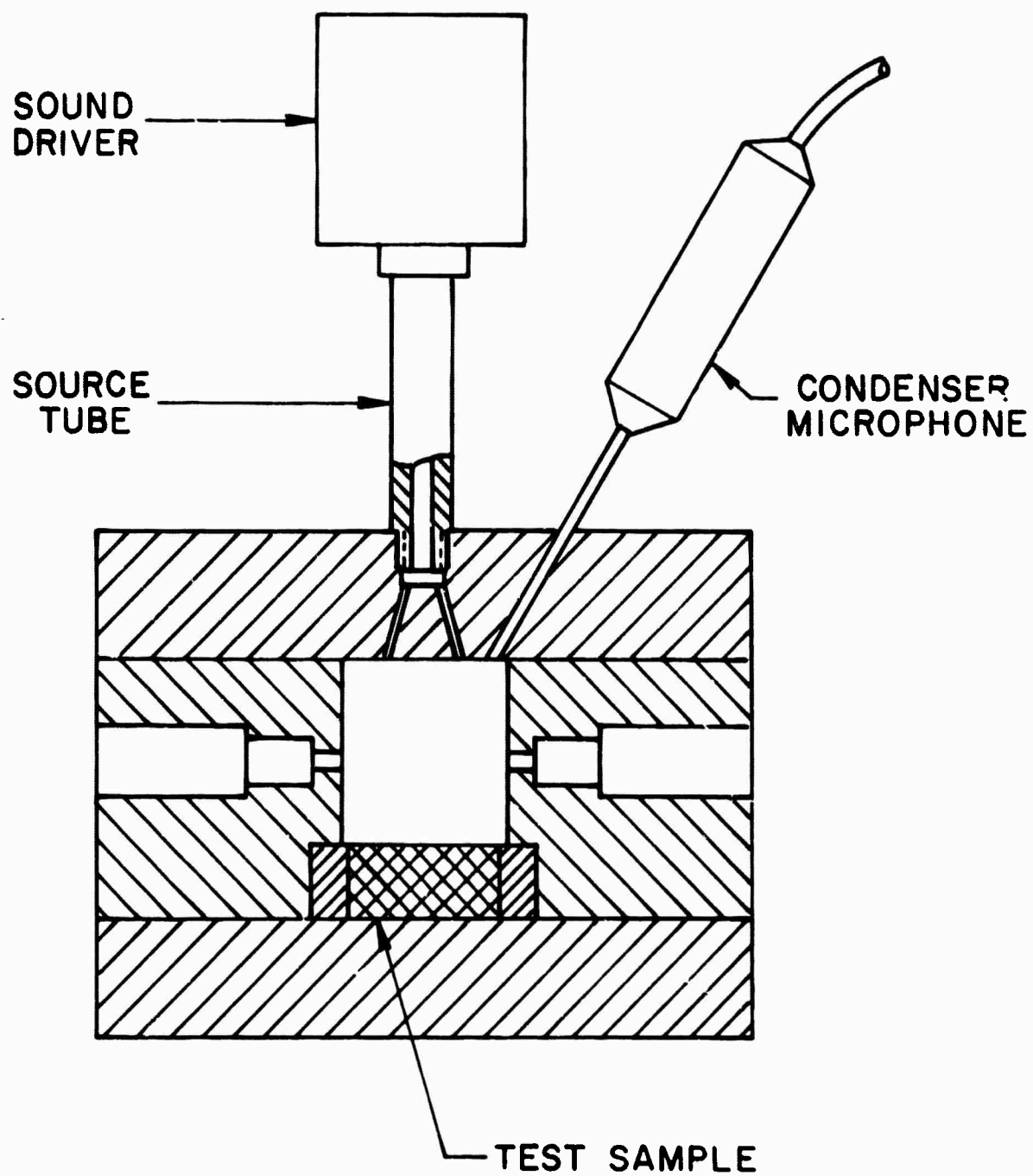


FIGURE 37

SOLID-PROPELLANT ACOUSTIC OSCILLATOR WITH TRANSPARENT (QUARTZ)
COMBUSTION CHAMBER USED BY NACHBAR

(REF. 225)

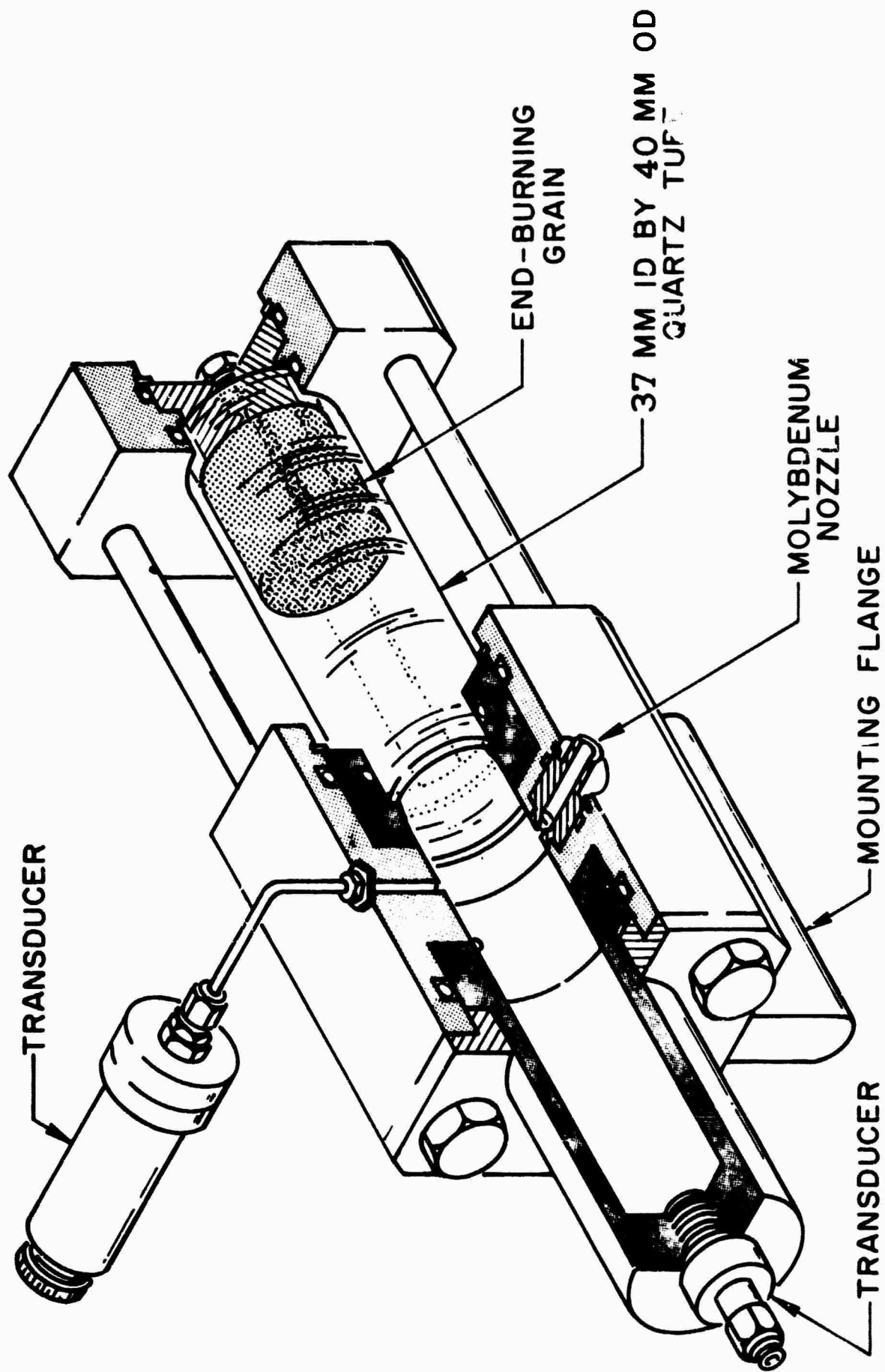


FIGURE 38

WAVE SPLITTER APPARATUS USED BY LAWHEAD

(REF. 233)

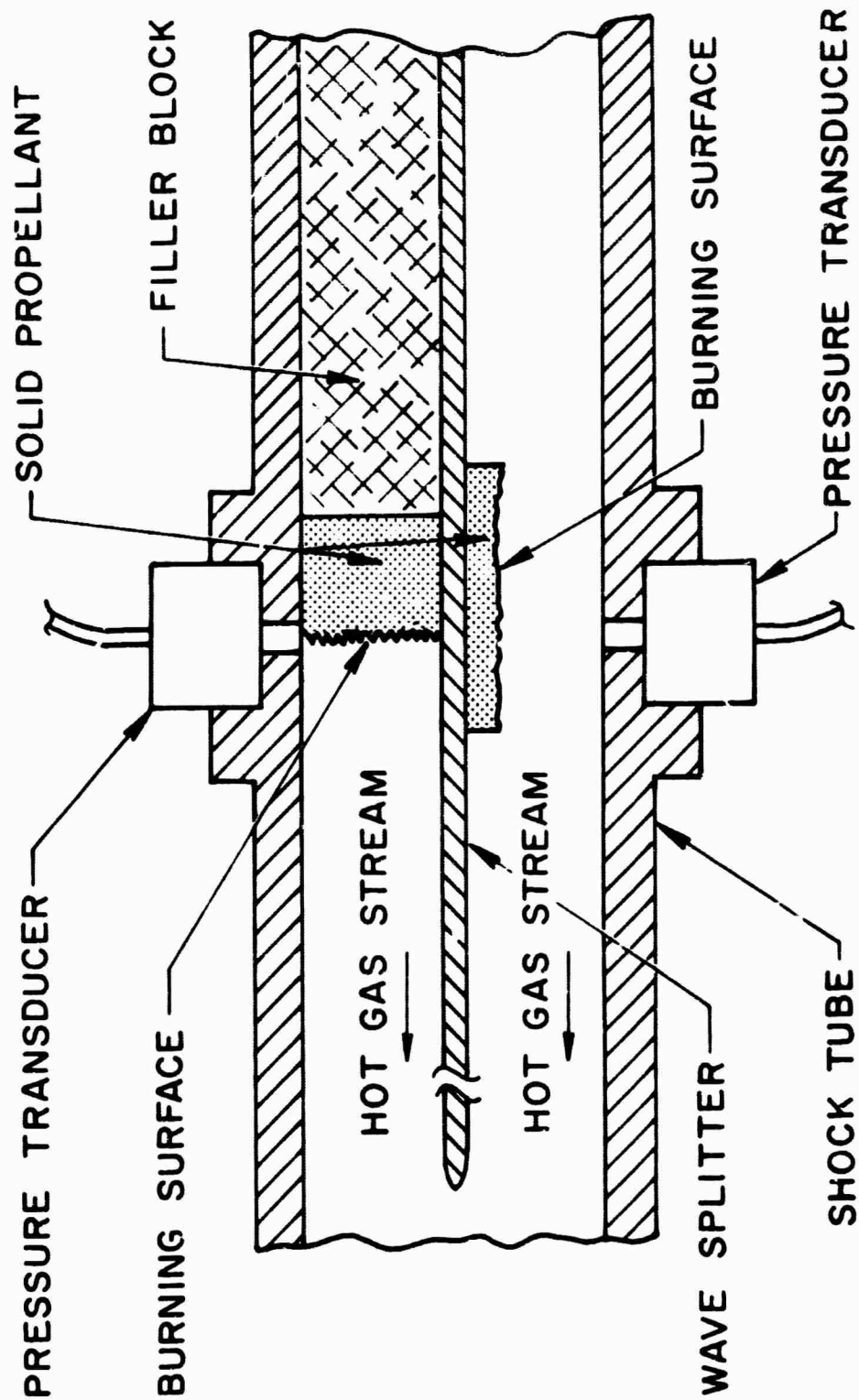


FIGURE 39

PRESSURE ALONG A TUBE

$$|p| = 2P_i e^{-\pi a} \sqrt{\cosh^2(\pi a) - \cos^2(\pi \beta)}$$

$a = \text{CONSTANT}$

$$\beta = \beta_\ell + \left(\frac{2}{\lambda}\right)(\ell - x)$$

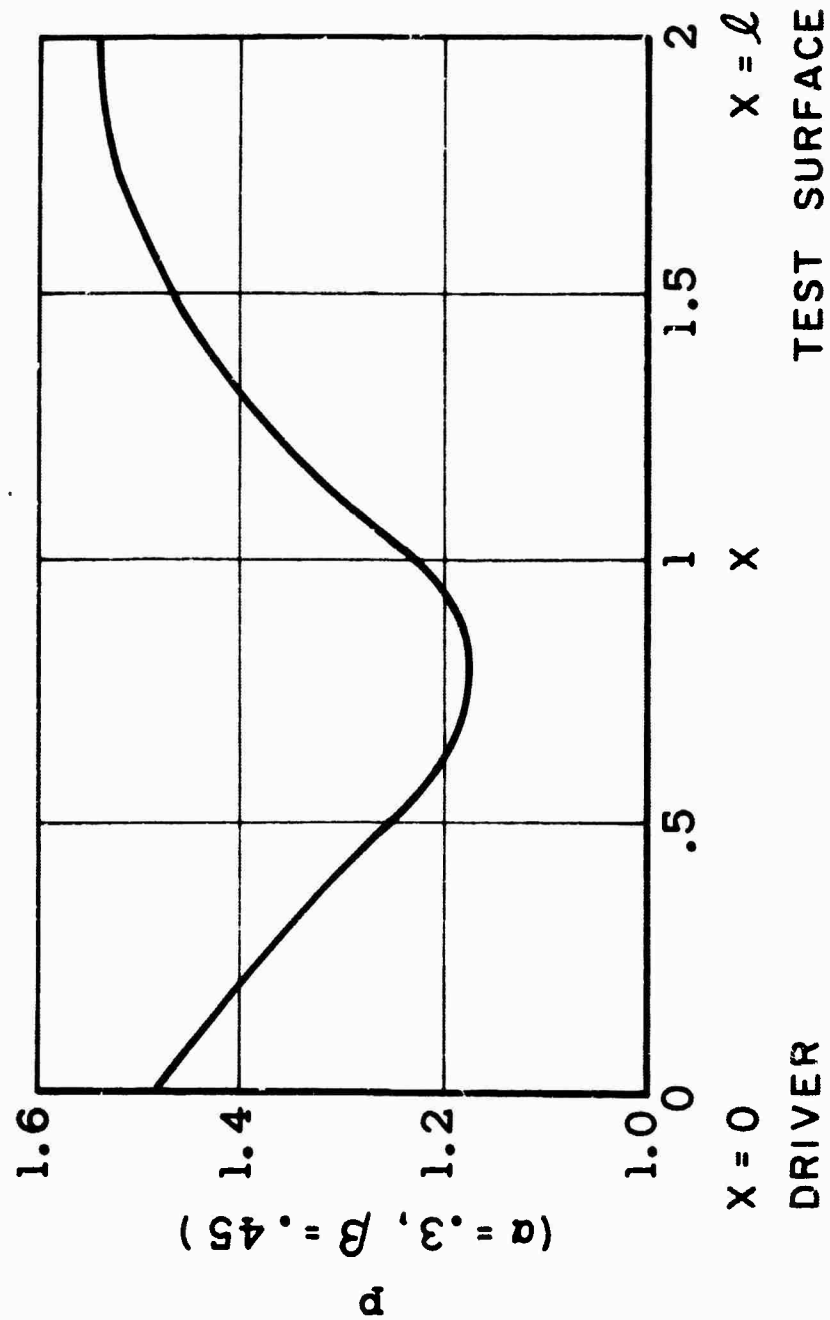


FIGURE 40

VARIATION OF MICROPHONE PRESSURE
WITH FREQUENCY

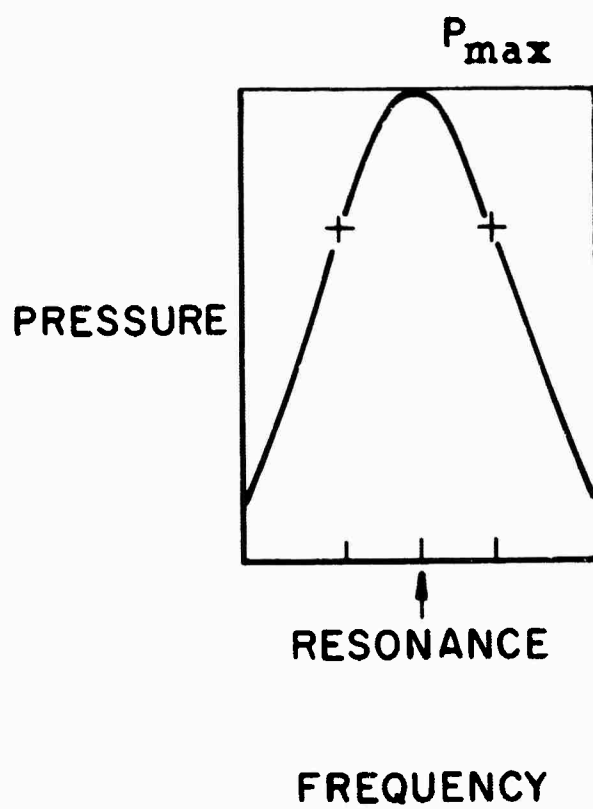


FIGURE 41

SHOCK REFLECTION FROM RIGID END WALL WITH OUTGASSING

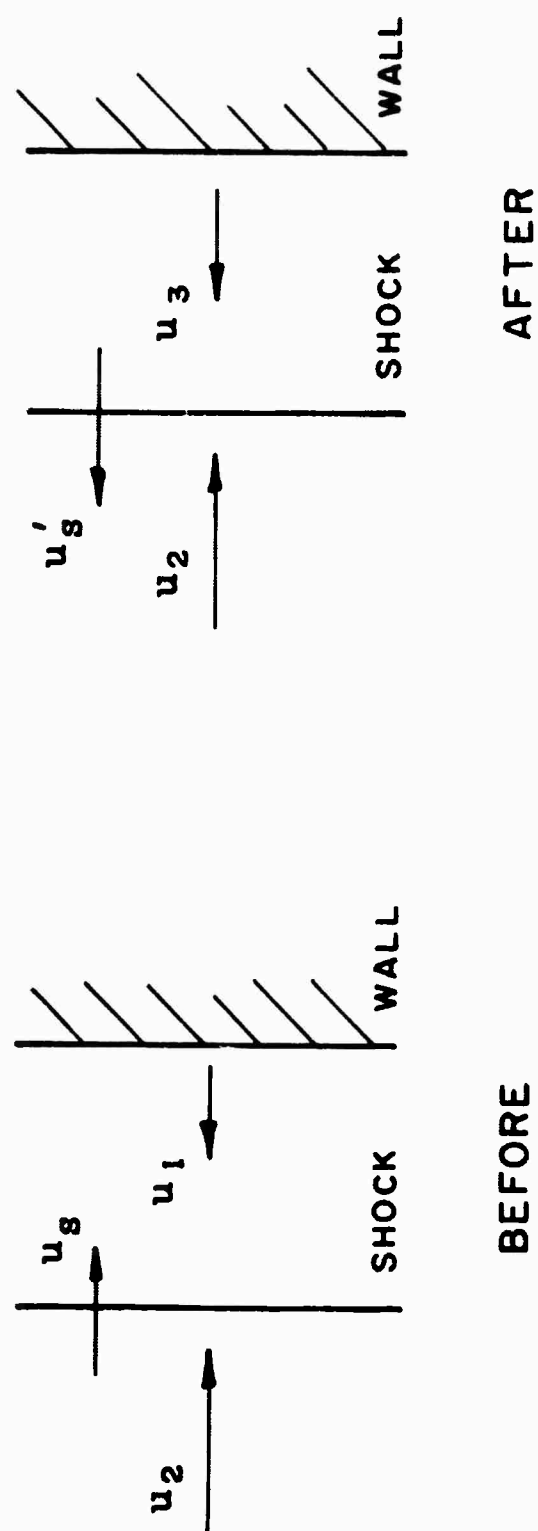


FIGURE 42

EXPECTED RESULT - PARTICLE TRACK METHOD

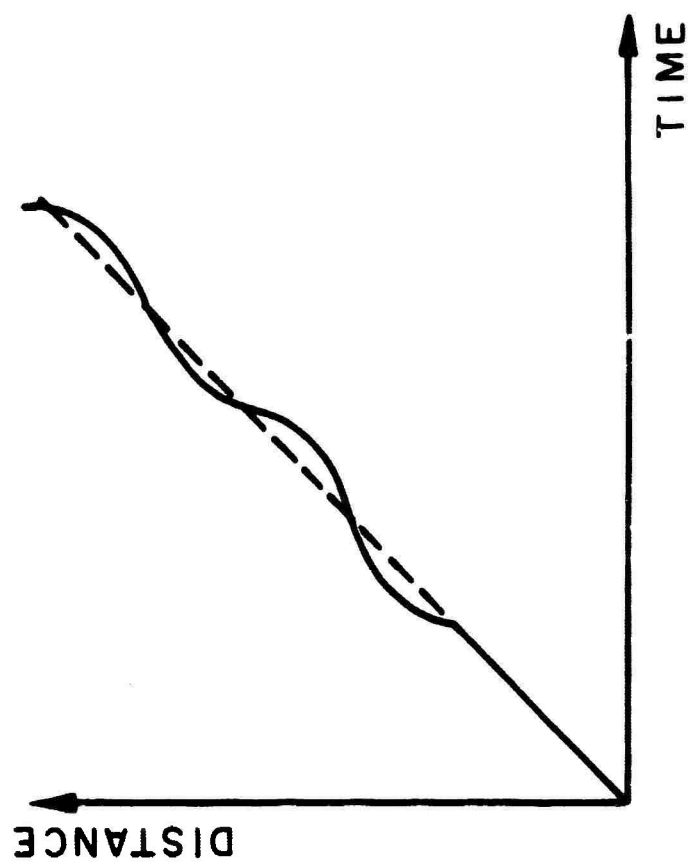


FIGURE 43

EXPERIMENT TO OBSERVE PARTICLE TRACK
IN PRODUCT GAS STREAM

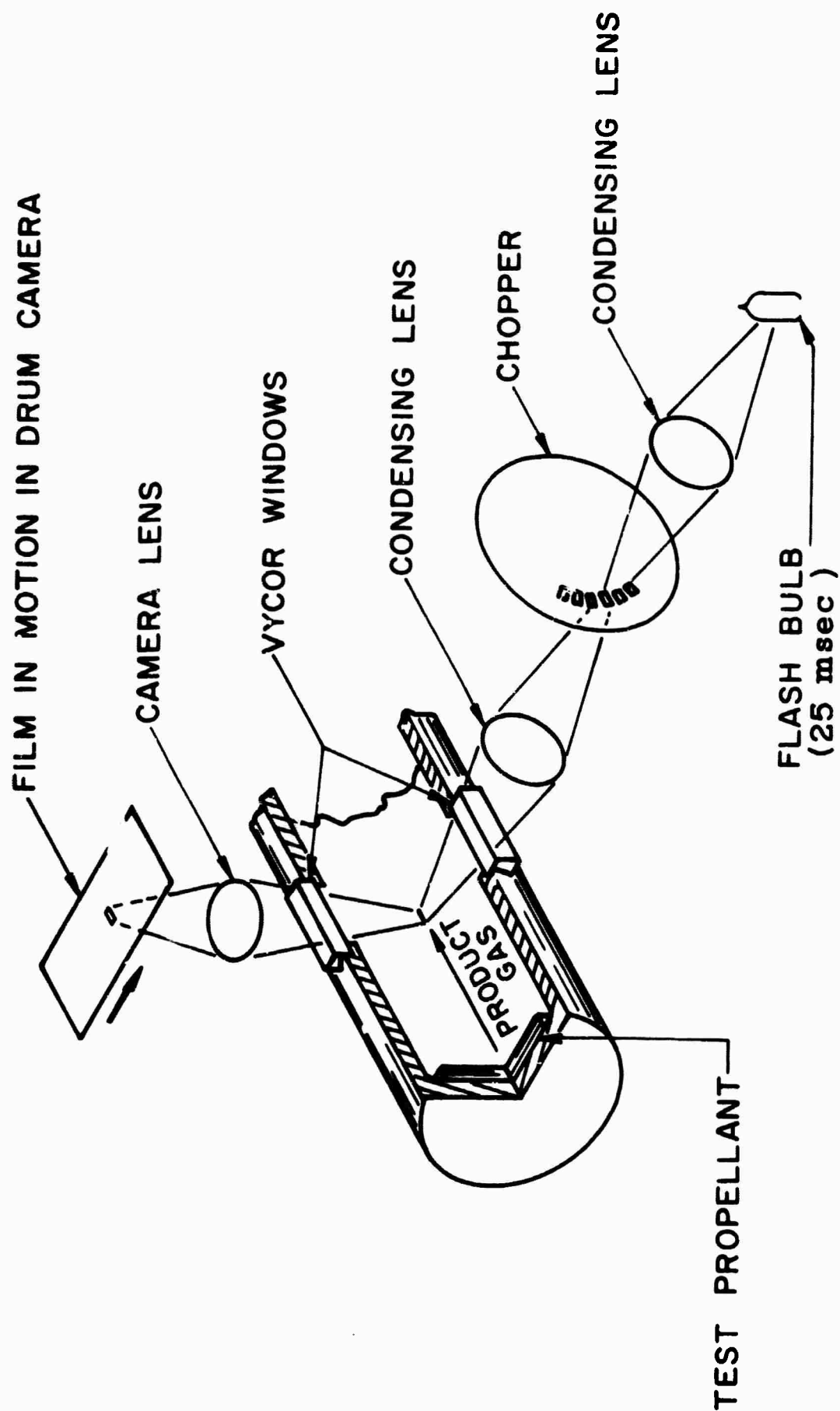


FIGURE 44

SIZE SELECTION CRITERION
FOR RELATIVE AMPLITUDE > 90 %

$$\frac{\omega}{a} < 0.5 \text{ OR}$$

$$\rho D^2 f < 8.8 \times 10^4 \text{ (D IN MICRONS)}$$

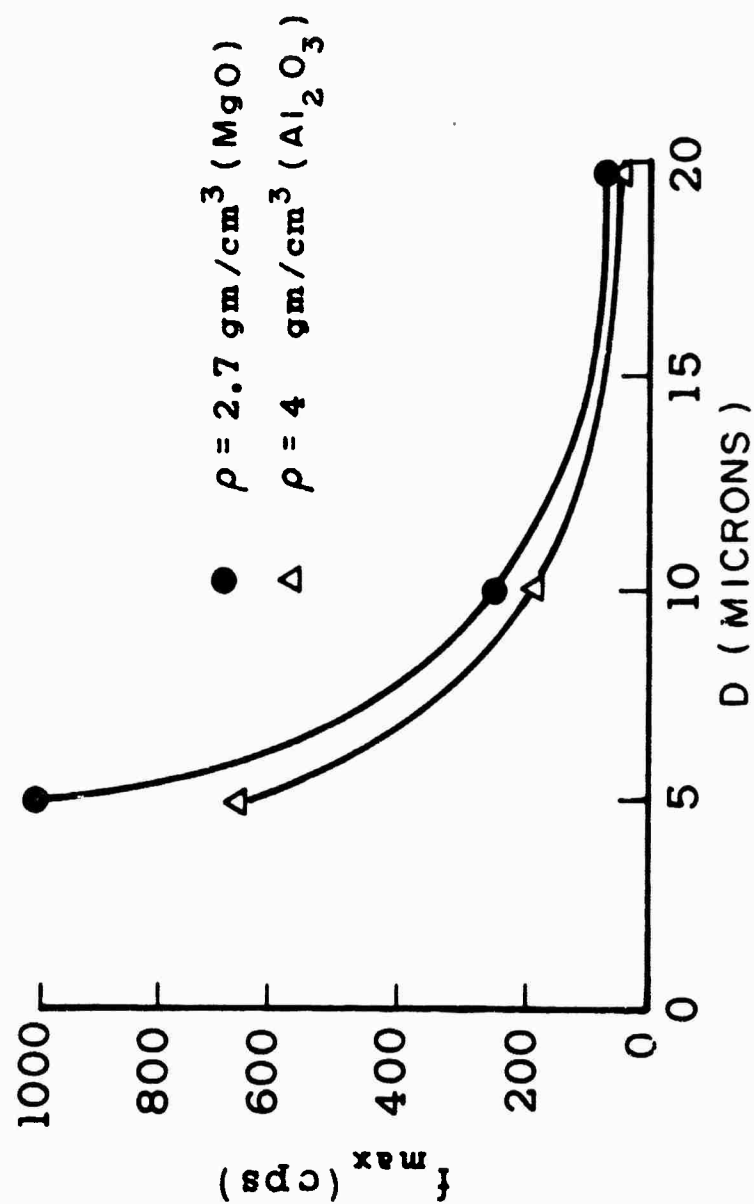
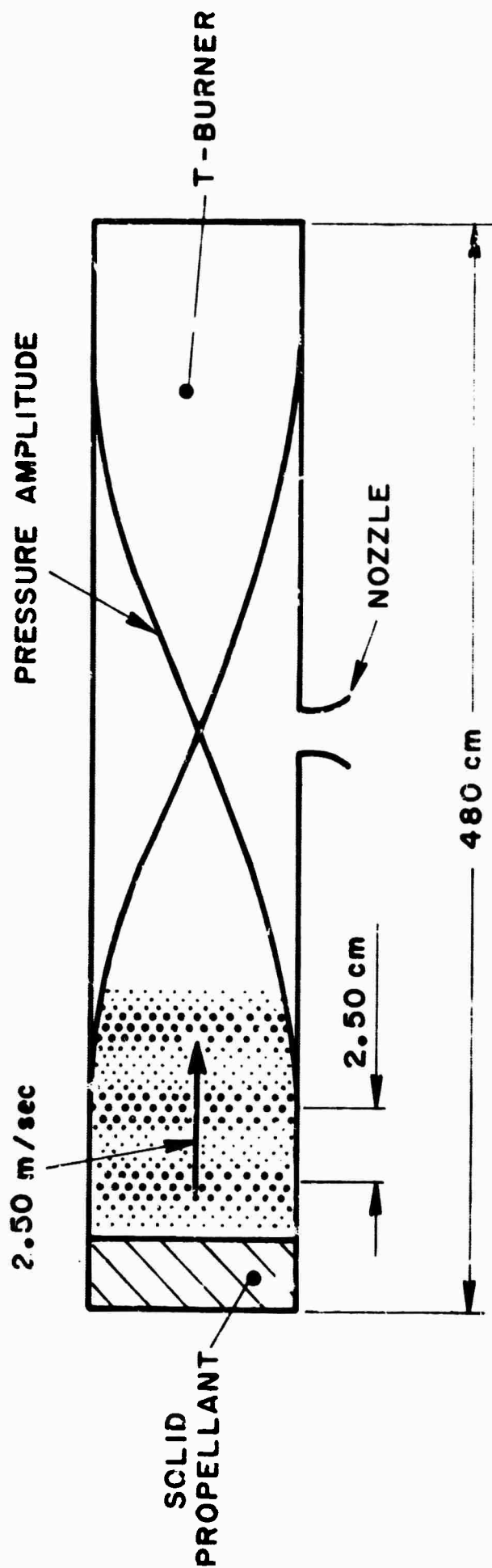


FIGURE 45

ENTROPY WAVE PROPERTIES IN AN ACOUSTIC FIELD



	ENTROPY WAVES	ACOUSTIC WAVES
FREQUENCY	100 cps	100 cps
VELOCITY	2.50 m/sec	960 m/sec
WAVE LENGTH	2.50 cm	960 cm

FIGURE 46

PRESSURE AND TEMPERATURE AS A FUNCTION OF
TIME FOR GAS PACKETS EMITTED FROM THE FLAME

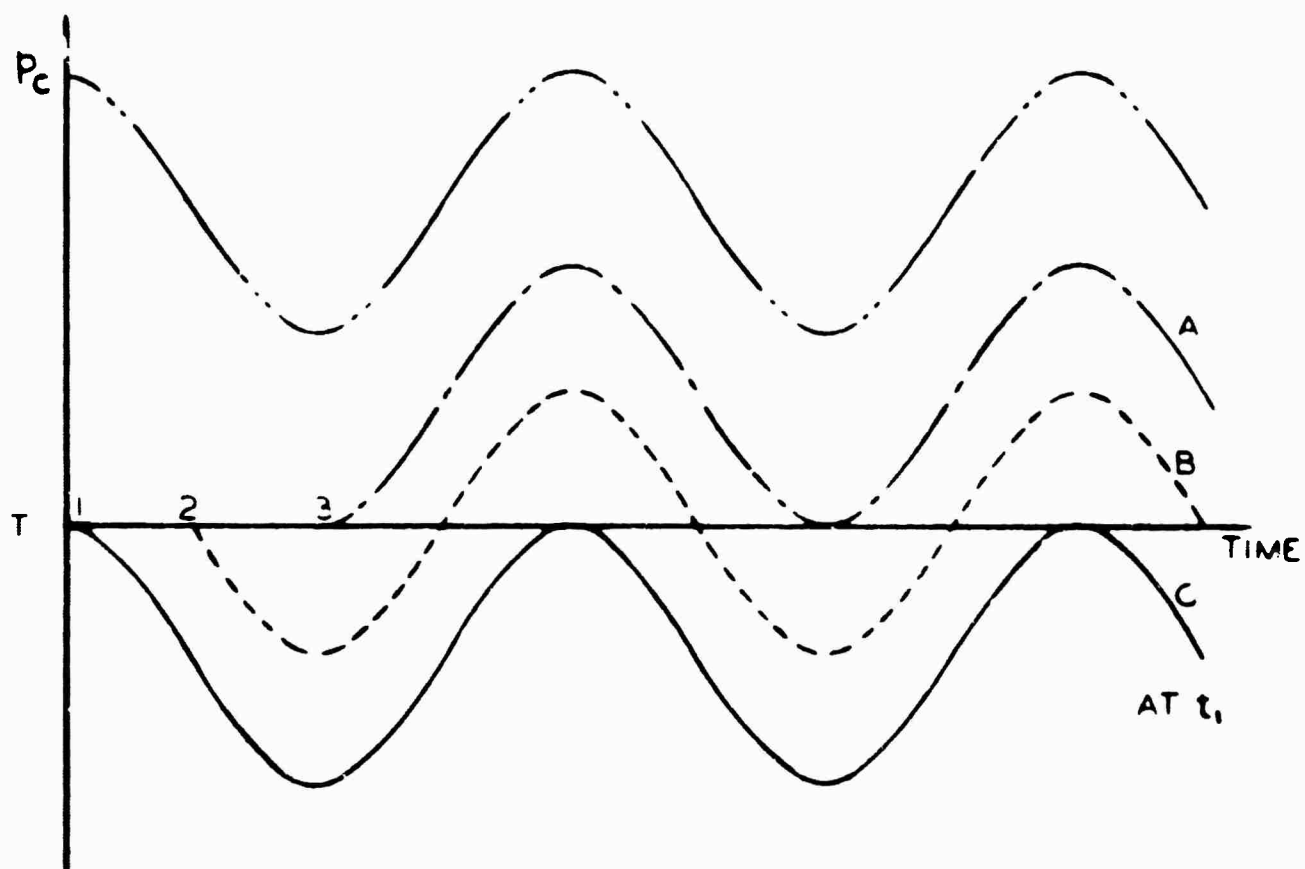


FIGURE 47

CROSS-SECTION OF T-BURNER

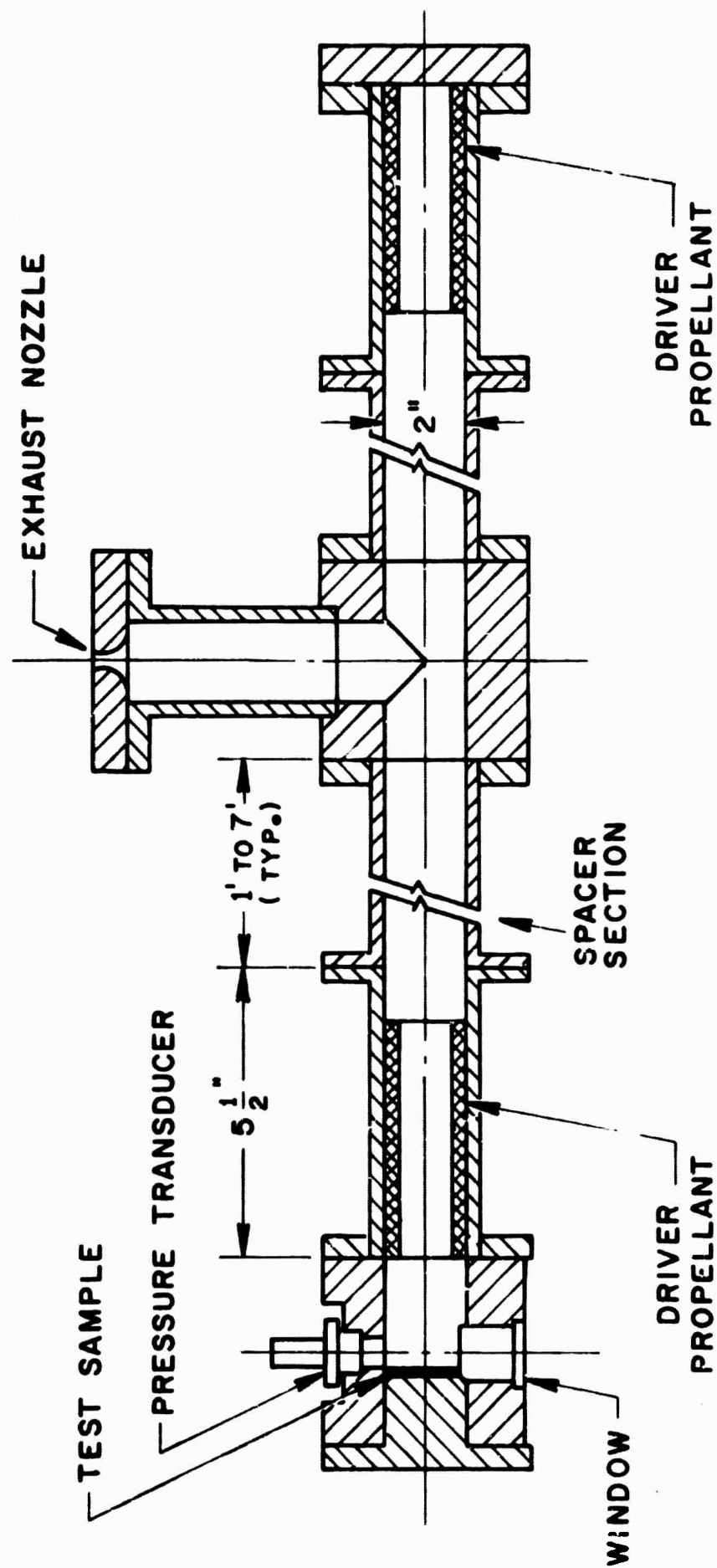
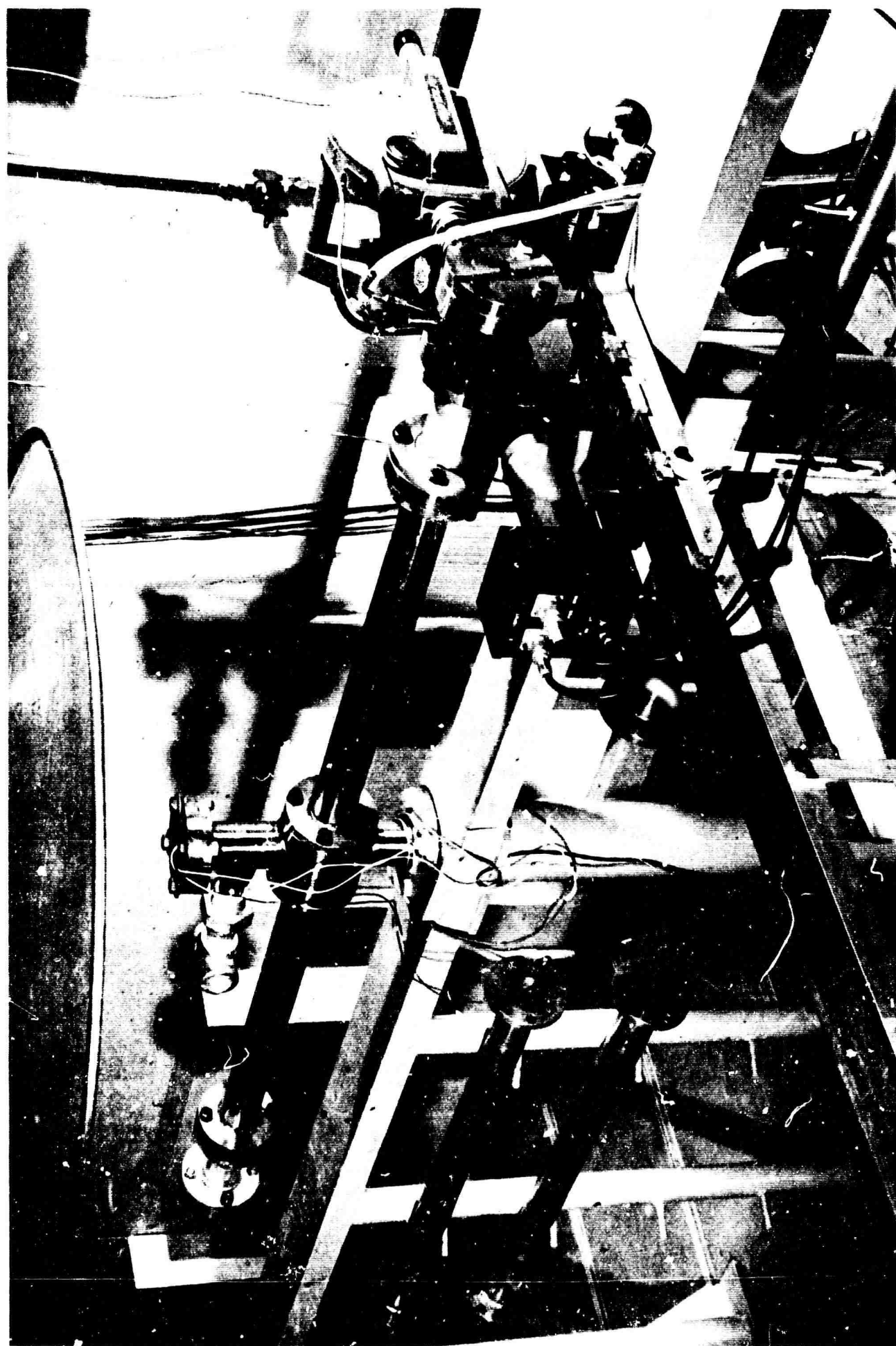
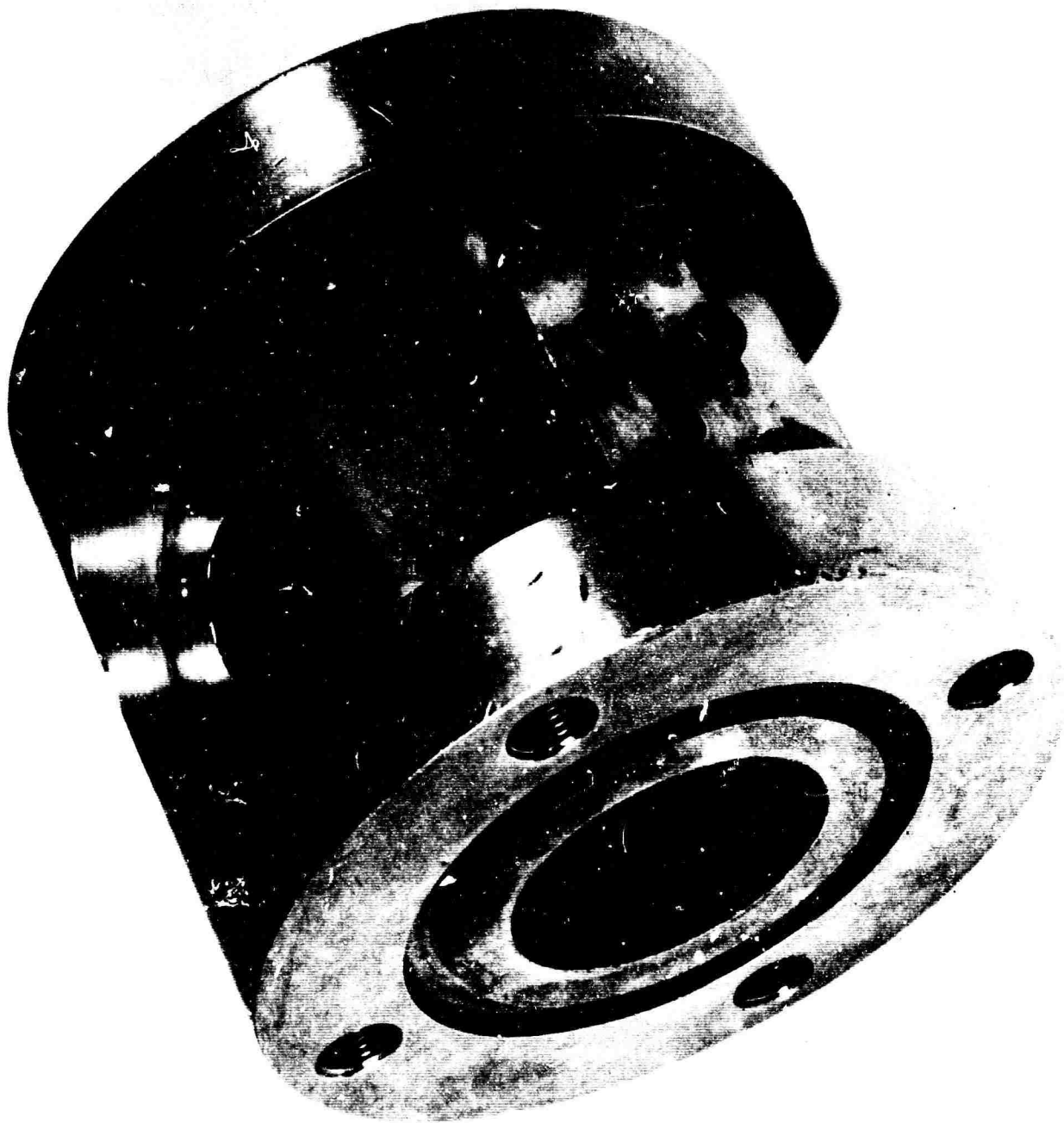


FIGURE 48



EXPERIMENTAL ARRANGEMENT FOR OBSERVATION OF TEMPERATURE WAVES
UNDER OSCILLATING PRESSURE IN T-BURNER



T-BURNER TEST SECTION



SAMPLE HOLDER

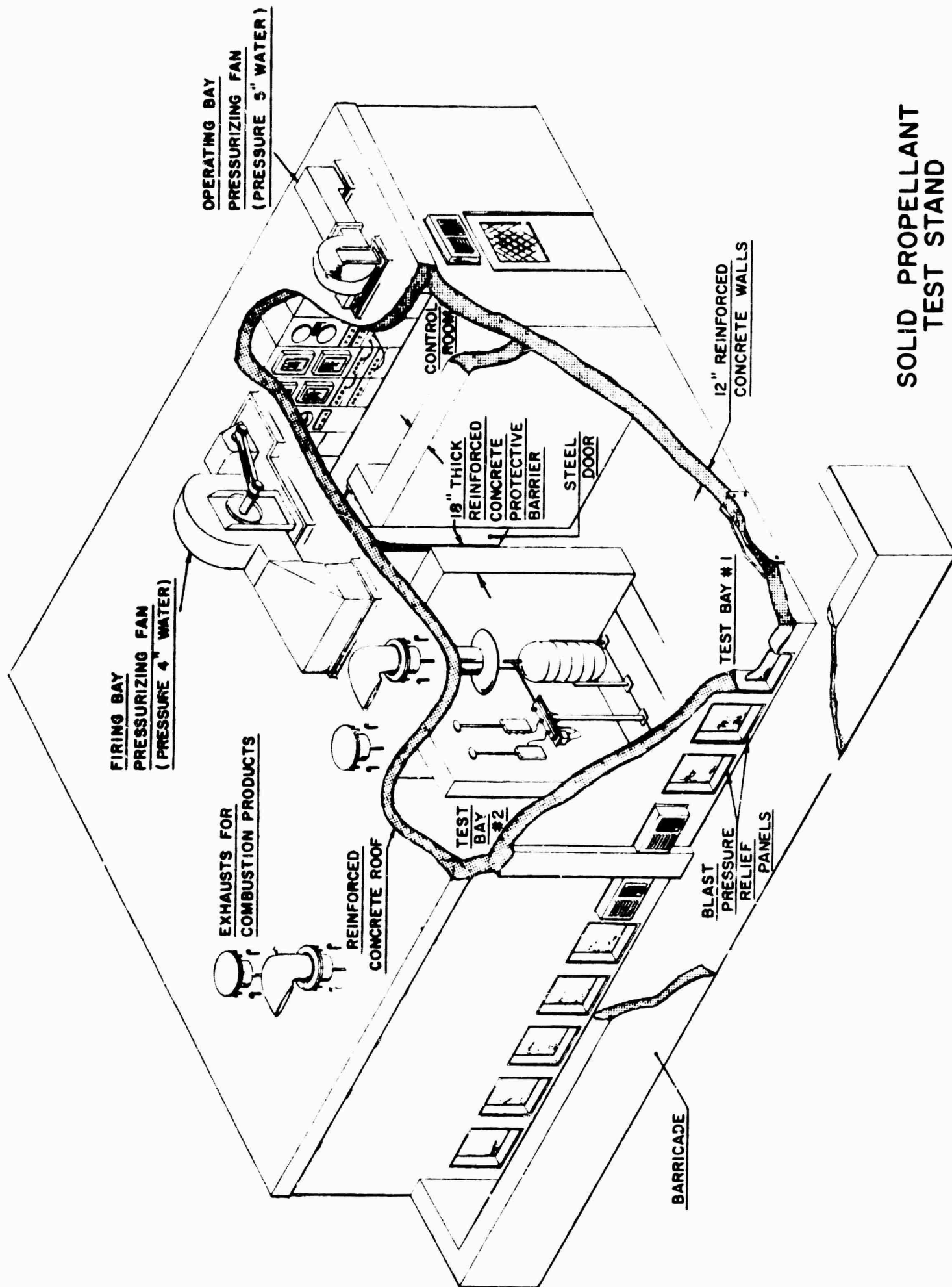
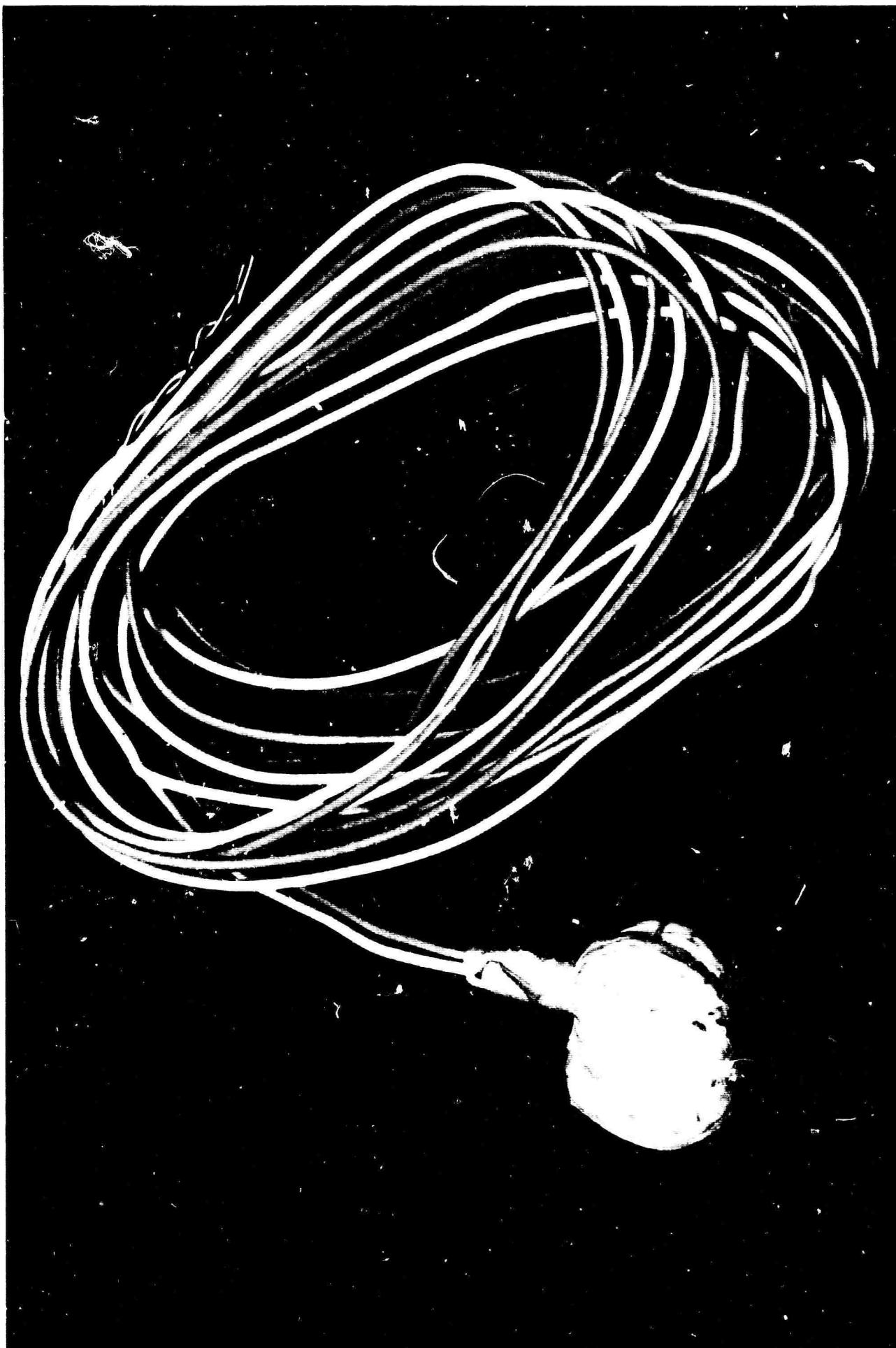


FIGURE 52



ASSEMBLED IGNITOR

FIGURE 53



IGNITOR COMPONENTS PRIOR TO ASSEMBLY

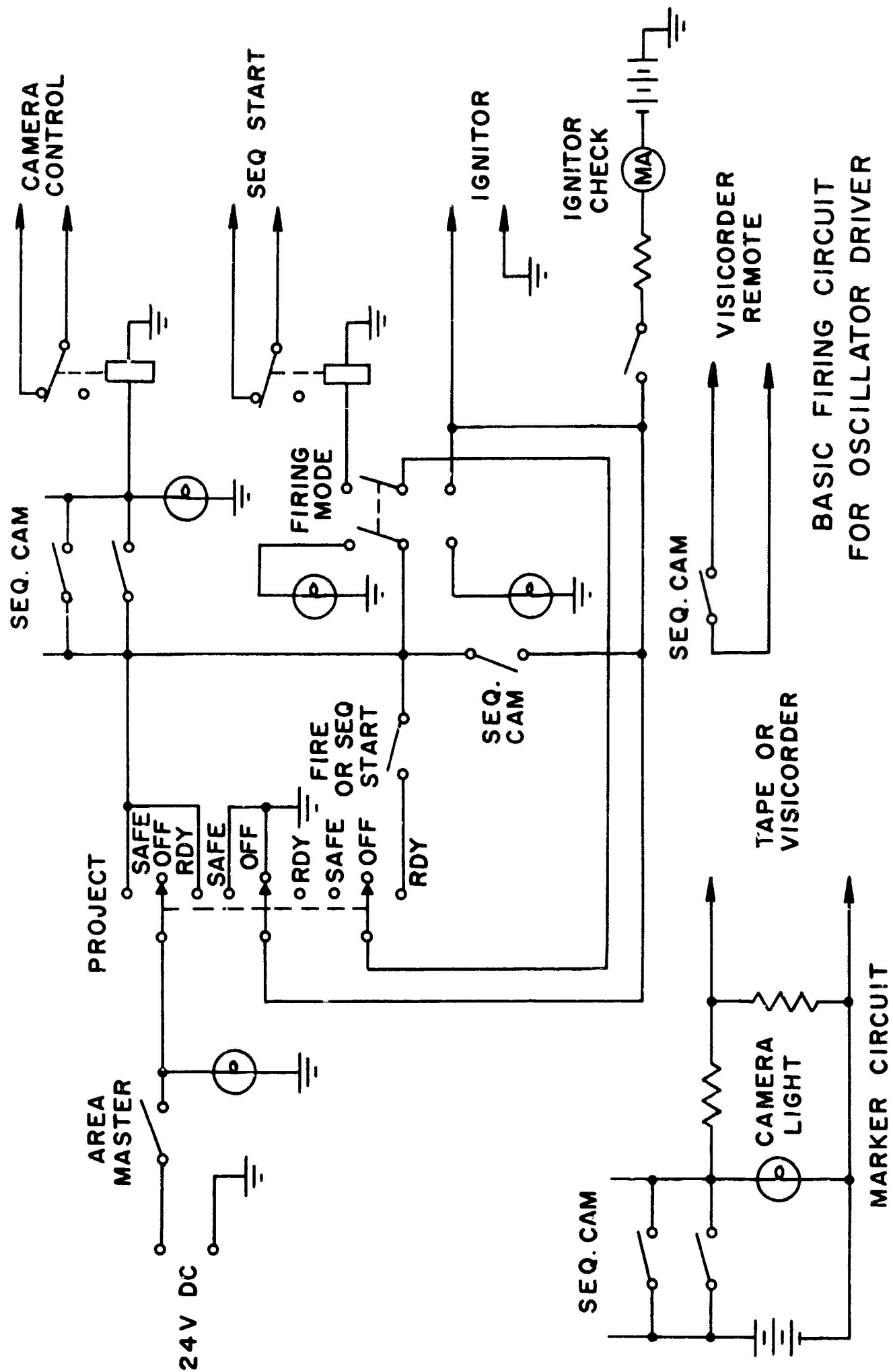
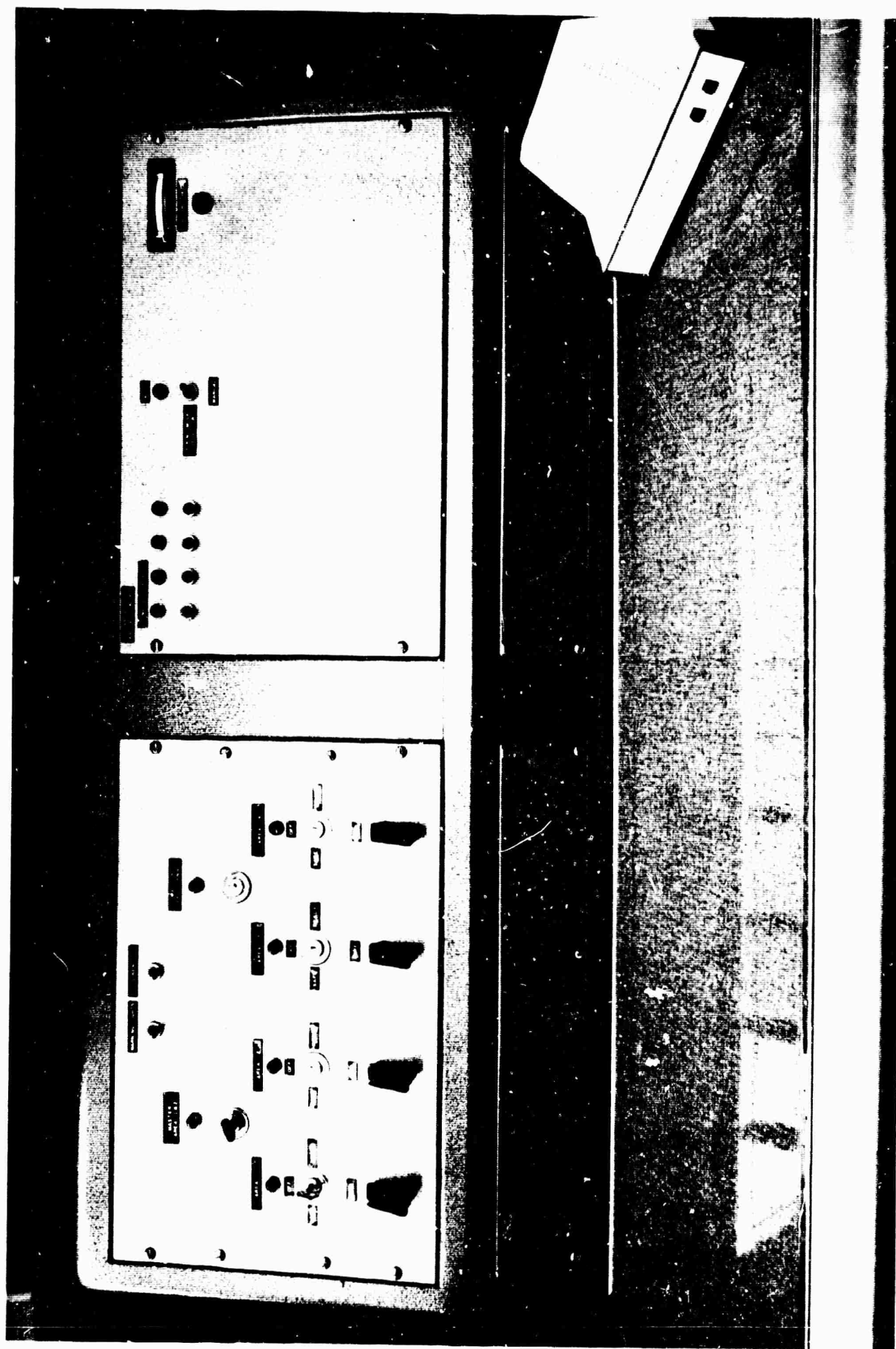
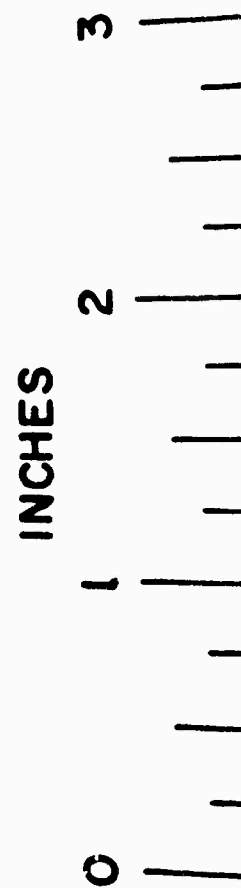


FIGURE 55

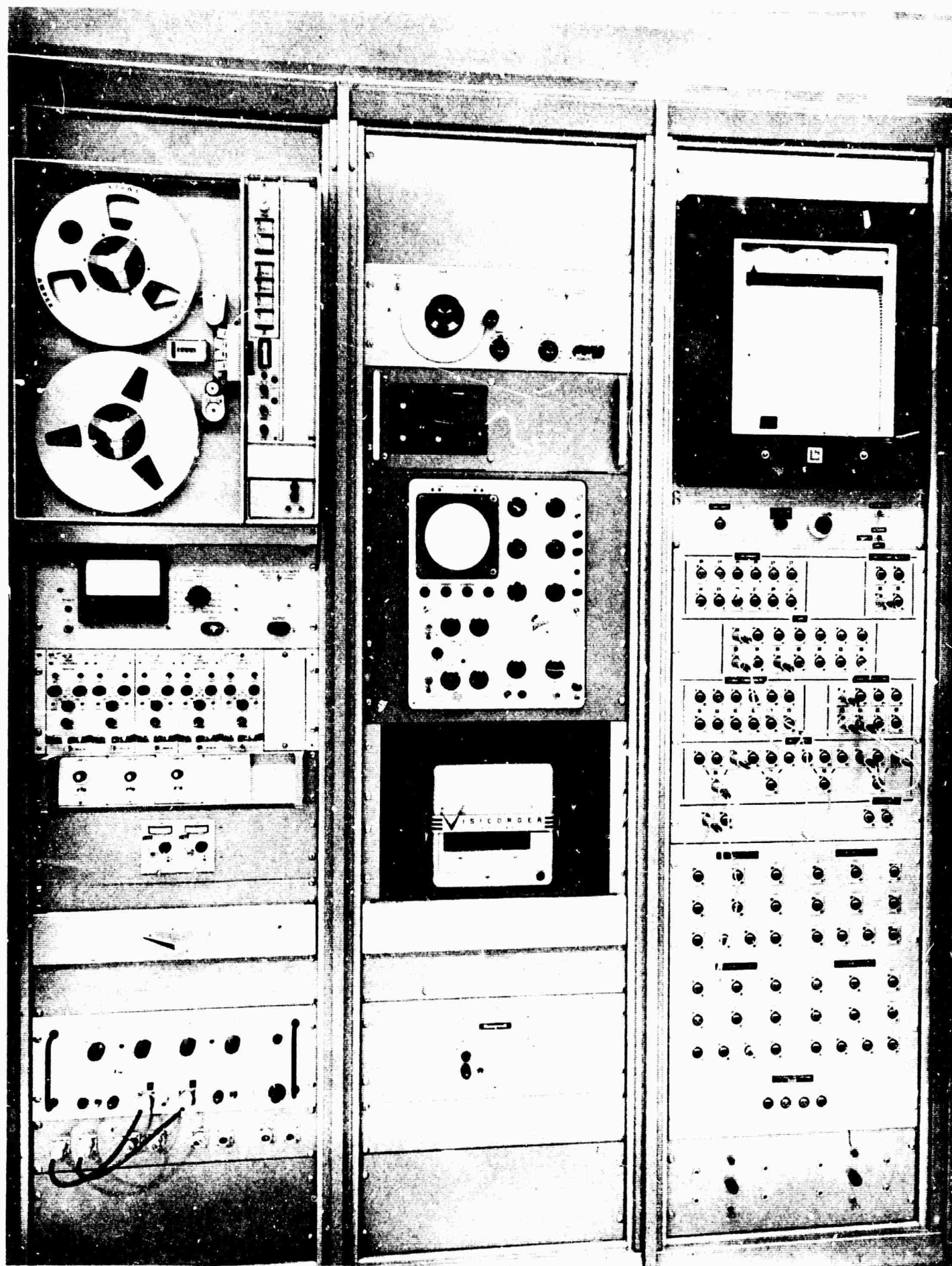
JP 23-PH-65



CONTROL PANEL



DYNISCO PRESSURE TRANSDUCERS



INSTRUMENTATION PANEL

FIGURE 58

JP23-P20-65

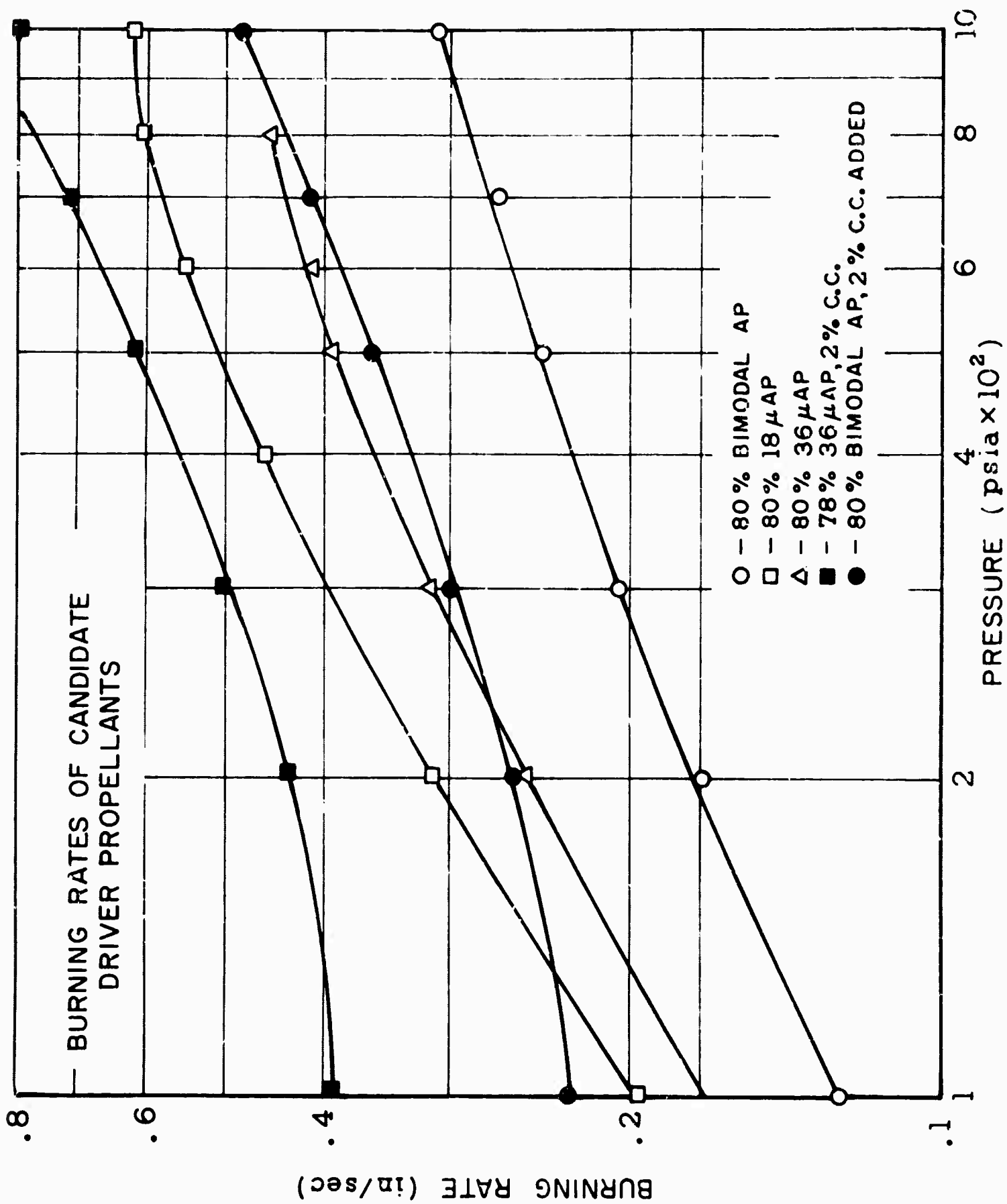


FIGURE 59

OPERATING CHARACTERISTICS OF T-MOTOR AT 430 CPS
WITH DRIVER CONTAINING 80% B.M. AP, 20% PBAA,
(2 % COPPER CHROMITE ADDED)

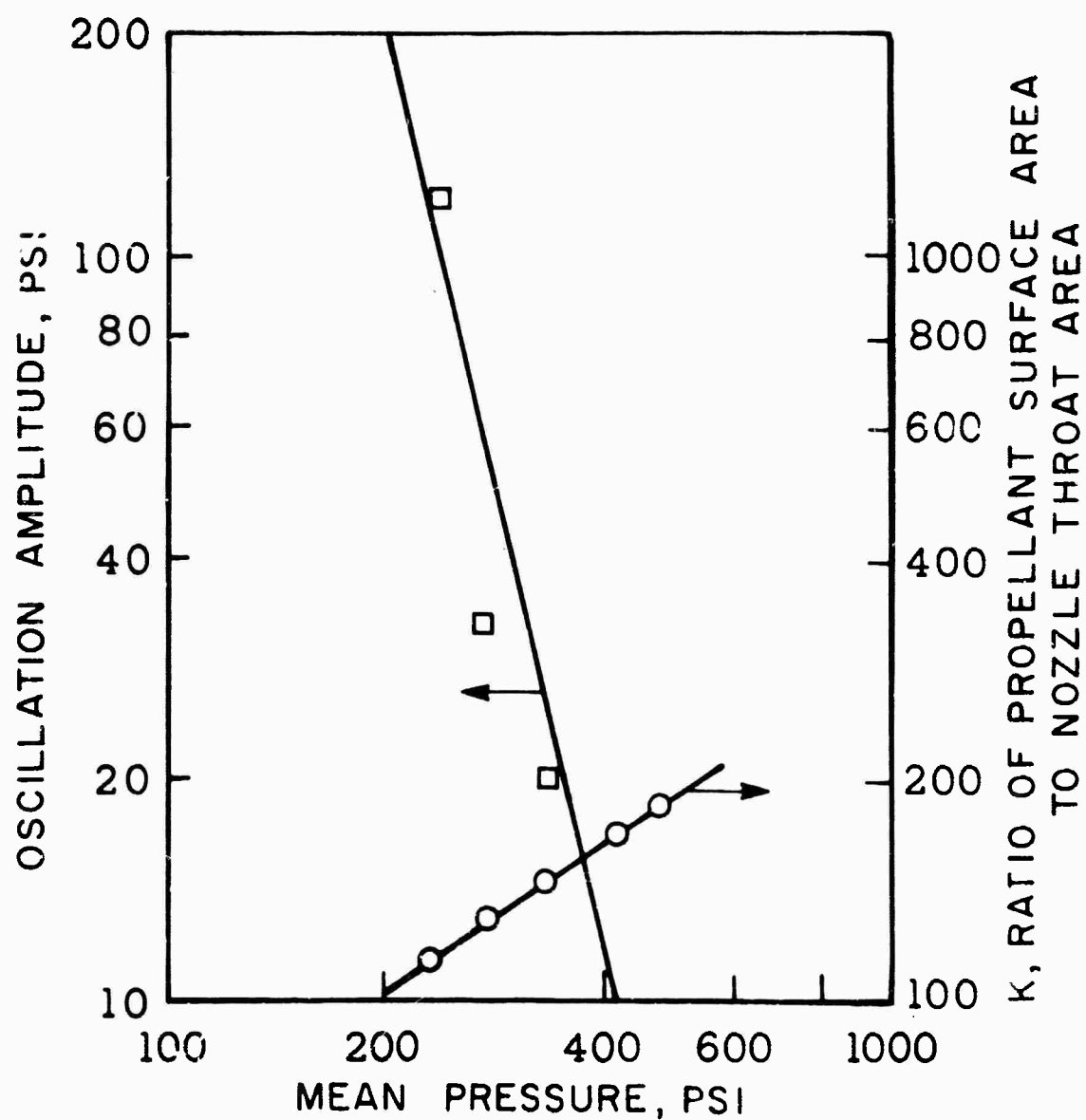


FIGURE 60

OPERATING CHARACTERISTICS OF T-MOTOR AT 270 CPS
WITH DRIVER CONTAINING 80% B.M. AP, 20% PBAA,
(2 % COPPER CHROMITE ADDED)

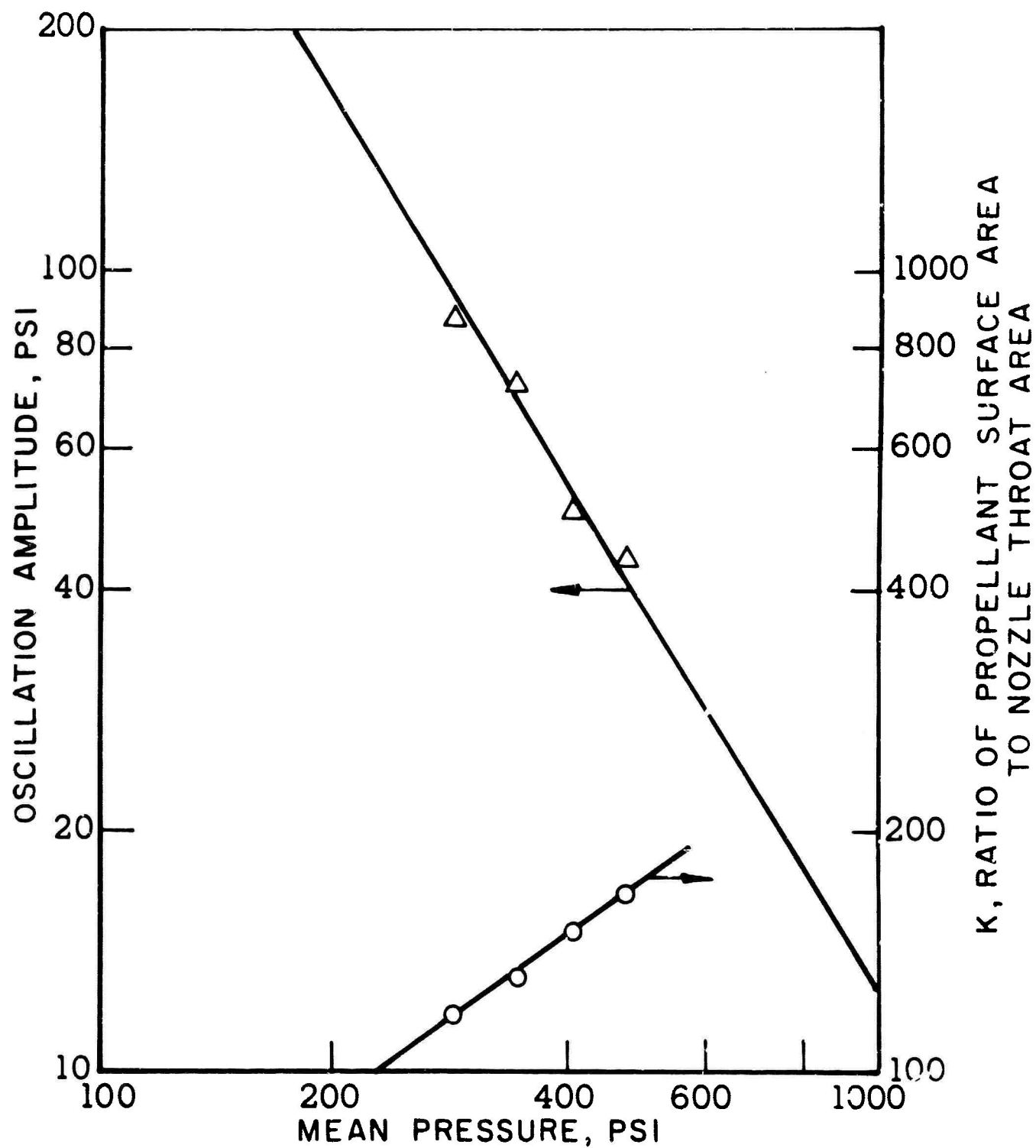


FIGURE 61

LP-3 BURNING RATE

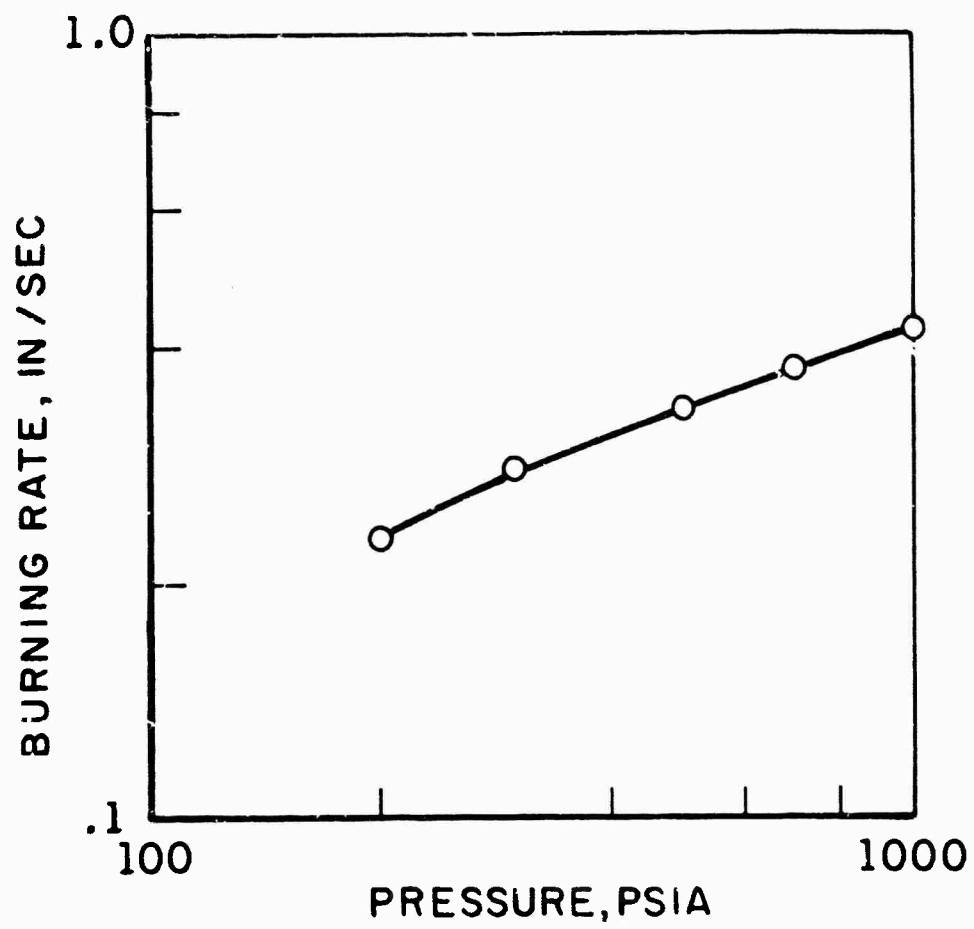


FIGURE 62

OPERATING CHARACTERISTICS OF T-MOTOR AT 430 CPS
WITH DRIVER CONTAINING 80% B.M. AP, 20% LP-3

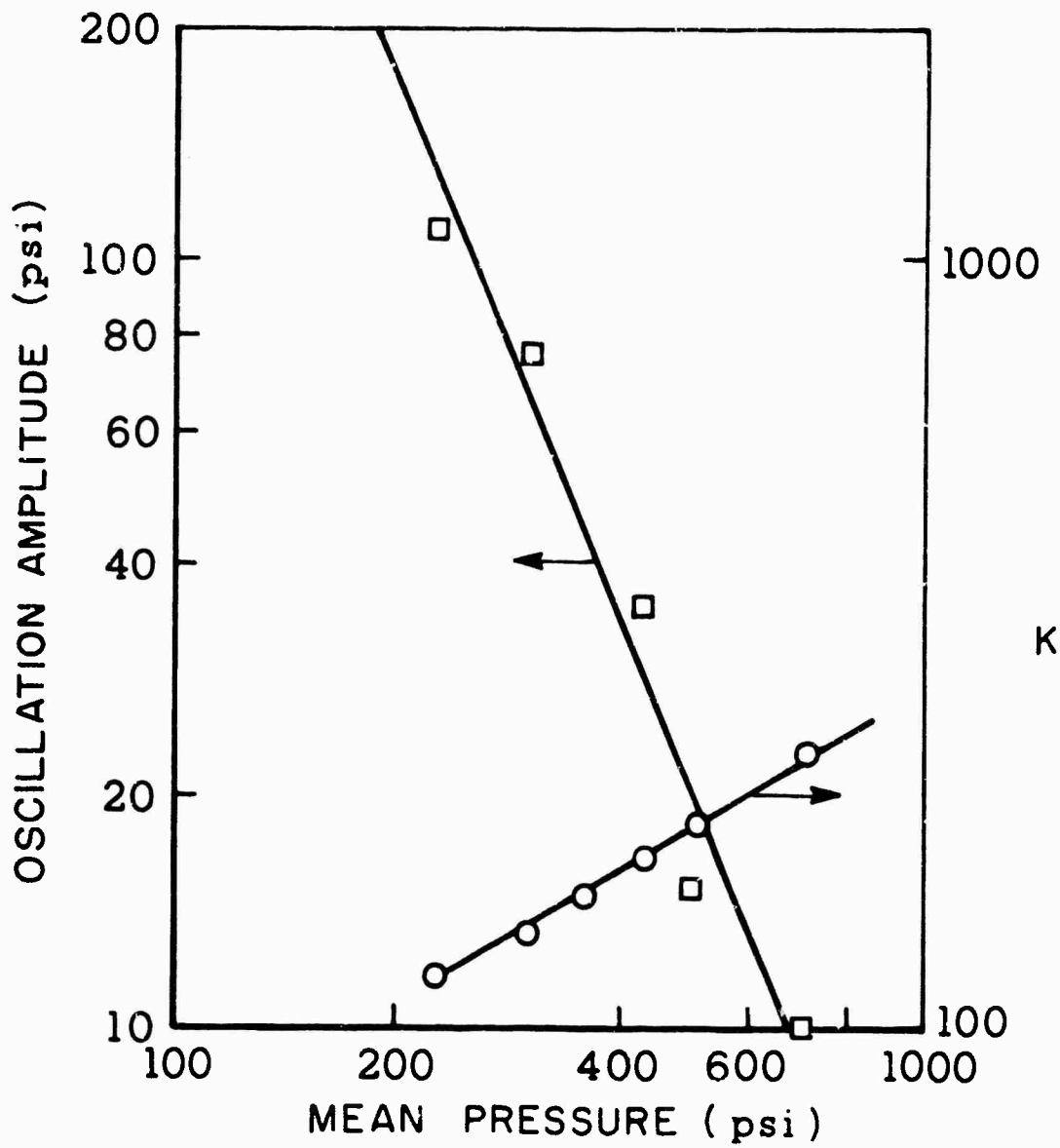


FIGURE 63

BURNING RATE vs PRESSURE FOR PROPELLANT
CONTAINING 85% TRIMODAL AP, 15% POLYURETHANE

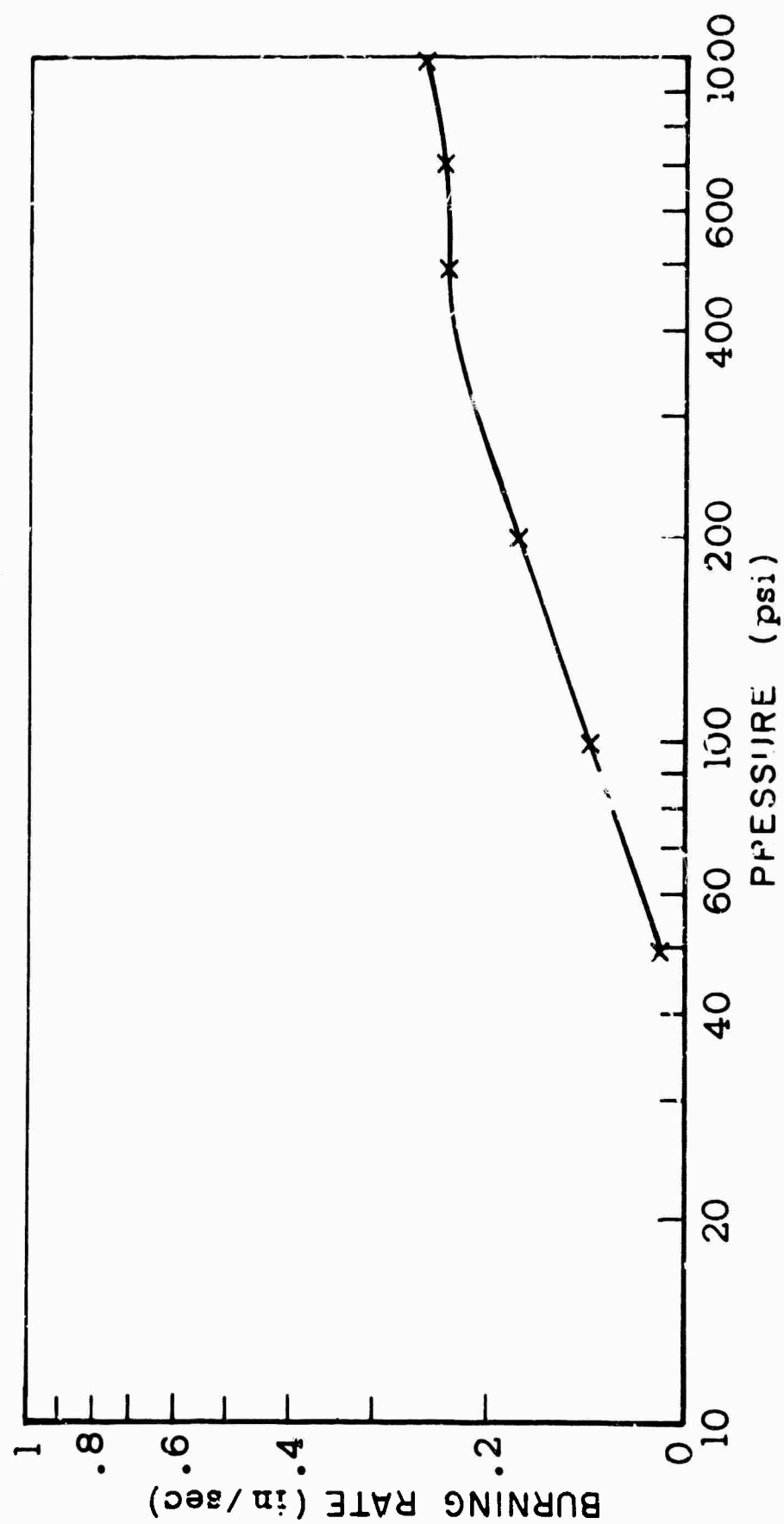


FIGURE 64

OPERATING CHARACTERISTICS OF T-MOTOR
WITH DRIVER CONTAINING 85% TRIMODAL AP,
15% POLYURETHANE

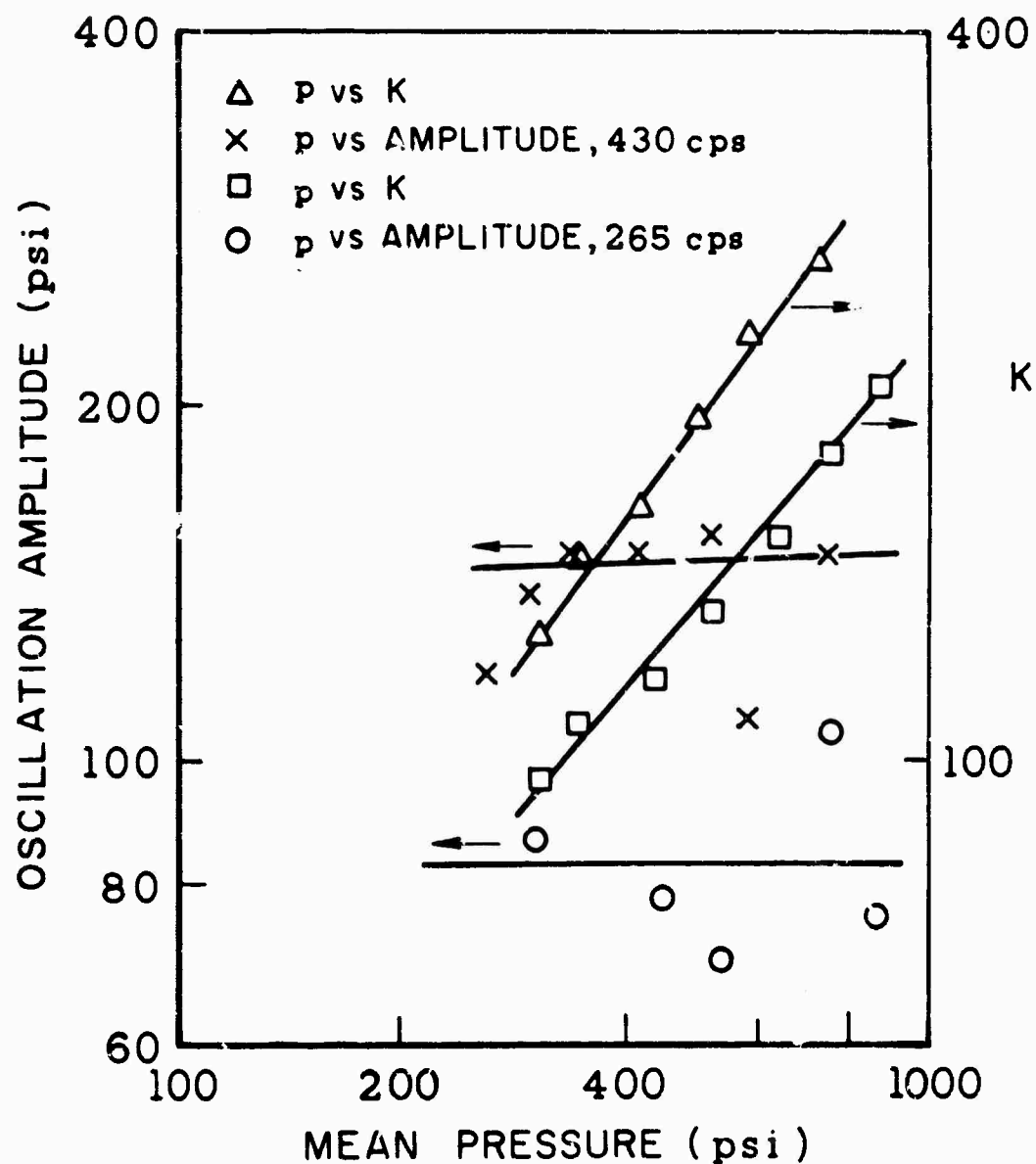


FIGURE 65

EFFECT OF MEAN PRESSURE AND FREQUENCY ON PRESSURE WAVE FORM IN T-BURNER



P=1150 psi
f=265 cps



P=1060 psi
f=190 cps



P=720 psi
f=265 cps



P=310 psi
f=150 cps



P=330 psi
f=265 cps



P=290 psi
f=105 cps



P=270 psi
f=190 cps



P=450 psi
f=77 cps

FIGURE 66

EFFECT OF SPACER LENGTH ON OSCILLATION AMPLITUDE
(AUP 85T, $\bar{p} = 900$, 3 FOOT EXTENSIONS)

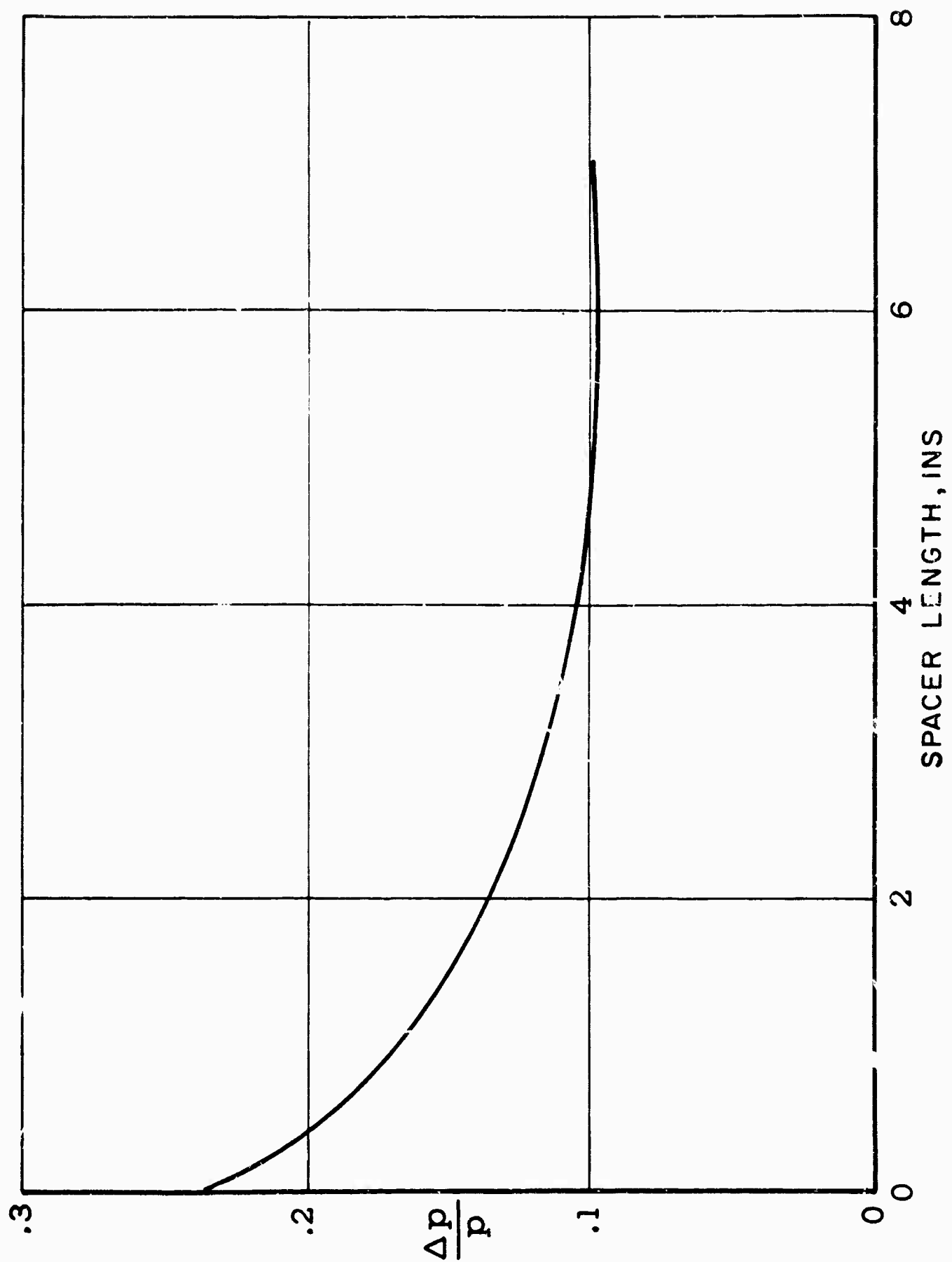


FIGURE 67

EFFECT OF DRIVER GRAIN LENGTH
ON OSCILLATION AMPLITUDE
(AUP 85T, $\bar{p} = 350$ psi, $f = 435$ cps)

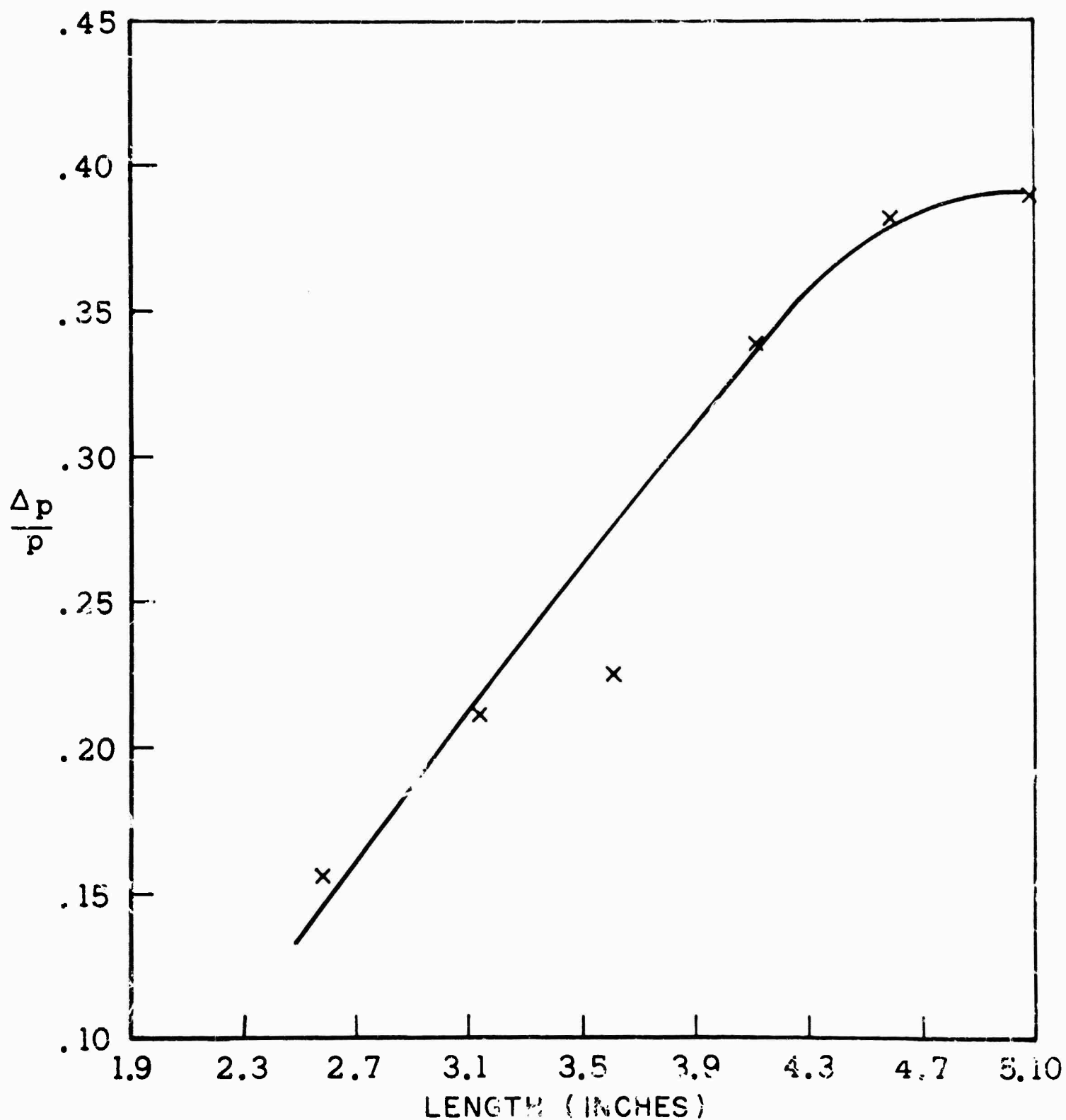
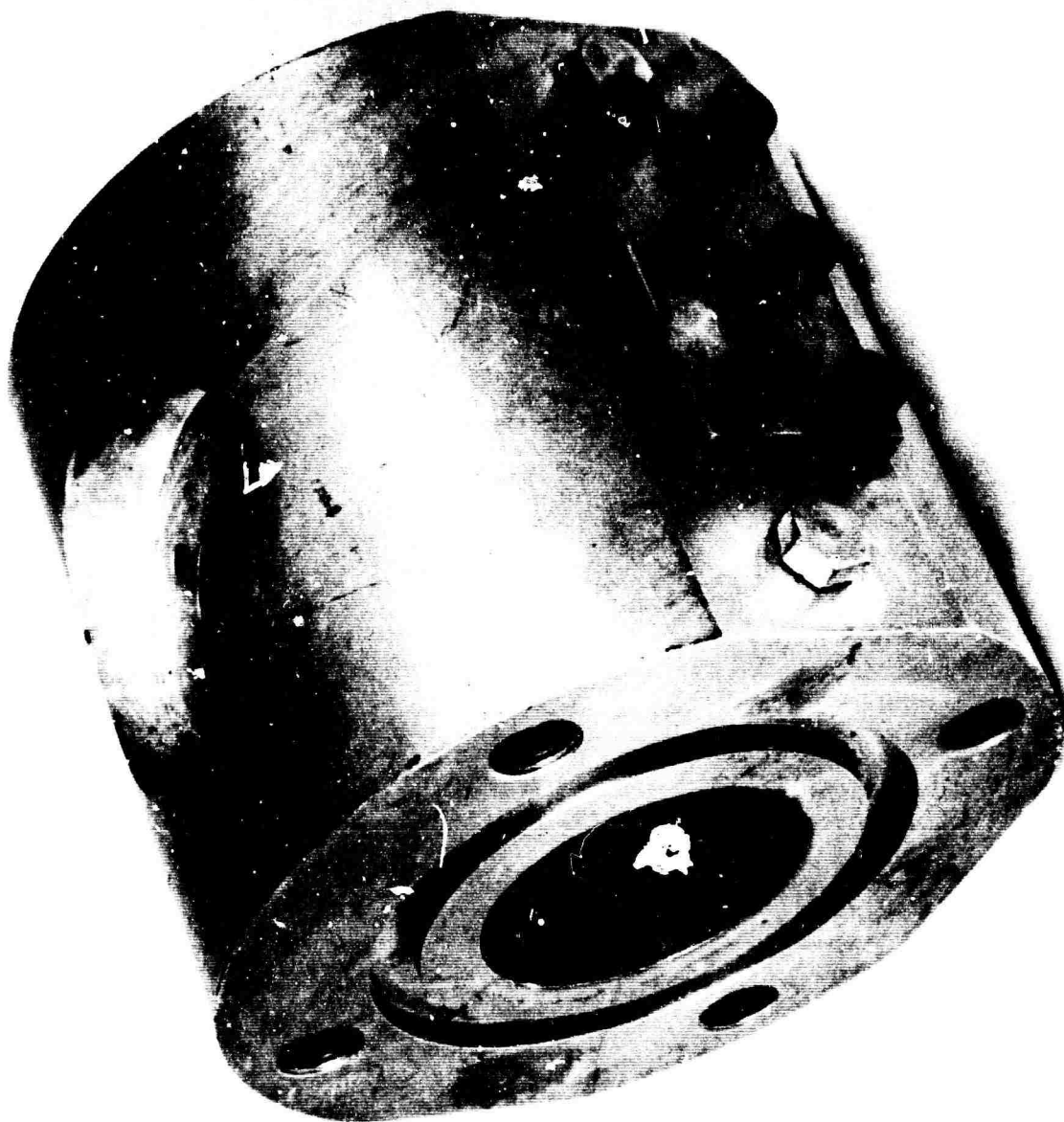
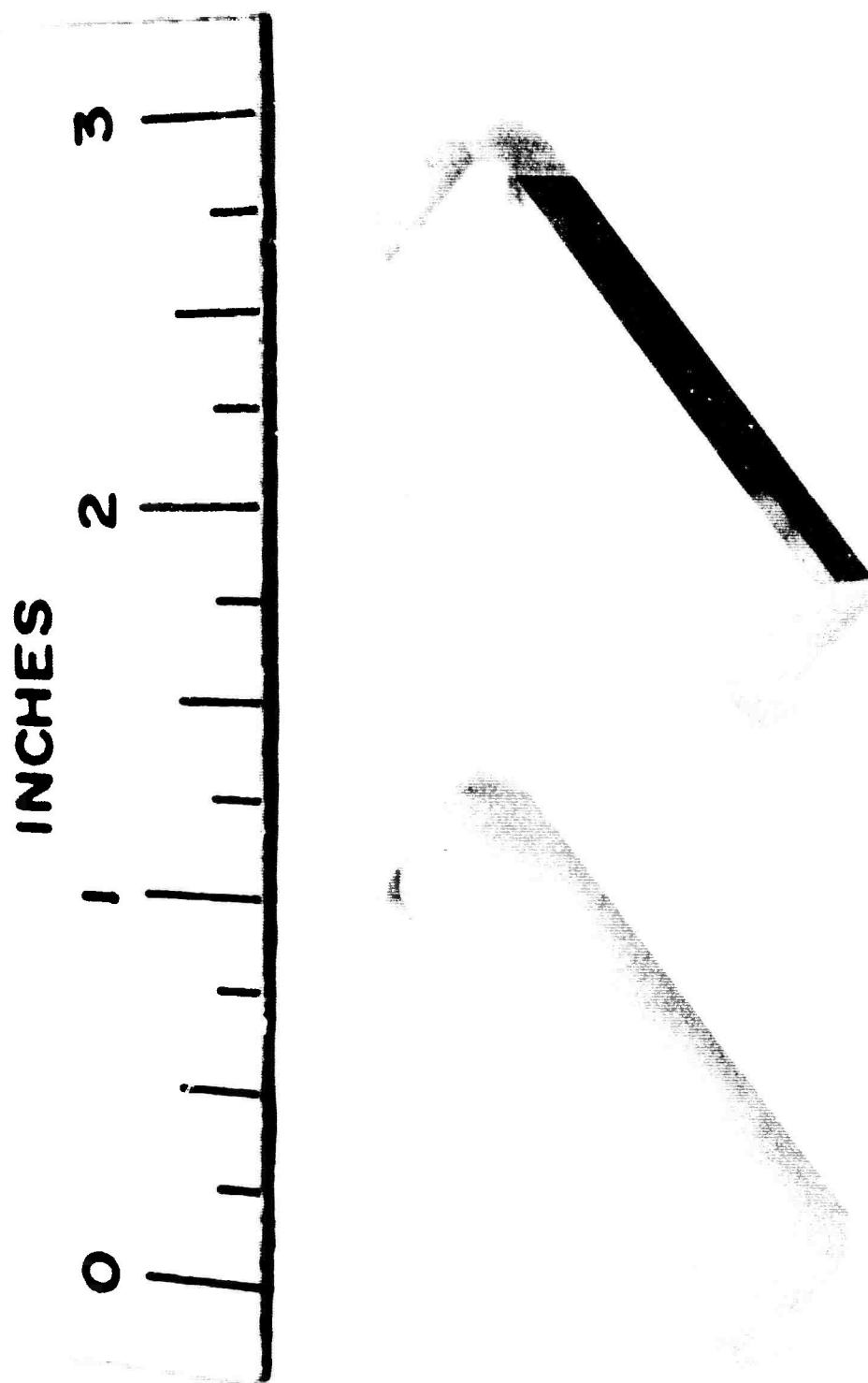


FIGURE 68



ORIGINAL TEST SECTION



COMPARISON OF NEW AND OLD WINDOWS
(NEW ON LEFT)

OPTICAL SYSTEM FOR OBTAINING SODIUM LINE WIDTH OF BURNING SOLID PROPELLANT

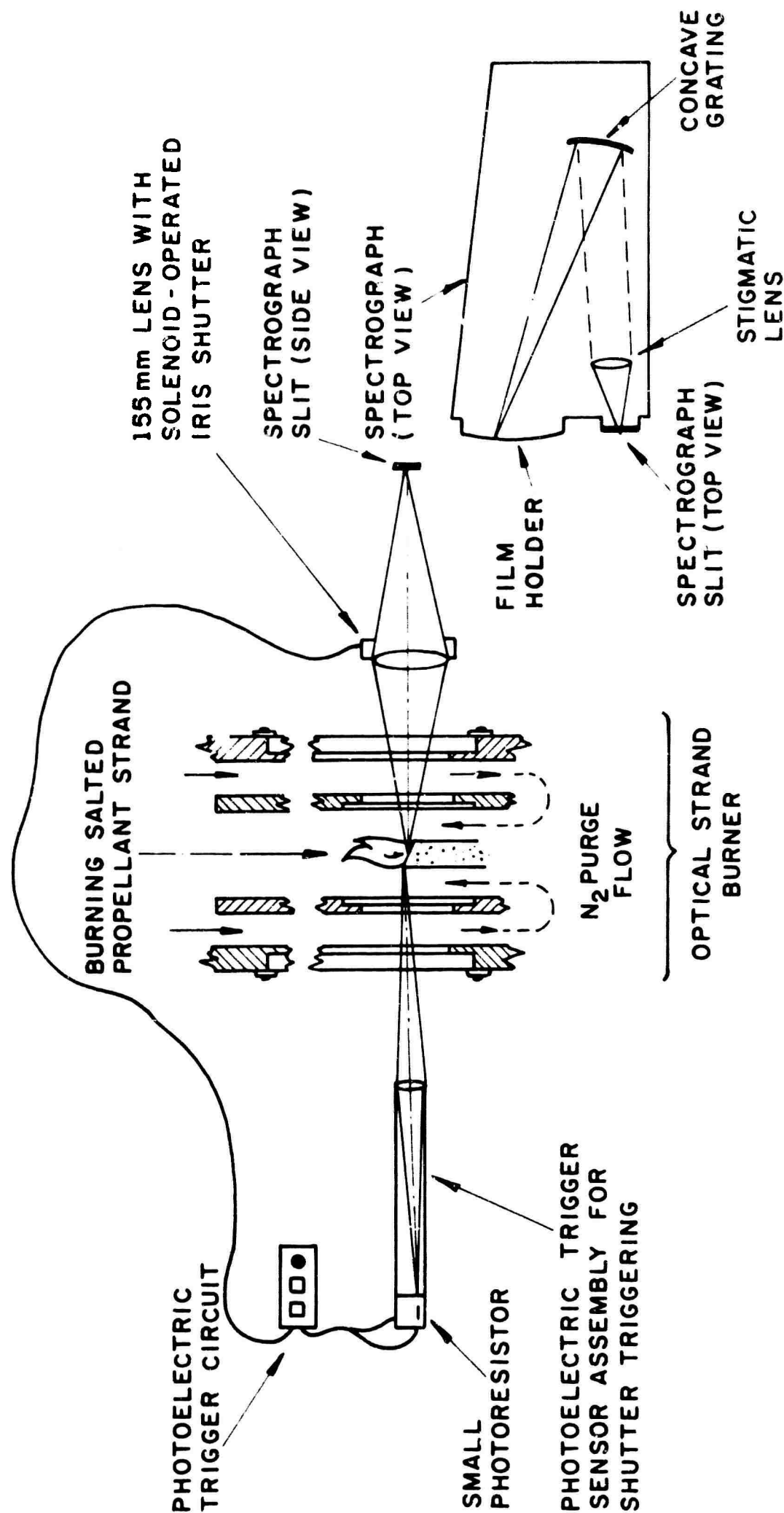
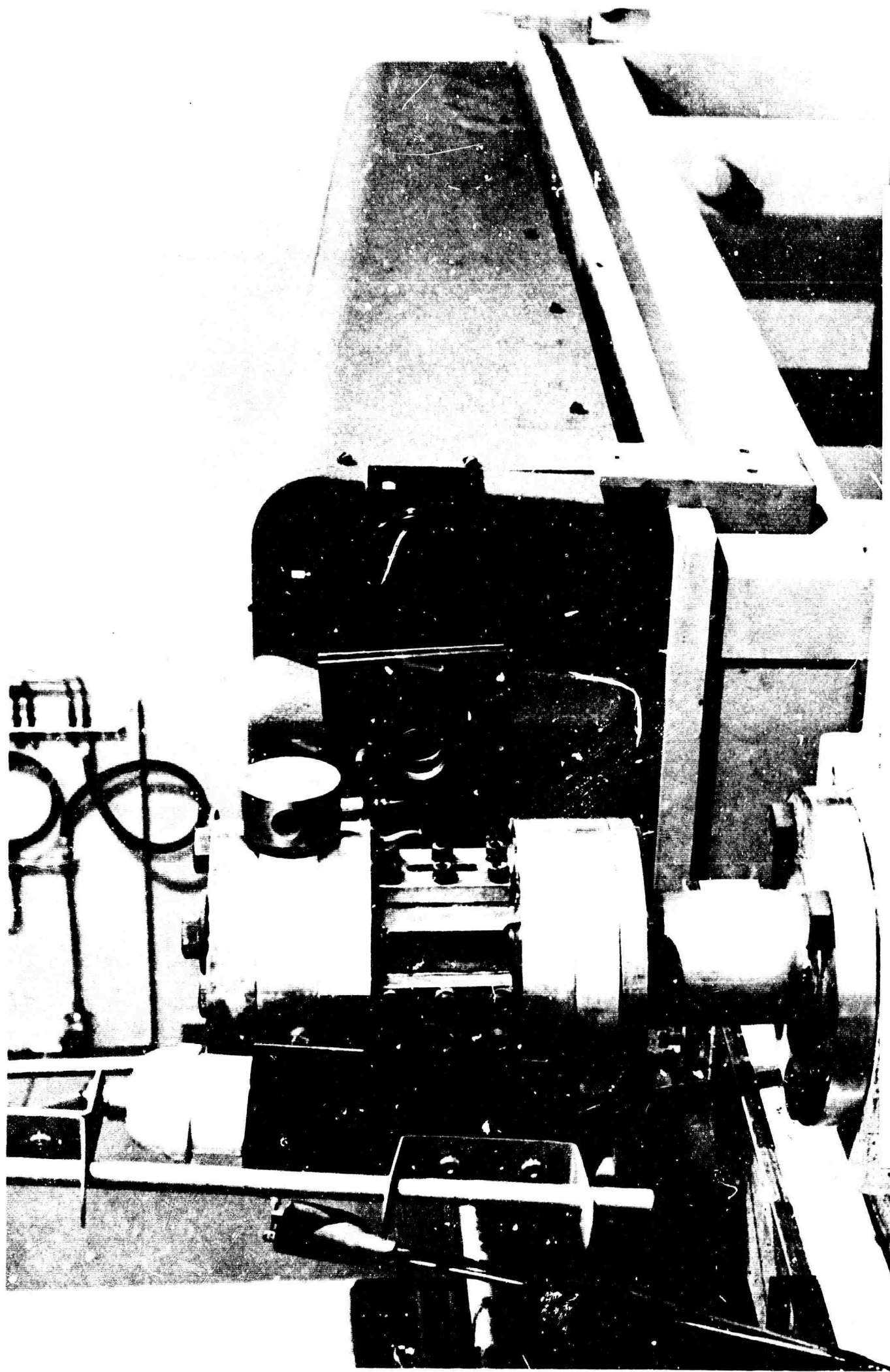
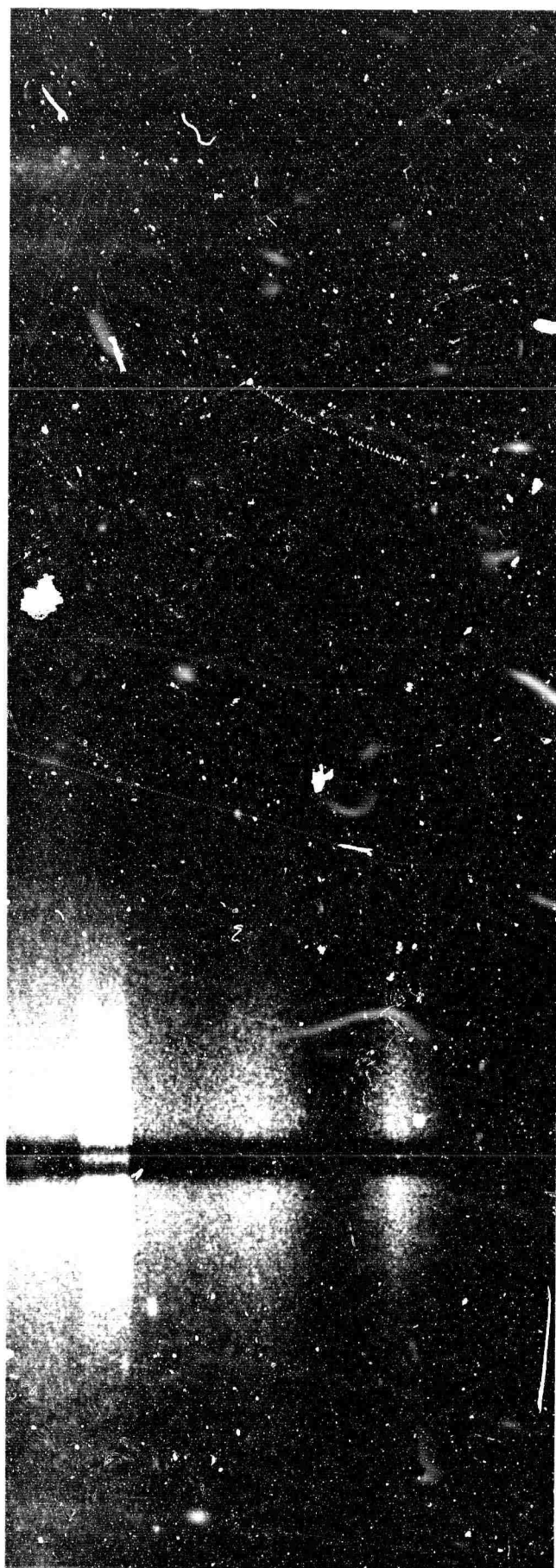


FIGURE 71

JP23-P2465



EXPERIMENTAL APPARATUS FOR OBTAINING SPECTRUM OF
PROPELLANT BURNING IN TEST SECTION



↑
SELF-REVERSED SODIUM D LINES

WAVELENGTH →

SPECTRUM OF PROPELLANT COMBUSTION GASES WITH
FILTERED RADIATION FROM TUNGSTEN LAMP SUPERIMPOSED

FIGURE 73

BLANK PAGE

PHOTOMETRIC TEMPERATURE MEASURING APPARATUS

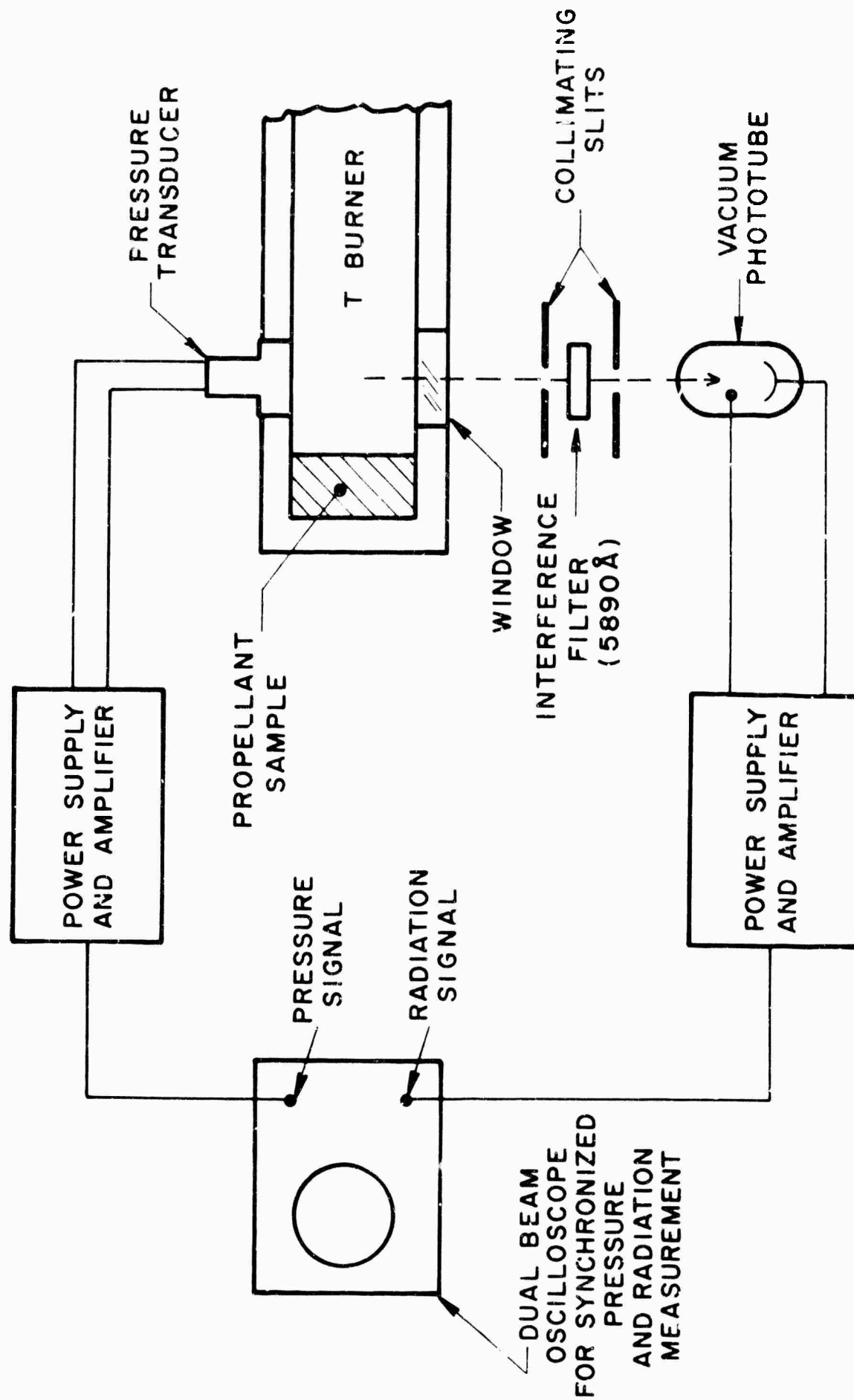


FIGURE 74

PHOTOMULTIPLIER CIRCUIT

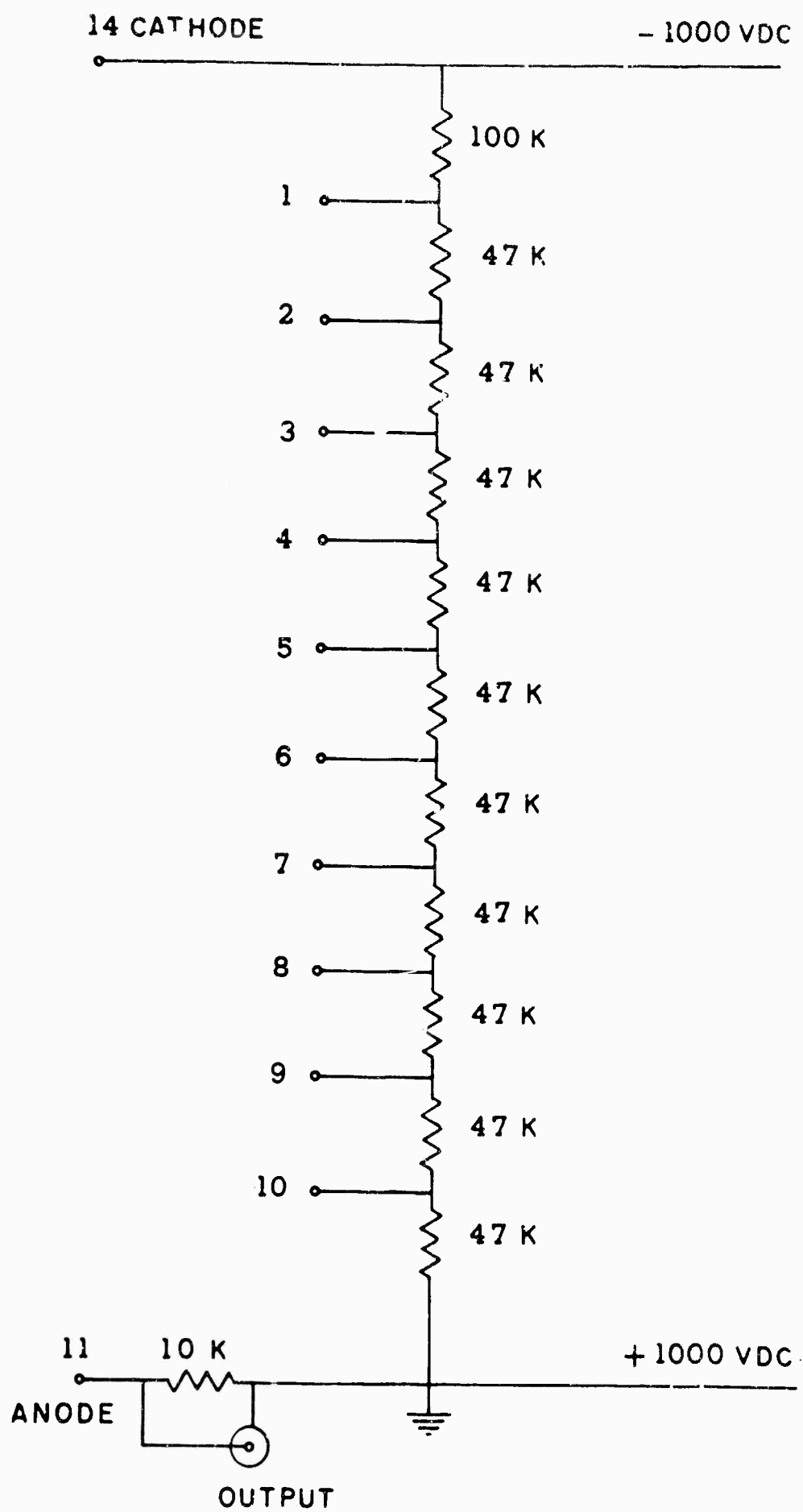


FIGURE 75

JP23-R4022-6J

BRIGHTNESS TEMPERATURE vs CURRENT FOR
18A/T10/2P-6V BULB
(BULB OUT OF TEST SECTION)

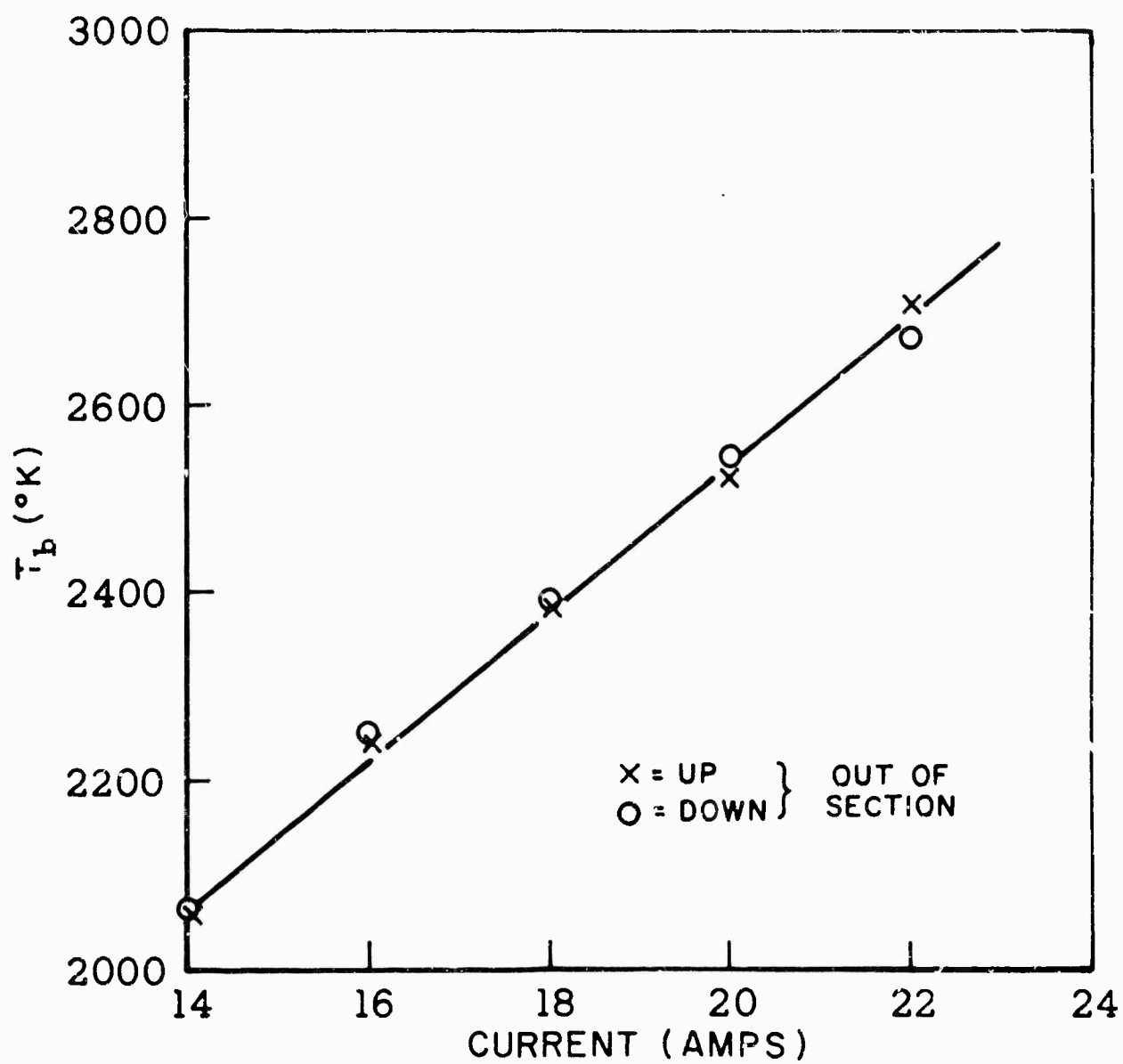


FIGURE 76

BRIGHTNESS TEMPERATURE vs CURRENT FOR
18A/T10/2P-6V BULB
(BULB IN TEST SECTION)

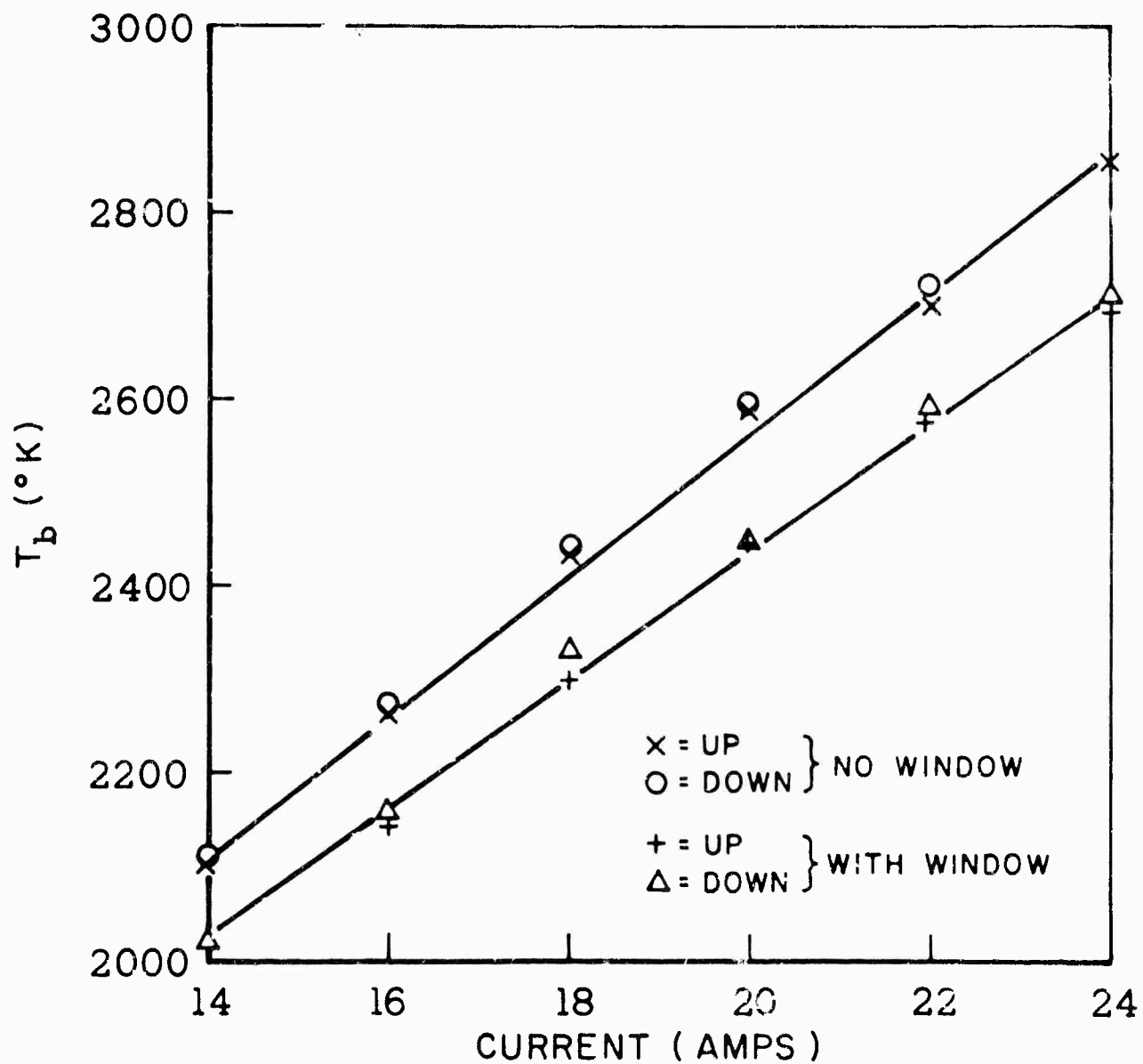


FIGURE 77

PHOTOMULTIPLIER OUTPUT vs BRIGHTNESS TEMPERATURE
(BULB OUT OF TEST SECTION)

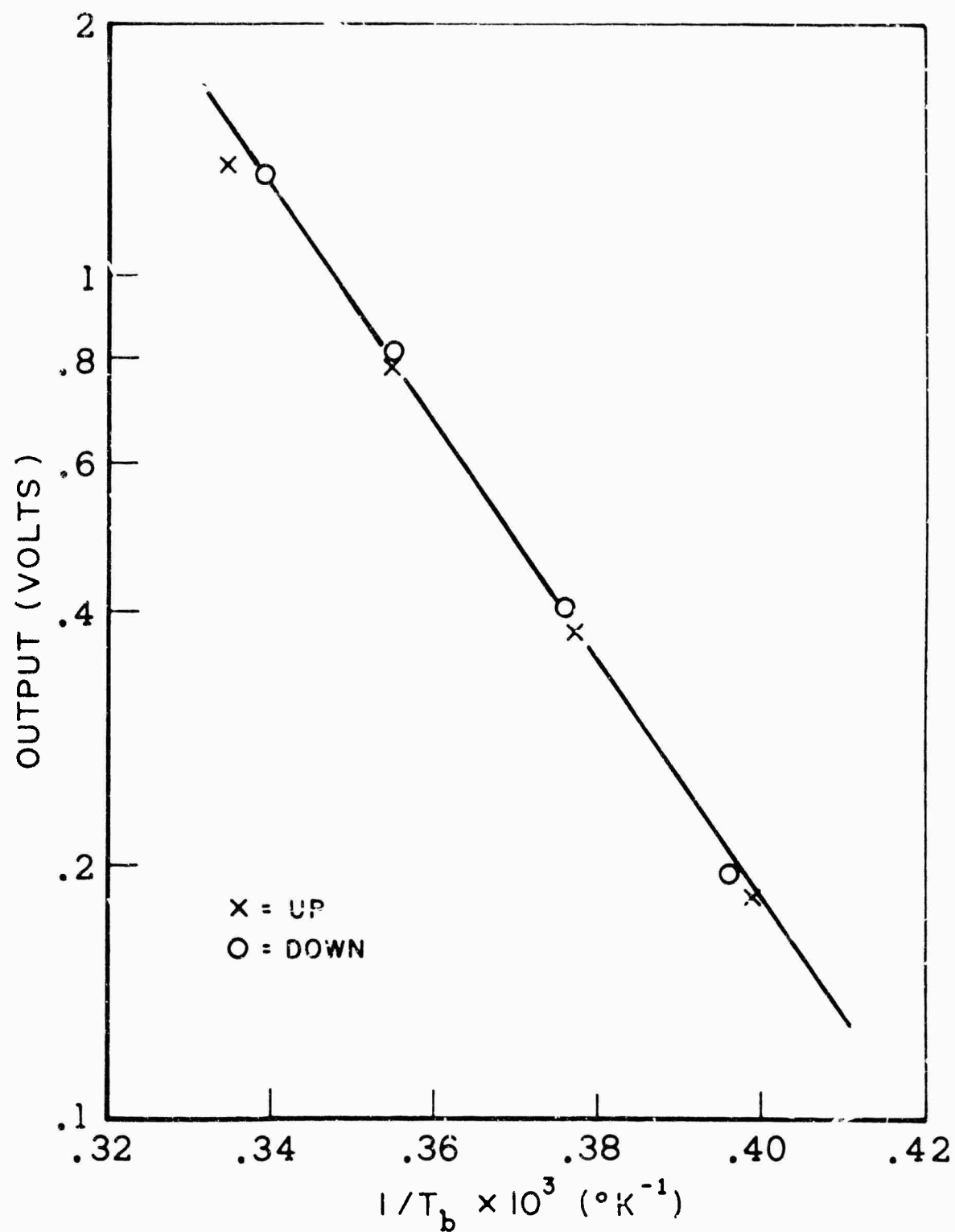


FIGURE 78

PHOTOMULTIPLIER OUTPUT vs BRIGHTNESS TEMPERATURE
(BULB IN TEST SECTION, WITH WINDOW)

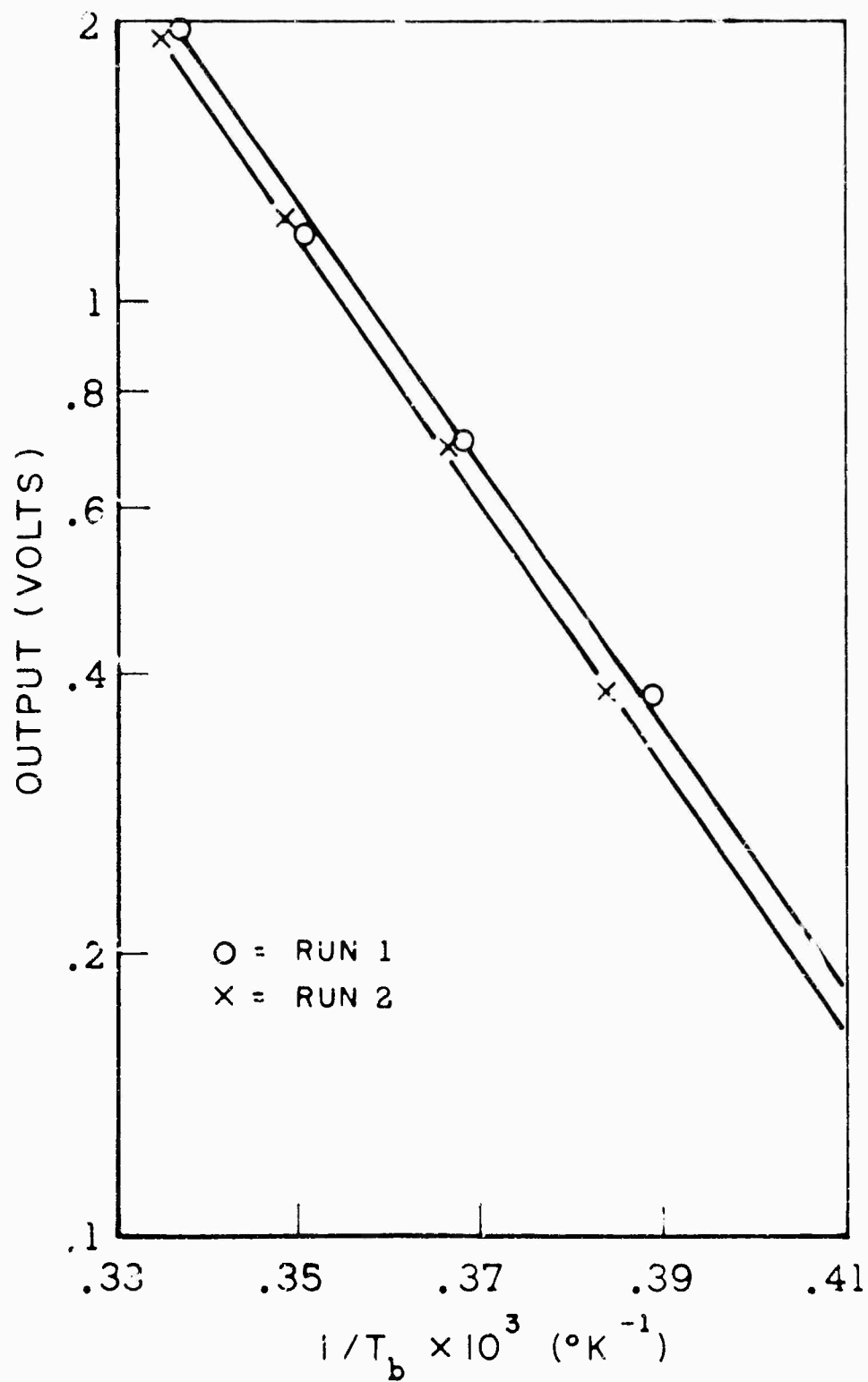


FIGURE 79

PHOTOMULTIPLIER OUTPUT vs BRIGHTNESS TEMPERATURE
(BULB IN TEST SECTION, NO WINDOW)

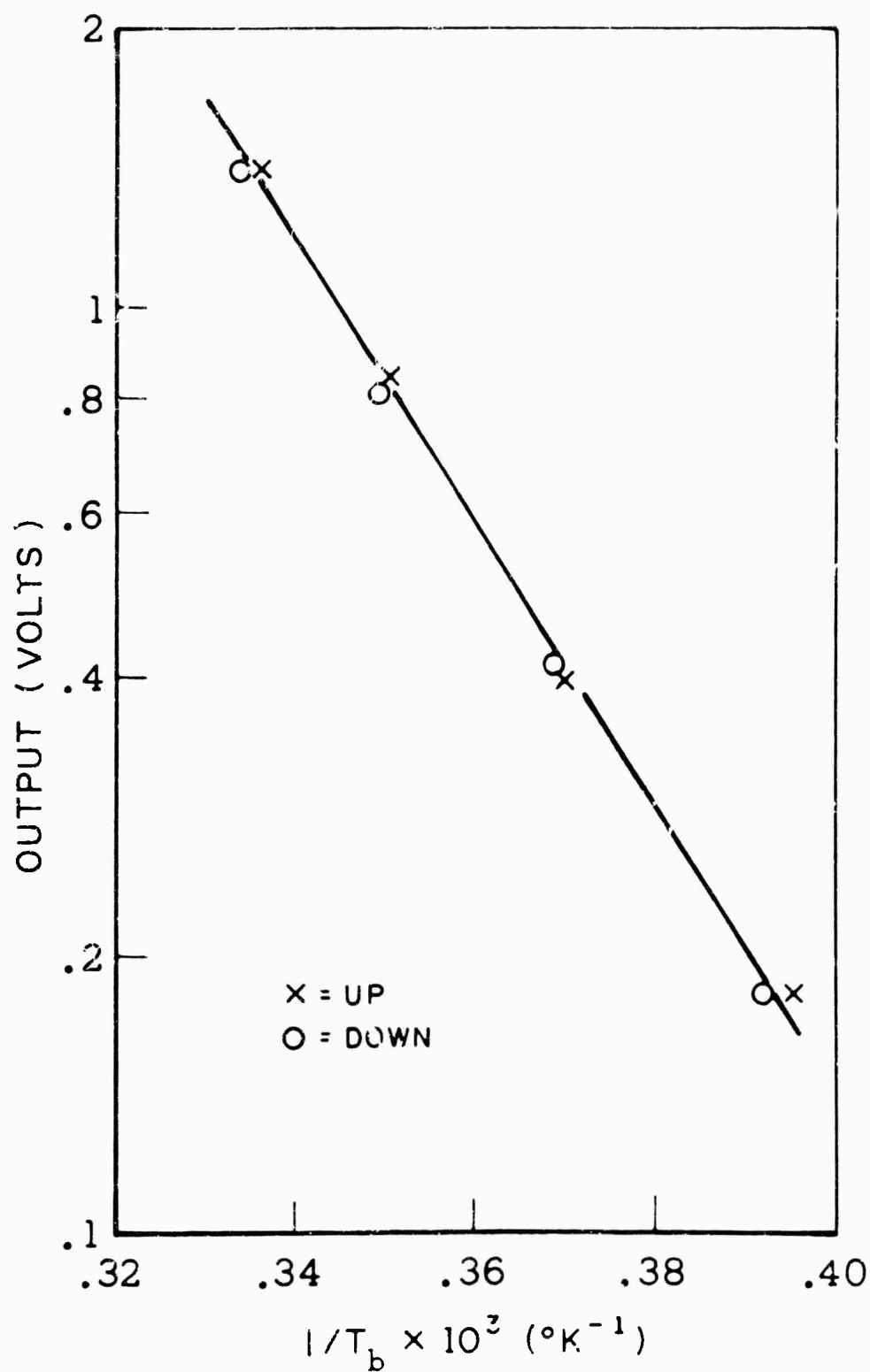
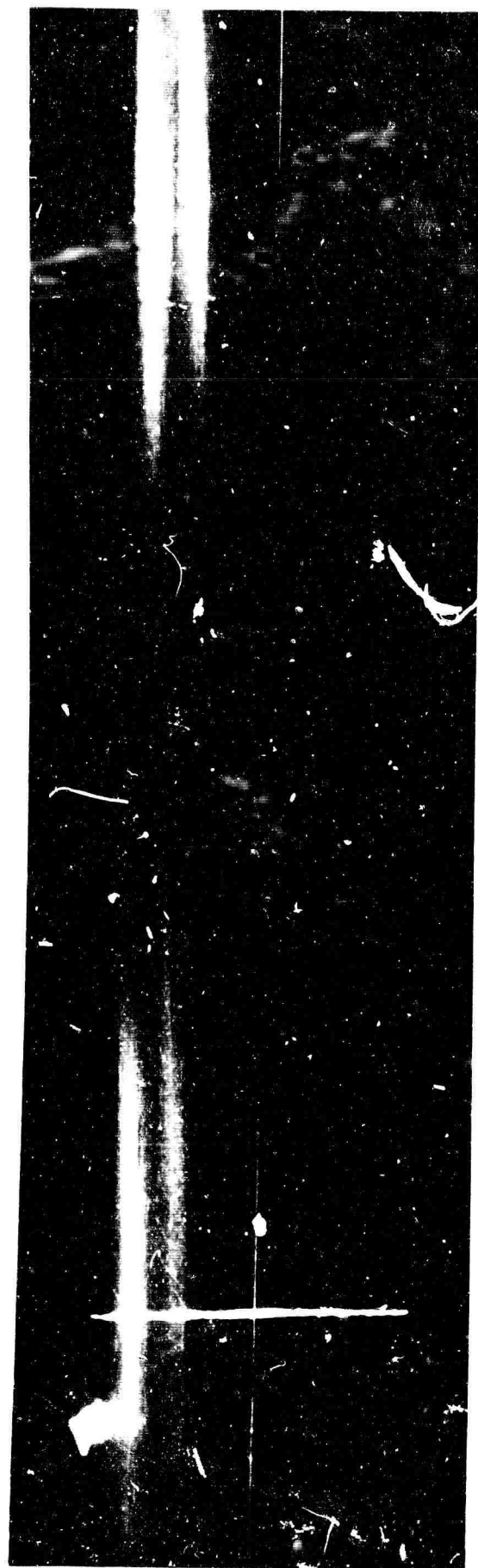


FIGURE 80

JP23-125-65



BURNING
SURFACE

DISTANCE

TIME —→

STREAK CAMERA RECORD FOR UNINHIBITED SAMPLE
(WOOD, REF. 193)

FIGURE 81

BURNING RATE vs PRESSURE
FOR PLASTISOL PROPELLANT P-5

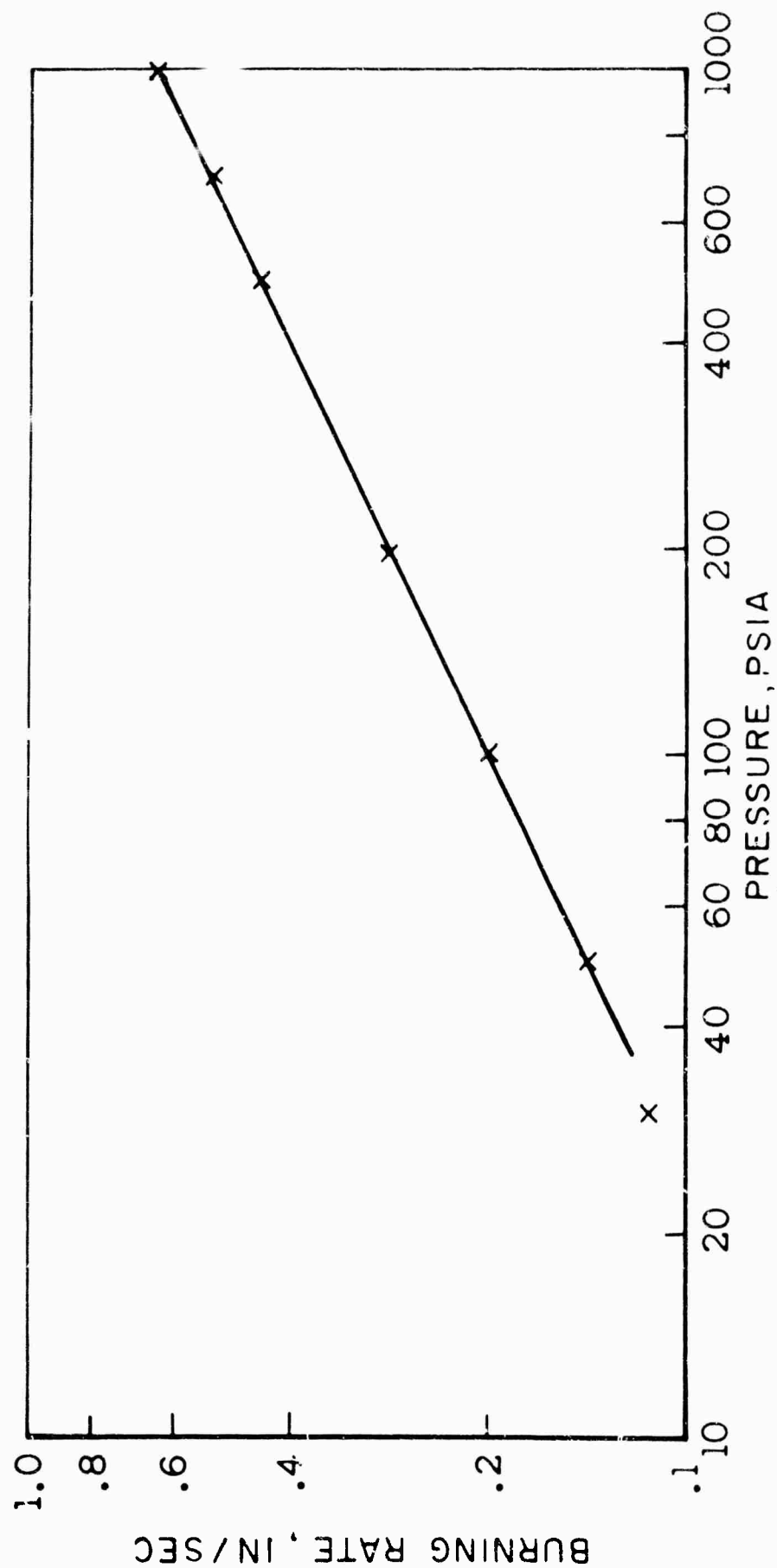


FIGURE 82



DISTANCE
↑

BURNING
SURFACE
↑

TIME →

STREAK CAMERA RECORD FOR AN INHIBITED SAMPLE
(PRINCETON)

FIGURE 83



STREAK CAMERA RECORD FOR UNINHIBITED SAMPLE
(PRINCETON)

BLANK PAGE

COMPUTED VARIATION OF $\text{Re}(\tilde{\theta}_f \bar{P} / \bar{T}_f \tilde{\phi})$ WITH
 FREQUENCY FOR DIFFERENT VALUES OF HEAT OF
 SURFACE REACTION (H) ($m=1$)

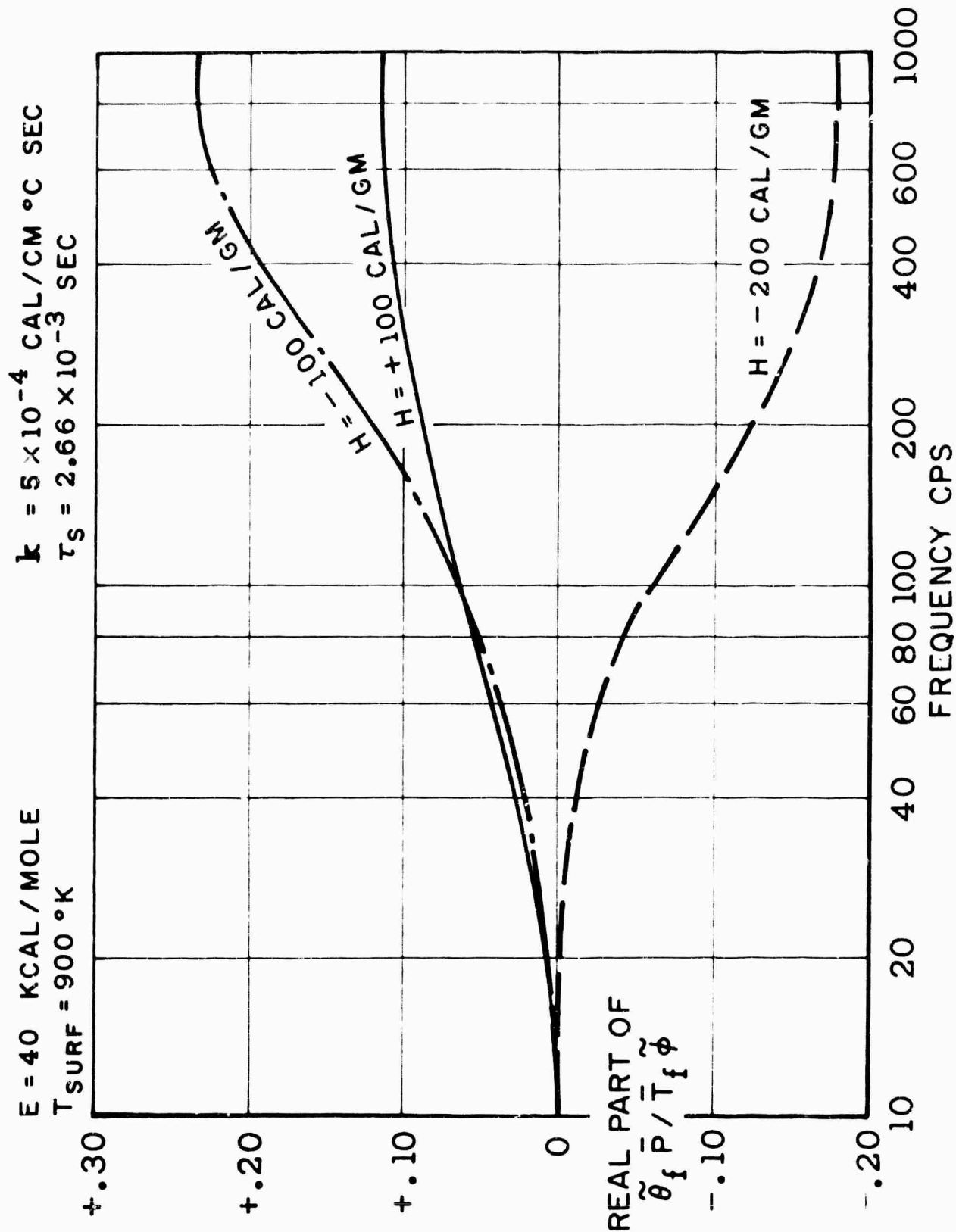


FIGURE 85

COMPUTED VARIATION OF $Re(y)$ WITH
FREQUENCY FOR DIFFERENT VALUES OF HEAT OF
SURFACE REACTION (H) ($m=1$)

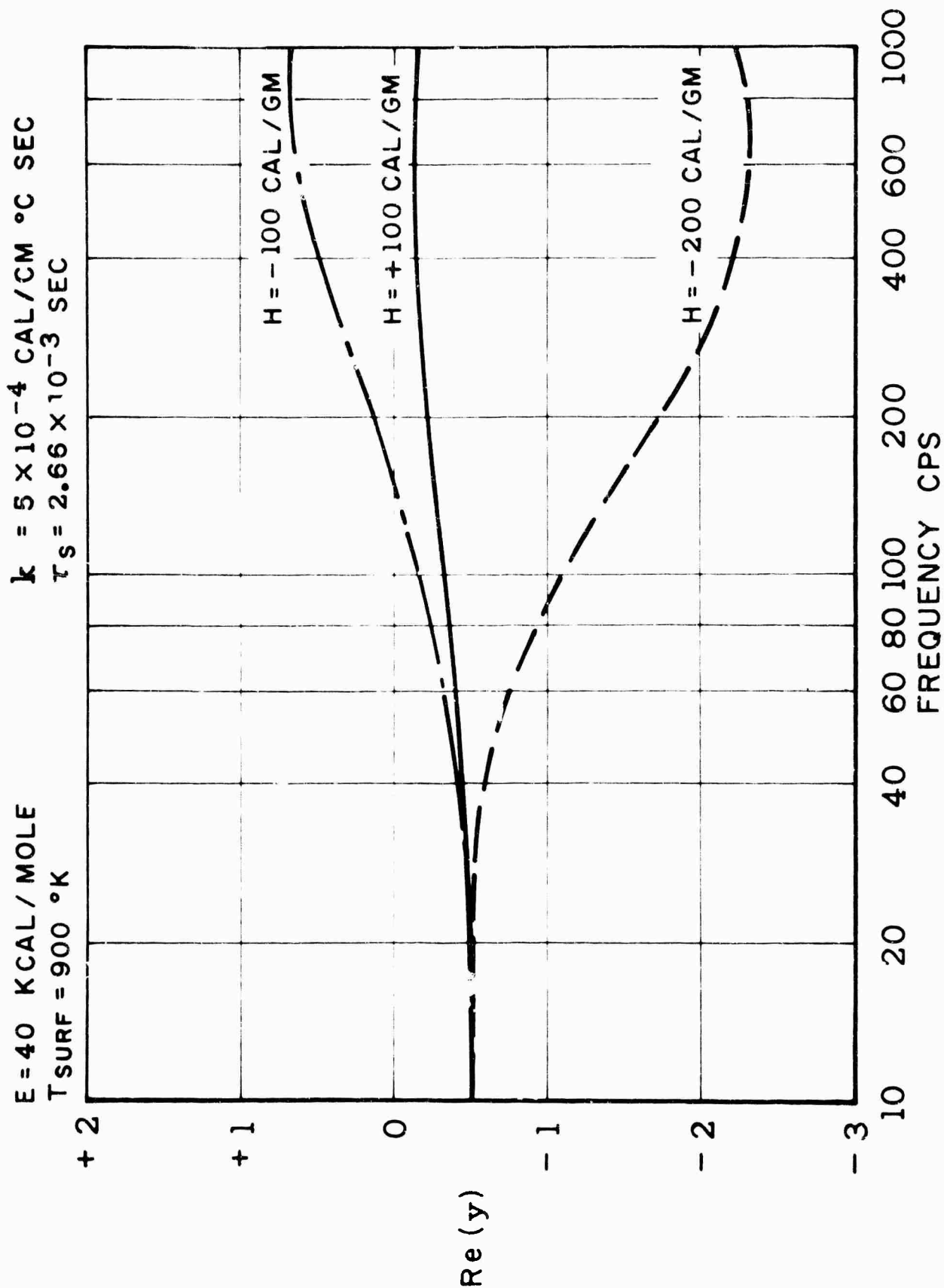


FIGURE 86

COMPUTED VARIATION OF PHASE ANGLE δ WITH
FREQUENCY FOR DIFFERENT VALUES OF HEAT OF
SURFACE REACTION (H) ($m = 1$)

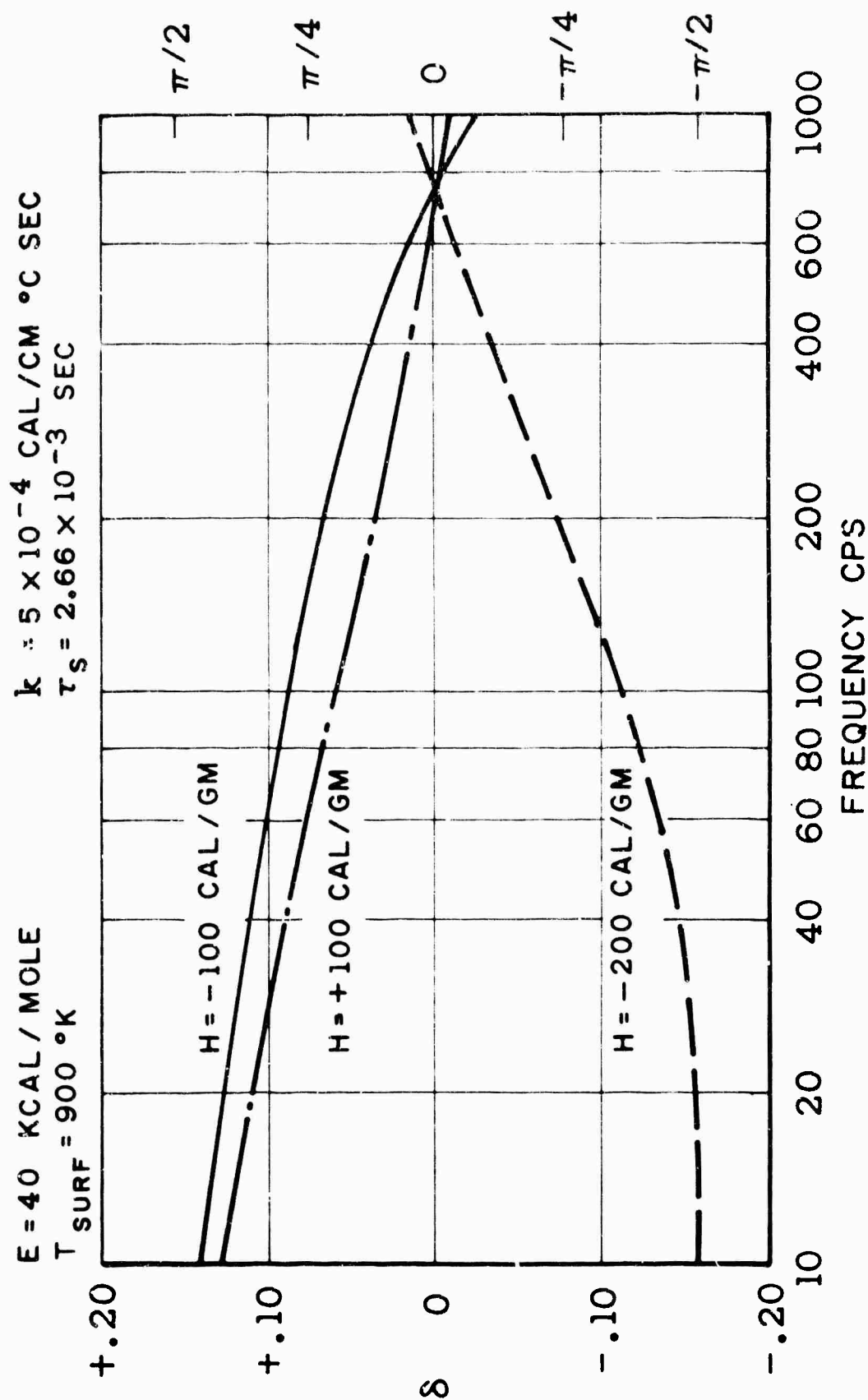


FIGURE 87

COMPUTED VARIATION OF $|\tilde{\theta}_f \bar{P} / \bar{T}_f \tilde{\phi}|$ WITH
 FREQUENCY FOR DIFFERENT VALUES OF HEAT OF
 SURFACE REACTION (H) (m=1)

E=40 KCAL/MOLE

k = 5×10^{-4} CAL/CM °C SEC

T_{SURF} = 900 °K

$\tau_s = 2.66 \times 10^{-3}$ SEC

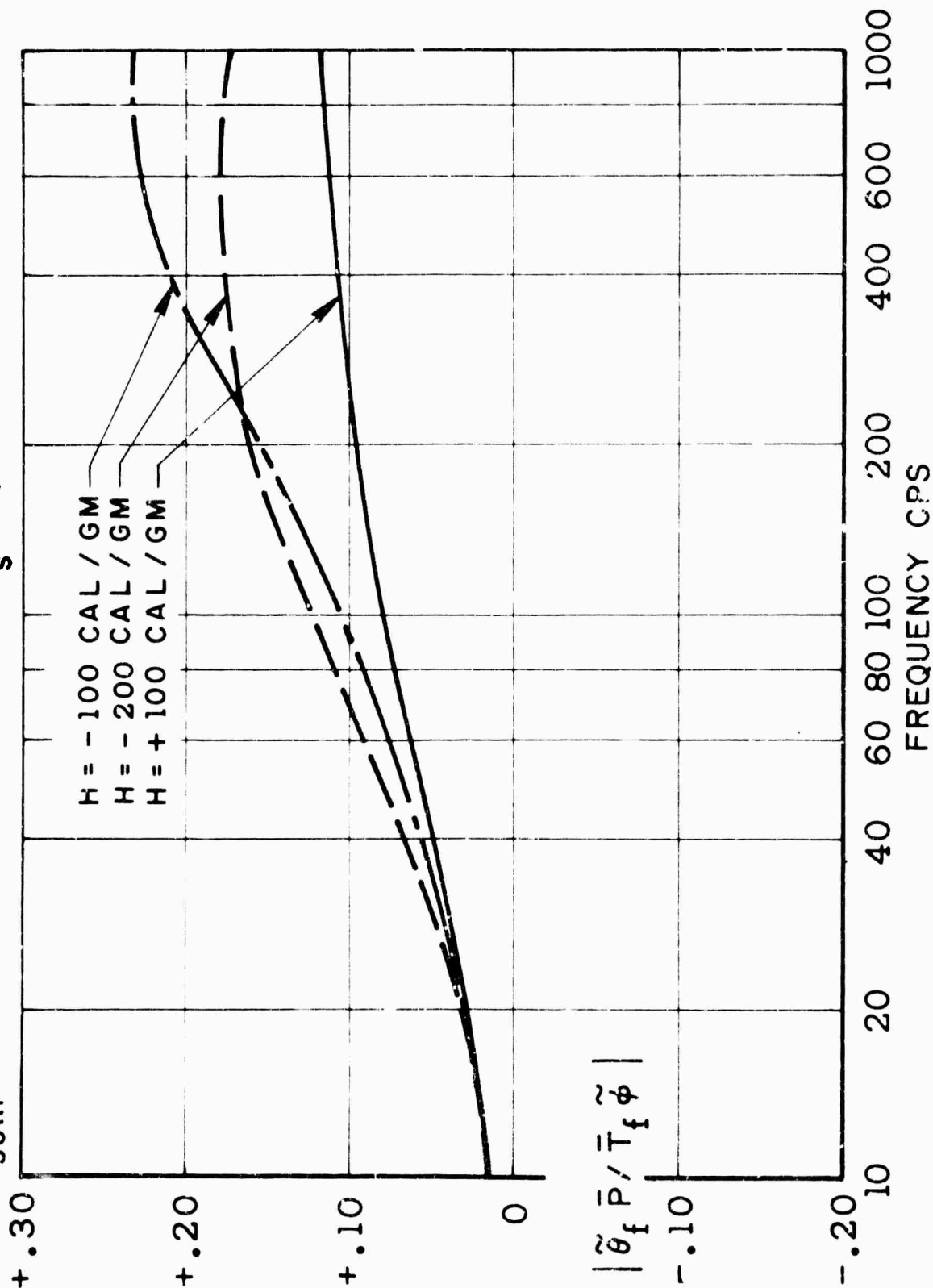


FIGURE 88

COMPUTED VARIATION OF $\text{Re}(\tilde{\theta}_f \bar{P} / \bar{T}_f \phi)$ WITH
 FREQUENCY FOR DIFFERENT VALUES OF BURNING RATE ($H = -200$)

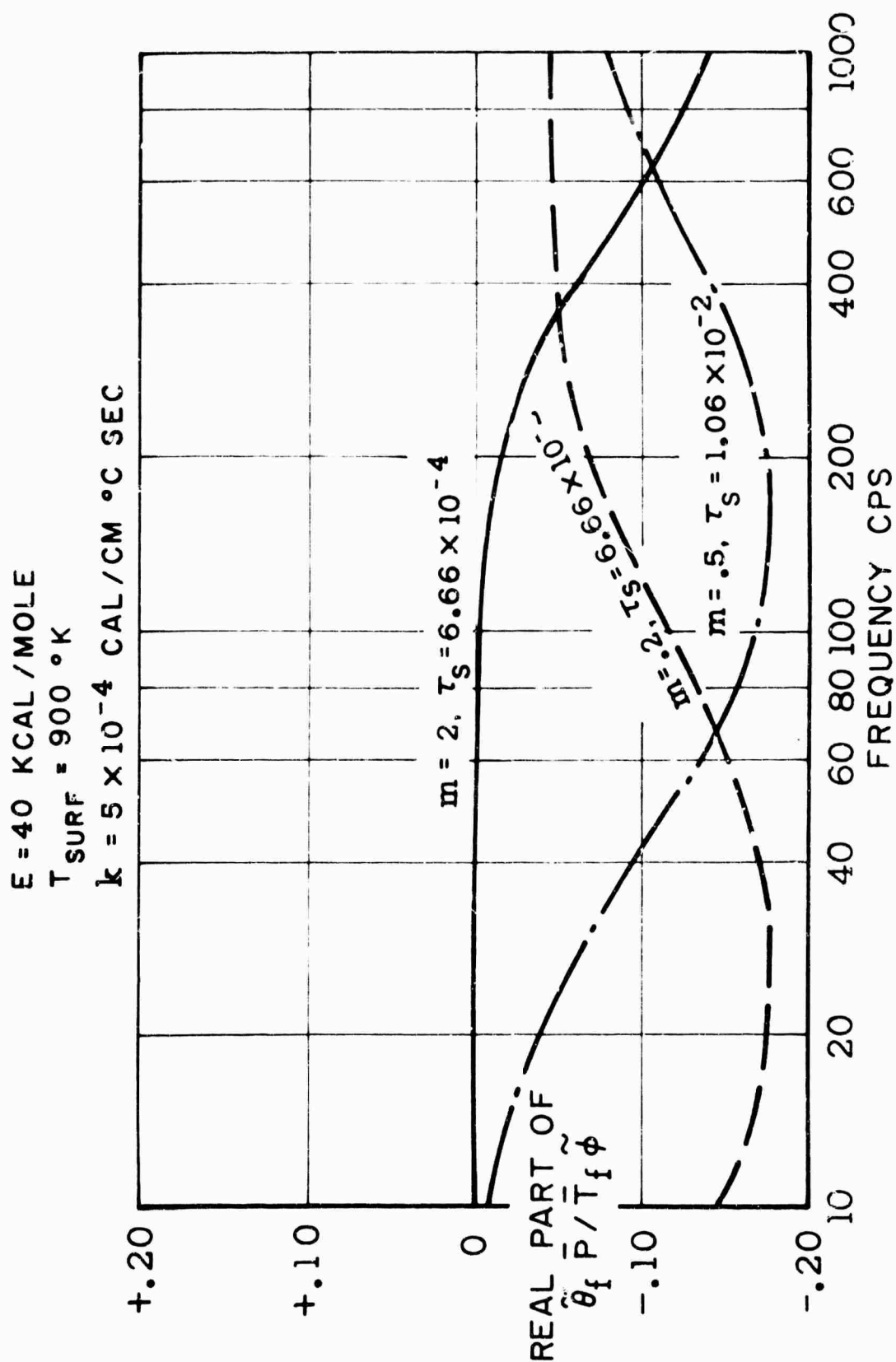


FIGURE 89

BLANK PAGE

COMPUTED VARIATION OF $\text{Re}(\tilde{\theta}_f \bar{P} / \bar{T}_f \phi)$ WITH
 FREQUENCY FOR TWO VALUES OF E, THE ACTIVATION
 ENERGY OF SURFACE REACTION ($H = -200$)

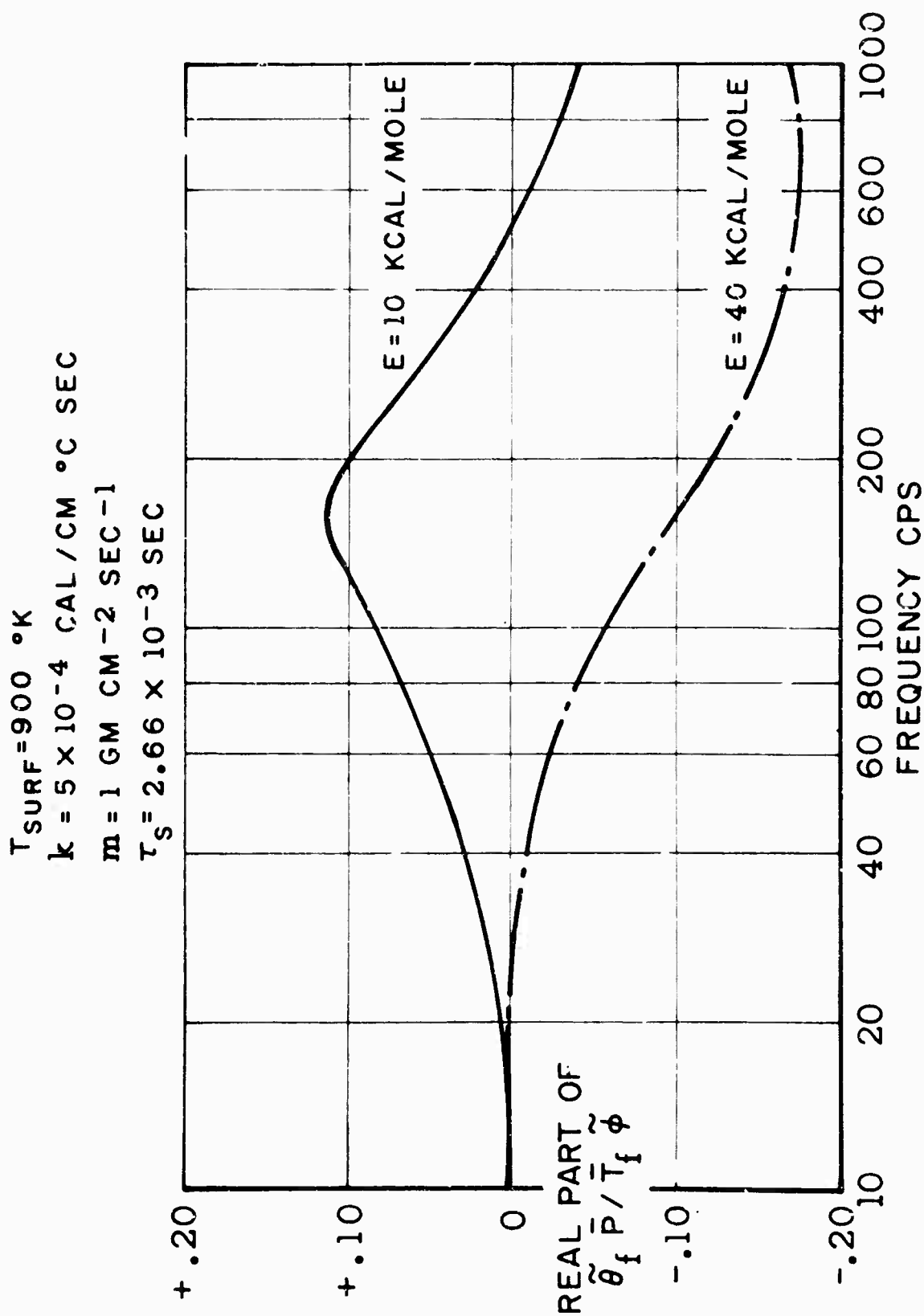


FIGURE 91

COMPUTED VARIATION OF $\text{Re}(\tilde{\theta}_f \bar{P} / \bar{T}_f \phi)$ WITH
 FREQUENCY FOR DIFFERENT VALUES OF SURFACE TEMPERATURE ($H = -100$)

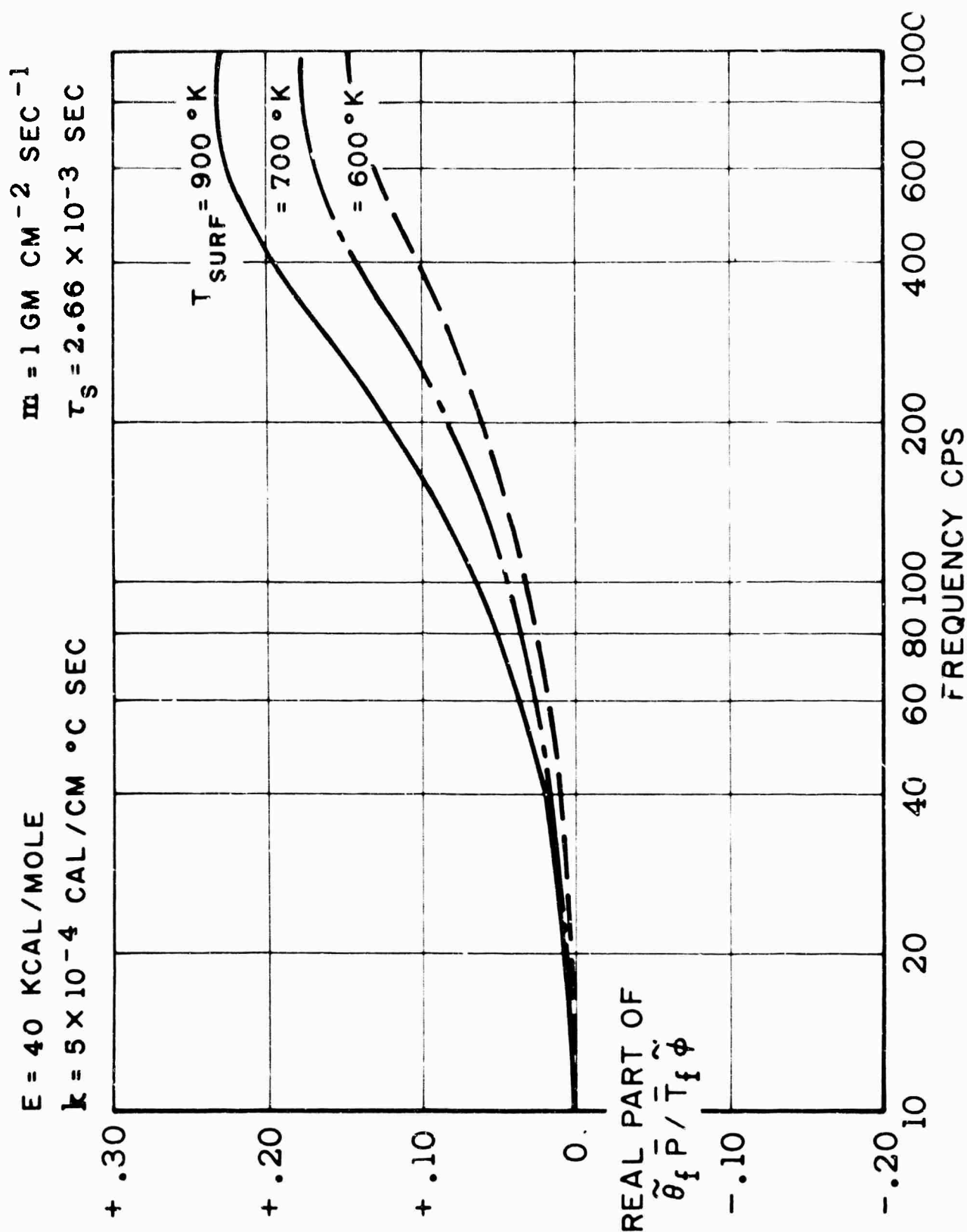


FIGURE 92

EFFECT OF HEAT TRANSFER PARAMETER α ON $\text{Re}(\tilde{\theta}_f \bar{P} / \bar{T}_f \tilde{\phi})$
($H = -200$)

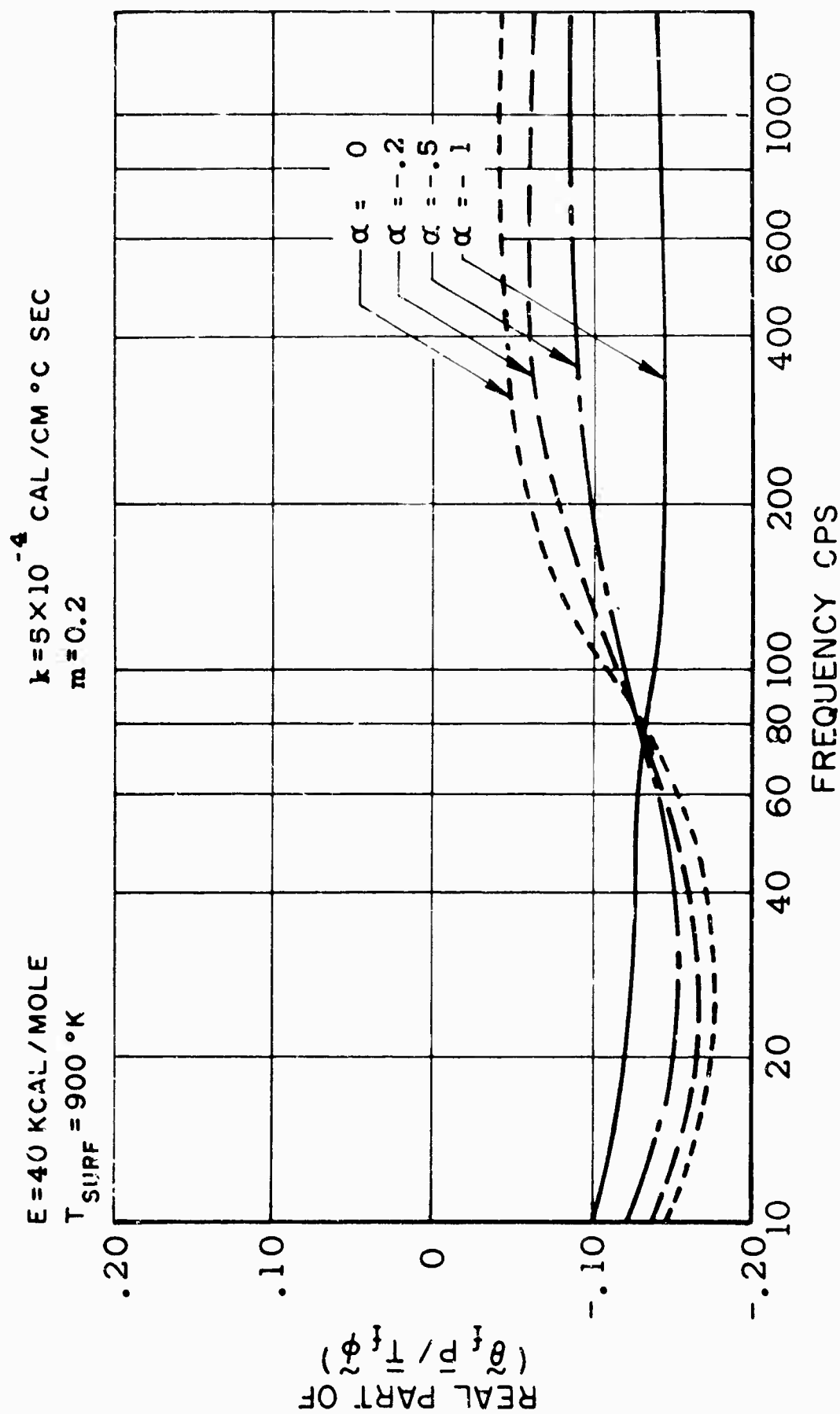


FIGURE 93

EFFECT OF HEAT TRANSFER PARAMETER α ON $\text{Re}(\tilde{\theta}_f \bar{P} / \bar{T}_f \phi)$
 (H = -100)

E = 40 KC/L/MOLE
 $k = 5 \times 10^{-4}$ CAL/CM °C SEC

$T_{\text{SURF}} = 900$ °K

$m = 0.2$

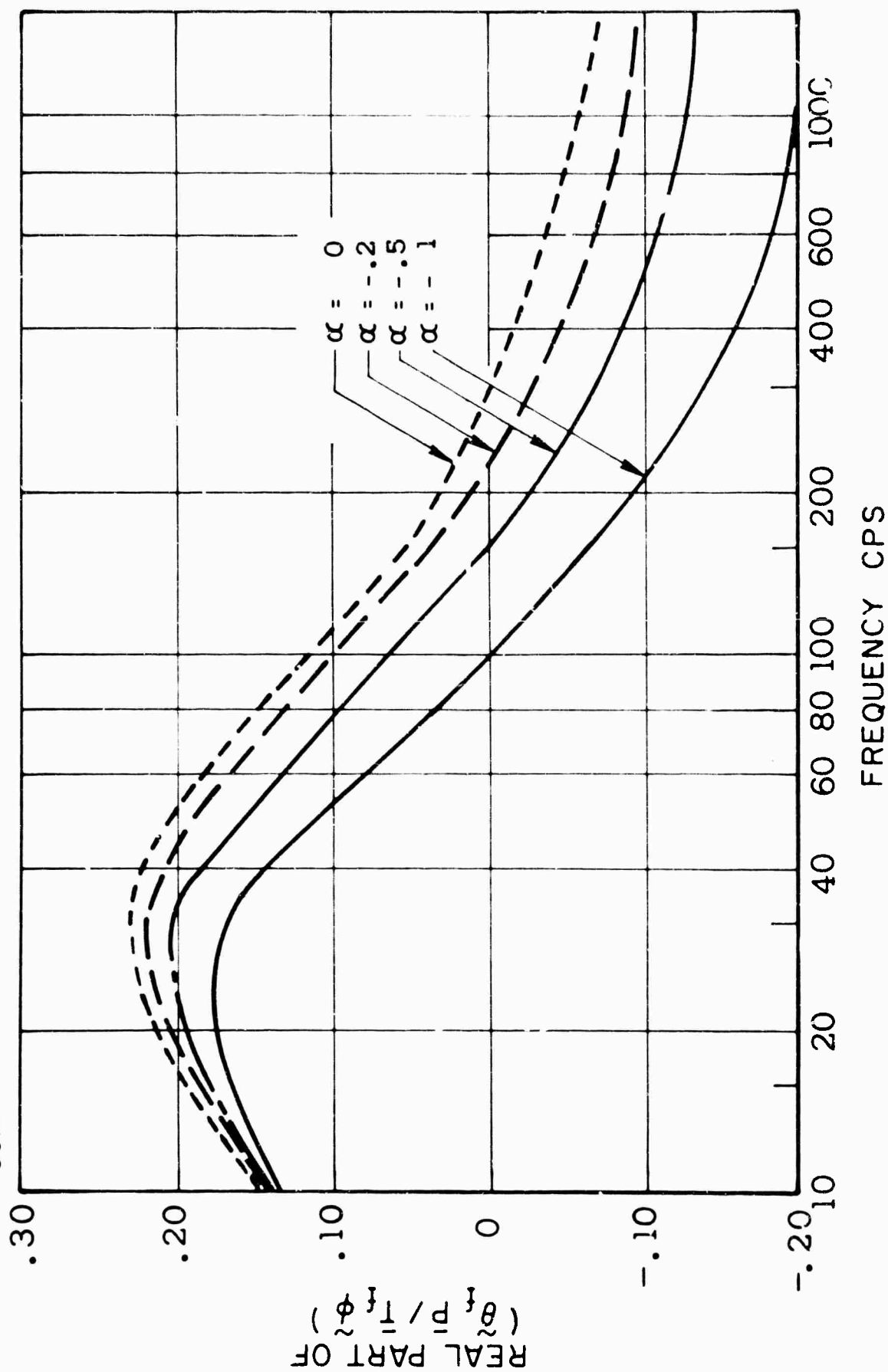


FIGURE 94

RADIOMETER
OUTPUT

PRESSURE

TIME →

PORTION OF THE OSCILLOGRAPH RECORD OF RADIOMETER AND PRESSURE OUTPUT

FIGURE 95

BLANK PAGE

STANDING AND SPINNING FORMS OF THE FIRST TANGENTIAL MODE

TIME

STANDING FORM

SPINNING FORM

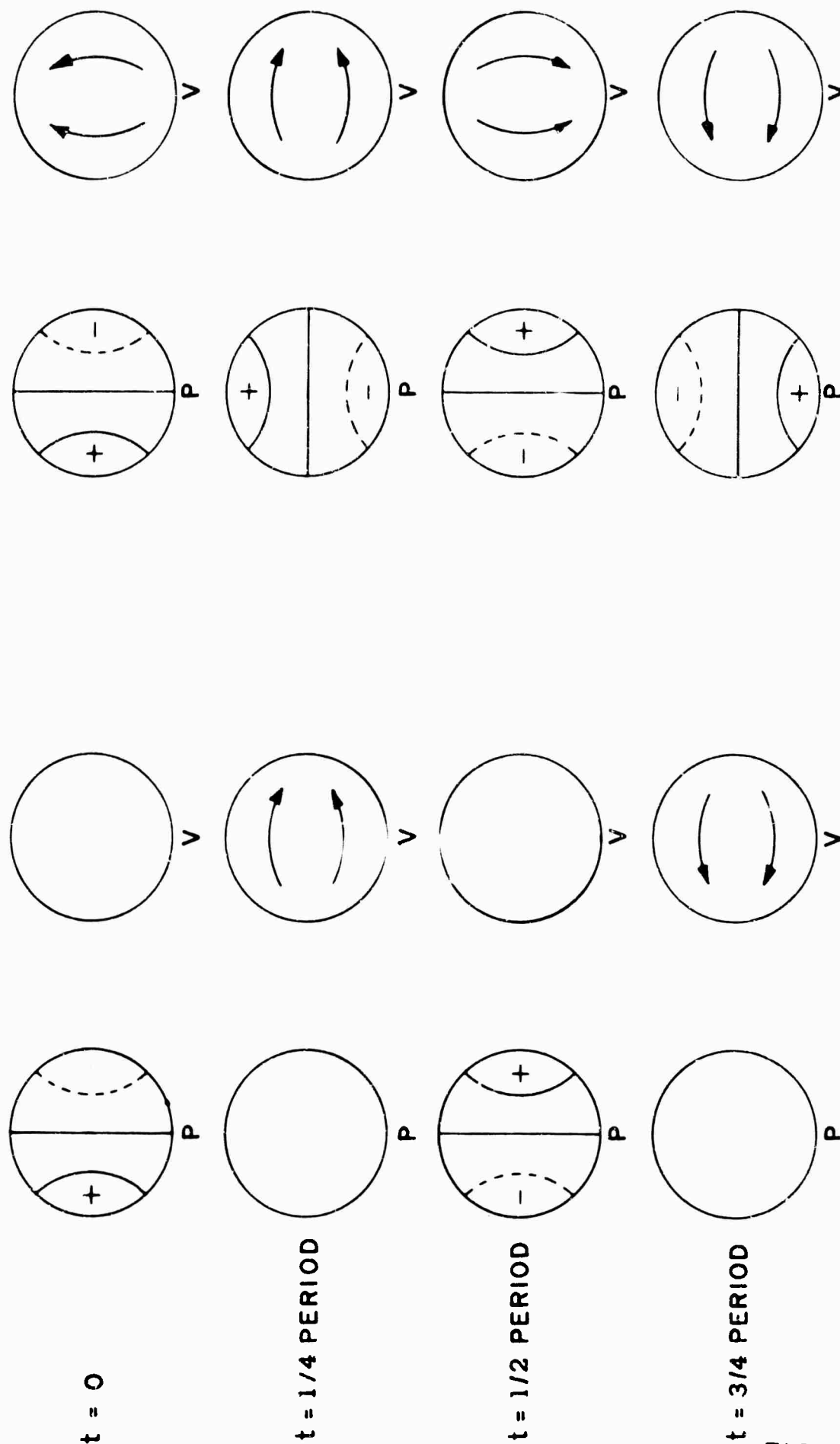
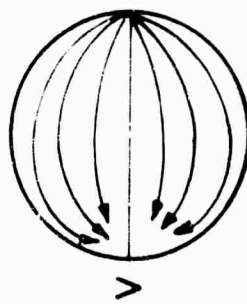
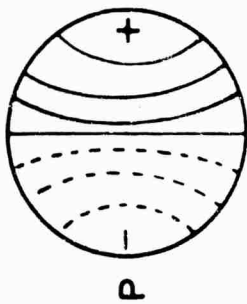


FIGURE B - 1

OSCILLATION PATTERN FOR TRANSVERSE MODES

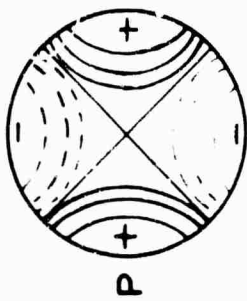
PURELY TANGENTIAL MODES

$S_{11} = 1.84129$



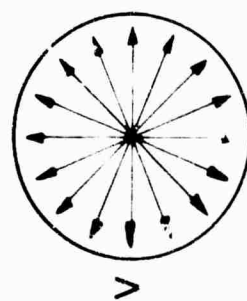
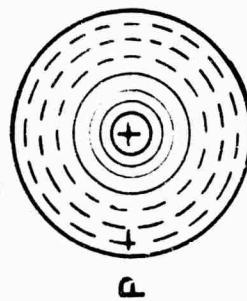
FIRST

$S_{21} = 3.0543$



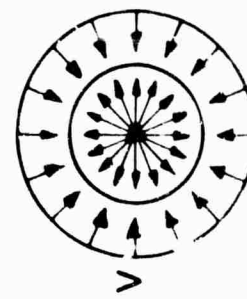
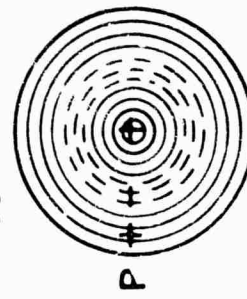
SECOND

$S_{02} = 3.8317$



FIRST

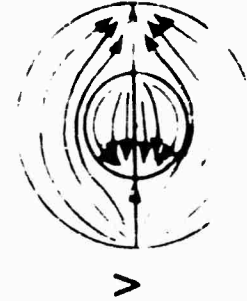
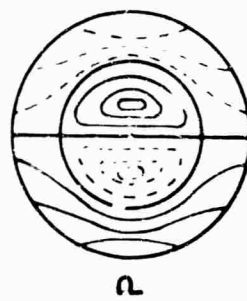
$S_{03} = 7.0156$



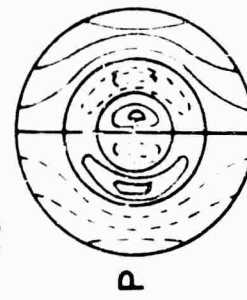
SECOND

COMBINED MODES

$S_{12} = 5.3313$



$S_{13} = 8.5263$



$S_{22} = 6.7060$

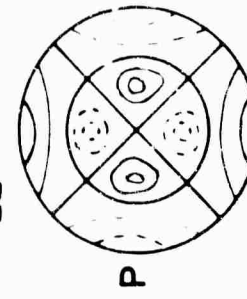


FIGURE B - 2

X-RAY THICKNESS MEASUREMENT

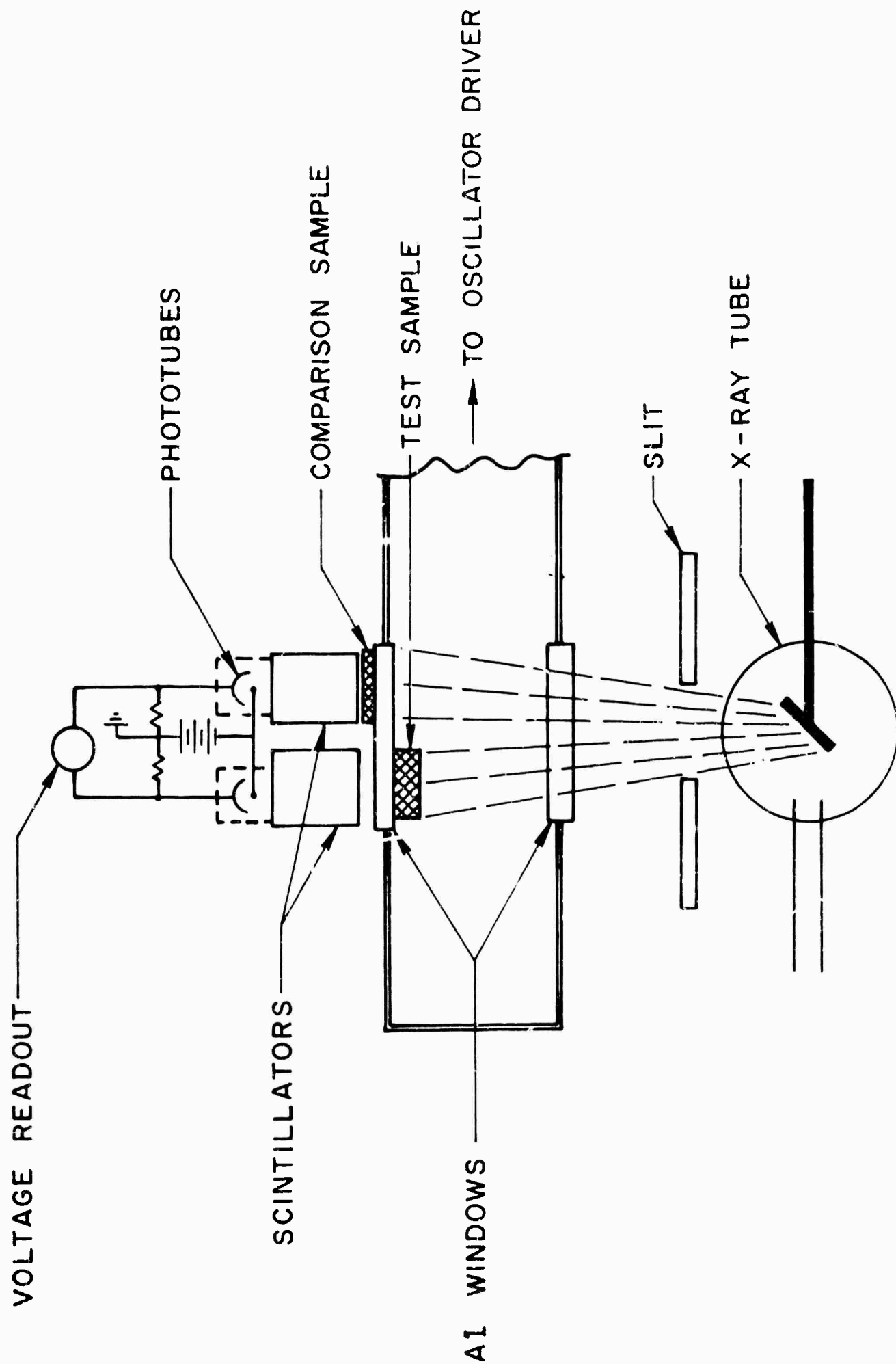


FIGURE C - 1

EMISSIONITY OF COMBUSTION GASES vs WAVE LENGTH

(IN THE NEIGHBORHOOD OF AN ISOLATED NaD LINE FOR A
SOLID PROPELLANT WITH 0.01 % NaCl AT 200 psi)

(SAMPLE THICKNESS IN CM. GIVEN ON CURVE)

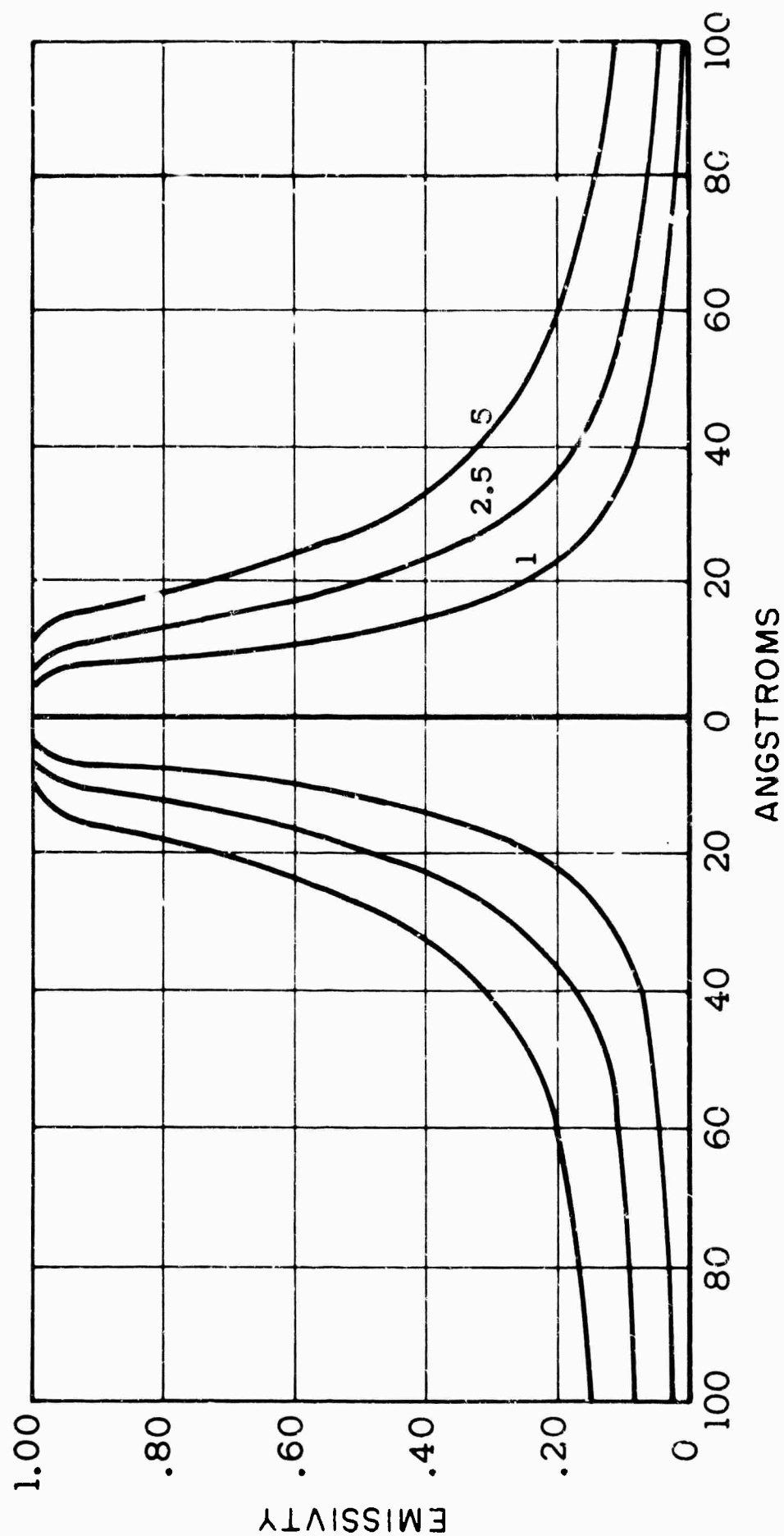


FIGURE F - 1

EMISSIVITY OF COMBUSTION GASES VS WAVE LENGTH

(IN THE NEIGHBORHOOD OF AN ISOLATED NaD LINE FOR A
SOLID PROPELLANT WITH 0.01% NaCl AT 400psi)

(SAMPLE THICKNESS IN CM. GIVEN ON CURVE)

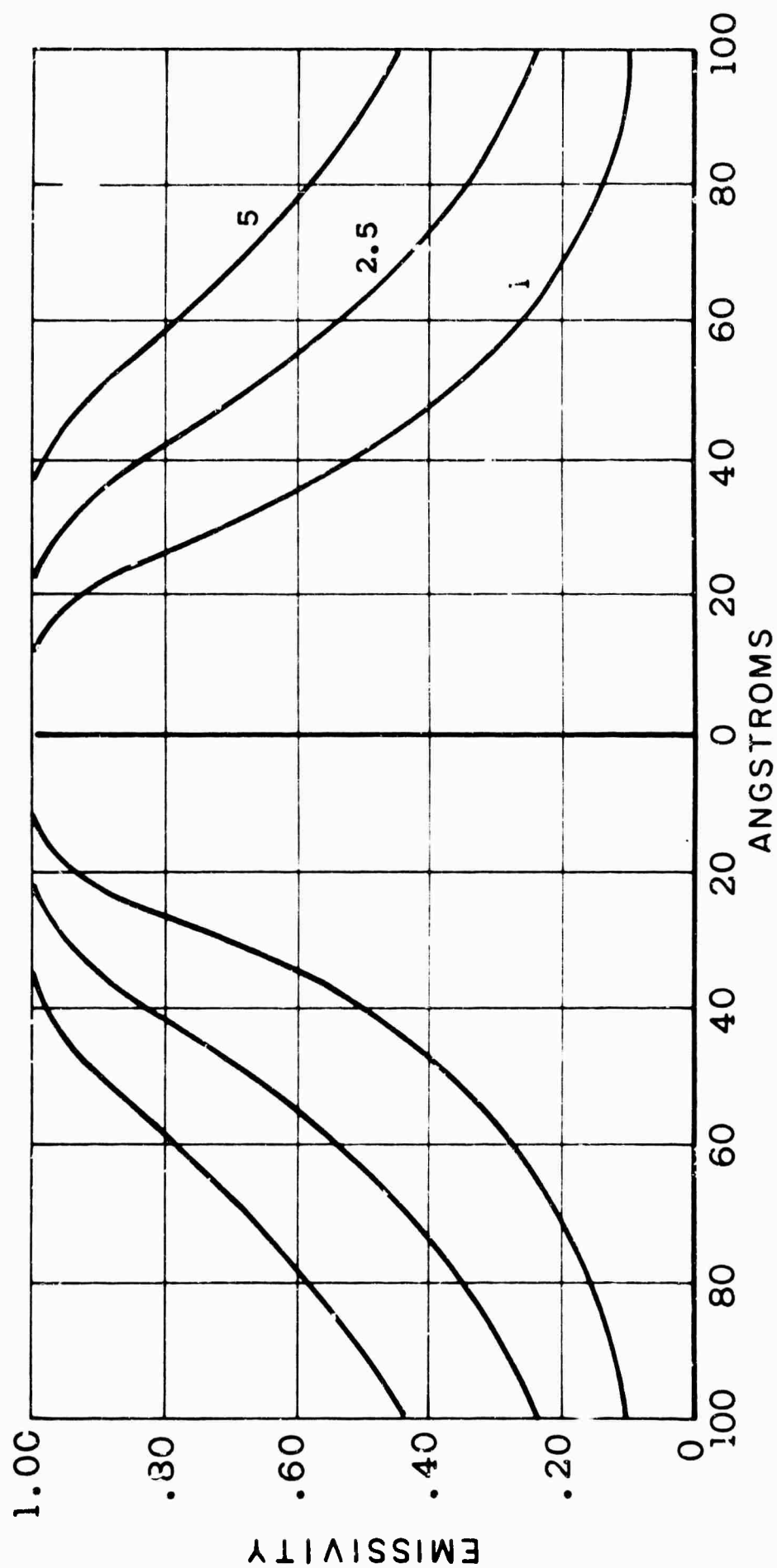


FIGURE F-2

EMISSIVITY OF COMBUSTION GASES vs WAVE LENGTH

(IN THE NEIGHBORHOOD OF A V ISOLATED NaD LINE FOR A
SOLID PROPELLANT WITH 0.1% NaCl AT 200 psi)

(SAMPLE THICKNESS IN CM. GIVEN ON CURVE)

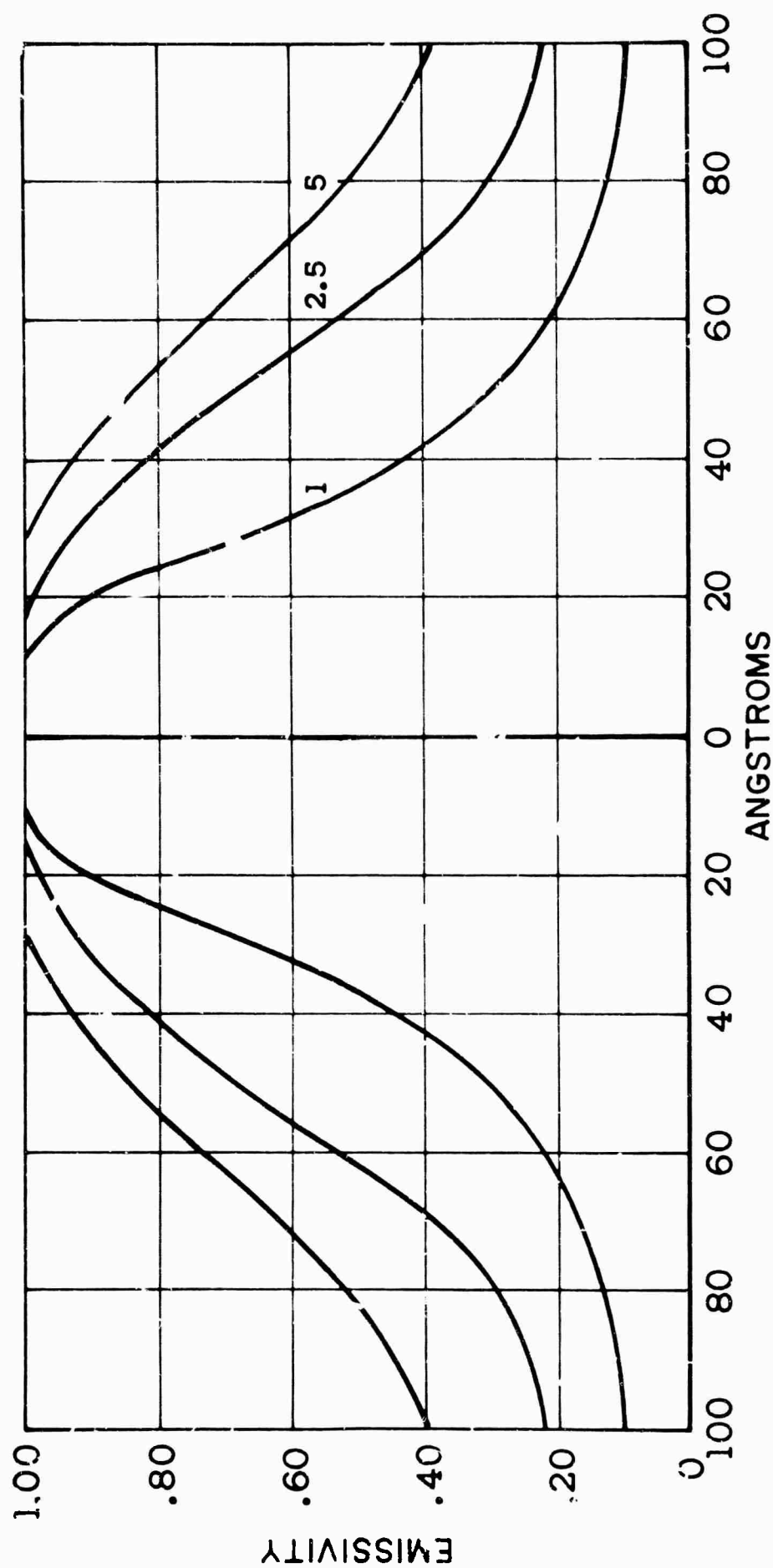


FIGURE F - 3

EMISSIVITY OF COMBUSTION GASES VS WAVE LENGTH

(IN THE NEIGHBORHOOD OF AN ISOLATED NaD LINE FOR A
SOLID PROPELLANT WITH 0.1% NaCl AT 400psi)

(SAMPLE THICKNESS IN CM. GIVEN ON CURVE)

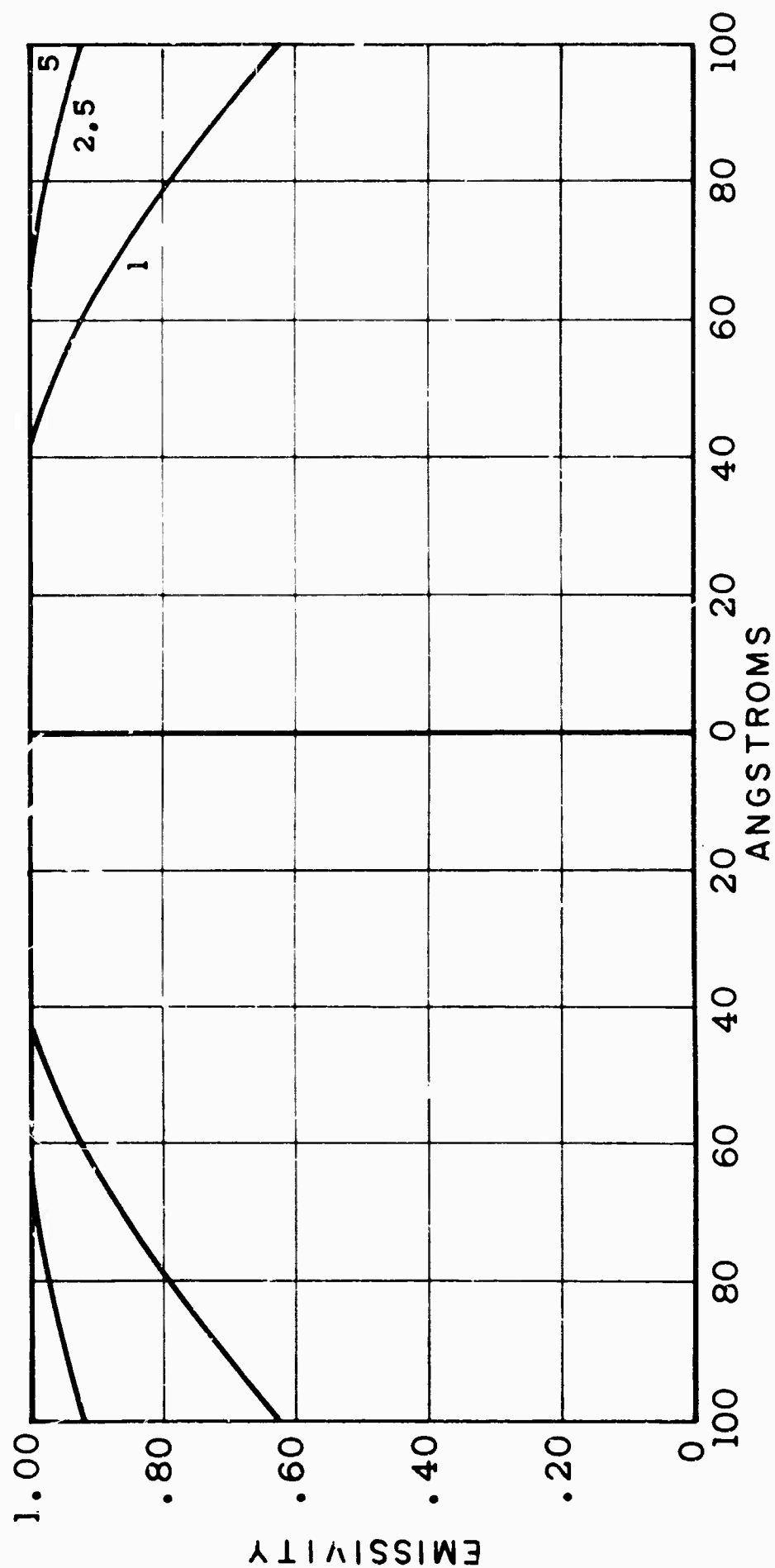


FIGURE F - 4

PRESSURE VS TIME IN (dp/dt) EXPERIMENT

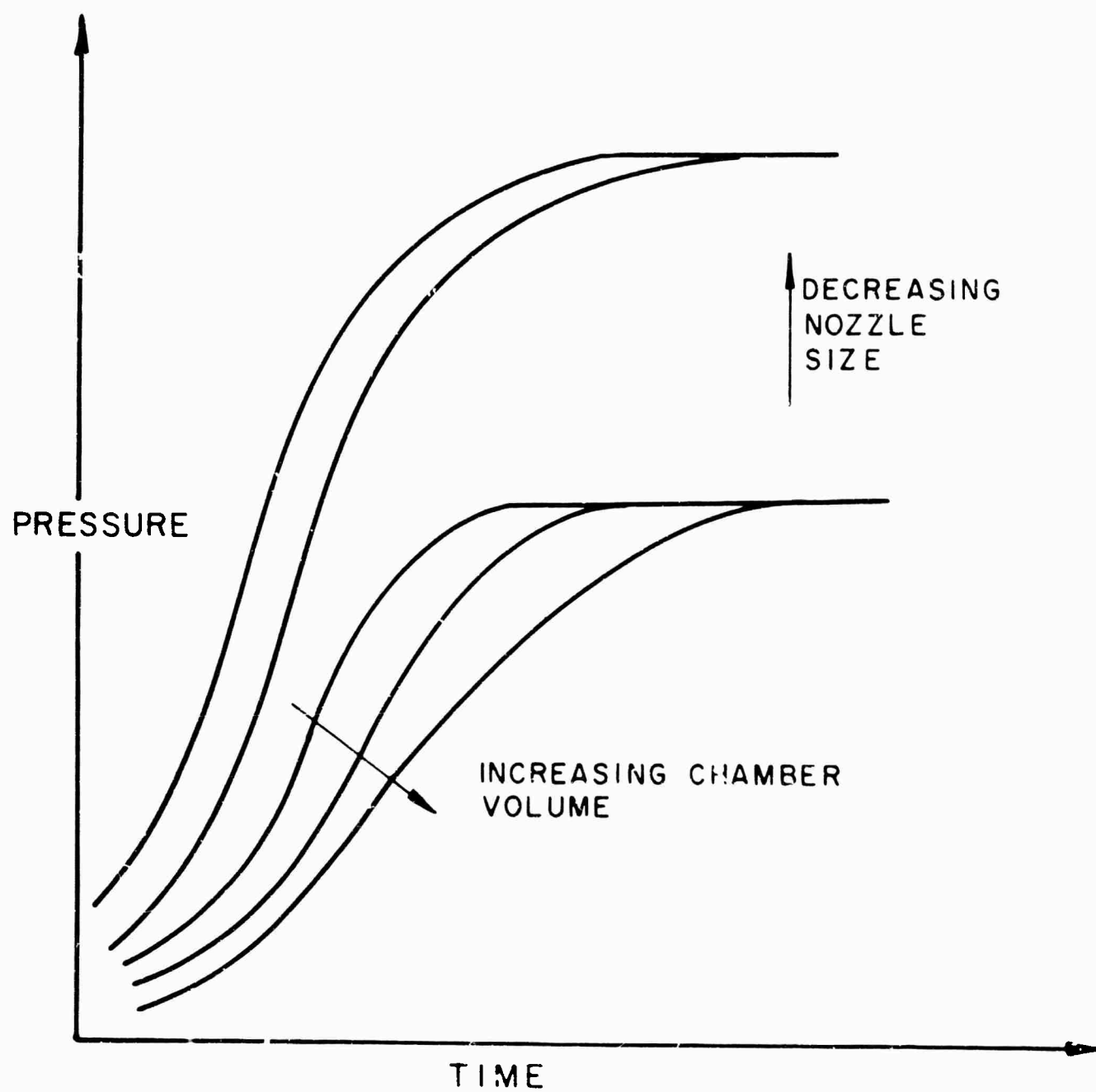


FIGURE H - 1

PRESSURE VS LUMINOSITY IN (dp/dt) EXPERIMENT

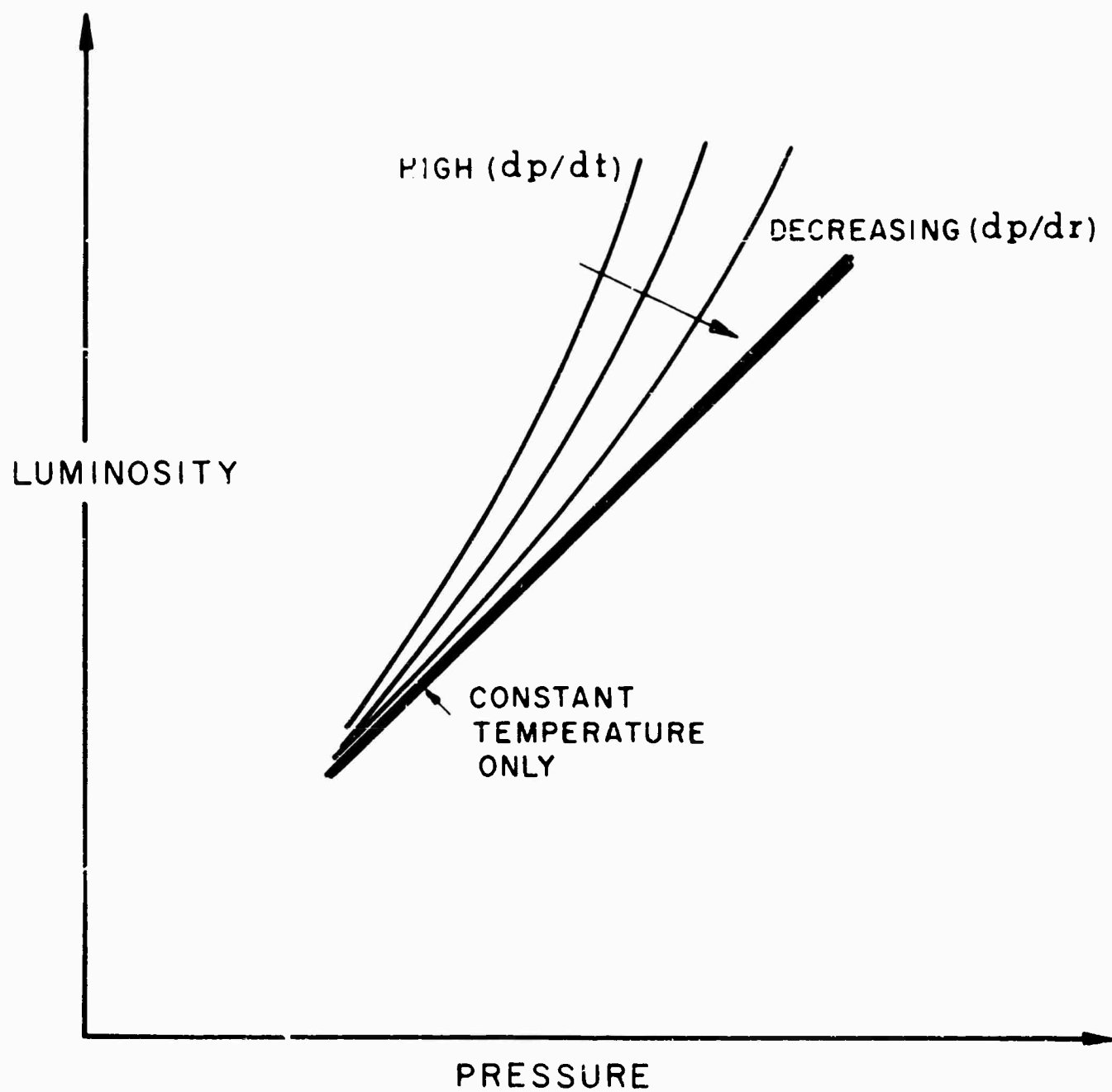


FIGURE H - 2

PRESSURE VS TEMPERATURE IN (dp/dt) EXPERIMENT

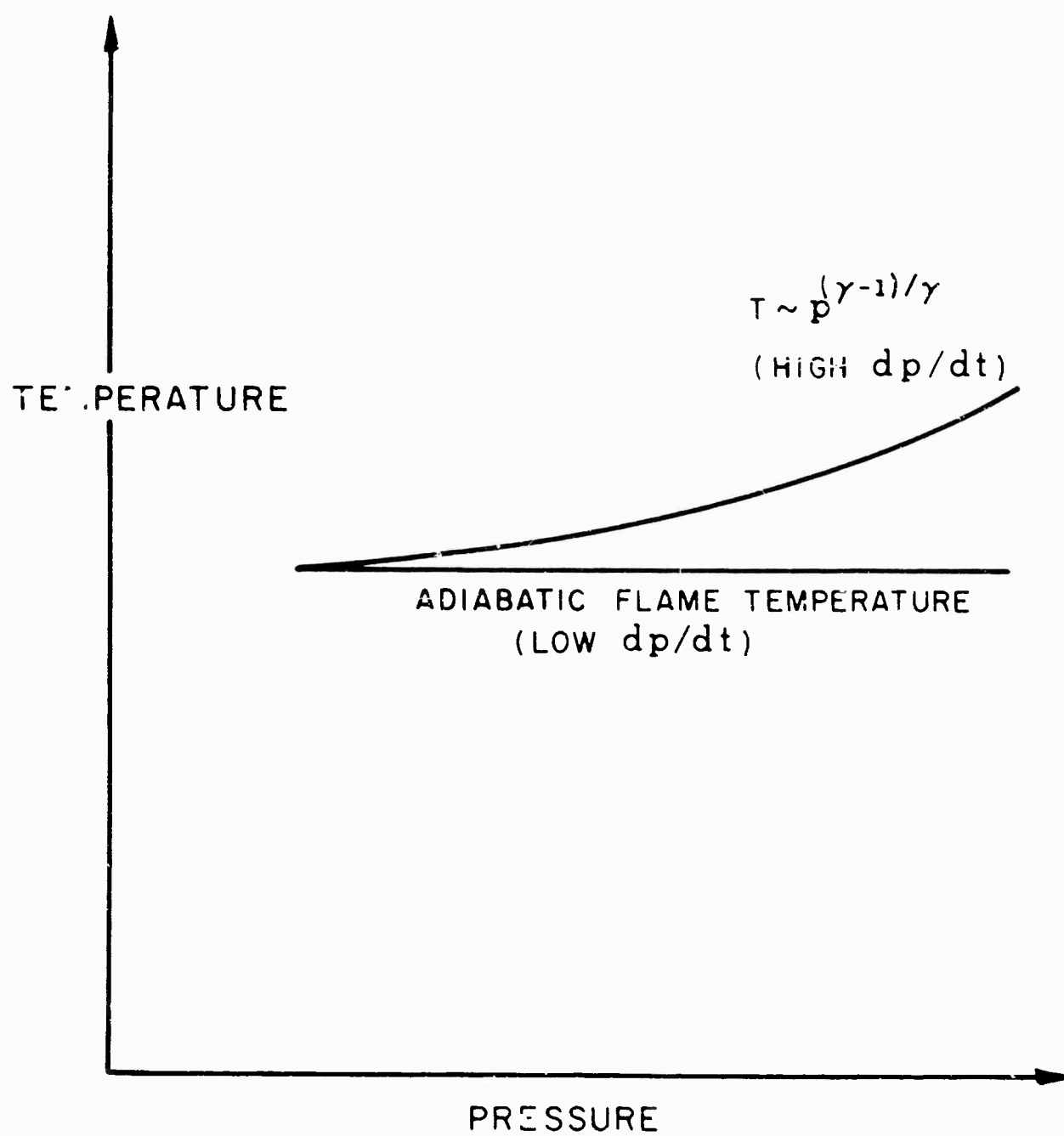


FIGURE H - 3

DOCUMENT CONTROL DATA - R&D

(Security Classification of title, body of abstract and indexing annotation must be entered when the overall report is classified)

1. ORIGINATING ACTIVITY (Corporate author)

Princeton University
Department of Aerospace & Mechanical Sciences
Princeton, New Jersey

2A. REPORT SECURITY CLASSIFICATION

☒ Unclassified
Other — Specify

2B. GROUP

3. REPORT TITLE

SOLID PROPELLANT COMBUSTION INSTABILITY: OSCILLATORY BURNING OF SOLID
ROCKET PROPELLANTS (U)

4. DESCRIPTIVE NOTES (Type of report and inclusive dates)

☒ Scientific Report ☐ Final Report ☐ Journal Article ☐ Proceedings ☐ Book

5. AUTHOR(S) (Last name, first name, initial)

Waesche Woodward R H
Summerfield Martin Prof (PI)

6. REPORT DATE AS PRINTED

August 1965

7A. TOTAL NO. OF PAGES

311

7B. NO. OF REFS

363

8A. CONTRACT OR GRANT NO.

AF-AFOSR-448-63

B. PROJECT NO

9711-01

C. 61445014

9A. ORIGINATOR'S REPORT NUMBER(S) (if given)

9B. OTHER REPORT NO.(S) (Any other numbers that may be assigned
this report)

AFOSR 46-0937
AD

10. AVAILABILITY LIMITATION NOTICES

Distribution of this document is unlimited

- ☒ Available from DDC
☐ Available from CFSTI
☐ Available from Source
☐ Available Commercially

11. SUPPLEMENTARY NOTES (Citation)

12. SPONSORING MILITARY ACTIVITY

AF Office of Scientific Research (SERP)
Office of Aerospace Research
Washington, D. C. 20333

13. ABSTRACT

This research was concerned with the problem of combustion instability in solid propellant rocket motors and, in particular, with the nature of the dynamic coupling between the oscillating pressure and the combustion process at the propellant surface. A T-tube rocket motor was used to generate a high amplitude pressure oscillation, in the range from 75 to 1600 cycles/second and 250 to 1150 psi mean pressure. Various test specimens of ammonium perchlorate composite propellants were exposed to this oscillating pressure field in a combustion chamber connected to the T-motor. Through windows in the chamber, observations of flame gas temperature were made by measuring the luminous radiation with a photocell receiver, and spatial gas temperature variations (entropy waves) were investigated by high speed photography. It was found that, for all the different propellants, in the entire range of frequency and pressure noted above, the flame temperature responded isentropically to the oscillating pressure, and no entropy waves were seen in the combustion gas stream. This is completely contrary to theoretical expectations and it obviously means that the physical nature of the pressure-flame interaction is not well understood. Because of the importance of this interaction, further experiments with a different approach are proposed.

14.

KEY WORDS

**Solid Propellant
Combustion
Instability
Research
Oscillatory Combustion
Experiments**

LINK A

LINK B

LINK C

ROLE

WT

ROLE

WT

ROLE

WT

INSTRUCTIONS

1. **ORIGINATING ACTIVITY:** Enter the name and address of the contractor, subcontractor, grantee, Department of Defense activity or other organization (corporate author) issuing the report.

2a. **REPORT SECURITY CLASSIFICATION:** Enter the overall security classification of the report. Indicate whether "Restricted Data" is included. Marking is to be in accordance with appropriate security regulations.

2b. **GROUP:** Automatic downgrading is specified in DoD Directive 5200.10 and Armed Forces Industrial Manual. Enter the group number. Also, when applicable, show that optional markings have been used for Group 3 and Group 4 as authorized.

3. **REPORT TITLE:** Enter the complete report title in all capital letters. Title in all cases should be unclassified. If a meaningful title cannot be selected without classification, show title classification in all capitals in parenthesis immediately following the title.

4. **DESCRIPTIVE NOTES:** If appropriate, enter the type of report, e.g., interim, progress, summary, annual, or final. Give the inclusive dates when a specific reporting period is covered.

5. **AUTHOR(S):** Enter the name(s) of author(s) as shown on or in the report. Enter last name, first name, middle initial. If military, show rank and branch of service. The name of the principal author is an absolute minimum requirement.

6. **REPORT DATE:** Enter the date of the report as day, month, year, or month, year. If more than one date appears on the report, use date of publication.

7a. **TOTAL NUMBER OF PAGES:** The total page count should follow normal pagination procedures, i.e., enter the number of pages containing information.

7b. **NUMBER OF REFERENCES:** Enter the total number of references cited in the report.

8a. **CONTRACT OR GRANT NUMBER:** If appropriate, enter the applicable number of the contract or grant under which the report was written.

8b, 8c, & 8d. **PROJECT NUMBER:** Enter the appropriate military department identification, such as project number, sub-project number, system numbers, task number, etc.

9a. **ORIGINATOR'S REPORT NUMBER(S):** Enter the official report number by which the document will be identified and controlled by the originating activity. This number must be unique to this report.

9b. **OTHER REPORT NUMBER(S):** If the report has been assigned any other report numbers (either by the originator or by the sponsor), also enter this number(s).

10. **AVAILABILITY/LIMITATION NOTICES:** Enter any limitations on further dissemination of the report, other than

those imposed by security classification, using standard statements such as:

(1) "Qualified requesters may obtain copies of this report from DDC."

(2) "Foreign announcement and dissemination of this report by DDC is not authorized."

(3) "U. S. Government agencies may obtain copies of this report directly from DDC. Other qualified DDC users shall request through

(4) "U. S. military agencies may obtain copies of this report directly from DDC. Other qualified users shall request through

(5) "All distribution of this report is controlled. Qualified DDC users shall request through

If the report has been furnished to the Office of Technical Services, Department of Commerce, for sale to the public, indicate this fact and enter the price, if known.

11. **SUPPLEMENTARY NOTES:** Use for additional explanatory notes.

12. **SPONSORING MILITARY ACTIVITY:** Enter the name of the departmental project office or laboratory sponsoring (paying for) the research and development. Include address.

13. **ABSTRACT:** Enter an abstract giving a brief and factual summary of the document indicative of the report, even though it may also appear elsewhere in the body of the technical report. If additional space is required, a continuation sheet shall be attached.

It is highly desirable that the abstract of classified reports be unclassified. Each paragraph of the abstract shall end with an indication of the military security classification of the information in the paragraph, represented as (TS), (S), (C), or (U).

There is no limitation on the length of the abstract. However, the suggested length is from 15 to 225 words.

14. **KEY WORDS:** Key words are technically meaningful terms or short phrases that characterize a report and may be used as index entries in cataloging the report. Key words must be selected so that no security classification is required. Identifiers, such as equipment model designation, trade name, military project code name, geographic location, may be used as key words but will be followed by an indication of technical context. The assignment of links, roles, and weights is optional.